INVESTIGATION OF LATTICE PHYSICS PHENOMENA WITH UNCERTAINTY ANALYSIS AND SENSITIVITY STUDY OF ENERGY GROUP DISCRETIZATION FOR THE CANADIAN PRESSURE TUBE SUPERCRITICAL WATER-COOLED REACTOR

INVESTIGATION OF LATTICE PHYSICS PHENOMENA WITH UNCERTAINTY ANALYSIS AND SENSITIVITY STUDY OF ENERGY GROUP DISCRETIZATION FOR THE CANADIAN PRESSURE TUBE SUPERCRITICAL WATER-COOLED REACTOR

By
AHMAD MOGHRABI, B.Sc., M.A.Sc.

A Thesis
Submitted to the School of Graduate Studies
in Partial Fulfilment of the Requirements
for the Degree

Doctor of Philosophy

McMaster University

DOCTOR OF PHILOSOPHY (2017) McMaster University
(Department of Engineering Physics) Hamilton, Ontario, Canada

TITLE: Investigation of Lattice Physics Phenomena with Uncertainty Analysis and Sensitivity Study of Energy Group Discretization for the Canadian Pressure Tube Type Supercritical Water-Cooled Reactors

AUTHOR: Ahmad Moghrabi, B.Sc., M.A.Sc.
Beirut Arab University, Lebanon

SUPERVISOR: Professor David Novog

NUMBER OF PAGES: xv, 132

Abstract

The Generation IV International Forum (GIF) has initiated an international collaboration for the research and development of the Generation IV future nuclear energy systems. The Canadian PT-SCWR is Canada's contribution to the GIF as a GEN-IV advanced energy system. The PT-SCWR is a pressure tube reactor type and considered as an evolution of the conventional CANDU reactor. The PT-SCWR is characterized by bi-directional coolant flow through the High Efficiency Re-entrant Channel (HERC). The Canadian SCWR is a unique design involving high pressure and temperature coolant, a light water moderator, and a thorium-plutonium fuel, and is unlike any operating or conceptual reactor at this time. The SCWR does share some features in common with the BWR configuration (direct cycle, control blades etc…), CANDU (separate low temperature moderator), and the HTGR/HTR (coolant with high propensity to up-scatter), and so it represents a hybrid of many concepts. Because of its hybrid nature there have been subtle feedback effects reported in the literature which have not been fully analyzed and are highly dependent on these unique characteristics in the core. Also given the significant isotopic changes in the fuel it is necessary to understand how the feedback mechanisms evolve with fuel depletion. Finally, given the spectral differences from both CANDU and HTR reactors further study on the few-energy group homogenization is needed. The three papers in this thesis address each one of these issues identified in literature. Models were created using the SCALE (Standardized Computer Analysis for Licensing Evaluation) code package.

Through this work, it was found that the lattice is affected by more than one large individual phenomenon but that these phenomena cancel one another to have a small net final change. These phenomena are highly affected by the coolant properties which have major roles in neutron thermalization process since the PT-SCWR is characterized by a tight lattice pitch. It was observed that fresh and

depleted fuel have almost similar behaviour with small differences due to the Pu depletion and the production of minor actinides, ^{233}U and xenon.

It was also found that a higher thermal energy barrier is recommended for the two-energy-group structure since the PT-SCWR is characterized by a large coolant temperature compared to the conventional water thermal reactors. Two, three and four optimum energy group structure homogenizations were determined based on the behaviour of the neutron multiplication factor and other reactivity feedback coefficients. Robust numerical computations and experience in the physics of the problem were used in the few-energy group optimization methodology. The results show that the accuracy of the expected solution becomes highly independent of the number of energy groups with more than four energy groups used.

Co-Authorship

Chapters 4-6 are original journal papers written by myself, Ahmad Moghrabi. Chapter 4 is a journal paper that was published by Canadian Nuclear Laboratories Nuclear Review, Vol. 5, No. 2, 2016, pp. 253-268, doi:10.12943/CNR.2016.00031. Chapter 5 is a journal paper that was published by the Journal of Nuclear Engineering and Radiation Science with digital object identifier doi:10.1115/1.403789, Vol. 4(1), 011011-011011-11, 2018. Chapter 6 stands for the third paper that was published by the Annals of Nuclear Engineering, Volume 115, May 2018, Pages 27-38, ISSN 0306-4549, https://doi.org/10.1016/j.anucene.2018.01.011.

I grant an irrevocable, non-exclusive license to McMaster University to reproduce this material as part of this thesis.

Acknowledgements

A special thanks goes to my direct supervisor Professor David Novog as this work wouldn't have been possible without his direct guidance and inputs. I am grateful for the opportunity of being part of his research group and its conscientious experiences to be able to accomplish this work under his supervision. Also, thank you to all my committee members including my direct supervisor, Dr. Jeremy Pencer, and Dr. Adriaan Buijs.

I would like to thank my wife for all her help, support and standing beside me throughout the last five years to accomplish this work. She is the driving force for all my success and achievements. She has been my inspiration and motivation for continuing to enhance my knowledge and move my career forward. I also thank my wonderful kids for understanding my dedication and passion for completing my career goals.

A special thanks also goes to Dr. David Hummel for his helpful editing feedback and discussions.

I could not be where I am without the support and motivation from these great people.

Table of Contents

List of Figures

List of Tables

Nomenclature

Abbreviations

AECL	Atomic Energy of Canada Limited
ASAP	Adjoint Sensitivity Analysis Procedure
BWR	Boiling Water Reactor
CANDU	CANada Deuterium Uranium
CNL	Canadian Nuclear Laboratories
CRD	Control Rod Drive
CTC	Coolant Temperature Coefficient
CVR	Coolant Void Reactivity
DF	Dancoff Factor
ESC	Extended Step Characteristics
FA	Fuel Assembly
FORSS	Fantastic Oak Ridge Sensitivity System
FTC	Fuel Temperature Coefficient
FQT	Fuel Qualification Testing
GEN IV	Generation IV
GFR	Gas-cooled Fast Reactor
GGA	Gulf General Atomic
GIF	Generation IV International Forum
HERC	High Efficiency Re-entrant Channel
HM	Heavy Metal
HPLWR	High Performance Light Water Reactor
HTGR	High Temperature Gas-cooled Reactor
HTR	High Temperature Reactor
HWPR	Heavy Water Pressurized Reactor
ICV	Inner Coolant Void
LFR	Lead-cooled Fast Reactor
LOCA	Loss-of-Coolant Accident
LWR	Light Water Reactor
M&C	Materials and Chemistry
MCDANCOFF	Monte Carlo Dancoff

MOX	Mixed OXide
MSR	Molten Salt Reactor
MTC	Moderator Temperature Coefficient
NEWT	New Extended step characteristics-based Weighting Transport code
NOC	Normal Operating Condition
NRCan	Natural Resources Canada
NSERC	Natural Science and Engineering Research Council
OAT	One-At-A-Time Method
OCV	Outer Coolant Void
PARCS	Purdue Advanced Reactor Core Simulator
PHWR	Pressurized Heavy Water Reactor
PT-SCWR	Pressure Tube SuperCritical Water-cooled Reactor
PWR	Pressurized Water Reactor
R&D	Research and Development
RBMK	Reaktor Bolshoy Moshchnosti Kanalniy (Russian: High Power Channel-Type Reactor)
RPV	Reactor Pressure Vessel
SAMS	Sensitivity Analysis Model for SCALE
SCALE	Standardized Computer Analysis for Licensing Evaluation
SCW	SuperCritical Water
SCWR	SuperCritical Water-cooled Reactor
SCW-FFP	SuperCritical Water Fossil Fired Plant
SCWR-SM	SuperCritical Water-cooled Reactor with Solid Moderator
SCWR-M	SuperCritical Water-cooled Reactor with Mixed core design
SFR	Sodium-cooled Fast Reactor
SI&A	System Integration and Assessments
Super FR	Super Fast Reactor
Super LWR	Super Light Water Reactor
TCV	Total Coolant Void
TH&S	Thermal-hydraulics and Safety
TRITON	Transport Rigor Implemented with Time-dependent Operation for Neutronic depletion
TSUNAMI	Tools for Sensitivity and Uncertainty Analysis Methodology Implementation
VHTR	Very-High-Temperature Reactor

Letters

C	Neutron precursor density [neutrons.cm^{-3}]
C	Covariance matrix
E	Energy [eV]
f	Thermal utilization factor
k	Neutron multiplication factor
N	Neutron density [neutrons.cm^{-3}]
P	Legendre polynomial
p	Resonance escape probability
Q	Neutron source [neutrons.cm^{-3}.s^{-1}]
r	Position (space: x,y,z) [cm,cm,cm]
s	Sensitivity
S	Sensitivity matrix
t	Time [s]
v	Speed [cm.s^{-1}]

β	Delayed neutron fraction
ε	Fast fission factor
η	Reproduction factor
λ	Decay constant [s^{-1}]
ν	Average number of neutrons released per fission event
ρ	Reactivity [mk]
σ	Microscopic cross-section [cm^2]
Σ	Macroscopic cross-section [cm^{-1}]
ϕ	Scalar neutron flux density [neutrons.cm^{-2}.s^{-1}]
ψ	Neutron angular flux density [neutrons.cm^{-2}.s^{-1}]
χ	Neutron fission spectrum
Ω	Direction of neutron flight [sr]

Subscript and Superscript

†	Adjoint
γ	Capture interaction
eff	Effective
g	Energy group
f	Fission interaction
∞	Infinite lattice
p	Prompt neutron
s	Scattering interaction
t	Total
T	Transpose

Chapter 1

Introduction

1.1. Introduction

Growth in the world's population and in the standard of living in developing countries is leading to an increase in energy demands, placing greater pressure on the world's energy resources and increases in CO_2 emissions. This has increased interest in clean and sustainable energy resources since fossil fuel systems (like coal and natural gas) are a significant source of greenhouse gases. Nuclear power is highly important because of its high power density, economics, sustainability, and low carbon dioxide emissions. This technology is based on the neutron fission reaction which produces thermal energy that can be converted to useful electrical energy. As of November 2016, there are 450 operating nuclear reactors worldwide which produce 14 percent of the world's electricity, and there are 60 new nuclear plants under construction [1]. The evolution of nuclear technology extends from the first prototype designs (Generation I), to the second generation (Generation II) commercial designs, through to Generation III designs which improve economics and safety through design standardization, improved fuel technology and enhanced safety systems. Most of today's operating reactors belong to the second or the third generations (Generation II and III), while reactors presently under construction belong to the new evolutionary design (Generation III+) [2, 3]. The percentage share of the nuclear energy in the energy matrix varies worldwide, as an example nuclear energy accounts for 75.2 percent of France's electricity, and 1.9 percent in China [4]. It is expected that nuclear energy will remain an integral part of the global energy mix. Particularly, China has plans to substantially increase the number of operating nuclear power plants by 2020 [5].

Although nuclear energy is becoming increasingly important as an alternative low-Carbon energy production option, it faces many challenges. These include factors affecting economics, safety, proliferation resistance, sustainability and efficiency. Knowing that the public safety is the key of the social acceptance which considered as one of the major challenges. Consequently, the Generation IV International Forum (GIF) has been established as an international collaboration in research to develop the next generation of nuclear energy systems.

1.2. The Generation-IV International Forum

GIF was established to foster international collaboration in developing innovative advanced nuclear energy systems through renewed research and development so that such systems would be available for international deployment by 2030. The challenging technology goals of the Gen-IV nuclear energy systems are summarized in the following four areas [2, 3]:

- **Sustainable nuclear energy**

  Focusing on nuclear waste management and resource utilization, Gen-IV nuclear energy systems will generate sustainable energy that promotes long-term nuclear fuel availability with effective fuel utilization. The revolutionary designs aim to minimize and manage nuclear waste and reduce the long-term nuclear waste repository requirements.

- **Economics**

  Generation IV nuclear energy systems will have a clear life-cycle cost advantage and a level of financial risk comparable to other energy sources. This includes the innovative enhancements in plant and fuel cycle efficiency, design simplifications, and plant sizes. Also, it involves the flexible utilization of nuclear energy as a primary energy source for a secondary application such as the production of hydrogen, fresh water, district heating, and other energy products to be produced where they are needed.

- **Safety and reliability**

  One of the priority requirements of future nuclear energy systems is an enhancement in safety and reliability. Gen-IV energy systems will excel in

safety and reliability by improving accident management and decreasing the likelihood and consequences of reactor core damage. This also includes the use of inherent safety features which reduce the need for offsite emergency response and enhance the public confidence in the safety of nuclear energy.

- **Proliferation resistance and physical protection**
  To focus on controlling and securing nuclear energy systems, facilities, and materials through design features. This includes the increase of physical protection against terrorists by increasing the robustness of the new facilities. Gen-IV nuclear energy systems will be very unattractive targets with the least desirable route for diversion or theft of weapons-usable materials.

To meet all these goals and to enhance the future role of nuclear energy, GIF has developed a technology roadmap that covers the research and development requirements to support future innovative nuclear energy systems. GIF has identified six Gen-IV nuclear energy systems for future research: Gas-cooled Fast Reactor (GFR), Lead-cooled Fast Reactor (LFR), Sodium-cooled Fast Reactor (SFR), Molten Salt Reactor (MSR), Very High Temperature Reactor (VHTR), and SuperCritical Water Reactor (SCWR) [2, 3]. It was agreed that each of the GIF's members would pursue a research and development program on at least one of these reactor systems. Three members of GIF (Canada, Japan, and the European Union) started a research and development program for the Gen-IV SCWR concept focusing on materials and chemistry, themalhydraulics and safety, system integration and core and reactor design [5]. The SCWR is the only Gen-IV reactor concept that utilizes water as the main coolant or moderator and it is the subject of this work.

1.3. The SCWR advantages and challenges

The SCWR is a high temperature and pressure water-cooled reactor designed to operate above the thermodynamic critical point of water (22.1 MPa). The concept of the SCWR was investigated in the '50s and '60s as discussed by Oka [6] but was never built. New attention has been given to the SCWRs in the last two decades owing to the large improvements in SuperCritical Water Fossil Fired Plant (SCW-

FFP) technology. A previous study [7] has shown that similar approaches and efficiencies can be achieved for nuclear power plants. Consequently, several countries initiated a research and development (R&D) program into the SCWR. In addition to the potential improvements in efficiency, other benefits include [8]:

- Plant simplifications with a direct cycle (compact turbine system) which will simplify the heat transport system and eliminate the secondary side that includes the steam handling components (steam generators, separators, dryers, recirculation jet pumps, pressurizer). This will also decrease the containment size and reduce the capital cost, which is considered to be 50-60% of existing light water reactors [9].
- Leveraging the technical experience in SCW-FFPs. Thus, the technology used in operating SCW-FFPs can be directly utilized in the design of out-of-core SCWR components. This includes high temperature and pressure turbines already being used in SCW-FFPs at similar operating conditions.
- The expertise and the accumulated body of knowledge from the existing Light Water Reactors (LWRs) and Pressurized Heavy Water Reactors (PHWRs) can be leveraged in the development of the SCWR concepts.
- The supercritical water exists in only one thermodynamic phase which eliminates any possibilities of boiling crises which are considered a main safety concern in LWRs.

Above the thermodynamic critical point, water behaves as a supercritical fluid in a single thermodynamic phase. Supercritical fluids undergo a drastic variation in their thermo-physical properties which impact their neutronic and thermalhydraulic behaviour. The density variation at supercritical pressure (25 MPa) decreases continuously as function of temperature as shown in Figure 1 [10]. Other properties which are related to the heat transfer are also highly affected including the thermal conductivity, viscosity and heat capacity. For example, the specific heat is

maximized at what is referred to as the pseudo-critical temperature as shown in Figure 1 [10].

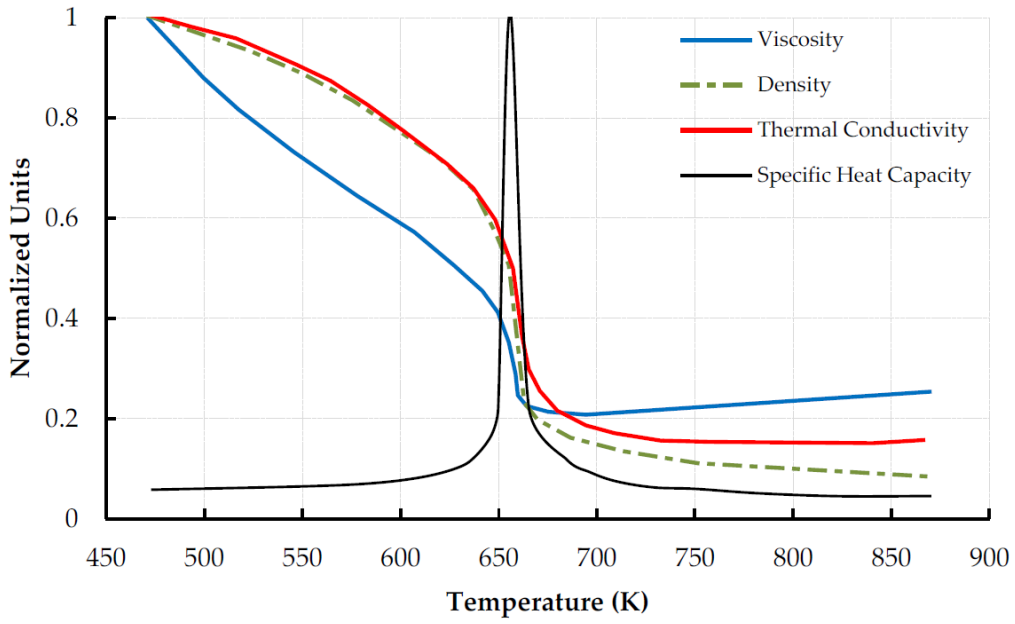

Figure 1:Variation of physical properties as function of temperature of supercritical water at 25 MPa [10].

The SCWR uses light water above its thermodynamic critical point as a coolant. Thus, several technological challenges that are correlated to the development of the SCWR arise from the large variation of coolant properties under the required operating conditions. A recent GIF report [5] has categorized the SCWR technological challenges into four domains: System Integration and Assessments (SI&A), Thermal-hydraulics and Safety (TH&S), Materials and Chemistry (M&C) and Fuel Qualification Testing (FQT). GIF [11] also highlights many future challenges for the SCWR project in many domains especially for the transient heat transfer models (including depressurization from supercritical to subcritical conditions). Moreover, it discusses the need to investigate qualified in-core materials that accommodate such high pressures and temperatures, corrosion, and high neutron radiation. GIF [11] further notes safety concerns which are considered challenges for the SCWR, such as controlling the coolant flow rate instead of coolant inventory and the use of a passive safety systems.

Another recent study [12] has classified the common SCWR design challenges into four domains as:

- **Materials:** Although the out-core materials and components can be selected based on the previous experience in operating SCW-FFPs, there is still a lack of knowledge for the in-core materials (reactor internals and fuel cladding). Thus, a large amount of research is required to investigate materials that are structurally robust and resist corrosion in high neutron flux density.
- **Chemistry:** It was confirmed experimentally that the chemical properties and density of the SCW coolant show large changes near the critical and pseudo-critical point which have a large influence on corrosion and stress corrosion cracking of the in-core materials. The in-core radiolysis effects in the SCWR are also noticeably different from the conventional light water reactors which complicate the behaviour.
- **Thermalhydraulic:** Unlike phase changes in subcritical water the SCW coolant exists with only one phase. Thus, the design criteria are now limited by the cladding temperature of the fuel rather than the traditional Critical Heat Flux (CHF). Therefore, accurate calculation of the SCW heat transfer is necessary for safety margin considerations. This requires experimental heat transfer data for the appropriate bundle geometry at the required conditions. Most of the available experimental data of SCW heat transfer is applicable to the SCW-FFPs, but not SCWR bundle geometries and conditions.
- **Safety:** There are many safety considerations related to the SCWR design that require investigation to establish a design and beyond design accident bases. These include, but are not limited to: transient experimental data on SCW heat transfer, experimental SCW data that covers the critical flow and depressurization of the system, experimental data and analytical models for the prediction of the onset of instability in the system, and coupled neutronics and themalhydraulics analyses**.**

Many SCWR designs have been proposed which can be classified based on the design features and neutron energy spectrum [13]. Depending on the design, the SCWR can be categorised into two main types: the pressure vessel reactor types analogous to the PWRs and BWRs, and the pressure tube reactor type which is similar to CANDU nuclear reactors. Moreover, some SCWR designs consider thermal, fast or mixed-neutron energy spectrum reactor concepts.

As a member of the GIF, Canada aims to perform research and development work on at least one of the GIF six reactor concepts. Due to the experience accumulated with the successful CANDU (CANada Deuterium Uranium) reactor, it was decided that Canada would initiate an R&D program for a thermal-spectrum pressure tube reactor, referred to as the Canadian PT-SCWR.

1.4. The Canadian PT-SCWR

The Canadian Pressure Tube Super Critical Water-cooled Reactor (PT-SCWR) is an advanced Gen-IV reactor concept that meets the goals for future innovative designs proposed by the GIF including resource sustainability, improved safety and reliability, economic benefits, and improved proliferation resistance and physical protection [14]. It is considered an evolution from the fleet of operating CANDU reactors [15]. The Canadian PT-SCWR design is proposed by Canadian Nuclear Laboratories (CNL), formerly named Atomic Energy of Canada Limited (AECL) [16], and shares some of the advantages of the conventional Heavy Water Pressurized Reactor (HWPR) and Boiling Water Reactor (BWR). The PT-SCWR is a pressure tube reactor type characterized by the separation of the coolant and the low temperature and low pressure heavy water moderator and the arrangement of fuel pins in annular fuel rings similar to the traditional CANDU reactor. It also shares some features of the BWRs such as the vertical orientation of the reactor core, large axial variations of fuel temperature and coolant properties along the fuel channel, a direct thermodynamic cycle design, and a long fuel assembly that spans the entire reactor core.

Unlike the traditional CANDU reactor, the Canadian PT-SCWR uses batch refuelling with an enriched mixture of plutonium-thorium oxide fuel [17, 18]. As depicted in Figure 2 [19], the fuel channel is characterized by the bi-directional flow path of the coolant through the High-Efficiency Re-Entrant channel (HERC) [17, 18]. The coolant enters the fuel channel from the inlet plenum at the top of the core and flows downwards through the central flow tube, reverses direction at the bottom of the channel, then flows upward through the outer flow tube and passes through the two annular fuel rings. Finally, it exits the fuel channel to the outer plenum. A combination of the liner, ceramic insulator, and pressure tube are used to separate the hot coolant from the low temperature and low pressure heavy water moderator, eliminating the calandria tube used in CANDU reactors (See Figure 3).

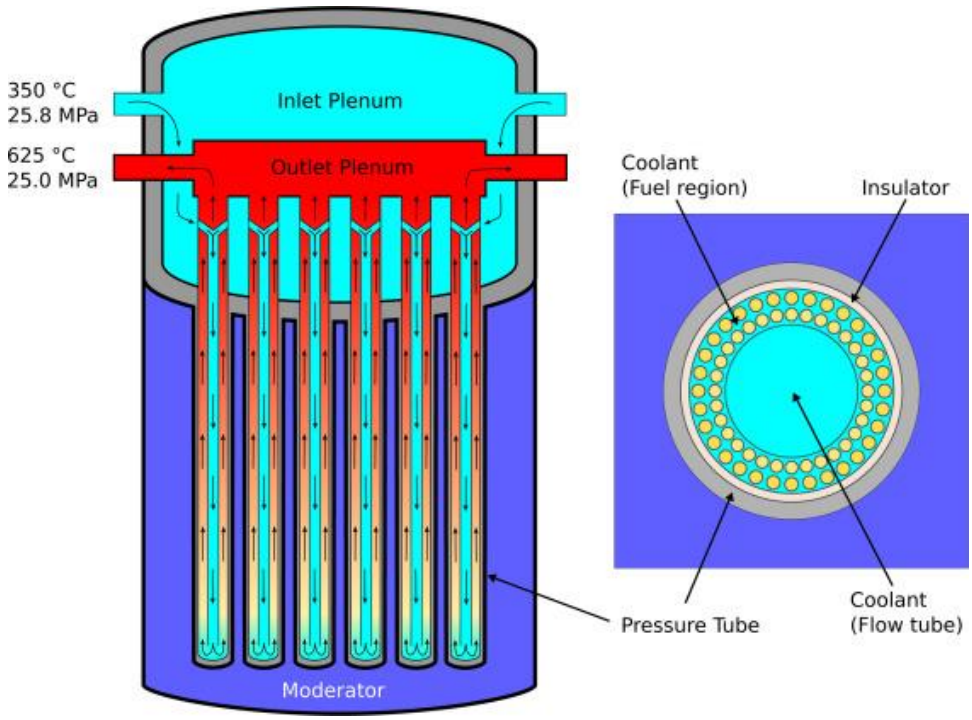

Figure 2: Core and lattice cell cross-section view of the PT-SCWR HERC concept with the 64-element fuel assembly [19].

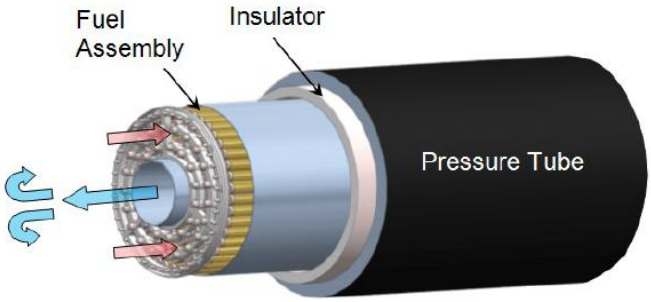

Figure 3: The fuel channel design in the Canadian PT-SCWR with illustration of the coolant flow through the HERC [17].

1.5. Thesis objectives and outlines

The Canadian PT-SCWR uses light water above its thermodynamic critical point as a coolant. The PT-SCWR experiences a large axial variation in coolant density and temperature along the fuel channel [20]. Such large variation in coolant properties introduces many challenges to the thermalhydraulic and the neutronic analysis of the PT-SCWR. In the PT-SCWR the heavy water moderator is separated from the supercritical light water coolant (kept at high temperature and pressure) causing fewer impacts on the core-neutronics than, e.g. in the light water cooled and moderated high pressure light water reactors [21]. However, the large coolant density variation and the high reduction of coolant density under normal operating conditions affect the neutron spectrum, which might complicate and influence the flux gradients [15]. The changes in the coolant density further impact the PT-SCWR neutronics by affecting several neutron-nuclei interactions and their corresponding rates. Many studies as outlined in Chapter 2, have been performed on the thermalhydraulics feedback and its coupling with the neutronics to have a better understanding of the physical behaviour of such designs. However, there is still a lack of knowledge on the some of the lattice cell phenomena taking place for the PT-SCWR.

In general reactor physics calculations, after the dilution dependent data are generated in a neutron cross section analysis package such as NJOY, the calculations are executed in two main stages. First, lattice cell transport calculations are performed based on lattice properties and geometry, using finite energy groups

to generate lattice homogenized constants and cross sections in a multi-energy group structure. Such calculations are performed using the neutron transport equation, the processed multi-group cross section library, the lattice geometry and suitable boundary conditions. The aim of this first stage is to generate suitably homogenized few group (generally 2 to 8) nuclear cross sections over an entire lattice. Knowing that the generated homogenized cross-sections are flux weighted, the condensed group structure is highly affected by the neutron spectrum. Then, full-core diffusion simulations are performed using the pre-calculated homogenized cross-sections generated from the lattice cell transport calculations. The neutron energy spectrum for thermal reactors is usually divided into two main portions: thermal and fast with an energy cut-off located at 0.625eV. However, the 0.625eV thermal energy barrier is not standard and depends on the reactor design, fuel type, coolant and moderator characteristics, etc. Given the changes in Gen-IV reactor designs (especially coolant density reductions and variations), many studies have dealt with the problem of optimizing a discretized broad/few energy group structure [22, 23, 24, 25]. In particular [26] has recommended that the conventional two-energy group diffusion approach is not sufficient to capture the spectral change in the analysis of the Canadian PT-SCWR.

The objectives of this thesis are to generate an improved understanding of the neutronic characteristics of the Canadian SCWR lattice cell under fresh fuel (publication #1) and depleted conditions (publication #2). An additional objective is to utilize this understanding to develop appropriate energy group structures for this SCWR fuel (publication #3). The three papers included in this thesis address each one of these issues and objectives. The different modules in Standardized Computer Analysis for Licensing Evaluation (SCALE) package were used in this work.

This thesis consists of 7 chapters including the current introductory chapter that are outlined as follows:

A scientific literature review that discusses the present study motivations, aims, goals, needs and requirements is established in Chapter 2. Additional information

on the different SCWR designs and concepts discussed in the past relevant studies is also presented in this chapter. Chapter 3 introduces the theoretical framework including the basic theory related to the neutron transport equation and general information about the methods that are used to solve it. Chapter 4 is a journal paper that was published by Canadian Nuclear Laboratories Nuclear Review, Vol. 5, No. 2, 2016, pp. 253-268, doi:10.12943/CNR.2016.00031 examining the lattice physics phenomena of the SCWR under fresh conditions. Chapter 5 is a journal paper that discuss the effects of fuel burnup on lattice behaviour which was published by the Journal of Nuclear Engineering and Radiation Science with digital object identifier given by doi:10.1115/1.4037895, Vol. 4(1), 011011-011011-11, 2018. Chapter 6 includes the final paper related to energy group structure optimization that was published by the Annals of Nuclear Energy, Volume 115, May 2018, Pages 27-38, ISSN 0306-4549, https://doi.org/10.1016/j.anucene.2018.01.011. Conclusions drawn from the models used and the results analysis are presented in Chapter 7 in conjunction with the recommendation for future work and the contributions to knowledge from this work.

Chapter 2

Literature Review

In this chapter the different SCWR designs will be discussed, highlighting in particular the characteristics and some of the technical challenges of the Canadian PT SCWR design. The SCWR is the only GEN IV reactor design that uses light water as coolant and moderator. The available literature on lattice physics characteristics and analysis of the SCWR will also be discussed. Finally, literature on energy group structure and optimization is reviewed.

2.1. The Super Critical Water-cooled Reactor

The Super Critical Water-cooled Reactor is one of the six GEN IV reactor technologies identified by the GIF that promises to fulfil its proposed goals. Given that the majority of nuclear power plants are water cooled reactors, the SCWR technology is considered as the natural evolutional and extension of the current conventional light water reactor concepts [27]. Two main types of SCWR reactor concepts have thus far been considered: the large reactor pressure vessel type and the pressure tube reactor. The SCWR was designed to operate with a thermal, fast or mixed neutron spectrum core.

2.2. Super Light Water Reactor and Super Fast Reactor

A large experience base has been accumulated in Japan with many years of operating the SCW-FFP since Anegasaki No. 1 started its operation in 1967 [9]. This was the driving force to motivate an R&D program on the GEN IV SCWR. The idea of using SCW coolant in nuclear reactor system has been investigated at the University of Tokyo and at the Waseda University through computational simulations since 1989 [9]. It was first presented to the GIF by Oka and Koshizuka

[28]. The Japanese SCWR technology is divided into two designs: The Super Light Water Reactor (Super LWR) utilizing the thermal neutron spectrum and the Super Fast Reactor (Super FR) with a fast neutron spectrum. The Super LWR is cooled and moderated by light water and characterized by a square fuel assembly [29]. The Super FR is cooled by light water utilizing Mixed Oxide (MOX) fuel with a hexagonal fuel assembly [29]. Both of the designs use a Reactor Pressure Vessel (RPV) and a once-through direct coolant cycle as depicted in Figure 4 [29].

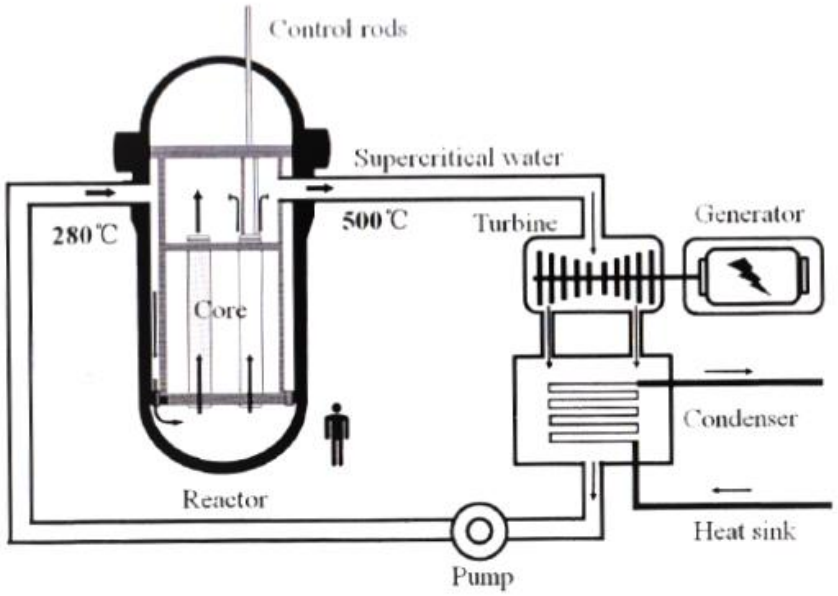

Figure 4: Super LWR and Super FR plant system design description [29].

Many coolant flow designs such as double-tube water rods, two-pass, and single-pass coolant flow schemes have been investigated to achieve a negative void reactivity. In general, the coolant provided through the inlet nozzles mainly flows upwards to the upper dome and then downwards through the water rods of the fuel assemblies (FA) which are classified into two groups: the inner core assembly and the peripheral core assembly [13, 29]. The coolant then travels upwards through the fuel region of the core to the upper plenum. The Control Rod Drives (CRDs) are clustered cruciform control rods (similar to those of BWR) inserted from the bottom of the core.

Oka and Mori [29] introduce 9, 10 and 12 energy group structure based on the lattice cell homogenized cross-sections for the Super FR with the SCW coolant. In

all cases they recommended a higher thermal energy cut-off barrier as shown in Table 1. The seventh group in the 9 energy group structure covers the transition energy range between the epithermal and the thermal energy regions. The main difference between the 10 and the 9 energy group structures is the detailed structure introduced by splitting that seventh group. The 12 energy group structure differs significantly from the 9 group structure with fine structure proposed between the fifth and the eighth energy group. They recommend a 12 energy group structure with more detailed group divisions in the thermal energy range to obtain acceptable accuracy.

Table 1:A detailed structure of the energy group structures proposed by Oka and Mori [28].

<table>
<tr><th colspan="2" rowspan="2">Energy Range (eV)</th><th colspan="2">Energy Group Structure</th><th colspan="2" rowspan="2">Energy Range (eV)</th><th rowspan="2">12 Energy Groups</th></tr>
<tr><th>9 G</th><th>10 G</th></tr>
<tr><td>1.00×10^{7}</td><td>8.21×10^{5}</td><td>1</td><td>1</td><td>1.00×10^{7}</td><td>8.21×10^{5}</td><td>1</td></tr>
<tr><td>8.21×10^{5}</td><td>6.74×10^{4}</td><td>2</td><td>2</td><td>8.21×10^{5}</td><td>6.74×10^{4}</td><td>2</td></tr>
<tr><td>6.74×10^{4}</td><td>5.53×10^{3}</td><td>3</td><td>3</td><td>6.74×10^{4}</td><td>5.53×10^{3}</td><td>3</td></tr>
<tr><td>5.53×10^{3}</td><td>4.54×10^{2}</td><td>4</td><td>4</td><td>5.53×10^{3}</td><td>4.54×10^{2}</td><td>4</td></tr>
<tr><td>4.54×10^{2}</td><td>3.73×10^{1}</td><td>5</td><td>5</td><td>4.54×10^{2}</td><td>7.89×10^{1}</td><td>5</td></tr>
<tr><td>3.73×10^{1}</td><td>2.38</td><td>6</td><td rowspan="2">6</td><td>7.89×10^{1}</td><td>1.37×10^{1}</td><td>6</td></tr>
<tr><td>2.38</td><td>1.86</td><td rowspan="4">7</td><td>1.37×10^{1}</td><td>1.86</td><td>7</td></tr>
<tr><td>1.86</td><td>8.76×10^{-1}</td><td>7</td><td>1.86</td><td>1.13</td><td>8</td></tr>
<tr><td>8.76×10^{-1}</td><td>4.14×10^{-1}</td><td>8</td><td>1.13</td><td>6.83×10^{-1}</td><td>9</td></tr>
<tr><td>4.14×10^{-1}</td><td>3.65×10^{-1}</td><td rowspan="2">9</td><td>6.83×10^{-1}</td><td>4.14×10^{-1}</td><td>10</td></tr>
<tr><td>3.65×10^{-1}</td><td>9.71×10^{-2}</td><td>8</td><td>4.14×10^{-1}</td><td>9.71×10^{-2}</td><td>11</td></tr>
<tr><td>9.71×10^{-2}</td><td>1.00×10^{-5}</td><td>9</td><td>10</td><td>9.71×10^{-2}</td><td>1.00×10^{-5}</td><td>12</td></tr>
</table>

2.3. European High Performance Light Water Reactor

The High Performance Light Water Reactor (HPLWR) is an SCWR concept developed by the European Union. The HPLWR is a pressure vessel reactor type with light water coolant (at the system pressure of 25 MPa) where part of the coolant flows first through the water rods within the Fuel Assembly (FA) to provide moderation. The coolant is then directed through the fuel-containing region of the assembly in a 3- pass arrangement. In the first pass, the coolant flows through the

evaporator and undergoes a change from liquid to steam-like state. Then the coolant changes direction in two superheating stages as shown in Figure 5 [30]. The coolant mixing between each stage eliminates enthalpy imbalances which might occur over the burnup of each assembly thus keeping the fuel cladding temperature below the required design constraints. Similar to the conventional PWR design, the control rods are inserted from the top of the core. According to Schulenberg and Starflinger [30] the conceptual design phase has been completed.

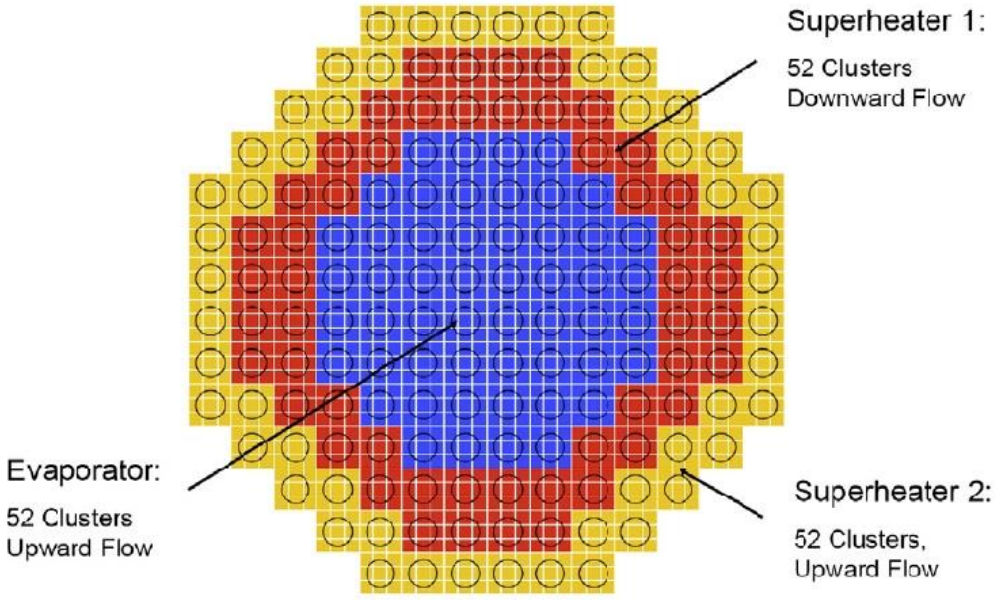

Figure 5: Description of evaporator and assembly cluster in the HPLWR core [30].

2.4. Alternative SCWR designs

An alternative SCWR design was developed in the republic of Korea that is moderated by the solid ZrH_2 and is referred to the SuperCritical Water-cooled Reactor with Solid Moderator (SCWR-SM). The solid moderator was introduced to simplify the coolant flow in the upper reactor dome. The SCWR-SM concept provided 1400 MWe with a four-batch fuel loading scheme [13]. Another mixed core design (SCWR-M) was developed at Shanghai Jiao Tong University in China [31]. The SCWR-M is a pressure vessel type that uses a mixed neutron spectrum through which the reactor core is divided into two zones: the thermal and the fast

zones. Firstly, the coolant entering the pressure vessel flows downwards through the thermal zone and then upwards through the fast zone [31].

2.5. The Canadian Pressure Tube Super Critical Water-Cooled Reactor

As part of the GIF, Canada has initiated an R&D program for a Gen IV pressure tube SCWR. The Canadian SCWR is referred to the "Pressure Tube Super Critical Water-cooled Reactor (PT-SCWR)" by its developers. Details of the design are reviewed below.

2.5.1. Development History

The Canadian SCWR concept has changed significantly since its earliest proposal. The earliest design was very similar to the traditional CANDU and was referred to the "CANDU-SCWR", where the major change was the change of the coolant type from heavy water to SCW while keeping the key design feature of CANDU, the separation of the moderator and the coolant [15].

A large number of changes have been proposed to this concept as a consequence of numerous optimization, analytical and theoretical studies. The idea of using a fuelling machine with a high temperature and pressure SCW channel was abandoned and thus the enriched fuel option was introduced [32]. The removal of online fuelling from the design also removed the requirements for a horizontal core geometry, and hence all future designs considered vertical cores. A three batch refuelling scheme and several plutonium and thorium mixture fuel assembly designs were investigated in McDonald et al. [33]. McDonald et al. also performed an optimization study of fuel-to-moderator ratio in order to achieve a high burnup and negative Coolant Void Reactivity (CVR). Based on these results the lattice pitch was selected to be 25 cm. A large non-fuel pin was introduced at the centre of the lattice with annular fuel rings to optimize CVR. However, it was observed that the radial power distribution was biased towards the outer fuel ring, negatively affecting the cladding temperatures. Consequently, the fuel element design was segmented into a larger number of pins, i.e., the 54-element, 78-element, and 62-

element designs. Finally, given the large diameter required for SCW feeder pipes, and to remove the possibility of pipe breaks at elevations below the reactor core, a re-entrant fuel channel design was selected. Such a design allows for both the inlet and outlet plena to be located above the active fuel and is the basis for the High Efficiency Re-entrant Channel (HERC) design proposed by AECL. The reference design introduced by Pencer et al. [18] is referred to as the Canadian Pressure Tube type SuperCritical Water-cooled Reactor (PT-SCWR) 64-element design.

2.5.2. The reference PT-SCWR design specifications

The current Canadian PT-SCWR conceptual design includes 336 fuel channels that operate with a total thermal power of 2540 MW. With the implementation of the direct cycle and the high temperature SCWR coolant, it is assumed that the thermodynamic cycle efficiency is 48% producing approximately 1200 MW of electric energy. As depicted in Figure 2, the PT-SCWR fuel channel is characterized by a unique bi-directional flow of coolant through HERC. The coolant enters the inlet plenum through the inlet nozzles at 350 °C and 25 MPa, is then distributed to each of the individual fuel assemblies and flows downward through the central flow tube in each channel. At the bottom of the channel, the coolant reverses direction and flows upward exchanging the heat with the fuel elements and exiting the fuel channel to the outlet plenum at 650 °C and 25 MPa. The low temperature and pressure heavy water moderator is separated from the high temperature and pressure light SCW coolant by liner tubes (inner and outer), ceramic insulator and pressure tube. The average fuel channel power is 7.56 MW_{th} and the average radial power peaking factor is expected to be 1.32 [8]. The PT-SCWR core is vertically oriented and 3-batch fuelled with a long fuel assembly that spans the whole core length [14]. The fuel assembly has a 5 m active fuel length with zirconium-modified stainless steel cladding and annular fuel pin distribution [34]. This reactor is powered by a Pu-Th fuel mixture which is arranged in two concentric 32-element fuel rings with 12% and 15% concentration of reactor grade plutonium in thorium in the outer and the inner rings, respectively. Descriptions of the HERC and the fuel compositions are shown in Table 2 and Table 3.

Table 2: Description of the HERC [19].

Component	Dimension (cm)	Material	Composition [wt%]	Density [g.cm^{-3}]
Center Tube Coolant	4.60 radius	Light Water	H_2O: 100 %	variable
Center Flow Tube	4.60 IR Thickness: 0.1	Zr-modified 310 Stainless Steel	C: 0.034; Si: 0.51; Mn: 0.74; P: 0.016; S: 0.0020; Ni: 20.82; Cr: 25.04; Fe: 51.738; Mo: 0.51; Zr: 0.59	7.9
Coolant		Light Water	H_2O: 100 %	variable
Liner Tube	7.20 IR Thickness: 0.05	Zr-modified 310 Stainless Steel	As above	7.9
Insulator	7.25 IR Thickness: 0.55	Yttria Stabilized Zirconia	Zr: 72.32; O: 27.68	5.37
Outer Liner Tube	7.80 IR Thickness: 0.05	Excel (Zirconium Alloy)	Sn: 3.5; Mo: 0.8; Nb: 0.8; Zr: 94.9	6.52
Pressure Tube	7.85 cm IR Thickness: 1.2	Excel (Zirconium Alloy)	As above	6.52
Moderator lattice pitch	25 square	Heavy Water	D_2O: 99.833; H_2O: 0.167	1.0851

Table 3: PT-SCWR fuel description and materials composition [19].

	Inner Ring	Outer Ring
Number of Rods	32	32
Pitch Circle Radius (cm)	5.4	6.575
Radius of Fuel Pins (cm)	0.415	0.440
Thickness of Fuel Cladding (cm)	0.06	0.06
Materials of Fuel Pins wt% PuO_2/ThO_2	15	12
Materials of Fuel Cladding	Zr-mod SS	Zr-mod SS
Fuel Pins Composition [wt%]	Pu:13.23; Th:74.70; O:12.07	Pu:10.59; Th:77.34; O:12.08
Fuel Cladding Composition [wt%]	C: 0.034; Si: 0.51; Mn: 0.74; P: 0.016; S: 0.0020; Ni: 20.82; Cr: 25.04; Fe: 51.738; Mo: 0.51; Zr: 0.59	Same as inner
Fuel Pins density (g/cm^3)	9.91	9.87
Fuel Cladding density (g/cm^3)	7.9	7.9
Plutonium Isotopics [wt%]	Pu238: 2.75; Pu239: 51.96; Pu240: 22.96; Pu241: 15.23; Pu242: 7.10	Pu238: 2.75; Pu239: 51.96; Pu240: 22.96; Pu241: 15.23; Pu242: 7.10

2.6. Reactor physics analyses

In the reactor core, the neutron flux is a function of time, space and energy. At a fundamental level, the interaction of a neutron with an in-core material is dependent on the material's microscopic cross section at the energy of the incident neutron. These interactions can be characterized into scattering (elastic and inelastic) and absorption and are strongly dependent on energy.

One of the most important aims in reactor physics calculations is to obtain the spatial and energy dependence of flux in the reactor core under steady-state conditions. The criticality search problem is investigated by introducing an eigenvalue referred to ($1/k_{\text{eff}}$) to the time-independent neutron transport equation where k_{eff} is called the effective multiplication factor. Such approach allows the number of neutrons emitted per fission to vary by a factor of ($1/k_{\text{eff}}$). The ratio of the neutron density between two consecutive generations with an iterative approach converges to a constant value which is independent of space, angle and energy and is given by [35]:

$$\lim_{\tau} \frac{N_\tau}{N_{\tau-1}} = \text{constant} = k_{\text{eff}}, \tag{2.1}$$

Usually, the controlled parameters of interest in steady-state and controlled conditions nuclear reactor are the k_{eff} and the neutron flux which are necessary to determine the different neutron reaction rates and particularly the balance between the neutron loss and production. Stochastic methods use the previous definition of k_{eff} that represents the ratio of neutron production from fission in the i^{th} generation to the neutron absorption and leakage in the generation (i+1). The reaction rates are used to calculate the approximate heat production from the fission reaction and the fuel utilization which is referred to the "burnup".

Although stochastic methods use the previous definition of k_{eff}, deterministic methods calculate k_{eff} based on different neutron physical interaction processes that occur within the nuclear reactor core which are given by the six-factor formula as:

$$k_{\text{eff}} = \eta f p \varepsilon P_F P_T, \tag{2.2}$$

where η is the neutron reproduction factor defines as the ratio of fast fission neutrons to the thermal neutrons absorbed in fuel. The thermal utilization factor f represents the probability of thermal neutron absorption within the fuel with respect to the other materials. The resonance escape probability p defines the probability that a neutron is slowing down to thermal energies without being absorbed. The ratio of total number of fast fission neutrons produced at all energies to number of

thermal fission neutrons defines the fast fission factor ε. Neutron leakage is included in the fast non leakage (P_F) and thermal non leakage (P_T) factors. The neutron life cycle based on the definition of the six factors is depicted in Figure 6. In infinite medium neutron leakage is neglected and thus Equation (3.2) can be simplified to what is referred to the four-factor formula that defines the infinite neutron multiplication factor k_∞ as:

$$k_\infty = \eta f p \varepsilon, \tag{2.3}$$

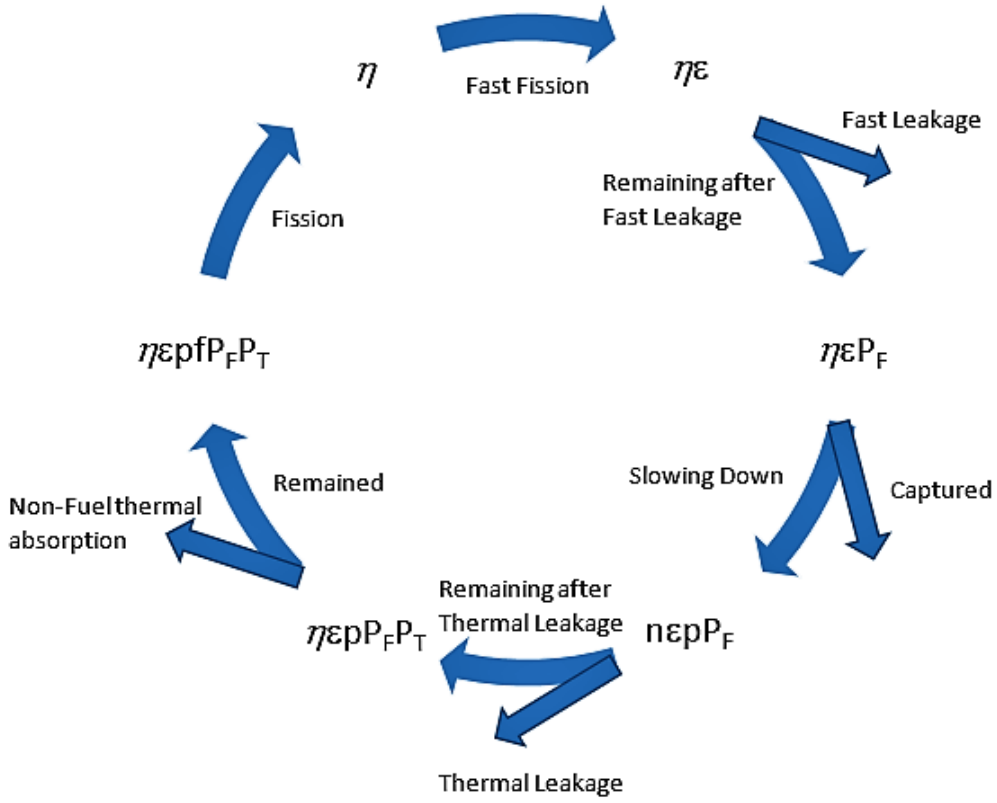

Figure 6: Neutron Life Cycle with k_{eff} = 1.

Generally, deterministic reactor physics calculations are performed in three-steps. First the continuous-energy nuclear data library is processed using NJOY to prepare a discrete energy dependent cross-section library for each different isotope (i.e., the so called multi-group library). Then, lattice cell transport calculations are performed to determine the spatially dependent flux spectra based on the problem

specific material composition, lattice geometry and boundary conditions. Based on the lattice level flux solutions the multi-group cross sections are homogenized in space over a lattice-cell and also into few energy groups. In the third step of the process, the computed few-group cross-sections are utilized to perform the full-core simulation based on the diffusion theory approximation.

The methodology described above is employed in many reactor analyses, however the number of few group cross sections and the energy boundaries used to define each group must be established a priori. The challenging problem that arises is to find the best values for the cut-off barriers of the energy divisions that fit the material compositions, fuel nature, geometry and reactor design. The selection of the few-energy group structure is unique and depends on the reactor type and design [36]. A review of some common approaches is given below.

2.6.1. Guidelines from literature for energy group structure

The general guidelines for the energy group structure found in the literature can be categorized into methods based on changes in neutron cross-sections, dominant physics within energy interval, or the variation in neutron spectrum. These guidelines can be summarized as follows:

- Bell & Glasstone [35] and Koclas [37] recommend the placement of the energy group barriers where the cross section of the most important isotopes (mainly fuel isotopes) experiences significant variations.
- Duderstadt and Hamilton [38] divided the neutron energy range into three main regions based on the physical interaction types as shown in Figure 7 and summarized as follows:
    - Neutron Thermalization Region (approximately from 0 eV to ~1 eV) which includes typically the highest magnitude cross sections and where phenomena related to up-scattering, chemical binding and diffraction may be important.
    - Neutron Moderation or Slowing Down Region (approx. from 1 eV to 10^5 eV) over mostly the resolved resonance regions and where only elastic scattering is expected with no up-scattering.

- Fast Fission Region (approx. from 10^5 eV to 10^7 eV) includes the energies for fission neutrons as well as many delayed neutron precursors. Here both elastic and inelastic scattering occurs (with no up-scattering) and cross sections cover mostly the unresolved resonance regions.

Duderstadt and Hamilton also recommend that the group structure selection basis take into account the neutron spectrum behaviour, shape and changes stating:

> *"... neutron energy spectrum is the key to the generation of group constants that yield an accurate few-group description of nuclear reactor behaviour."*

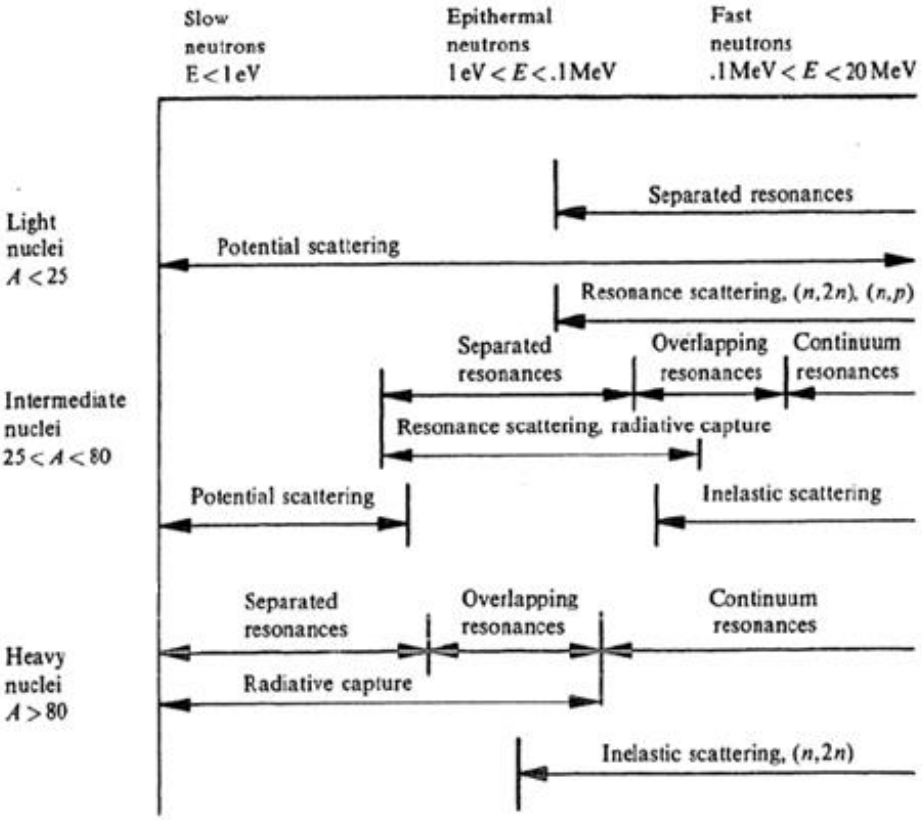

Figure 7: Summary of cross-section physical behaviour [38].

- Glasstone and Sesonske [39] recommend selecting energy group barriers based on the dominating physical phenomena and suggest a 4-group structure for water moderated nuclear reactors as follows:

- Thermal Region (Between 0 eV and 0.625 eV)
  - Down-scattering and up-scattering between energy groups can exist.
  - Absorption can occur.
- Resonance region (Between 0.625 eV and 500 eV)
  - Neutron slowing down occurs by elastic scattering.
  - Absorption by resolved resonances.
- Slowing-down region (Between 500 eV and 0.05 MeV)
  - Neutron slowing down by elastic scattering
  - Absorption by unresolved resonances.
- The fast region (Between 0.05 MeV and 10 MeV)
  - Basically, all the fission and decay neutrons have energies in this group.
  - Neutron slowing down takes place through both types of scattering: elastic and inelastic.

Glasstone and Sesonske also mention that graphite moderated reactors may require more than four energy groups and at least two thermal groups.

- Yigal Ronen [40] supports the energy group selection basis that identifies the important energy intervals based on the neutron population in these intervals.
- Massimo [41] supports the use of the minimum number of energy groups that ensure an acceptable accuracy in either the transport or diffusion calculation. He also highlights that accurate power distribution in regions where the neutron spectrum is highly spatially dependent such as at the core boundaries (core-reflector regions) demands several thermal groups. Such a proposal can be supported by Figure 8. He recommends to have an energy group structure that includes an energy interval for the fast fission source, an energy range for the resolved and the unresolved resonances and a thermal range with particular groups to include the low lying Pu resonances in case of utilizing a fuel that is characterized by high Pu loading. Moreover, Massimo illustrates that the effect of Doppler broadening on the low lying

resonances is small and treating those resonances with a single broad group is acceptable. Such discussion of the grouping is closely related to the SCWR fuel which has a high temperature (i.e., high potential for up-scattering) and a reactor-grade Pu-Th fuel (i.e., with many important low lying resonances).

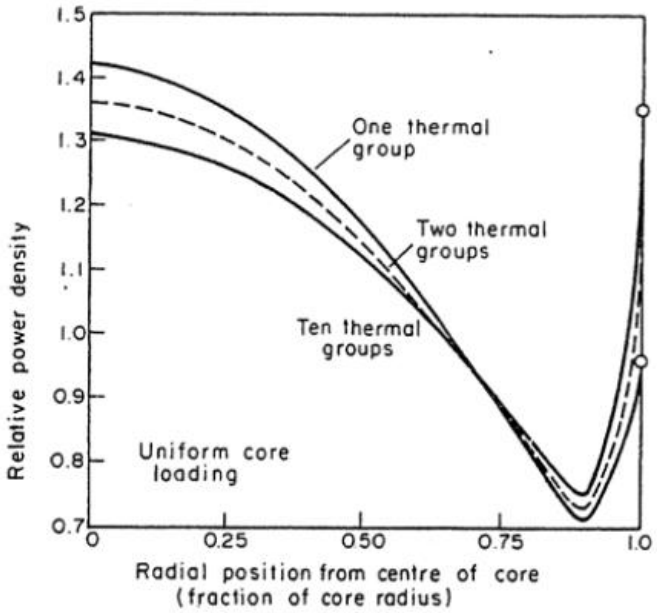

Figure 8: Demonstration of the effect of the number of energy groups on the average radial power distribution for Peach bottom HTGR [41].

- Merrill in the Gulf General Atomic (GGA) report [42] splits the neutron energy range into regions based on the dominant physical phenomena. There he also recommends to divide the resolved and the unresolved resonance ranges for the most important fuel isotopes (fissile and fertile isotopes). Moreover, he supports forming separate groups that might include the fission sources, fast fissions, inelastic thresholds, and the large thermal energy resonances. The GGA report on nuclear reactor design methods and energy group structure methodology is considered the most detailed document in the literature [43] and it was cited by Massimo and Duderstadt and Hamilton. The GGA group structure selection methodology was used in the design and the analysis of Fort Saint Vrain (FSV) which was a High Temperature Gas-cooled Reactor (HTGR) that was developed

and built in the US. The GGA energy group structure used for the FSV reactor was based on the neutron spectrum shown in Figure 9 [42].

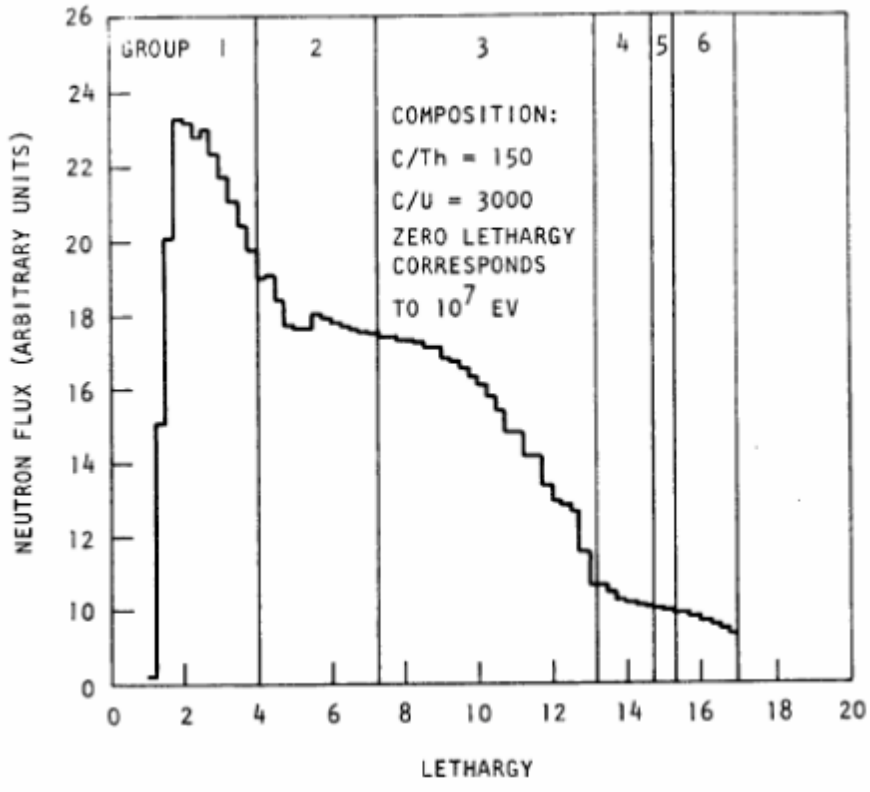

Figure 9: The fast neutron spectrum of the Fort Saint Vrain reactor along with the fast group structure [42].

- Oka and Mori in [29] introduce a modified energy group structure for analyzing the fast and thermal coupled core of the Super FR and recommend up to 12 energy groups to increase the accuracy and capture the low lying Pu peaks, the different isotopes of the MOX fuel, the effects of the blanket and the zirconium hydride layer in the hexagonal shaped FA.

2.6.2. Thermal Energy Boundary

Historically, most of the water moderated reactors such as the CANDU and LWR reactors have been analyzed using a two energy group structure with the thermal cut-off barrier placed at 0.625 eV. Such two-group models have provided very accurate and acceptable solutions [38]. However, the High Temperature Reactors (HTRs), which are characterized by a higher coolant temperature than the traditional light water thermal reactor require a higher thermal cut-off value. The

driver related to the selection of the two-group barrier is that in most applications it is desirable to differentiate regions where up-scatter occurs solely within a group and ensures important resonances are not subdivided. Such drivers are consistent with literature that suggests the thermal energy cut-off to be high enough in order to ignore the up-scattering from the thermal energy group for the HTR as discussed below.

Massimo [41] indicates that the typical thermal energy cut-off for HTRs should be between 2 eV and 4 eV with a standard value located at 2 eV. He also suggests that a high thermal cut-off (at 2 eV) might include all the neutron up-scattering possibilities with negligible probability of having neutrons scattering above that value. Duderstadt and Hamilton recommend the boundary to be between 0.5 eV and 1 eV for the water moderated reactors and to be as high as 3 eV for the HTR for the same rationale.

Massimo also provides the recommended energy group structure for the Fort Saint Vrain reactor in Table 4. The first group is designed to include the dominant fission sources. The second and the third groups are aimed to separate the resolved and the unresolved resonances of the main resonance absorber, which is ^{232}Th. The thermal energy rangy range was set at 2.38 eV with a set of thermal energy groups that conform to changes in the scattering matrix and the low lying Pu resonances. An energy barrier was set at 17.6 eV since the first resonance peak of ^{232}Th occurs at 21.9 eV. A small group was selected between 2.38 eV and 3.93 eV with the assumption that most neutron up-scattering goes from thermal range into the lowest energy group in the fast range confining the up-scatter to reasonable epi-thermal energies. Although the FSV reactor was fueled by 93% enriched uranium, it utilized the same fertile isotope as the Canadian PT-SCWR which is the ^{232}Th (ThO_2 for PT-SCWR and ThC_2 for FSV) and contains appreciable Pu at higher burnup.

Table 4: The 4, 7, and 9 energy group structure used for the analysis of Fort Saint Vrain Reactor [41].

Energy boundaries (eV)				
upper	lower	9 groups	7 groups	4 groups
1.5×10^7	1.83×10^5	1	1	1
1.83×10^5	961	2	2	2
961	17.6	3		
17.6	3.93	4	3	3
3.93	2.38	5		
2.38	0.414	6	4	4
0.414	0.10	7	5	
0.10	0.04	8	6	
0.04	0.0	9	7	

2.7. Lattice physics uncertainty analysis

The uncertainties associated with nuclear data library cross sections (such as ENDF/VII) impact the computation of multi-group and few-group cross sections and hence impact the computation of important full core quantities such as local powers and burnup. They are defined through the covariance matrix which describes the variations of random variables with respect to each other. The covariance of two random variables α and β can be expresses as:

$$cov(\alpha, \beta) = E[(\alpha - E(\alpha))(\beta - E(\beta))] , \quad (2.4)$$

Where $E(\alpha)$ is the expected value of the variable α. The covariance of a variable with itself is the variance, which is basically the diagonal of the covariance matrix. Additional uncertainties in geometry, local coolant conditions, fuel temperatures etc. may also impact the power distribution in the core through feedback effects. Since the uncertainty in some of the important thermalhydraulic predictions is not yet quantified for the SCWR the focus of most work has been on the impact of cross section uncertainties.

Assessments of the current reactor modelling methods and uncertainties are important for accurate design modelling procedure of the SCWR. Many studies [44, 45, 46, 47] discussed the importance, needs, and the effects of the sensitivity of the calculations to the nuclear data on the modelling of the advanced nuclear energy systems and the corresponding challenges in the Gen-IV reactor design. In

particular, many studies were performed on older design versions of the Canadian SCWR. A sensitivity study of the calculations to the nuclear data for the CANDU-SCWR was performed by Kozier et al. [48]. Another study involving an experimental work in the ZED-2 facility in chalk river was presented in Langton et al. [49]. A sensitivity and uncertainty analysis for the Canadian SCWR 54-element for fresh fuel was presented recently by Blomeley et al. [50]. This study shows that the neutron multiplication factor and the reactivity coefficient are highly sensitive to ^{2}H, ^{239}Pu and ^{232}Th. Where the ^{239}Pu represents the dominant fuel fissile isotope and ^{232}Th is a strong neutron absorber as a fertile fuel isotope. The highest sensitivity of the ^{2}H is due its role in neutron moderation process. Blomeley et al. [50] work also suggests the need to examine and re-evaluate the nuclear data library especially for some isotopes by which the system is highly sensitive which might decrease the total uncertainty.

Chapter 3

Theoretical Background

The primary aim in nuclear reactor physics is to provide an accurate estimate of the neutron density in the nuclear reactor which is a function of time, space, energy and direction. This can be done by solving the neutron transport equation, also called the linear Boltzmann equation, which describes the neutron density as neutrons move through matter. Such solutions cannot be determined exactly, and even approximate numerical solutions can only be obtained on a small section of a core at reasonable CPU cost. On the other hand, diffusion calculations while fast, cannot provide accurate solutions at small spatial scales and near strongly absorbing media. Thus a hybrid of lattice-level transport solutions and full-core diffusion calculations are often used in order to make reactor physics calculations tractable.

3.1. Neutron transport equation

The derivation of the neutron transport equation is beyond the scope of this report and is discussed in many nuclear engineering books; however, the notations, symbols, and equations included in this report are as in [51]. The time-dependent neutron transport equation that describes the different interactions involved with a neutron as it travels through matter including fission, leakage, streaming, scattering and capture is given as:

$$\frac{1}{\nu}\frac{\partial \psi}{\partial t}(\boldsymbol{r},\boldsymbol{\Omega},E,t)$$

$$= \int_0^{\infty}\int_{4\pi} \Sigma_s(\boldsymbol{\Omega}'\cdot\boldsymbol{\Omega},E'\to E)\,\psi\,(\boldsymbol{r},\boldsymbol{\Omega}',E',t)d\boldsymbol{\Omega}'dE'$$

$$+\frac{\chi_p(E)}{4\pi}\int_0^{\infty}\int_{4\pi}[1-\beta(E')]\nu\Sigma_f(E')\,\psi\,(\boldsymbol{r},\boldsymbol{\Omega}',E',t)d\boldsymbol{\Omega}'dE'$$

$$+\frac{1}{4\pi}\sum_{j=1}^{6}\chi_j(E)\,\lambda_j C_j(\boldsymbol{r},t)+\frac{1}{4\pi}Q(\boldsymbol{r},E,t)-\boldsymbol{\Omega}\cdot\nabla\,\psi(\boldsymbol{r},\boldsymbol{\Omega},E,t)$$

$$-\Sigma_t(E)\psi(\boldsymbol{r},\boldsymbol{\Omega},E,t), \qquad (3.1)$$

This equation is referred to as "a first-order integro-differential equation" [51] and includes the delayed neutron precursors and the neutron sources from fission. The neutron transport equation is a balance equation that describes the rate of change of the angular neutron density due to the different reactions taking place [51], where:

$$\frac{1}{\nu}\frac{\partial \psi}{\partial t}(\boldsymbol{r},\boldsymbol{\Omega},E,t)$$

$=$ time rate of change of angular neutron density $N(\boldsymbol{r},\boldsymbol{\Omega},E,t)$ at time t

$=$ (rate of gain) $-$ (rate of loss) , (3.2)

$$\int_0^{\infty}\int_{4\pi} \Sigma_s(\boldsymbol{\Omega}'\cdot\boldsymbol{\Omega},E'\to E)\,\psi\,(\boldsymbol{r},\boldsymbol{\Omega}',E',t)d\boldsymbol{\Omega}'dE'$$

$=$ In $-$ scattering rate at which neutrons about r scatter from $d\boldsymbol{\Omega}'dE'$ about $(\boldsymbol{\Omega}',E')$ into $d\boldsymbol{\Omega}\,dE$ about $(\boldsymbol{\Omega},E)$ at time t , (3.3)

$$\frac{\chi_p(E)}{4\pi}\int_0^{\infty}\int_{4\pi}[1-\beta(E')]\nu\Sigma_f(E')\,\psi\,(\boldsymbol{r},\boldsymbol{\Omega}',E',t)d\boldsymbol{\Omega}'dE'$$

$=$ rate at which prompt fission neutrons are produces about $(\boldsymbol{r},\boldsymbol{\Omega},E,t)$ at time t , (3.4)

$$\frac{1}{4\pi}\sum_{j=1}^{6}\chi_j(E)\,\lambda_j C_j(\boldsymbol{r},t) = \text{the rate at which delayed neutrons are}$$

born about (r,Ω,E,t) at time t , (3.5)

$$\frac{1}{4\pi}Q(\boldsymbol{r},E,t) = \text{Source rate} \quad , \tag{3.6}$$

$$\begin{aligned}(\text{rate of gain}) = {} & \text{In} - \text{scattering rate} \\ & + \text{prompt fission neutron production rate} \\ & + \text{delayed neutrons production rate} + \text{source rate} \\ = {} & \int_0^\infty \int_{4\pi} \Sigma_s(\boldsymbol{\Omega}' \cdot \boldsymbol{\Omega}, E' \to E)\, \psi\,(\boldsymbol{r},\boldsymbol{\Omega}',E',t) d\boldsymbol{\Omega}' dE' \\ & + \frac{\chi_p(E)}{4\pi} \int_0^\infty \int_{4\pi} [1-\beta(E')] \nu\Sigma_f(E')\, \psi\,(\boldsymbol{r},\boldsymbol{\Omega}',E',t) d\boldsymbol{\Omega}' dE' \\ & + \frac{1}{4\pi}\sum_{j=1}^{6} \chi_j(E)\, \lambda_j C_j + \frac{1}{4\pi} Q(\boldsymbol{r},E,t), \text{with} \sum_{j=1}^{6} \beta_j(E) = \beta(E) \end{aligned} \tag{3.7}$$

$$\boldsymbol{\Omega} \cdot \nabla\, \psi(\boldsymbol{r},\boldsymbol{\Omega},E,t) = \text{Net leakage rate} \quad , \tag{3.8}$$

$$\Sigma_t(E)\psi(\boldsymbol{r},\boldsymbol{\Omega},E,t) = \text{Collision rate} \quad , \tag{3.9}$$

$$(\text{rate of loss}) = \text{Net leakage rate} + \text{Collision rate} =$$

$$\Omega \cdot \nabla\, \psi(\boldsymbol{r},\boldsymbol{\Omega},E,t) + \Sigma_t(E)\psi(\boldsymbol{r},\boldsymbol{\Omega},E,t)\,, \tag{3.10}$$

The precursor density $C_j(\boldsymbol{r},t)$ is given as follows:

$$\frac{1}{\nu}\frac{\partial C_j}{\partial t}(\boldsymbol{r},t) = \int_0^\infty \int_{4\pi} \beta_j(E')\nu\Sigma_f(E')\, \psi\,(\boldsymbol{r},\boldsymbol{\Omega}',E',t) d\boldsymbol{\Omega}' dE' - \lambda_j C_j(\boldsymbol{r},t)\,, \tag{3.11}$$

Similar to the neutron transport equation, each term in Equation (3.11) represents a physical process that causes either a gain or loss of group-j neutron precursor nuclei, where:

$$\frac{1}{\nu}\frac{\partial C_j}{\partial t}(\boldsymbol{r},t) = \text{the rate of change of the number of group} - j \text{ precursor nuclei}$$
$$= (\text{Rate of gain}) - (\text{Rate of loss}), \quad (3.12)$$

$$\int_0^\infty \int_{4\pi} \beta_j(E')\nu\Sigma_f(E')\,\psi(\boldsymbol{r},\boldsymbol{\Omega}',E',t)d\boldsymbol{\Omega}'dE'$$
$$= \text{the rate at which group} - j \text{ precursor nuclei are produced}$$
$$= \text{rate of gain}, \quad (3.13)$$

$$\lambda_j C_j(\boldsymbol{r},t)$$
$$= \text{the rate at which group} - j \text{ precursor nuclei undergo radioactive decay}$$
$$= \text{rate of loss due to decay with a radioactive decay constant } \lambda_j, \quad (3.14)$$

In general, the neutron angular flux $\psi(\boldsymbol{r},\boldsymbol{\Omega},E,t)$ and the precursor densities $C_j(\boldsymbol{r},t)$ are obtained by solving equations (3.1) and (3.11) simultaneously using specified initial and boundary conditions. In most computer codes, such as SCALE or DRAGON, steady-state assumptions are often applied in order to further reduce the complexity of the solution.

3.2. Steady-state neutron transport equation

The neutron transport equation can be simplified assuming a steady-state [51] by setting $\frac{\partial\psi}{\partial t} = 0$ in equation (3.1). Consequently, such an approximation would also eliminate the precursors' densities by substituting $\frac{\partial C_j}{\partial t} = 0$ in equation (3.11) to get:

$$\lambda_j C_j(\boldsymbol{r},t) = \int_0^\infty \int_{4\pi} \beta_j(E')\nu\Sigma_f(E')\,\psi(\boldsymbol{r},\boldsymbol{\Omega}',E',t)d\boldsymbol{\Omega}'dE', \quad (3.15)$$

Then by direct substitution in equation (3.1), one can get a steady-state neutron transport equation with delayed neutrons as [51]:

$$\boldsymbol{\Omega}\cdot\nabla\,\psi(\boldsymbol{r},\boldsymbol{\Omega},E)+\Sigma_t(E)\psi(\boldsymbol{r},\boldsymbol{\Omega},E)$$
$$=\int_0^{\infty}\int_{4\pi}\Sigma_s(\boldsymbol{\Omega}'\cdot\boldsymbol{\Omega},E'\rightarrow E)\,\psi\,(\boldsymbol{r},\boldsymbol{\Omega}',E')d\boldsymbol{\Omega}'dE'$$
$$+\frac{\chi_p(E)}{4\pi}\int_0^{\infty}\int_{4\pi}[1-\beta(E')]\nu\Sigma_f(E')\,\psi\,(\boldsymbol{r},\boldsymbol{\Omega}',E')d\boldsymbol{\Omega}'dE'$$
$$+\frac{1}{4\pi}\sum_{j=1}^{6}\chi_j(E)\int_0^{\infty}\int_{4\pi}\beta_j(E')\nu\Sigma_f(E')\,\psi\,(\boldsymbol{r},\boldsymbol{\Omega}',E')d\boldsymbol{\Omega}'dE'$$
$$+\frac{1}{4\pi}Q(\boldsymbol{r},E)\ , \qquad (3.16)$$

It should be noted that applying the steady-state assumption with reflective boundary conditions has the effect of transforming the transport equation to an eigenvalue problem given by [50]:

$$\boldsymbol{\Omega}\cdot\nabla\,\psi(\boldsymbol{r},\boldsymbol{\Omega},E)+\Sigma_t(E)\psi(\boldsymbol{r},\boldsymbol{\Omega},E)$$
$$=\int_0^{\infty}\int_{4\pi}\Sigma_s(\boldsymbol{\Omega}'\cdot\boldsymbol{\Omega},E'\rightarrow E)\,\psi\,(\boldsymbol{r},\boldsymbol{\Omega}',E')d\boldsymbol{\Omega}'dE'$$
$$+\frac{\chi_p(E)}{4\pi k}\int_0^{\infty}\int_{4\pi}\nu\Sigma_f(E')\,\psi\,(\boldsymbol{r},\boldsymbol{\Omega}',E')d\boldsymbol{\Omega}'dE', \qquad (3.17)$$

Where the fission source is modified by a factor of 1/k, the delayed neutrons are neglected, and the source Q and the boundary source are set to zero.

3.3. Methods for solving the neutron transport equation

3.3.1. Approximations

The neutron transport equation involves seven independent variables to provide an accurate description of neutron density in terms of space, energy, direction and time. Moreover, each cross section depends on neutron energy as well as position because of the heterogeneity of most reactor cores [35]. Finally, the isotopic composition evolves in time such that the atomic number densities used to compute the macroscopic cross sections also evolve in time. The methods developed to solve

the neutron transport equation can be categorized into two main groups: the stochastic approach using Monte Carlo method and the deterministic methods. The deterministic approaches are used in this work and summarized below.

3.3.2. Deterministic approach

Due to the approximations applied in the different deterministic methods developed, the neutron transport equation is suitably modified. As an example, the spherical harmonics P_n and the discrete ordinates S_N methods use the integro-differential form of neutron transport equation, the method of characteristics uses the characteristic form, and the collision probability uses the integral form [51]. Deterministic methods use many approximations for either the spatial or angular discretization while all utilize some form of multi-group energy discretization.

3.3.2.1. The continuous-energy equations

In continuous energy, the 3D neutron transport equation without delayed neutrons in steady state is given by [51]:

$$\begin{aligned}\boldsymbol{\Omega}\cdot\nabla\psi(\boldsymbol{r},\boldsymbol{\Omega},E)+\Sigma_t(E)\psi(\boldsymbol{r},\boldsymbol{\Omega},E)&\\ =\int_0^\infty\int_{4\pi}\Sigma_s(\boldsymbol{r},\boldsymbol{\Omega}'\cdot\boldsymbol{\Omega},E'\to E)\,\psi(\boldsymbol{r},\boldsymbol{\Omega}',E')d\boldsymbol{\Omega}'dE'&\\ +\frac{\chi(\boldsymbol{r},E)}{4\pi}\int_0^\infty\int_{4\pi}\nu\Sigma_f(\boldsymbol{r},E')\,\psi(\boldsymbol{r},\boldsymbol{\Omega}',E')d\boldsymbol{\Omega}'dE'&\\ +\frac{1}{4\pi}Q(\boldsymbol{r},E)\quad,&\end{aligned}\tag{3.17}$$

With a boundary condition that would be initially stated:

$$\psi(\boldsymbol{r},\boldsymbol{\Omega},E)=\psi^b(\boldsymbol{r},\boldsymbol{\Omega},E),\quad \boldsymbol{\Omega}\cdot\mathbf{n}<0, 0<E<\infty \tag{3.18}$$

Knowing that the cross-sections and the fission spectrum in these equations satisfy the following identities [51]:

$$\Sigma_t(E)=\Sigma_s(E)+\Sigma_\gamma(E)+\Sigma_f(E)\quad, \tag{3.19}$$

$$\Sigma_s(E)=\int_0^\infty\int_{4\pi}\Sigma_s(\boldsymbol{\Omega}\cdot\boldsymbol{\Omega}',E'\to E)\,d\boldsymbol{\Omega}'dE'\quad, \tag{3.20}$$

$$\int_0^{\infty} \chi(E) dE = 1 \quad , \tag{3.21}$$

$$\Sigma_s(\mathbf{\Omega}' \cdot \mathbf{\Omega}, E' \to E) = \sum_{n=0}^{N} \frac{2n+1}{4\pi} \Sigma_{s,n}(E' \to E) P_n(\mathbf{\Omega}' \cdot \mathbf{\Omega}) \quad , \tag{3.22}$$

3.3.2.2. Multigroup approximations

One of the most important approximations used by almost all deterministic methods is the multigroup approximation by which the neutron energy (which varies up to 10 MeV) is divided into a finite number of energy intervals or energy groups. The basic concept of the multigroup approximation is to average the cross sections within each energy group and consider the cross sections to be constant and independent of energy within each group. A finite number G of energy groups (bins) is to be selected as [1]:

$$E_{\min} = E_G < E_{G-1} < \cdots < E_g < E_{g-1} < \cdots < E_2 < E_1 = E_{\max} \ , \tag{3.23}$$

$E_{\min}$ is considered to be very small so neutrons with energies less than $E_{\min}$ are neglected, and $E_{\max}$ is considered to be very large so that neutrons with energies more than $E_{\max}$ are also neglected. Within this approximation the energy interval of g^{th} energy group is expressed as [51]:

$$E_g < E < E_{g-1} \quad , \tag{3.24}$$

It should be noted that the conventional order of energy groups in all references and including [51] is such that the index g decreases as the energy increases. Fast energy neutrons are thus slowing down through increasing order of the indices g. For each $1 \leq g \leq$ G, we define [51]:

$$\psi_g(\boldsymbol{r}, \mathbf{\Omega}) = \int_{E_g}^{E_{g-1}} \psi(\boldsymbol{r}, \mathbf{\Omega}, \mathrm{E})\, dE = \text{ Angular flux for group } g \quad , \tag{3.25}$$

$$\chi_g(\boldsymbol{r}) = \int_{E_g}^{E_{g-1}} \chi(\boldsymbol{r}, \mathrm{E})\, dE = \text{Multigroup fission spectrum for group } g \ , \tag{3.26}$$

$$Q_g(\boldsymbol{r}) = \int_{E_g}^{E_{g-1}} Q(\boldsymbol{r}, \mathrm{E})\, dE = \text{Internal multigroup source to group } g\ , \qquad (3.27)$$

By using Equation (3.26) and the definition of the fission spectrum, the multigroup fission spectrum obeys the following condition:

$$\sum_{g=1}^{G} \chi_g(\boldsymbol{r}) = \sum_{g=1}^{G} \int_{E_g}^{E_{g-1}} \chi(\boldsymbol{r}, E) dE = \int_{E_{\min}}^{E_{\max}} \chi(\boldsymbol{r}, E) dE = 1\ , \qquad (3.28)$$

Now, by integrating the neutron transport equation (3.17) in case of steady state per energy group g, one can get [51]:

$$\begin{aligned} \boldsymbol{\Omega} \cdot \nabla \psi_g(\boldsymbol{r}, \boldsymbol{\Omega}) + & \int_{E_g}^{E_{g-1}} \Sigma_t\,(\boldsymbol{r}, E) \psi(\boldsymbol{r}, \boldsymbol{\Omega}, E) \mathrm{dE} \\ & = \sum_{g'=1}^{G} \int_{E_g}^{E_{g-1}} \int_{E_{g'}}^{E_{g'-1}} \int_{4\pi} \Sigma_s(\boldsymbol{r}, \boldsymbol{\Omega}' \cdot \boldsymbol{\Omega}, E' \to E)\, \psi\,(\boldsymbol{r}, \boldsymbol{\Omega}', E') d\boldsymbol{\Omega}' dE' dE \\ & + \frac{\chi_g(\boldsymbol{r})}{4\pi} \sum_{g'=1}^{G} \int_{E_{g'}}^{E_{g'-1}} \int_{4\pi} \nu\Sigma_f(\boldsymbol{r}, E')\, \psi\,(\boldsymbol{r}, \boldsymbol{\Omega}', E') d\boldsymbol{\Omega}' dE' \\ & + \frac{Q_g(\boldsymbol{r})}{4\pi}\ , \end{aligned} \qquad (3.29)$$

Which is equivalent to,

$$\begin{aligned} & \boldsymbol{\Omega} \cdot \nabla \psi_g(\boldsymbol{r}, \boldsymbol{\Omega}) + \left[\frac{\int_{E_g}^{E_{g-1}} \Sigma_t\,(\boldsymbol{r}, E) \psi(\boldsymbol{r}, \boldsymbol{\Omega}, E) \mathrm{dE}}{\int_{E_g}^{E_{g-1}} \psi(\boldsymbol{r}, \boldsymbol{\Omega}, E) \mathrm{dE}} \right] \psi_g(\boldsymbol{r}, \boldsymbol{\Omega}) \\ & = \sum_{g'=1}^{G} \int_{4\pi} \left[\frac{\int_{E_g}^{E_{g-1}} \int_{E_{g'}}^{E_{g'-1}} \Sigma_s(\boldsymbol{r}, \boldsymbol{\Omega}' \cdot \boldsymbol{\Omega}, E' \to E) \psi\,(\boldsymbol{r}, \boldsymbol{\Omega}', E') dE' dE}{\int_{E_{g'}}^{E_{g'-1}} \psi(\boldsymbol{r}, \boldsymbol{\Omega}', E') \mathrm{dE}'} \right] \psi_{g'}(\boldsymbol{r}, \boldsymbol{\Omega}') d\boldsymbol{\Omega}' \\ & + \frac{\chi_g(\boldsymbol{r})}{4\pi} \sum_{g'=1}^{G} \int_{4\pi} \left[\frac{\int_{E_{g'}}^{E_{g'-1}} \nu\Sigma_f(\boldsymbol{r}, E') \psi(\boldsymbol{r}, \boldsymbol{\Omega}', E') dE'}{\int_{E_{g'}}^{E_{g'-1}} \psi(\boldsymbol{r}, \boldsymbol{\Omega}', E') \mathrm{dE}'} \right] \psi_{g'}(\boldsymbol{r}, \boldsymbol{\Omega}') d\boldsymbol{\Omega}' \\ & + \frac{Q_g(\boldsymbol{r})}{4\pi}\ , \end{aligned} \qquad (3.30)$$

Or,

$$\boldsymbol{\Omega}\cdot\nabla\,\psi_g(\boldsymbol{r},\boldsymbol{\Omega})+\ \hat{\Sigma}_{t,g}(\boldsymbol{r},\boldsymbol{\Omega})\,\psi_{\,g}(\boldsymbol{r},\boldsymbol{\Omega})$$
$$=\sum_{g'=1}^{G}\int_{4\pi}\hat{\Sigma}_{s,g'\to g}(\boldsymbol{r},\boldsymbol{\Omega}'\cdot\boldsymbol{\Omega})\psi_{g'}(\boldsymbol{r},\boldsymbol{\Omega}')d\boldsymbol{\Omega}'$$
$$+\ \frac{\chi_g(\boldsymbol{r})}{4\pi}\sum_{g'=1}^{G}\int_{4\pi}\hat{\nu}\hat{\Sigma}_{f,g}(\boldsymbol{r},\boldsymbol{\Omega}')\,\psi_{g'}(\boldsymbol{r},\boldsymbol{\Omega}')d\boldsymbol{\Omega}'$$
$$+\frac{Q_g(\boldsymbol{r})}{4\pi}\ , \tag{3.31}$$

Where,

$$\hat{\Sigma}_{t,g}(\boldsymbol{r},\boldsymbol{\Omega})=\left[\frac{\int_{E_g}^{E_{g-1}}\Sigma_t\,(\boldsymbol{r},E)\psi(\boldsymbol{r},\boldsymbol{\Omega},E)\mathrm{dE}}{\int_{E_g}^{E_{g-1}}\psi(\boldsymbol{r},\boldsymbol{\Omega},E)\mathrm{dE}}\right]\ , \tag{3.32}$$

$$\hat{\Sigma}_{s,g'\to g}(\boldsymbol{r},\boldsymbol{\Omega}'\cdot\boldsymbol{\Omega})$$
$$=\left[\frac{\int_{E_g}^{E_{g-1}}\int_{E_{g'}}^{E_{g'-1}}\Sigma_s(\boldsymbol{r},\boldsymbol{\Omega}'\cdot\boldsymbol{\Omega},E'\to E)\psi\,(\boldsymbol{r},\boldsymbol{\Omega}',E')dE'dE}{\int_{E_{g'}}^{E_{g'-1}}\psi(\boldsymbol{r},\boldsymbol{\Omega}',E')\mathrm{d}E'}\right], \tag{3.33}$$

$$\hat{\nu}\hat{\Sigma}_{f,g}(\boldsymbol{r},\boldsymbol{\Omega}')=\left[\frac{\int_{E_{g'}}^{E_{g'-1}}\nu\Sigma_f(\boldsymbol{r},E')\psi(\boldsymbol{r},\boldsymbol{\Omega}',E')dE'}{\int_{E_{g'}}^{E_{g'-1}}\psi(\boldsymbol{r},\boldsymbol{\Omega}',E')\mathrm{d}E'}\right]\ , \tag{3.34}$$

Where the g^{th} energy group boundary condition can be obtained by integrating Equation (3.20) over the energy interval of the g^{th} energy group:

$$\psi_g(\boldsymbol{r},\boldsymbol{\Omega})=\ \psi_g^b(\boldsymbol{r},\boldsymbol{\Omega})=\int_{E_g}^{E_{g-1}}\psi^b(\boldsymbol{r},\boldsymbol{\Omega},E)\mathrm{d}E\ ,\ \ \boldsymbol{\Omega}\cdot\ \mathbf{n}<0 \tag{3.35}$$

As it was discussed in [51], it would appear that the problem can be addressed easily by simply solving the neutron transport Equation (3.31) per energy group with an energy interval $E_g\le E\le E_{g-1}$ and using the boundary condition in Equation (3.35). However, this is impossible as the hatted cross-sections of Equation (3.31) and expressed in Equations (3.32-3.34) shows an angular dependence and also depends

on the flux solution of the continuous energy equation. Another approximation is needed to proceed forward and solve the problem. An approximation can be applied by choosing a form of the angular dependence of the flux and then integrating per energy group. The form of the flux with the multigroup approximation can be as follows:

$$\psi(\boldsymbol{r},\boldsymbol{\Omega},\mathrm{E}) \approx \Psi(\boldsymbol{r},E) f(\boldsymbol{r},\boldsymbol{\Omega}), \tag{3.36}$$

Where $\Psi(\boldsymbol{r},E)$ is a specified neutron spectrum [51]. By substituting Equation (3.36) in Equations (3.32-3.34) and canceling the function $f(\boldsymbol{r},\boldsymbol{\Omega})$ from both the denominator and numerator, the multigroup cross-sections can be written as [51]:

$$\Sigma_{t,g}(\boldsymbol{r}) = \left[\frac{\int_{E_g}^{E_{g-1}} \Sigma_t(\boldsymbol{r},E)\Psi(\boldsymbol{r},E)\mathrm{dE}}{\int_{E_g}^{E_{g-1}} \Psi(\boldsymbol{r},E)\mathrm{dE}}\right], \tag{3.37}$$

$$\Sigma_{s,g'\to g}(\boldsymbol{r},\boldsymbol{\Omega}'\cdot\boldsymbol{\Omega}) = \left[\frac{\int_{E_g}^{E_{g-1}}\int_{E_{g'}}^{E_{g'-1}} \Sigma_s(\boldsymbol{r},\boldsymbol{\Omega}'\cdot\boldsymbol{\Omega},E'\to E)\Psi(\boldsymbol{r},E')dE'dE}{\int_{E_{g'}}^{E_{g'-1}} \Psi(\boldsymbol{r},E')\mathrm{dE}'}\right], \tag{3.38}$$

$$\nu\Sigma_{f,g}(\boldsymbol{r}) = \left[\frac{\int_{E_{g'}}^{E_{g'-1}} \nu\Sigma_f(\boldsymbol{r},E')\Psi(\boldsymbol{r},E')dE'}{\int_{E_{g'}}^{E_{g'-1}} \Psi(\boldsymbol{r},E')\mathrm{dE}'}\right], \tag{3.39}$$

Substituting these expressions into Equation (3.31) give the multigroup transport equation per energy group as:

$$\begin{aligned}\boldsymbol{\Omega}\cdot\nabla\psi_g(\boldsymbol{r},\boldsymbol{\Omega}) + \Sigma_{t,g}(r)\,\psi_g(\boldsymbol{r},\boldsymbol{\Omega}) &= \sum_{g'=1}^{G}\int_{4\pi}\Sigma_{s,g'\to g}(\boldsymbol{r},\boldsymbol{\Omega}'\cdot\boldsymbol{\Omega})\,\psi_{g'}\left(\boldsymbol{r},\boldsymbol{\Omega}'\right)d\boldsymbol{\Omega}' \\ &+ \frac{\chi_g(\boldsymbol{r})}{4\pi}\sum_{g'=1}^{G}\int_{4\pi}\nu\Sigma_{f,g}(\boldsymbol{r})\,\psi_{g'}\left(\boldsymbol{r},\boldsymbol{\Omega}'\right)d\boldsymbol{\Omega}' \\ &+ \frac{Q_g(\boldsymbol{r})}{4\pi}, \end{aligned} \tag{3.40}$$

By which the multigroup fluxes $\psi_g(r,\Omega)$ are obtained by solving these equations with multigroup boundary conditions (3.35). By using the multigroup

approximation, the expressions of different multigroup cross-sections can be written as:

$$\Sigma_{t,g}(\boldsymbol{r}) = \Sigma_{s,g}(\boldsymbol{r}) + \Sigma_{\gamma,g}(\boldsymbol{r}) + \Sigma_{f,g}(\boldsymbol{r}), \tag{3.41}$$

$$\Sigma_{s,g'\to g}\left(\boldsymbol{r}, \boldsymbol{\Omega}' \cdot \boldsymbol{\Omega}\right) = \sum_{n=0}^{N} \frac{2n+1}{4\pi} \Sigma_{s,n,g'\to g} P_n\left(\boldsymbol{\Omega}' \cdot \boldsymbol{\Omega}\right), \tag{3.42}$$

$$\sum_{g'=1}^{G} \int_{4\pi} \Sigma_{s,g'\to g}\left(\boldsymbol{r}, \boldsymbol{\Omega}' \cdot \boldsymbol{\Omega}\right) d\,\boldsymbol{\Omega}' = \Sigma_{s,g}(\boldsymbol{r}), \tag{3.43}$$

A comparison between the continuous energy and the multigroup expressions are important and should be given extra attention. Based on [51], Equations (3.28, 3.41-3.43) are referred to the multigroup expressions while equations (3.19-3.22) represents the continuous energy counterparts. A direct comparison of these equations would explain the physical meaning between them. First of all, Equations (3.19) and (3.41) show that the interactions between the neutrons and the different nuclei follow the same behaviour in both cases for the multigroup and the continuous energy. Equations (3.20) and (3.43) [51]:

"*Guarantee that the continuous-energy and multigroup scattering operators are conservative – they neither create nor destroy neutrons. (These operators only rearrange neutrons in* $(\boldsymbol{\Omega}, \mathrm{E})-$*space.)"*

Moreover, Equations (3.21) and (3.28) make sure that the neutron fission spectrum in continuous energy and in the multigroup approach have the same normalization condition. Finally, Equations (3.22) and (3.42) show that the multigroup and continuous energy cross-sections are consistent in terms of being expressed within the same type of Legendre polynomial expansions [51].

The previous comparison and discussion show that the multigroup transport equations is quite similar to the continuous transport equation in terms of structure, form, and shape [51]. However, in the multigroup approximation, the energy range

is discrete as opposed to continuous energy approach. Knowing that the approximation is illustrated in the representation of the angular dependence of the flux and thus replacing the Equations (3.32 - 3.34) by (3.37 - 3.39). Additionally, it should be noted that:

1. In deriving the multigroup cross-sections, it was assumed that the continuous flux has the form of Equation (3.36) with a condition that Ψ is known. But this is true only in particular cases as stated by [51]:
   "Requires the angular flux to have the same energy spectrum for each direction of flight and the same direction-dependence for each energy."
   This can occur only in an infinite homogeneous medium with isotropic flux which doesn't generally describe spatially dependent problems.
2. The actual cross-sections versus energy graphs are curvilinear and continuous but in the multigroup case cross-sections versus energy graphs are discontinuous and the cross-sections value are constant and averaged per energy group (see Figure 10). In other words, the multigroup cross-sections are independent of energy within the respective energy group.

Usually, in the multigroup case where the number of energy bins used is relatively high (few hundreds) and consequently the energy group width ($\Delta E = E_{g-1} - E_g$) is relatively small. Since the energy group width size decreases as the number of energy groups increases, it would appear that at a large number of energy groups G (within certain limit) the multigroup cross-sections curves become very similar to and approach the continuous energy cross-sections graphs. The assumption of considering the cross-sections independent of Ψ (energy) becomes valid and applicable.

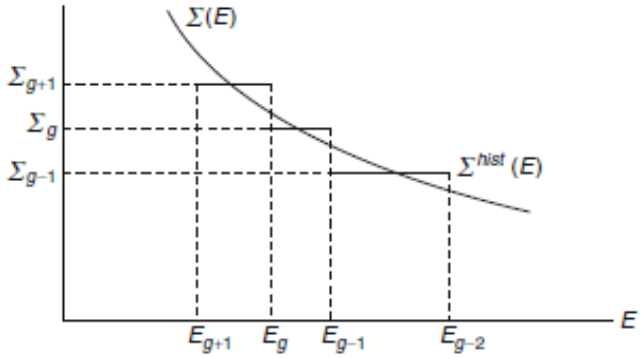

Figure 10: Continuous-energy histogram cross-sections [50].

3.3.3. Importance of proper selection of energy group structure

Neutron energy is an important parameter that plays a vital role in its interaction with the material. Cross section defines the neutron reaction probability parameter which highly depends on the energy of the incoming neutron. The basic assumption of the multigroup approximation is to divide the neutron energy range into finite number of energy groups within which the cross-section is averaged and considered to be constant. That means the cross-section is considered to be energy independent within each individual energy group. The lattice level calculations undergo a spatial homogenization and energy condensation processes by which the lattice cell homogenized cross sections are averaged and calculated for few number of energy groups (usually between 2 and 8). Although these cross sections are flux weighted but they highly depend on the energy barriers of the energy group structure used. Changing the energy barriers of the energy group structure would impact the group homogenized cross sections due to the effects of the resonances of different isotopes. An example that demonstrates the effects of the appropriate selection of the energy group structure is shown in figure 1. In Figure 11(a) and 11(b), different energy barriers are used to show how the calculated homogenized cross sections are impacted when energy group structure with different energy barriers are used. Consequently, the adequate selection of the energy group structure is very important and have a direct impact on the estimated solution. Such group structure should account and take into consideration the special resonances of the fuel isotopes especially at the thermal region. Multigroup selection basis criteria are

addressed in many references, however, most of them agree with general guidelines that depends on the behaviour of the neutron cross-section. It was recommended to analyze the neutron energy spectrum before the selection of the energy group structure as stated by [35]:

"In order to obtain useful group cross-sections in the energy regions where cross-section versus energy curves have fine structure, it is necessary to perform careful analysis of the neutron energy spectrum through these regions"

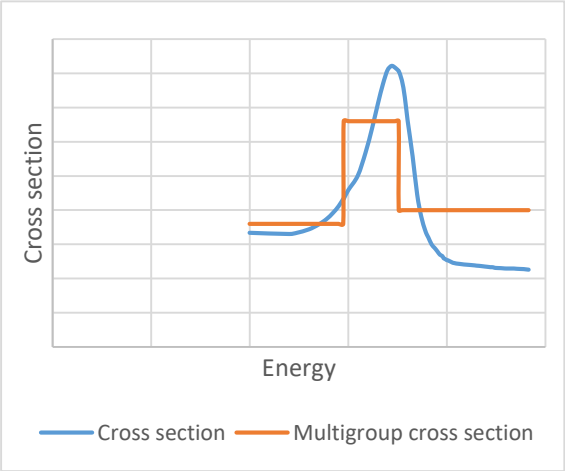

(a)

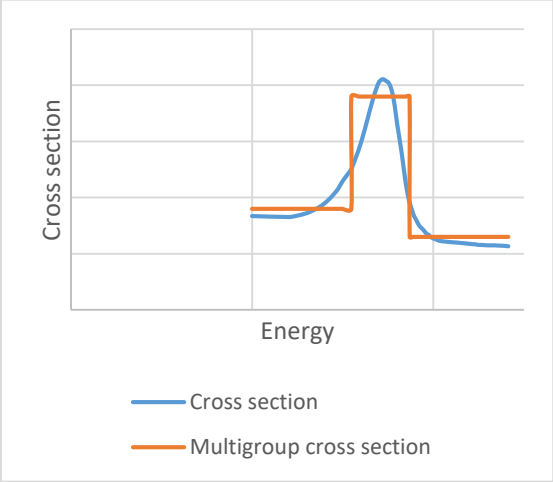

(b)

Figure 11: The change in multigroup cross section with different energy group barrier.

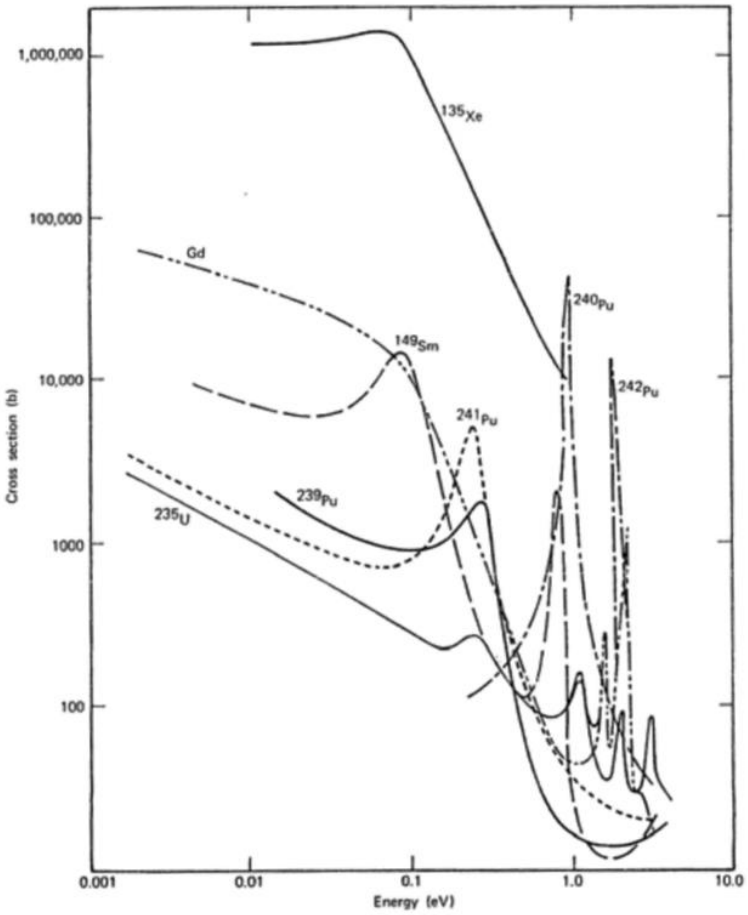

Figure 12: The low energy cross sections of some selected important isotopes [38].

Moreover, it was recommended by [51] that the cross-sections of the low-energy resonances, like the low lying Pu peaks, be precisely discretized. In addition to this, the other resolved resonances of the cross-section energy curves should be included in an energy group. For HTRs, Massimo suggests a list of special isotopes with high degree of importance illustrated by ^{239}Pu, ^{240}Pu, ^{241}Pu, ^{135}Xe, ^{149}Sm, ^{103}Rh. He mentioned that those isotopes have importance resonances within the energy range where neutron up-scattering starts to be considered as an important phenomenon. The low lying resonances of the previously mentioned isotopes are shown in Figure 12 [38]. Here it is convenient to mention that there is a trade-off between the number of energy groups used, the accuracy of the calculations, the size of the domain and spatial accuracy, and the temporal evolution of the neutron fluxes and isotopic compositions.

3.3.4. Resonance self-shielding

Almost all the deterministic methods use the multigroup approximation method by which the cross sections are averaged per energy group. However, averaging the cross section should satisfy an important condition which is the conservation of the reaction rate. Since the reaction rate is equal to the product of the cross section and the flux, the best option is to average the cross section with respect to the average flux. "Flux weighted average cross-sections" are calculated per each energy group which can be expressed as [52]:

$$\bar{\sigma}_g = \frac{\int_g \sigma(E)\,\phi(E)dE}{\int_g \phi(E)dE}\,, \tag{3.44}$$

But this leads to an immediate complication because the flux is unknown and the primary purpose of the whole calculation is to calculate the value of the flux. Of particular interests are resonances where the flux and cross-sections vary substantially within a group. This problem can be solved with another approximation which is referred to the resonance self-shielding correction. There are different types of approximations and methods developed for the resonance self-shielding process that are used by many computer codes. SCALE code uses the Bondarenko method [52].

The Bonderenko method for self-shielding will be discussed briefly based on [52]. In the Bonderenko method, the flux is expressed in an infinite homogenous medium as:

$$\phi(E) \sim \frac{1}{\Sigma_t(E)}\,, \tag{3.45}$$

Where $\phi(E)$ is the flux and $\Sigma_t(E)$ is the macroscopic total cross-section. Direct substitution of Equation (3.45) in equation (3.44) yields:

$$\bar{\sigma}_g^i = \frac{\int_g \frac{\sigma^i(E)\,dE}{\Sigma_t(E)}}{\int_g \frac{dE}{\Sigma_t(E)}}\,, \tag{3.46}$$

Which is equivalent to,

$$\bar{\sigma}_g^i = \frac{\int_g \frac{\sigma^i(E)\,dE}{N_i\sigma_t^i(E) + \sum_{j\neq i} N_j\sigma_t^j(E)}}{\int_g \frac{dE}{N_i\sigma_t^i(E) + \sum_{j\neq i} N_j\sigma_t^j(E)}} \quad , \tag{3.47}$$

Where i represents the nuclide under investigation, N is the number density and σ_t represent the microscopic total cross-section [52]. It is convenient to define σ_0^i as [52]:

$$\sigma_0^i = \sum_{j\neq i} \frac{N_j\sigma_t^j(E)}{N_i} \quad , \tag{3.48}$$

Where σ_0^i term represents the cross-section of nuclide i for all nuclides in the mixture other than nuclide i itself [52]. The average expression of the cross-section can be given by:

$$\bar{\sigma}_g^i = \frac{\int_g \frac{\sigma^i(E)\,dE}{\sigma_t^i(E) + \sigma_0^i(E)}}{\int_g \frac{dE}{\sigma_t^i(E) + \sigma_0^i(E)}} \quad , \tag{3.49}$$

Where σ_0^i is called the "background cross-section", also known as the "dilution cross-section" [53]. The dilution in a self-shielding calculation refers to the cross sections of all other material other than the isotope of interest. It important here not to be confused with the word "Dilution", since dilution in self-shielding is not the traditional definition of dilutions as "concentration" but rather refers to a cross-section. Since the problem dilution is not known initially, the average cross-section is evaluated at different dilutions and stored in the nuclear data library. When the lattice transport code (such as SCALE, for example) uses the nuclear data library, it first calculates the problem dilution based on the simulated geometry and composition. Then, it selects up the cross-section corresponding to the calculated dilution from the library. An example on how the dilution, whether it is high or low, affects the evaluation of the averaged multigroup cross-section is shown in Figure 13 and Figure 14.

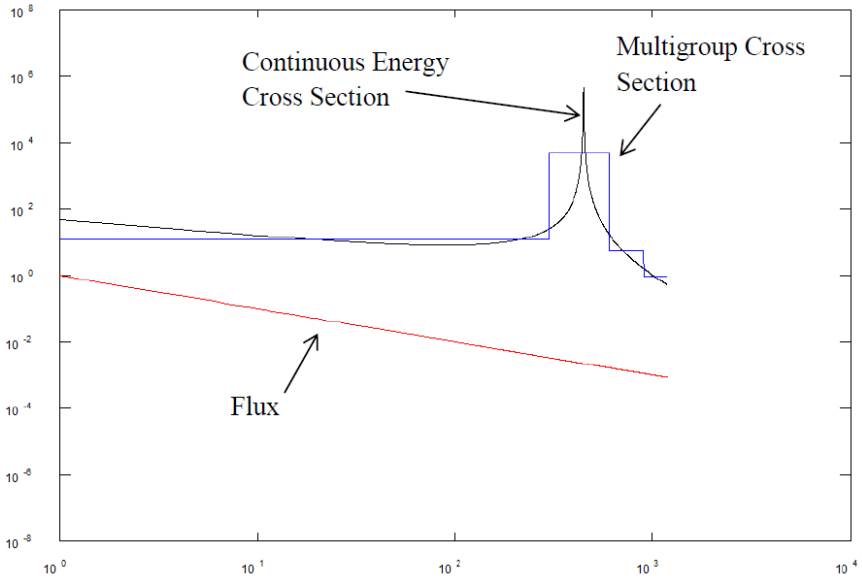

Figure 13: Continuous Energy Cross Section and Corresponding Multigroup Cross Section at Infinite Dilution [53].

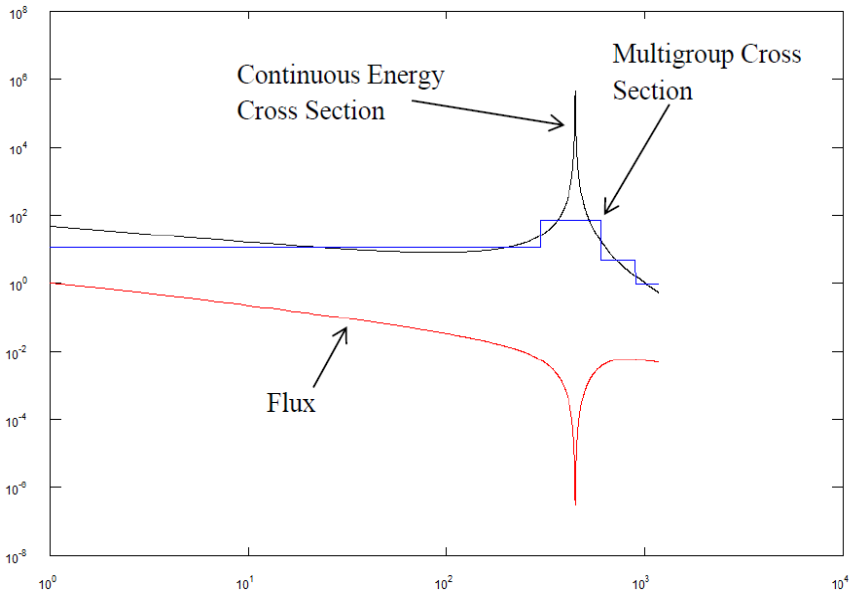

Figure 14: Continuous Energy Cross Section and Corresponding Multigroup Cross Section at a Dilution of 10 barns [53].

3.4.Methods of sensitivity and uncertainty analysis

Uncertainty quantification is a major outcome of software validation in the nuclear industry. Uncertainties may arise during experiments due to instrumentation errors either in the dependent or independent variables. Such experiments are then used

to assess the code accuracy where prediction uncertainties may arise from approximations in the physical models, deviation in geometry/composition of the domain, uncertainty in material properties or their state (i.e., a materials temperature), uncertainties in the numerical approximations used in the solution process, and/or uncertainties in the boundary/initial conditions. Such errors are estimated and provided either as single uncertainties (assuming no covariance), groups of uncertainties (with some covariance quantified) or as full covariance matrices (where all covariances are defined).

Sensitivity analysis is used extensively both to compute the uncertainty (via the sandwich rule with the covariance matrix) and also to better understand the physical phenomena involved. In this thesis, sensitivity analysis is used extensively to understand the relative importance of some nuclear processes and hence better understand the larger scale phenomena (such as CVR).

Solving the neutron transport equation would yield the neutron multiplication factor k_{eff}. However, k_{eff} calculations would include uncertainties that arise from the nuclear data library, boundary conditions, material properties or arrangement and/or from the computational method itself. In general, the multiplication factor k_{eff} depends on many parameters and this dependence can be represented mathematically as [51]:

$$k_{\text{eff}} = k_{\text{eff}}(\boldsymbol{\alpha}), \qquad \text{where } \boldsymbol{\alpha} = (\alpha_1, \dots, \alpha_N) \tag{3.50}$$

With $\boldsymbol{\alpha}$ a vector with N components representing the different parameters of the system such as cross-sections and number density. By using a Taylor series [54], the uncertainty in k_{eff} can be expressed as [51]:

$$\delta k_{\text{eff}} = \sum_{n=1}^{N} \left(\frac{\partial k_{\text{eff}}}{\partial \alpha_n} \right) \delta \alpha_n \ , \ \delta \alpha_n = \alpha_n - \alpha_n^0 \tag{3.51}$$

The partial derivatives in Equation (3.51) are called the sensitivities of the system $k_{\text{eff}}(\boldsymbol{\alpha})$ with respect to each of the system parameters α_n individually and can be expressed as [51]:

$$s_n = \left(\frac{\partial k_{\text{eff}}}{\partial \alpha_n}\right), \tag{3.52}$$

Knowing that the covariance matrix $\mathbf{C}_\alpha$ of the parameter $\boldsymbol{\alpha}$ and the variance matrix of k_{eff} are given by [51]:

$$\mathbf{C}_\alpha = \langle \delta\boldsymbol{\alpha}\delta\boldsymbol{\alpha}^{\boldsymbol{T}} \rangle \ , \tag{3.53}$$

$$\text{var}\ (k_{\text{eff}}) = \langle (k_{\text{eff}})^2 \rangle = \mathbf{S}\, \langle \delta\boldsymbol{\alpha}\delta\boldsymbol{\alpha}^{\boldsymbol{T}} \rangle\, \mathbf{S}^{\boldsymbol{T}} = \mathbf{S}\, \mathbf{C}_\alpha \mathbf{S}^{\boldsymbol{T}} \ , \tag{3.54}$$

With "T" represents the "transpose of the matrix" and the bold **S** represents the sensitivity matrix with N components system parameters and it can be written as [51]:

$$\mathbf{S} = \left\{ \left(\frac{\partial k_{\text{eff}}}{\partial \alpha_1}\right), \ldots, \left(\frac{\partial k_{\text{eff}}}{\partial \alpha_N}\right) \right\}, \tag{3.55}$$

Equation (3.54) is the so-called sandwich rule which may be used for uncertainty calculations. It is clearly shown that the sandwich rule depends on the system sensitivities. However, with a system of many parameters (like a nuclear reactor), it is quite difficult to calculate the system sensitivities. As a result, many methods have been developed to calculate the sensitivities of system parameters and are briefly presented below.

3.4.1. Stochastic methods

Many methods have been developed to calculate the different parameter sensitivities in case of a stochastic mathematical approach. The most famous and popular one is the One-At-A-Time method (OAT).

3.4.2. The One-At-A-Time method (OAT)

This method is considered to be one of the simplest and easiest methods in terms of its concept. However, it requires many calculations and is considered "computationally expensive" [53]. At first, a simulation is performed with all the nominal values of the system parameters. Then, each parameter will be perturbed individually satisfying the rule "one parameter at a time" until all the system

parameters are perturbed. Finally, a comparison between the simulations output would provide a clear description of the sensitivity of each parameter (See Figure 15). Although this method is very simple, it is very difficult to apply to a system with a large number of parameters. However, its advantage beside simplicity is the ability to provide a short list of the important parameters affecting the system.

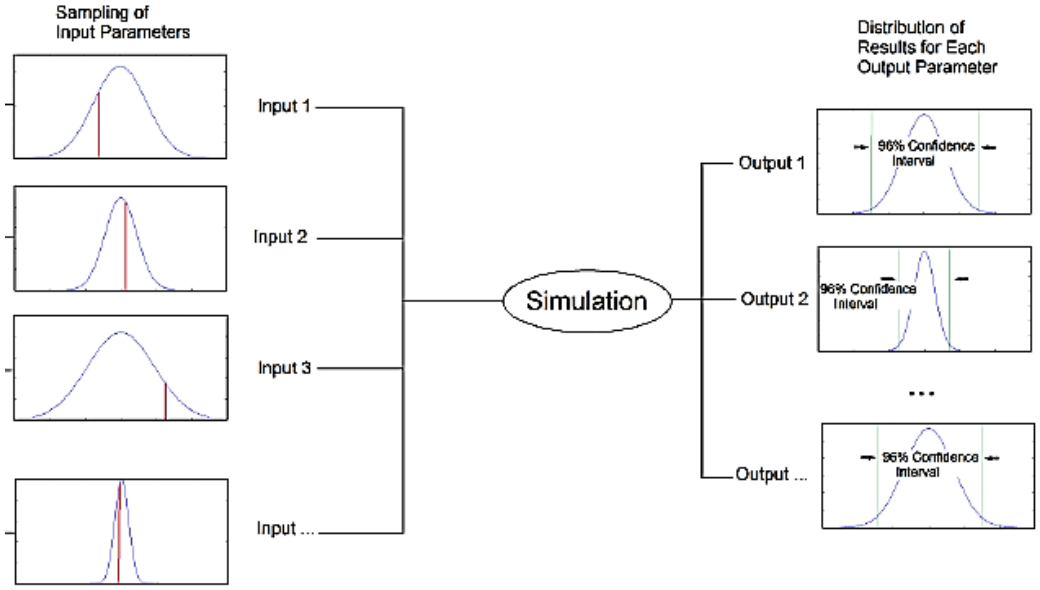

Figure 15: OAT Method for sensitivity propagation [53].

3.4.3. Deterministic methods

Deterministic methods for sensitivity and uncertainty calculation differ from stochastic methods in terms of the methodology and the way by which the problem has been approached. As an example, all stochastic or statistical methods first start with the uncertainty calculations and then perform the sensitivity analysis [51, 55]. However, deterministic methods start with the sensitivity calculation followed by the uncertainty calculations using the sandwich rule. Literature reflects the advantages of deterministic methods for sensitivity calculations over the stochastic methods. As an example based on [55] the actual response sensitivities to parameters cannot be computed exactly by using statistical methods and can be done only by using deterministic methods. The most popular method for the

sensitivity calculation in case of deterministic approach is the Adjoint Sensitivity Analysis Procedure (ASAP).

3.4.4. Adjoint Sensitivity Analysis Procedure (ASAP)

The Adjoint method is not as simple as the OAT method. However, its efficiency and advantages appear when dealing with a system of many parameters (e.g. a nuclear reactor). The Adjoint Sensitivity Analysis Procedure (ASAP) proposed by Cacuci [51, 55] is one of the most popular methods used for a deterministic approach and many computer codes use it for the sensitivity calculation. Adjoint methods depend on the forward and the adjoint solutions of the neutron transport equation. The detailed derivation of this method is beyond the scope of this report. Rather, a brief description of the sensitivity calculation in the SCALE code will be discussed based on [52]. In fact, the SCALE code depends on adjoint-based perturbation theory [52] to calculate the explicit sensitivity coefficients of k_{eff} which will be discussed briefly using the same notations expressed in [52].

The Boltzmann transport equation can be written as [52]:

$$[A - \lambda B]\phi = 0 \ , \tag{3.56}$$

Where, ϕ represents the neutron flux, λ represents the eigenvalues with λ=1/k_{eff}, A and B are operators where A represents all of the transport equation except the fission term and B represents the fission [52]. Perturbation of the transport equation operators and the eigenvalues are given by:

$$A' = A + \delta A \ , \tag{3.57}$$

$$B' = B + \delta B \ , \tag{3.58}$$

$$\lambda' = \lambda + \delta\lambda \ , \tag{3.59}$$

δA and δB are small linear perturbation in the operators A and B respectively. $\delta\lambda$ represents the resulting change in the eigenvalue due the operator's perturbations. The perturbed transport equation can be written as:

$$[A' - \lambda' B']\phi' = 0 \ , \tag{3.60}$$

The adjoint equation of equation (3.56) is:

$$[A^{\dagger} - \lambda^{\dagger} B^{\dagger}]\phi^{\dagger} = 0 \ , \tag{3.61}$$

Where $\phi^{\dagger}$is the adjoint flux, $A^{\dagger}$ and $B^{\dagger}$ are the adjoint operators of the operators A and B respectively. Multiplying the Equation (3.60) by $\phi^{\dagger}$ and integrating yields:

$$\langle \phi^{\dagger}(A' - \lambda' B')\phi' \rangle = 0 \ , \tag{3.62}$$

Now substituting Equations (3.57 - 3.59) in Equation (3.61) and rearranging yields,

$$\langle \phi^{\dagger}(A - \lambda B + \delta A - \lambda \delta B - B\delta\lambda - \delta\lambda\delta B)\phi' \rangle = 0 \ , \tag{3.63}$$

By using Equation (3.61) with the adjoint property ($\langle \phi^{\dagger}(A - \lambda B)\phi' \rangle = \langle \phi'(A^{\dagger} - \lambda^{\dagger} B^{\dagger})\phi^{\dagger} \rangle$**,** Equation (3.63) can be reduced to:

$$\langle \phi^{\dagger}(\delta A - \lambda \delta B - B\delta\lambda - \delta\lambda\delta B)\phi' \rangle = 0 \ , \tag{3.64}$$

Equation (3.64) can be simplified by applying some approximations. First, the second order perturbation term ($\delta\lambda\delta B$) can be ignored. Also, replacing ϕ' with ϕ assumes that the perturbation of the operators in the transport equation does not reflect a significant change in the flux solution. Applying the discussed approximations and rearranging Equation (3.64) gives:

$$\frac{\delta\lambda}{\lambda} = \frac{\langle \phi^{\dagger}(\delta A - \lambda \delta B)\phi \rangle}{\langle \phi^{\dagger}(\lambda B)\phi \rangle} \ , \tag{3.65}$$

The perturbation terms of Equation (3.65) can represent the partial derivatives of the macroscopic cross-sections of the transport equation (Σ). Such substitution in Equation (3.65) gives:

$$\frac{\delta\lambda}{\lambda} = \frac{\langle \phi^{\dagger}(\xi) \left(\frac{\partial A[\Sigma(\xi)]}{\partial \Sigma(r)} - \lambda \frac{\partial B[\Sigma(\xi)]}{\partial \Sigma(r)} \right) \phi(\xi) \rangle}{\langle \phi^{\dagger}(\xi)(\lambda B[\Sigma(\xi)])\phi(\xi) \rangle} \ , \tag{3.66}$$

It should be noted that ξ represents the vector space and the brackets $\langle \quad \rangle$ represents an integration over space, energy, and direction. As $\lambda = 1/k_{\text{eff}}$, then:

$$\frac{\partial\lambda}{\lambda} = -\frac{\partial k}{k} \ , Where \ k = \ k_{\text{eff}} \tag{3.67}$$

Using the Equation (3.67), the final expression of the sensitivity of k as a result of small perturbation (which was the basic assumption of the approximations made within the previous derivation) in the macroscopic cross-sections (Σ) of the transport equation can be expressed by:

$$S_{k,\Sigma(\mathrm{r})} = \frac{\Sigma(r)}{k}\frac{\partial k}{\partial \Sigma(r)} = -\frac{\Sigma(r)}{k}\frac{\langle \phi^{\dagger}(\xi)\left(\frac{\partial A[\Sigma(\xi)]}{\partial \Sigma(r)} - \frac{1}{k}\frac{\partial B[\Sigma(\xi)]}{\partial \Sigma(r)}\right)\phi(\xi)\rangle}{\langle \phi^{\dagger}(\xi)\left(\frac{1}{k^2}B[\Sigma(\xi)]\right)\phi(\xi)\rangle}\ , \quad (3.68)$$

Chapter 4

Investigation of Reactor Physics Phenomena in the Canadian Pressure Tube Supercritical Water Reactor

This paper was published by the Canadian Nuclear Laboratories Nuclear Review and it is cited as:

'Moghrabi, A., and Novog, D. R., 2016, "Investigation of Reactor Physics Phenomena in the Canadian Pressure Tube Supercritical Water Reactor," Can. Nucl. Lab. Nucl. Rev., 5(2), pp. 253–268.'

In this paper, a sensitivity and uncertainty analysis is used to identify the changes in the different lattice physic phenomena and neutronic behaviour of the Canadian PT-SCWR 64-element with fresh fuel. The lattice physics modules in standardized computer analysis for licensing evaluation were used in the analysis.

FULL ARTICLE

INVESTIGATION OF REACTOR PHYSICS PHENOMENA IN THE CANADIAN PRESSURE TUBE SUPERCRITICAL-WATER REACTOR

Ahmad Moghrabi* and David Raymond Novog

McMaster University, Hamilton, ON L8S 4L8, Canada

Article Info
Keywords: Reactor physics, supercritical water reactor, lattice physics, neutron multiplication.
Article History: Received 29 February 2016, Accepted 8 June 2016, Available online 25 October 2016.
DOI: http://dx.doi.org/10.12943/CNR.2016.00031

*Corresponding author: moghraam@mcmaster.ca

The Canadian pressure-tube supercritical-water-cooled reactor is an advanced Generation IV reactor concept that uses water above its thermodynamic critical pressure as its coolant. The higher operating pressure dictates changes in the design and configuration of the reactor core and fuel assemblies as compared with existing CANDU designs. In addition, the reference Canadian design considers a plutonium-driven thorium fuel with high-pressure light-water coolant and a separate low-pressure heavy-water moderator. The salient features of this core design include a vertically orientated re-entrant channel where the coolant passes from an inlet plenum above the core downwards through the internal annulus flow tubes in each fuel assembly, then through a 180° bend, then upwards through the fuel region of the assembly where it absorbs thermal energy, and finally into the outlet plenum located above the core. Given the multiple flow paths through a fuel assembly, the significant coolant property variations along the fuel channel caused by transitions through the pseudo-critical temperature, the external low-pressure moderator, and the Pu–Th fuel composition, the lattice physics phenomena are significantly different from those in conventional CANDU power plants. In this paper, the changes in lattice physics phenomena are identified and analyzed through sensitivity and uncertainty analyses using the lattice physics modules in standardized computer analysis for licensing evaluation.

1. Introduction

Through the Generation IV International Forum (GIF) the next generation of advanced nuclear energy systems, known as Generation IV (GEN-IV) nuclear reactors, are being developed. These designs focus on resource sustainability, improved safety and reliability, economic benefits, and improved proliferation resistance and physical protection [1]. Canada's contribution to the GIF is the Canadian pressure tube supercritical water-cooled reactor (PT-SCWR) [2], which is considered as an evolution of the Canada Deuterium Uranium (CANDU) reactor.

The PT-SCWR has characteristics similar to both the pressurized heavy-water reactor (PHWR) designs like CANDU and boiling water reactors (BWRs). The Canadian PT-SCWR uses supercritical light water (SCW) as a coolant coupled directly to a turbine similar to BWR designs. The combination of higher temperatures and direct cycles lead to efficiency approaching 48%. The PT-SCWR is also vertically oriented, batch fuelled, and has fuel assemblies that span the entire length of the core similar to BWR technology. A key distinction from other SCWR designs is the separation of the high-pressure coolant and the low-temperature and pressure heavy-water moderator [2]. The separation of the coolant and moderator in the reactor is similar to existing CANDU designs. The reference design features a high-efficiency re-entrance channel (HERC) [3–5] where the coolant flows downwards through the central flow tube and upwards around the fuel elements through the outer flow tube section of the fuel channel.

A fundamental design requirement was that the power coefficient of reactivity be negative for all postulated transients and that the overall coolant density reactivity coefficient also be positive for loss-of-coolant accident (LOCA) events to have negative coolant void reactivity. Given the significant differences of the fuel design compared with existing physics code applications, a large number of studies have been performed comparing the 2-dimensional (2-D) lattice level neutronic behavior [6–8]. Moreover, research has also been performed on the coupled thermalhydraulic feedback effects in the PT-SCWR [9–11]. The key findings of many of these studies show that overall the design has a negative

power and positive coolant density reactivity coefficient as expected. However, there exists the possibility of nonequilibrium coolant density distributions that can give rise to brief periods of positive reactivity during some stylized LOCA events. For the purposes of this paper, these effects are named void reactivity, or differential void reactivity, for consistency with other CANDU literature. However, strictly speaking, the concept of void fraction is not applicable to coolants above the thermal physical critical point, and what is actually meant are reactivity effects resulting from strong coolant density variations. Although this existing body of knowledge has provided significant benefit in the design and assessment of the PT-SCWR concept, there is a lack of detailed understanding of the unique and subtle phenomenological differences in the HERC fuel design and a conventional CANDU reactor, in particular for cases where differential (nonequilibrium) densities occur across the fuel channel. The objective of this paper is to study the lattice physics details of the SCWR with fresh fuel and obtain a firm understanding of the important phenomena and unique behavior of this fuel design.

2. Calculation Methods

The lattice level transport calculations in this work were performed using the NEWT [12] code which is part of the SCALE (Standardized Computer Analysis for Licensing Evaluation) 6.1.3 [13] package. All the 2-D lattice cell simulations were performed using the 238 energy group ENDF/B-VII.0 library included in SCALE 6.1.3 release. NEWT is a deterministic code that solves the Boltzmann transport equation using the discrete ordinate approach followed by the extended step characteristics (ESC) approximation employing the method of characteristics along discrete angular directions within the computational cell or mesh. Although the ESC approximation method is powerful, it requires a fine mesh, so mesh sensitivity studies are performed as outlined below. A large number of NEWT simulations were performed as a benchmark to confirm its suitability and agreement with other lattice transport codes used for SCWR analysis [8].

The PT-SCWR is characterized by concentric fuel rings that are different from the typical light-water reactor (LWR) square pitch lattice often analyzed with NEWT. To handle the concentric fuel array NEWT uses Dancoff factors for accurate self-shielding treatment. The SCWR-specific Dancoff factors were calculated for each case using MCDANCOFF [14], which is part of SCALE. It was observed that the computed Dancoff factors values vary slightly with the fuel pin position within the assembly. A sensitivity study showed that these small variations in Dancoff factors have a minor effect on the transport calculations and, therefore, the average value in each fuel ring was used (consistent with the SCALE manual [15] recommendations). Before executing the neutron transport calculations, NEWT performs a resonance self-shielding process using the dan2pitch card to calculate the equivalent lattice pitch from the Dancoff factors of the fuel pins. The self-shielding calculation within NEWT has a limitation depending on many factors and in particular the density of the coolant [16]. Consequently, an altered coolant density with value of 0.4 g/cm^3 was used in the self-shielding calculation as this strategy showed the most consistent results when the coolant density within the fuel region drops below 0.4 g/cm^3 [16]. Using the input geometry, materials specification, boundary conditions, and Dancoff factors along with the 238-group nuclear data library the NEWT code solves the transport equation and predicts the neutron multiplication factor (k_∞). NEWT also provides the components of the 4-factor formula, reaction rates, and local flux spectrum. Further processing of the results provided the space and energy homogenized cross-sections.

One of the advantages of NEWT code is the capability to analyze complex geometries in the 2-D transport calculations. However, as stated above the methods are somewhat dependent on mesh and geometry details. For example, in NEWT, any defined geometrical circle is represented by an equilateral dodecagon as a default condition. A sensitivity study was performed investigating the influence of this approximation on the calculation of k_∞ confirming the results presented previously in Canuti et al. [17]. Additional sensitivity studies were performed for all cases of the mesh refinement and the optimum meshes that have a minimal sensitivity of results to mesh size were selected and used in the subsequent analyses.

The nuclear data sensitivity and uncertainty analysis presented in this work were performed using TSUNAMI-2D (Tools for Sensitivity and Uncertainty Analysis Methodology Implementation) code [13, 15, 18–20]. For TSUNAMI-2D, NEWT is used to calculate the forward and the adjoint flux solutions and then the SAMS (sensitivity analysis module for SCALE) [13, 21, 22] module generates sensitivity coefficients for k_∞ with respect to each cross-section.

The SAMS code calculates the sensitivity coefficients spectrum by calculating its value for each discrete energy group and reaction. The sensitivity coefficients are dimensionless quantities defined as percentage effect on the system's neutron multiplication factor, k, to a percentage change in the nuclear reaction cross-sections [21]. The sensitivity can be expressed as function of the neutron multiplication factor as [21]:

$$\text{Sensitivity} = \frac{dk}{k}\frac{\Sigma^i_{x,g}}{d\Sigma^i_{x,g}} \quad (1)$$

where $\Sigma^i_{x,g}$ represents the cross-section nuclear data component for the process x of nuclide i in energy group g.

The complete sensitivity of the neutron multiplication factor, k, due to perturbation of $\Sigma^i_{x,g}$ including contributions from all perturbations consists of 2 phenomena: the implicit and the explicit components. The explicit component represents the sensitivity of k to perturbations of the group-wise cross-section data [21] and is calculated using the same methodology used in the Fantastic Oak Ridge Sensitivity System (FORSS) [23] code system for fast reactor application. The implicit component represents the sensitivity of the resonance self-shielding multigroup cross-section data to the self-shielding phenomena [21], usually manifesting as a change in group fluxes that are subsequently used in the homogenization process. The complete sensitivity can be expressed as [21]:

$$\left(S_{k,\Sigma^i_{x,g}}\right)_{\text{complete}} = \left(S_{k,\Sigma^i_{x,g}}\right)_{\text{explicit}} + \left(S_{k,\Sigma^i_{x,g}}\right)_{\text{implicit}} = \frac{\Sigma^i_{x,g}}{k}\frac{\partial k}{\partial \Sigma^i_{x,g}} + \sum_j \sum_h \frac{\Sigma^j_{y,h}}{k}\frac{\partial k}{\partial \Sigma^j_{y,h}} \times \frac{\Sigma^i_{x,g}}{\Sigma^j_{y,h}}\frac{\partial \Sigma^j_{y,h}}{\partial \Sigma^i_{x,g}} \quad (2)$$

where $\Sigma^j_{y,h}$ represents the cross-section nuclear data component for the process y of nuclide j in energy group h. The first term in Equation (2) represents the explicit component of the sensitivity while the implicit component is included in the second term and represents the effect of perturbing the cross-section $\Sigma^i_{x,g}$ on the resonance self-shielding values of $\Sigma^j_{y,h}$ [21].

The nuclear data covariance data is a symmetric $\mathbf{M} \times \mathbf{M}$ matrix, which includes all the correlations between the nuclides reaction cross-sections with the relative variances located on diagonal elements and covariances in off-diagonal elements, is given by [24]:

$$C_{\alpha\alpha} = \left[\frac{\text{COV}(\alpha_m, \alpha_p)}{\alpha_m \alpha_p}\right],\ \alpha = 1,\ 2,\ \ldots,\ M;\ p = 1,\ 2,\ \ldots,\ M \quad (3)$$

where M is the number of nuclide reaction pairs × the number of energy groups. With the nuclear data parameters, describing the nuclide reaction cross-sections per energy groups, are represented by the vector [23]:

$$\alpha \equiv (\alpha_m),\ m = 1,\ 2,\ \ldots,\ M \quad (4)$$

The uncertainty matrix for the system of k values due to the nuclear data covariances, C_{kk}, can be determined using the covariance matrix, sensitivity matrix and its transpose as [23]:

$$C_{kk} = S_k C_{\alpha\alpha} S_k^{\dagger} \quad (5)$$

knowing that within the uncertainty matrix, C_{kk}, the diagonal terms represents the relative variance values for each nuclide, reaction, and energy. However, the off-diagonal elements represent the shared or common variance between the different nuclides, reactions, and energies.

3. Modelling Methods

This study focuses on the Canadian PT-SCWR 64-elemet fuel assembly geometry with Thoria mixed with reactor-grade Plutonium of isotopic composition given in Pencer et al. [25]. The fuel is arranged in 2 concentric 32-element rings with 15% and 12% by weight PuO_2 in ThO_2 in the inner and outer rings, respectively. The fuel assembly has a 5 m active length and zirconium modified stainless steel cladding [25]. The isotopic atomistic densities and geometric specifications [26] for the Canadian PT-SCWR 64-element fresh fuel assembly were used in this study. Coolant is provided to the channel from an upper inlet plenum through a central downwards flow channel in each fuel assembly. At the bottom of the channel, the flow in the center tube is redirected upwards through the fuel containing region of the assembly. The flow path is known as a re-entrant fuel design and is termed the high-efficiency re-entrant channel (HERC) by the developers (Figure 1 [26]). Flow from the inlet plenum is delivered at 350 °C and 25.8 MPa and exits the fuel channel at 625 °C and 25.0 MPa with each channel using an inlet orifice to obtain a flow such that each channel has approximately the same outlet temperature. Owing to the supercritical nature of the coolant, it undergoes significant variations in its thermophysical properties as it travels through the fuel channel, and such changes must be considered in the lattice physics simulations. To thermally isolate the fuel channel from the low-pressure and low-temperature moderator, a ceramic insulator is used on the inner surface of the pressure tube.

Although a previous study [8] showed that simulations at the mid-plane of the reactor where the property gradients may be the largest have similar behaviour of k_∞ as the top of the channel, such similarity in k_∞ may be misleading, individual phenomena may significantly change and having their effects cancelling each other so that the effect on k_∞ is small. The first position used in this study (at 25 cm from the bottom of the channel) is used to assess the lattice cell characteristics at the bottom of the channel or the inlet of the heated portion of the fuel assembly where the density of the coolant under normal operating conditions is the highest. The second position is at 475 cm, representing the channel outlet or the top of the channel where the coolant density under normal operating conditions is the lowest. The temperatures and properties of the different lattice cell components at 25 cm and 475 cm locations were taken from Sharpe et al. [8] and are listed in Table 1. The top and bottom of the channel are selected for analysis as they represent the largest change in fuel temperature and coolant properties in the channel. For self-shielding calculations in NEWT, the Dancoff factors are calculated on a ring-wise basis and are shown in Table 2 for the reference conditions as well as for each of the sensitivity cases examined in this work.

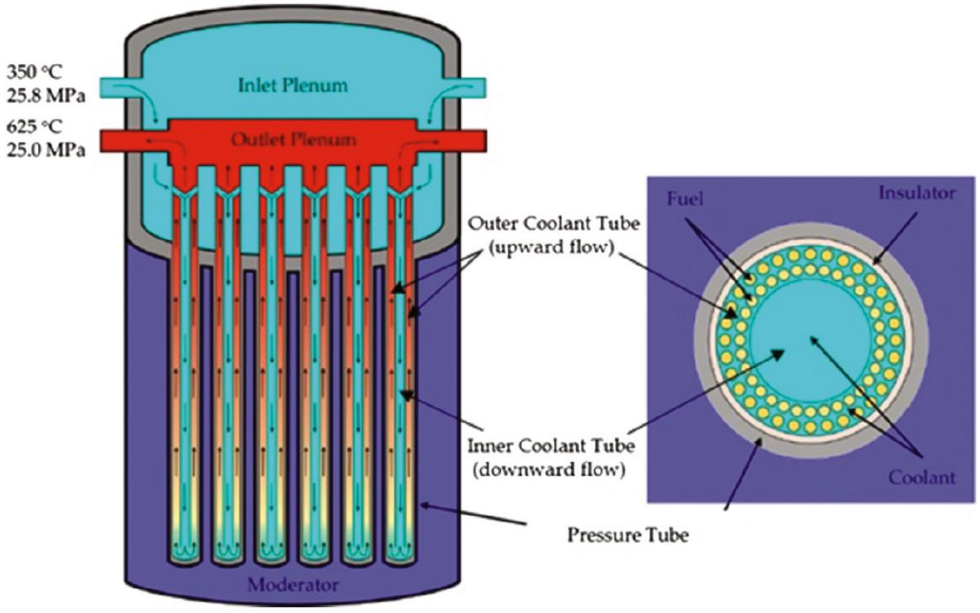

FIGURE 1. Core and lattice cell cross-section view of PT-SCWR HERC concept with the 64-element fuel assembly [25].

TABLE 1. Coolant density and component temperatures at the inlet and outlet of the channel.

Distance from bottom of the channel (cm)	Coolant density (g/cm^3)		Component temperatures (K)						
	ρ_{out}	ρ_{in}	Outer coolant	Cladding	Liner	Insulator	Pressure tube	Inner coolant	Fuel
25	0.51702	0.57896	647.40	683.04	640.78	537.68	410.38	636.45	1117.36
475	0.07014	0.61903	890.62	1006.99	859.82	673.29	452.28	625.81	1539.91

The research in this paper examines the lattice physics phenomena through sensitivity and uncertainty analysis to nuclear data for the normal operating conditions (NOC) as well as several perturbed scenarios. Simulations of the different scenarios listed in Table 3 were executed using NEWT and TSUNAMI-2D codes. The scenario selection was based on a set of preliminary sensitivity simulations in addition to the methodology proposed in Blomely et al. [27] and Langton et al. [28]. NEWT was used to investigate the reaction rates, flux spectrum, space homogenized cross-sections, the components of the 4-factor formula, and the neutron multiplication factor for the infinite lattice cell to observe and assess the important changes in lattice physics phenomena. TSUNAMI-2D was used to perform sensitivity and uncertainty analysis and was used to understand the phenomena that lead to changes in neutron multiplication constant. Moreover, the changes in the phenomena were also examined as a function of coolant void reactivity (CVR),[1] fuel temperature coefficient (FTC), coolant temperature reactivity coefficient (CTRC), and moderator temperature reactivity coefficient (MTRC).

4. Results and Discussion

As mentioned above, a series of NEWT and TSUNAMI-2D simulations were performed to examine the behavior of lattice cell phenomena at the bottom and the top of the fuel channel for NOC and the perturbed cases. The 4-factor

[1]Strictly speaking, in a coolant beyond its supercritical pressure the concept of coolant void is not applicable since there are no phase transitions. However, large density transitions may still occur in the SCWR and are similar in characteristic to classical CANDU transitions. Hence, the term CVR is used here for consistency to legacy CANDU terminology, but what is really inferred is the reactivity induced from a change in coolant density.

TABLE 2. Values of Dancoff factors for each ring for each configuration.

	At 25 cm from bottom of channel		At 475 cm from bottom of channel	
	Inner fuel ring	Outer fuel ring	Inner fuel ring	Outer fuel ring
Reference	0.333167	0.274634	0.463916	0.417592
Inner coolant voided	0.411945	0.276974	0.615624	0.426317
Outer coolant voided	0.494940	0.451323	0.494671	0.451321
Total coolant voided	0.664289	0.462187	0.664289	0.462187
Fuel hot	0.333167	0.274634	0.463916	0.417592
Coolant hot	0.333167	0.274634	0.463916	0.417592
Moderator hot	0.333167	0.274634	0.463916	0.417592

TABLE 3. Definition of sensitivity cases.

Case name	Description
Reference	Nominal temperatures and densities of different lattice cell components
Inner coolant voided (ICV)	Coolant density in the central flow tube (inner tube) decreases to 0.001 g/cm^3
Outer coolant voided (OCV)	Coolant density in the outer flow tube decreases to 0.001 g/cm^3
Total coolant voided (TCV)	Coolant density in both tubes (inner and outer) decreases to 0.001 g/cm^3
Fuel hot	Fuel temperature increased by 100 K
Coolant hot	Inner and outer coolant temperature increased by 100 K
Moderator hot	Moderator temperature increased by 20 K

TABLE 4. Values of neutron multiplication factor, k_∞, and the 4 factors at the channel inlet and outlet.

	Distance from bottom of channel		
Factor	25 cm	475 cm	Reactivity difference (mk)
Reproduction (η)	1.73674	1.739422	1.20
Thermal utilization (f)	0.861505	0.867537	5.41
Resonance escape probability (p)	0.675033	0.655916	−22.28
Fast fission (ϵ)	1.276447	1.302981	15.96
Multiplication (k_∞)	1.289201	1.289671	0.28

formula components are examined and the corresponding contribution of each factor to the reactivity in the perturbed cases is discussed. The phenomenological identification and assessment were based on the nuclear data sensitivities and the uncertainties in the neutron multiplication factor.

4.1. Normal operating conditions: reference case

4.1.1. Effect of properties on the 4-factor formula

Each factor in the 4-factor formula was examined to ascertain the various reactivity contributions at the bottom and top of the channel. The 4-factor formula can be written as:

$$k_\infty = \eta f p \epsilon$$

where the reproduction factor (η) is the average number of neutrons released per thermal absorption in fuel isotopes, the thermal utilization factor (f) represents thermal neutrons absorbed by fuel relative to thermal neutrons absorbed everywhere, the resonance escape probability (p) represents the fraction of fission neutrons being slowed to thermal energies without absorption with respect to the total fission neutrons, and the fast-fission factor (ϵ) defines the total number of fission neutrons relative to the number of thermal fissions. Table 4 summarizes the reference case 4 factors for the inlet and outlet lattice conditions as well as the net reactivity difference (in mk) between the inlet and outlet of the fuel channel.

The changes in the 4 factors along the length of the channel are explained in terms of the underlying phenomena:

1. Compared with the normal CANDU lattice physics phenomena the resonance escape probability phenomena are substantively different. In a typical CANDU lattice, there are 2 competing phenomena that give rise to a net increase in escape probability with decreasing coolant density. First, lower coolant densities reduce the scattering interactions for fast neutrons emerging from the fuel, thereby allowing these emerging neutrons to avoid resonance energies while on their path to the moderating material. In contrast, the neutron population returning from the moderator, while mostly thermal, has some of its spectrum still within the resonance

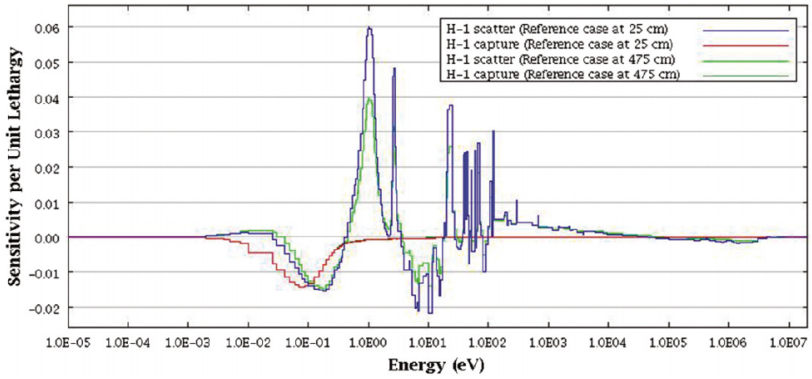

FIGURE 2. ^{1}H sensitivities for the reference case at 25 cm and 475 cm from the bottom of channel.

region, and therefore a reduction in coolant density means such returning epithermal neutrons remain within the resonance energies and hence may be captured. In the normal CANDU cell, the moderator volume is very large and hence the second effect is small since the returning neutron population has few neutrons outside the thermal range. Therefore, the first effect dominates and the resonance escape probability increases with decreasing coolant density. For the SCWR cell, the moderator volume (i.e., lattice pitch) is much smaller than CANDU and the spectrum of neutrons returning from the moderating material has a much larger portion of epithermal neutrons. Therefore, the coolant near the fuel plays a significant role in scattering these returning epithermal neutrons out of resonance energies and into the thermal portion of the spectra. Separate effect perturbations of the inlet lattice cell coolant density to the outlet conditions, holding all other lattice inputs constant, showed that the effect of coolant density contributes approximately −16 mk to the overall change in escape probability, with the remaining observed changes being a result of fuel temperature. Additional sensitivity studies were also performed for larger lattice pitch cells (larger heavy-water moderator regions). Examination of the returning neutron spectra showed that for larger lattice pitches, incoming neutrons were much more thermal, and hence the importance of the coolant in the fuel region for thermalization of these returning epithermal neutrons is decreased. Such large lattice pitch cases showed resonance escape probability behavior that is similar to those in a typical CANDU lattice cell. Further discussion of this resonance escape phenomena is provided in the discussion on coolant voiding effects. In addition to the coolant density effects, the fuel temperatures in the SCWR change significantly from the channel entrance to exit. A separate effect study perturbing only the fuel temperature from its inlet to outlet condition indicates that the Doppler effect contributes approximately −5 mk to the resonance escape probability.

2. The fast fission factor increases substantively from the bottom to the top of the channel (+15.96 mk) due to the reduction in the coolant density. As the coolant density decreases in the outer flow tube there is a hardening of the flux spectrum in the region surrounding the fuel, leading to an increase in the fast fission probability. This was confirmed by independently varying the coolant density in the lattice while keeping all other variables constant and examining the changes in the fast fissions factor.
3. The thermal utilization factor is larger at the channel outlet than the inlet (by 5.41 mk). Neutron absorption in ^{1}H mainly occurs within the thermal energy region as shown in Figure 2. As the coolant density decreases, the total thermal neutron absorption decreases since the ^{1}H atomic density decreases causing a positive contribution to the thermal utilization factor.
4. The reproduction factor increases from inlet to outlet (by 1.20 mk) largely resulting from higher neutron production rate of ^{240}Pu and ^{241}Pu fissions with the harder neutron spectra at the top of the channel that counterbalances the negative contributions of ^{232}Th and ^{239}Pu. This can be explained by the variation of nubar (average number of neutrons per fission reaction), fission and absorption sensitivities shown in Tables 5 and 6 and discussed in the following section.

4.1.2. Sensitivity studies on NOC lattice characteristics

The most significant k_{∞} sensitivities to nuclear data from TSUNAMI-2D for the reference case at the channel inlet and outlet are presented in Tables 5 and 6. These sensitivities are integrated over all energy levels and are given on a per-reaction and isotope basis. ^{239}Pu is the highest fissile

TABLE 5. The top sensitive nuclides and breakdown by reaction at 25 cm for the reference case.

Nuclide	Nubar	Fission	Capture	Scatter	Total
^{239}Pu	0.71068	0.30942	−0.20704	−0.00027119	0.10211
^{240}Pu	0.0053792	0.0031613	−0.082285	0.00098999	−0.078133
^{241}Pu	0.27523	0.12592	−0.049665	−0.00009864	0.076155
^{232}Th	0.0053486	0.002478	−0.082713	0.0059199	−0.074315
^{2}H	—	—	−0.00061228	0.063305	0.062693
^{56}Fe	—	—	−0.023137	−0.0019701	−0.025107
^{58}Ni	—	—	−0.012607	−0.0011497	−0.013757
^{91}Zr	—	—	−0.014507	0.0011508	−0.013356
^{1}H	—	—	−0.035327	0.026357	−0.0089698
^{53}Cr	—	—	−0.0085364	−0.00008434	−0.0086208

TABLE 6. The top sensitive nuclides and breakdown by reaction at 475 cm for the reference case.

Nuclide	Nubar	Fission	Capture	Scatter	Total
^{239}Pu	0.7055	0.30777	−0.20317	−0.00037424	0.10423
^{2}H	—	—	−0.00059909	0.085777	0.085178
^{232}Th	0.0057765	0.0026807	−0.090383	0.0071685	−0.080534
^{241}Pu	0.27906	0.1271	−0.050165	−0.00012743	0.076806
^{240}Pu	0.0059592	0.0035064	−0.079028	0.0009053	−0.074617
^{56}Fe	—	—	−0.021789	−0.0023401	−0.024129
^{58}Ni	—	—	−0.011985	−0.001357	−0.013342
^{91}Zr	—	—	−0.014115	0.0017585	−0.012357
^{1}H	—	—	−0.034902	0.026498	−0.0084037
^{53}Cr	—	—	−0.0079978	−0.00011367	−0.0081115

component in the fuel [25] and, consequently, its fission sensitivity is a dominant contribution to k_∞. Furthermore, ^{241}Pu is characterized by a large fission cross-section and, therefore, its fission cross-section sensitivity is also high. ^{232}Th and ^{240}Pu are characterized by large absorption cross-sections and hence also contribute significantly to k_∞. In the SCWR design, a significant fraction of neutron moderation occurs in the heavy water moderator and accordingly scattering in ^{2}H is also significant. The other significant contributors come from structural materials and the light-water coolant as discussed below. In general, the results in Tables 5 and 6 are consistent with expectations, with the relative sensitivity to deuterium being higher at the channel exit, reflecting its increasing importance due to the reduction in the fuel region moderation with lower coolant density.

Interestingly, ^{1}H appears in the list of the top 10 nuclides that have the highest contribution to k_∞ due to the relatively large volume of light water in the SCWR lattice cell. Investigation of the flux distribution explains the importance of the ^{1}H scattering and absorption and its impact on k_∞. The flux spectrum in the lattice cell shows a high concentration of thermal flux in the central coolant tube and at the corners of the lattice cell indicating the importance of both the heavy-water moderator and central light-water coolant to neutron moderation. The light water flowing through the central tube, therefore, contributes significantly to the moderation and the net absorption in the cell and this explains the relative importance of ^{1}H. This is evident over the whole energy spectrum as shown in Figure 2, with particular sensitivity to scattering at epithermal energies and absorption in the thermal range.

The central flow tube structure, fuel cladding, and the inner liner tubes are made from Zirconium modified stainless steel (mainly ^{56}Fe, ^{58}Ni, and ^{53}Cr), whereas the insulator, outer liner tube, and the pressure tube predominantly consist of ^{91}Zr. The large quantities of these materials as well as their absorption and the neutron capture cross-sections impacts k_∞, and this explains their high sensitivities. It should be noted that k_∞ is more sensitive to ^{56}Fe than ^{91}Zr despite the disparity in the amounts of these materials in the lattice as the ^{91}Zr has a lower thermal neutron absorption cross-section than iron ^{56}Fe [27].

The magnitudes of the sensitivities presented in Tables 5 and 6 and Figure 2 are used to further examine the phenomena affecting the 4 factors. Figure 2 shows the very large sensitivity to neutron scattering for energy ranges in the epithermal region. Such sensitivities arise from various phenomena including up-scattering from thermal into the low-lying Pu resonances and (or) the importance of ^{1}H in thermalizing the epithermal neutrons returning from the D_2O moderator. The negative scattering sensitivity of ^{1}H in the energy range between 0.1 and 0.3 eV and around the 10 eV represent the neutron scattering out of the ^{239}Pu fission resonances. However, the large positive scattering peak of ^{1}H at 1 eV represents the neutron down scattering into the low lying ^{239}Pu fission resonance. By examining the sensitivity spectra varying a single parameter at a time, it is observed that the dominant contribution to the sensitivity in this region is a result of the outer (fuel region) coolant density. Furthermore, repeating such sensitivity studies for a larger lattice pitch (larger D_2O volumes) shows the sensitivity to ^{1}H decreases substantively in the epithermal region. These studies clearly substantiate that the dominant mechanism leading to the decrease in resonance escape probability is the coolant density change in the outer fuel region and its subsequent effect on returning epithermal neutrons from the D_2O moderator. The fuel temperature contribution to the resonance escape probability change with elevation results from the high sensitivity of lattice calculations to absorption in ^{241}Pu and ^{232}Th and the overall broadening of these cross-sections due to the Doppler effect. Exceptions exist within the energy range between 0.1 and 1.0 eV where less absorption occurs at the channel exit than the channel inlet due to up-scattering by the higher coolant temperatures near the outlet, but the effect is small.

The slight increase in reproduction factor at the top of the channel is also expected given the sensitivities shown in Tables 5 and 6 for nubar and the capture-to-fission ratio. In general with a harder spectrum, nubar will tend to increase with elevation which tends to increase the reproduction factor in particular for the elements undergoing fast fissions. At the same time, the higher fuel temperatures will tend to increase the non-fission absorptions in the ^{232}Th and hence increase the capture-to-fission ratio, thereby offsetting some of the increase in reproduction. The net result is a small positive increase in reproduction factor with channel elevation. Similarly, the thermal utilization changes are consistent with the changes in ^{1}H sensitivity showing a decrease in the sensitivity to capture with elevation. Absorption and scattering sensitivities of ^{1}H decrease with less density coolant at the top of the channel confirming the previous discussion and its corresponding effects in increasing the fast fission factor and the thermal utilization factor. Finally, all the isotopes contributing to fast fissions show larger sensitivities at the channel outlet, which is consistent with the discussion relating to the expected increase in fast fission probability with the hardening of the neutron spectrum towards the outlet.

4.1.3. Uncertainty studies on NOC lattice cell

The uncertainty in k_∞ due to uncertainties in nuclear data library was found to be 6.96 mk and 6.90 mk at the bottom and top of the channel, respectively. Nuclides with uncertainty contribution of more than approximately 0.5 mk are listed in Table 7.

The results in Table 7 (in comparison with Tables 5 and 6) show that the highest contributors to sensitivity are not necessarily associated with the largest contributors to the uncertainty, with the results largely consistent with those in Blomeley et al. [27]. As an example, ^{92}Zr (n,γ) and ^{242}Pu (n,γ) appear to be on the list of the highest contributors to uncertainty at both positions of the fuel channel, but k_∞ is not significantly sensitive to any of these nuclides-reactions, indicating a high nuclear data covariance in these reactions. Similarly, ^{1}H appears in the list with the highest contributors to the sensitivity of k_∞ while it is not a dominant contributor to uncertainty. In general, contribution to uncertainty of most nuclides and reactions is less at the channel outlet compared with their values at the channel inlet, which explains the slight decrease in the uncertainty at the channel outlet. The exception to this behavior is the contribution of ^{2}H (n,2n) and ^{2}H (elastic) reactions to the total uncertainty in k_∞. This also demonstrates the importance and the influence of ^{2}H in the Canadian PT-SCWR modeling.

4.2. Coolant density reactivity

Previous literature has identified interesting lattice physics phenomena for the Canadian PT-SCWR design. In particular, for cases with uniform changes in the coolant density throughout the lattice, the reactivity reduces consistent with the design objectives. However, during some postulated transients nonuniform voiding can occur for brief periods of time. During these periods, the reactivity of the lattice may temporarily become positive. The term "total coolant void" (TCV) corresponds to lattice cases where the coolant density in both inner and outer tubes is decreased uniformly to a low value. Depending on the LOCA scenario, the lattice may be partially voided where the inner flow channel density remains relatively unperturbed but the outer channel density decreases (outer coolant void, OCV) or where the inner flow channel density drops while the outer channel remains relatively unchanged (inner coolant void, ICV). Lattice level calculations have shown that the TCV and ICV have a negative CVR, whereas OCV has a positive CVR. Hence some non-equilibrium cases may result in transients where core power may temporarily increases prior to TCV induced self-shutdown of the reactor [11]. The reactivity and 4 factors for each case (TCV, OCV, and ICV) were investigated at the

TABLE 7. Nuclear data contribution to k_∞ uncertainty in the reference, ICV, OCV, and TCV cases at 25 cm and 475 cm from the bottom of the channel.

		Contribution to uncertainty (mk)							
		25 cm				475 cm			
Covariance matrix element		NOC	ICV	OCV	TCV	NOC	ICV	OCV	TCV
^{239}Pu (ū)	^{239}Pu (ū)	5.63	5.68	5.45	5.51	5.60	5.63	5.52	5.53
^{239}Pu (fission)	^{239}Pu (fission)	1.82	1.80	1.77	1.78	1.82	1.81	1.80	1.79
^{239}Pu (n,γ)	^{239}Pu (n,γ)	1.72	1.63	1.62	1.51	1.68	1.56	1.65	1.52
^{239}Pu (fission)	^{239}Pu (n,γ)	1.57	1.44	1.47	1.31	1.52	1.34	1.50	1.31
^{240}Pu (n,γ)	^{240}Pu (n,γ)	1.07	1.08	1.00	0.98	1.01	1.00	1.00	0.97
^{56}Fe (n,γ)	^{56}Fe (n,γ)	1.05	0.98	0.97	0.92	1.00	0.94	0.98	0.92
^{2}H (n,2n)	^{2}H (n,2n)	1.04	1.22	1.14	1.34	1.13	1.34	1.14	1.35
^{92}Zr (n,γ)	^{92}Zr (n,γ)	1.01	1.35	0.89	1.26	0.91	1.30	0.88	1.26
^{2}H (n,2n)	^{2}H (elastic)	−1.00	−1.39	−1.18	−1.80	−1.22	−1.82	−1.22	−1.82
^{2}H (elastic)	^{2}H (elastic)	0.95	1.55	1.20	2.38	1.30	2.43	1.28	2.41
^{91}Zr (n,γ)	^{91}Zr (n,γ)	0.75	1.01	0.69	0.99	0.70	1.01	0.68	0.99
^{241}Pu (fission)	^{241}Pu (fission)	0.69	0.66	0.68	0.68	0.69	0.68	0.69	0.68
^{90}Zr (n,γ)	^{90}Zr (n,γ)	0.65	0.87	0.58	0.82	0.59	0.84	0.57	0.82
^{232}Th (n,γ)	^{232}Th (n,γ)	0.63	0.74	0.57	0.82	0.64	0.85	0.55	0.74
^{58}Ni (n,γ)	^{58}Ni (n,γ)	0.62	0.58	0.57	0.54	0.59	0.55	0.58	0.54
^{241}Pu (ū)	^{241}Pu (ū)	0.58	0.66	0.63	0.68	0.63	0.68	0.63	0.68
^{53}Cr (n,γ)	^{53}Cr (n,γ)	0.56	0.51	0.51	0.48	0.53	0.49	0.52	0.48
^{242}Pu (n,γ)	^{242}Pu (n,γ)	0.53	0.62	0.49	0.54	0.52	0.58	0.51	0.56
Total of contributions above		6.92	7.09	6.67	7.02	6.86	7.17	6.77	7.04
Total from all contributions		6.96	7.14	6.71	7.06	6.90	7.22	6.81	7.11

channel inlet and outlet to provide a more thorough understanding of the reactivity phenomena.

4.2.1. Inner coolant void case

The ICV case corresponds to a situation where the coolant density flowing downwards through the central flow tube decreases while the outer coolant region remains unaffected and results in a negative ICV reactivity of −20.00 mk and −21.90 mk at the channel inlet and outlet, respectively. When the central flow tube is voided, neutron moderation via scattering with ^{1}H in the central flow tube is eliminated and thus, the number of thermal neutrons drops sharply in the central region of the assembly. Given this lack of moderation, emitted neutrons would need to travel further prior to moderation in the D_2O and as such would be subjected to resonance capture phenomena. Although this leads to a reduction in the number of thermal fission occurrences, the harder spectrum alternatively leads to greater fast-fission interactions that, when taken together, give negative reactivity. This can be explained using Tables 8 and 9 and examining the 4 factors:

- As a consequence of the loss of moderating coolant in the central tube, many neutrons remain in the resonance region and the path length to a moderator material increases on average. The remaining moderating material in the outer coolant (fuel containing) region (light water) is insufficient to fully thermalize the neutrons in the center of the channel. The resonance escape probability, therefore, decreases by 108.52 mk and 133.73 mk at channel inlet and outlet, respectively. The effect is larger near the channel outlet where coolant moderation in the fuel region of the channel is already low due to the pre-existing low-coolant density in the outer region of the fuel.
- The increase of the thermal utilization factor has a positive contribution of +18.48 mk and +21.93 mk at the channel inlet and outlet, respectively. As discussed previously, the removal of the large ^{1}H in the center of the tube reduces the number of nonfission thermal absorptions in the H_2O thereby increasing the thermal utilization factor.
- Given the much harder neutron spectrum in the fuel region for the voided case, the fast fission factor increases by 72.28 mk and 90.72 at the channel inlet and outlet, respectively, predominantly driven by increases in the inner ring. In the inner-coolant void case, the neutron scattering interactions with the

TABLE 8. Neutron multiplication factor for the reference case and the reactivity change in each of the perturbed cases at the channel inlet (25 cm) with the corresponding components from the 4-factor formula.

		Contribution (mk)					
Factor	Reference case	ICV	OCV	TCV	FTC	CTC	MTC
Reproduction (η)	1.73674	−2.24	1.78	1.85	−0.03	−1.60	−0.19
Thermal utilization (f)	0.861505	18.48	10.60	28.36	0.02	4.22	0.94
Resonance escape probability (p)	0.675033	−108.52	−23.75	−150.64	−1.30	−0.57	−0.05
Fast fission (ϵ)	1.276447	72.28	21.46	109.13	0.17	−0.35	−0.14
k_∞ for reference case/net reactivity change for the perturbed cases	1.289201	−20.00	10.10	−11.31	−1.14	1.69	0.56

TABLE 9. Neutron multiplication factor for the reference case and the reactivity change in each of the perturbed cases at the channel outlet (475 cm) with the corresponding components in the 4-factor formula.

		Contribution (mk)					
Factor	Reference case	ICV	OCV	TCV	FTC	CTC	MTC
Reproduction (η)	1.739422	−0.82	0.62	0.33	−0.03	−1.08	−0.28
Thermal utilization (f)	0.867537	21.93	1.35	23.49	0.03	3.78	0.84
Resonance escape probability (p)	0.655916	−133.73	0.34	−135.39	−1.09	−0.35	−0.08
Fast fission (ϵ)	1.302981	90.72	1.83	93.41	0.10	−0.49	−0.10
k_∞ for reference case/net reactivity change for the perturbed cases	1.289671	−21.90	4.14	−18.15	−0.99	1.86	0.38

coolant nuclides flowing through the central flow tube are eliminated, which increases the probability of having the first neutron interaction within the fuel giving rise to higher fast fission phenomena. Knowing that fast fission occurrences are higher at the channel outlet than at the channel inlet due to pre-existing low-density coolant in the fuel region (i.e., slightly harder fission spectrum at the exit). In general, the voiding in any coolant region acts to reduce neutron–coolant interactions, thereby increase the probability of fast fission for all voided cases.

- The reproduction factor decreases slightly by −2.24 mk and −0.82 mk at the bottom and top of the channel, respectively. This decrease is driven mainly by the increase of absorption in ^{232}Th resonances. Examining the highest sensitive fuel isotopes shown in Table 10 shows that the large negative contribution of ^{232}Th is partially offset by the small positive contribution from ^{240}Pu and ^{241}Pu.

TSUNAMI-2D simulations for the ICV case also confirm the phenomenological understanding above, and the highest sensitivity contributions are presented in Table 10. In the ICV case, k_∞ becomes more sensitive to the fuel isotopes due to the increase in resonance absorption and fast-fission reactions. Specifically, k_∞ is more sensitive to contributions from ^{238}Pu and ^{242}Pu due to the increase in the number of fast fission events. The sensitivity of ^{2}H is higher at the outlet than the inlet since a majority of the coolant is voided near the channel outlet (inner coolant is voided and outer coolant density is low at the outlet), whereas the sensitivity is lower at the inlet since there is a significant amount of ^{1}H still present in the outer coolant region. In fact, although ^{1}H is a significant sensitivity contributor at the bottom of the channel due to the absorptions and scatterings occurring in the outer coolant region, the combination of voided inner volume and low outer volume coolant density decreases its sensitivity such that it no longer appears on the list of significant contributors. The sharp decrease in ^{1}H absorptions also explains the increase of the thermal utilization factor since the reduction in ^{1}H absorptions with the lower atomic number density will reduce the number of non-fission thermal absorption in the cell.

In the ICV case, ^{56}Fe, ^{91}Zr, and ^{58}Ni contribute significantly to the sensitivity in k. However, the sensitivity of ^{91}Zr becomes higher than that of ^{58}Ni compared with the reference NOC case. In the ICV case, neutrons are mainly thermalized in the heavy-water moderator and as such a larger fraction of neutrons must travel through the insulator and pressure

TABLE 10. The top nuclear data sensitivity components at 25 cm and 475 cm for the ICV case.

At 25 cm from the bottom of the channel				At 475 cm from the bottom of the channel			
Nuclide	Fission	Capture	Total	Nuclide	Fission	Capture	Total
^{239}Pu	0.31104	−0.19936	0.11133	^{2}H	—	−0.00085	0.15226
^{2}H	—	−0.00081132	0.099624	^{239}Pu	0.30833	−0.1913	0.11649
^{232}Th	0.0029128	−0.10069	−0.089008	^{232}Th	0.0032561	−0.11712	−0.10235
^{241}Pu	0.13356	−0.049301	0.084127	^{241}Pu	0.13618	−0.050159	0.085836
^{240}Pu	0.0038337	−0.085898	−0.08077	^{240}Pu	0.0044807	−0.079083	−0.073377
^{56}Fe	—	−0.021248	−0.02249	^{56}Fe	—	−0.020455	−0.022811
^{91}Zr	—	−0.019237	−0.017598	^{91}Zr	—	−0.020107	−0.017145
^{58}Ni	—	−0.011747	−0.012435	^{58}Ni	—	−0.011419	−0.012747
^{1}H	—	−0.0077939	0.009584	^{238}Pu	0.0017414	−0.0093749	−0.0076925
^{242}Pu	0.00091363	−0.0091638	−0.0081313	^{53}Cr	—	−0.0074147	−0.0075297

tube prior to thermalization. As a result, higher neutron absorption by ^{91}Zr occurs during the neutrons path either from or to the moderator.

The uncertainty due to the nuclear data library in the ICV case is 7.14 mk and 7.22 mk at the channel inlet and outlet, respectively. Nuclides and reactions whose contribution to the uncertainty is higher than 0.5 mk are presented in Table 7. In comparison with the reference NOC case, the total uncertainty in k_∞ increases slightly, largely stemming from the increase in contributions from ^{2}H and zirconium isotopes. The changes in uncertainty are small, and the dominant uncertainty (Pu nubar) is comparable with the NOC cases.

4.2.2. Outer coolant void case

The OCV case occurs when the coolant density flowing upwards in the outer flow tube decreases, whereas the inner flow tube coolant density remains fixed, resulting in a positive OCV reactivity of 10.10 mk and 4.14 mk at the inlet and outlet, respectively. Such reactivity insertion may be important in safety analyses of inlet LOCAs where the density of the outer flow tube may be reduced during the initial stage of the transient [26]. In particular for reversing flows, the coolant density in the outer flow tube will decrease since the supply under reverse conditions is from the outlet header. This continues for a brief period until such time as the flow transports the low-density coolant backward through the inner flow tube. At the outlet of the channel, all 4 factors affecting reactivity are positive and relatively small in magnitude giving a reactivity increase of 4.14 mk. At the inlet there are much larger changes in reactivity, however, the large positive contributions from the thermal utilization and fast-fission are partially offset by the negative contribution of resonance escape probability with the net being +10.10 mk. The changes in the 4 factors show similar behavior as that associated with the inlet-to-outlet axial variation discussed in Section 4.1, and are as follows:

- In this case, there is a more significant perturbation in the coolant density in the outer region as compared with the NOC inlet-to-outlet changes, and as such the dominant effect on escape probability results from the epithermal returning neutrons from the heavy-water moderator. As noted previously, the outer coolant provides additional moderation for these returning neutrons and thus many avoid capture. In the completely voided case, the returning epithermal neutrons undergo no moderation and a significant fraction are captured in the fuel. At the bottom of the channel, the resonance escape probability decreases by 23.75 mk where the change in outer flow tube coolant density is larger than that associated with the inlet-to-outlet variation. And thus, the impact of escape probability is larger than the sensitivity cases that examined only density perturbations from NOC inlet density to outlet density that was discussed previously (−18 mk). At the top of the channel, the change in coolant density between the voided case and the NOC is small. Consequently, the loss of neutron up-scattering with the lower numbers of hot coolant nuclides offsets the other negative contribution causing the resonance escape probability to increase slightly by 0.34 mk. This is further substantiated by perturbing the coolant temperature at the NOC outlet densities and observing the high sensitivity of the escape probability to coolant temperature at this location.
- In the OCV case, the fast fission factor increases by 21.46 mk and 1.83 mk at the bottom and top of the channel, respectively. As discussed previously for the normal axial variation in outer coolant density fast fissions increase with reduced outer coolant densities. It should also be noted that the increase rate in the fast fission factor is not as high as the ICV case due to the contribution of coolant flowing through inner flow tube to the moderation process.

TABLE 11. The top nuclear data sensitivity components at 25 cm and 475 cm for the OCV case.

At 25 cm from the bottom of the channel				At 475 cm from the bottom of the channel			
Nuclide	Fission	Capture	Total	Nuclide	Fission	Capture	Total
^{239}Pu	0.30485	−0.19981	0.10471	^{239}Pu	0.30605	−0.20112	0.10456
^{2}H	—	−0.00060615	0.080215	^{2}H	—	−0.00059691	0.084567
^{232}Th	0.0026177	−0.08609	−0.077601	^{232}Th	0.0026676	−0.088548	−0.079457
^{241}Pu	0.12783	−0.050587	0.077113	^{241}Pu	0.12745	−0.050474	0.076847
^{240}Pu	0.0034679	−0.079097	−0.074703	^{240}Pu	0.0035121	−0.078398	−0.074029
^{56}Fe	—	−0.021689	−0.024036	^{56}Fe	—	−0.021652	−0.024137
^{58}Ni	—	−0.011992	−0.013374	^{58}Ni	—	−0.011951	−0.013407
^{91}Zr	—	−0.014351	−0.012597	^{91}Zr	—	−0.014077	−0.012248
^{238}Pu	0.0012804	−0.0093472	−0.0081005	^{53}Cr	—	−0.0079564	−0.0080781
^{53}Cr	—	−0.0079813	−0.0080932	^{1}H	—	−0.034593	−0.0079826

- The thermal utilization factor increases by 10.60 mk and 1.35 mk at the channel inlet and outlet, respectively, due to the decrease in ^{1}H neutron absorption within the thermal energy range. The effect is larger at the channel inlet since the unperturbed coolant density has a higher initial value.
- The reproduction factor increases slightly causing the reactivity to increase by 1.78 mk and 0.62 mk at the bottom and top of the channel, respectively, resulting largely from higher neutron production rate of ^{240}Pu and ^{241}Pu consistent with the previous discussion for the NOC case.

The highest sensitivity nuclides at the channel inlet and outlet for the OCV case are listed in Table 11. The increase of fission sensitivities of ^{238}Pu, ^{240}Pu, and ^{232}Th explain the increase of the fast fission factor. The ^{2}H sensitivity increases as discussed previously, confirming the increase of neutron interactions with the heavy-water moderator nuclides. ^{1}H absorption and scattering sensitivities decrease slightly with fewer coolant interactions while the decrease in ^{1}H absorption sensitivity explains the increase of the thermal utilization factor. It is interesting to note that for the OCV case ^{1}H does not appear in the highest sensitivity list at the bottom of the channel while it is at the top of the channel. Further investigation shows that ^{1}H negative absorption sensitivity partially offsets the positive scattering sensitivity such that the net sensitivity is small. At the top of the channel the incremental change in absorption with voiding from an already low density is much smaller, therefore not offsetting the scattering sensitivity to the same extent. Thus, ^{1}H appears in the sensitivity list at the top of the channel but not at the bottom.

The uncertainty due to nuclear data was found to be 6.71 mk and 6.81 mk at the bottom and top of the channel, respectively. The highest contributors to uncertainty are presented in Table 7. In comparison with the reference NOC case, the uncertainty in k_{∞} due to the nuclear data library decreases slightly, mainly due to the decrease in the uncertainty contributions from the fuel isotopes. Compared with the ICV case, the uncertainty contributions differ in magnitude owing to the much harder spectra in the ICV relative to the OCV case.

4.2.3. Total coolant void case

The TCV case considers the perturbation in the density of coolant flowing through both the outer and the central flow tubes to decrease uniformly as would occur for equilibrium LOCA conditions. The TCV case shows a negative TCV reactivity with a value of −11.31 mk and −18.15 mk at the channel inlet and outlet, respectively. In the TCV case, the role of coolant in neutron moderation will be eliminated and consequently, neutron moderation would be restricted to the heavy-water moderator. Similar to the ICV case, resonance escape probability would decrease significantly. However, the thermal utilization factor increases due to fewer neutron absorptions in the coolant and fast-fission fraction would increase under the harder spectrum. The net negative TCV reactivity thus results from:

- The resonance escape probability decreases by −150.64 mk and −135.39 mk at the channel inlet and outlet, respectively. The phenomena and direction of the changes are consistent with the results from the previous sections, with the net effect being larger than the linear combination of the ICV and OCV cases.
- The reduction in cell moderation leads to an increase in the fast fission by +109.13 mk and +93.41 mk at the channel inlet and outlet, respectively. Pre-existing lower density coolant at the fuel region at the top of the channel causes a lower increase in the fast fission factor as compared with the inlet.
- The sharp drop of neutron thermal absorption causes the reactivity to increase by 28.36 mk at the channel

TABLE 12. The top nuclear data sensitivity components at 25 cm and 475 cm for the fuel temperature reactivity coefficient.

At 25 cm from the bottom of the channel				At 475 cm from the bottom of the channel			
Nuclide	Fission	Capture	Total	Nuclide	Fission	Capture	Total
^{239}Pu	0.30962	−0.20723	0.10212	^{239}Pu	0.30791	−0.20332	0.10422
^{240}Pu	0.0031731	−0.082277	−0.078137	^{2}H	—	−0.00059909	0.085757
^{241}Pu	0.1259	−0.049641	0.07616	^{232}Th	0.0026879	−0.090699	−0.080829
^{232}Th	0.0024898	−0.08316	−0.074685	^{241}Pu	0.12709	−0.05015	0.076809
^{2}H	—	−0.0006098	0.06344	^{240}Pu	0.003514	−0.078967	−0.074563
^{56}Fe	—	−0.023007	−0.02493	^{56}Fe	—	−0.021772	−0.024103
^{58}Ni	—	−0.012542	−0.013664	^{58}Ni	—	−0.011976	−0.013327
^{91}Zr	—	−0.014438	−0.013278	^{91}Zr	—	−0.014109	−0.01234
^{53}Cr	—	−0.0084876	−0.0085705	^{53}Cr	—	−0.0079915	−0.0081052
^{1}H	—	−0.035199	−0.0078181	^{1}H	—	−0.03489	−0.0080014

inlet and 23.49 mk at the channel outlet, largely driven by the removal of ^{1}H as an absorber.

- The reproduction factor increases slightly producing a positive reactivity of 1.85 mk and 0.33 mk at the bottom and top of the channel, respectively. Similar to the previous discussion, the reproduction factor increases with the higher production rate of ^{240}Pu and ^{241}Pu isotopes that offset the negative contribution of ^{239}Pu and ^{232}Th absorption.

TSUNAMI-2D simulations for the TCV case at the channel inlet and outlet confirms the previous discussion and is consistent with the results discussed in the ICV and OCV cases. The highest contributors to uncertainty in the TCV case at the top and bottom of the channel are given in Table 7. The total uncertainty due to the nuclear data library is 7.06 mk and 7.11 mk at the bottom and top of the channel, respectively. As it can be seen in Table 7, contributions of ^{2}H (n,2n), ^{2}H (elastic), and (n,γ) reactions of the different zirconium isotopes increases in TCV case relative to the reference NOC case. The net changes in total uncertainty are small among the cases considered.

4.3. Fuel temperature coefficient

The fuel temperature reactivity coefficient was investigated at the channel inlet and outlet, and a 100 K increase in the fuel temperature caused the reactivity to decrease by 1.14 mk and 0.99 mk, corresponding to a FTC of −0.0014 mk/K and −0.0099 mk/K, respectively.

The fuel temperature reactivity coefficient is negative due to the Doppler broadening effect as expected and is quite similar to the conventional behaviour of CANDU lattice cell, especially when considering the behaviour of the low-lying fission resonance peak of ^{239}Pu. In the conventional CANDU, the fuel temperature coefficient is negative. However, as the ^{239}Pu builds up with fuel burnup, the fuel temperature coefficient becomes less negative. Since the low-lying resonance peak of ^{239}Pu is a fission peak and the increase in absorption at that peak due to Doppler broadening causes the reactivity to increase, this leads to less negative fuel temperature coefficients as Pu builds up in CANDU fuel. The Canadian PT-SCWR lattice cell is characterized by high ^{239}Pu loading [25] and hence similar behaviour to CANDU is observed i.e., the fuel temperature coefficient is small and negative. Tables 8 and 9 show that the decrease in resonance escape probability is the main contributor to the reactivity difference when the fuel temperature is increased, which corresponds to −1.30 mk and −1.09 mk at the bottom and top of the channel, respectively. A slight increase of fast fission factor is also observed which partially offsets the negative contribution from escape probability.[2]

The highest contributors to nuclear data sensitivity at bottom and top of the fuel channel are presented in Table 12. Increasing of the absorption sensitivity of the fuel isotopes such as ^{232}Th, ^{240}Pu, and ^{241}Pu are consistent with the decrease in resonance escape probability with more fuel absorption. This also explains the decrease of capture sensitivity in ^{56}Fe, ^{58}Ni, ^{91}Zr, and ^{53}Cr due to higher fuel absorption.

4.4. Coolant temperature coefficient

Increasing the coolant temperature by 100 K causes the reactivity to increase by 1.69 mk and 1.86 mk, corresponding to a CTC of 0.0169 mk/K and 0.0186 mk/K at the channel inlet and outlet, respectively.

The most significant change with higher coolant temperature (+100 K) is an increase in thermal utilization factor of

[2]In NEWT, any fissions above 0.635 eV are considered in the fast range, and as such with increased fissions in the low-lying Pu resonance this appears as a small increase in fast fission factor.

4.22 mk and 3.78 mk driven by the up-scatter of neutrons into the low-energy Pu fission resonances. In this case it is the 0.3 eV resonance that plays the strongest role. Increasing the up-scattering of the thermal neutrons has the effect of shifting the thermal flux spectrum peak closer to the 0.3 eV fission resonance. This increases the number of thermal fissions relative to absorptions in other materials leading to a positive thermal utilization effect. The reproduction factor causes the reactivity to decrease by 1.60 mk and 1.08 mk at the channel inlet and outlet, respectively, resulting from a high portion of up-scattered neutrons, some of which are captured in non-fission resonances. It is also noteworthy that SCALE shows a small decrease in the fast fission factor which results from the change in the average neutron temperature in thermal range not from any substantive change in the true fast fission probability. SCALE computes the fast fission factor as the ratio of all fission neutrons to thermal fission neutrons and hence increases in the thermal fission reaction rate will appear as a decrease in the fast fission factor. The shift in the thermal spectra to slightly higher energy increases the portion of neutrons near the 0.3 eV ^{239}Pu peak, which increases thermal fissions, whereas higher energy fissions are less affected. Thus, the predicted changes in fast fission factor are consistent with expectations. Finally, the higher coolant temperatures in the central coolant shift the mean energy of the thermal neutrons in the interior of the cell to higher energy, thereby also increasing the epithermal neutron content. This small increase in the epithermal neutron content decreases the resonance escape probability by a small fraction.

The sensitivity study results shown in Table 13 indicate an increase in the sensitivity to ^{239}Pu, confirming the importance of the up-scattering discussion above. The sensitivity to ^{1}H absorption decreases since up-scattering phenomenon reduces the fraction of neutrons in the thermal absorption band of ^{1}H relative to those being absorbed in the 0.3 eV fission resonance. Due to the importance of ^{1}H absorption and scattering it is also included in the list.

4.5. Moderator temperature coefficient

The moderator temperature was perturbed by increasing its value by 20 K, which causes the reactivity to increase by 0.56 mk and 0.38 mk corresponding to a moderator temperature coefficient of 0.028 mk/K and 0.019 mk/K at the channel inlet and outlet, respectively.

Analysis of the 4-factor components shows that the primary contributor to moderator temperature reactivity is the thermal utilization factor that increases by 0.94 mk at the bottom of the channel and 0.84 mk at the top of the channel. Increasing the moderator temperature causes the energy spectrum of neutrons returning from the heavy-water moderator to shift to slightly higher energies. Such a shift causes a small increase in neutron absorption in the low-lying fission resonances and less absorption in the ^{1}H. Consequently, the thermal utilization factor increases with fewer thermal neutron absorptions. The same phenomena are observed in Figure 3 for MTC as for the CTC case, except an order of magnitude smaller in the MTC case. The discussion on resonance escape and fast fission factor for the CTC case also applies to the MTC case.

The highest sensitivity nuclides obtained by TSUNAMI-2D at the channel inlet and outlet are listed in Table 14. The sensitivity to ^{239}Pu is larger than the reference case again reinforcing the role of the low-lying ^{239}Pu resonances in the observed phenomena, albeit to a lesser extent than the CTC cases (a smaller perturbation was applied in the MTC case). The sensitivity to ^{2}H also increases marginally consistent with increased neutron interaction with the ^{239}Pu resonances at higher moderator temperatures.

TABLE 13. The top nuclear data sensitivity components at 25 cm and 475 cm for the coolant temperature reactivity coefficient.

At 25 cm from the bottom of the channel				At 475 cm from the bottom of the channel			
Nuclide	Fission	Capture	Total	Nuclide	Fission	Capture	Total
^{239}Pu	0.31076	−0.21113	0.099362	^{239}Pu	0.30857	−0.20578	0.10242
^{240}Pu	0.0031533	−0.081561	−0.077426	^{2}H	—	−0.00059788	0.084152
^{241}Pu	0.12457	−0.049309	0.075164	^{232}Th	0.002667	−0.08981	−0.079966
^{232}Th	0.0024705	−0.081722	−0.073255	^{241}Pu	0.12611	−0.049957	0.076022
^{2}H	—	−0.0006096	0.062165	^{240}Pu	0.0034922	−0.078581	−0.074184
^{56}Fe	—	−0.022411	−0.024247	^{56}Fe	—	−0.021398	−0.023645
^{58}Ni	—	−0.012239	−0.013314	^{58}Ni	—	−0.011786	−0.013092
^{91}Zr	—	−0.0144	−0.013249	^{91}Zr	—	−0.014089	−0.01234
^{53}Cr	—	−0.0082634	−0.008345	^{53}Cr	—	−0.0078509	−0.0079637
^{238}Pu	0.0011368	−0.0084472	−0.0073382	^{238}Pu	0.0012623	−0.0088058	−0.0075838
^{1}H	—	−0.033414	−0.0031853	^{1}H	—	−0.032884	−0.0026839

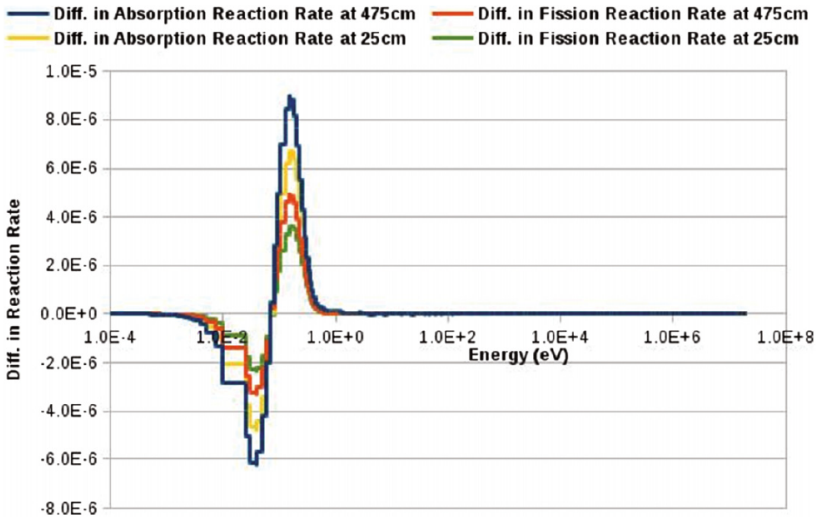

FIGURE 3. Differences in absorption and fission reaction rates between the MTC and reference cases at the top and bottom of the channel.

TABLE 14. The top nuclear data sensitivity components at 25 cm and 475 cm for the moderator temperature reactivity coefficient.

At 25 cm from the bottom of the channel				At 475 cm from the bottom of the channel			
Nuclide	Fission	Capture	Total	Nuclide	Fission	Capture	Total
^{239}Pu	0.30952	−0.20761	0.10164	^{239}Pu	0.3079	−0.20391	0.10363
^{240}Pu	0.0031612	−0.082223	−0.078081	^{2}H	—	−0.00058754	0.085755
^{241}Pu	0.12581	−0.049621	0.076094	^{232}Th	—	−0.090175	−0.080315
^{232}Th	0.0024781	−0.082563	−0.074109	^{241}Pu	0.12699	−0.050105	0.076762
^{2}H	—	−0.0005975	0.063543	^{240}Pu	—	−0.078884	−0.074475
^{56}Fe	—	−0.022895	−0.024798	^{56}Fe	—	−0.021647	−0.023954
^{58}Ni	—	−0.012484	−0.013595	^{58}Ni	—	−0.011912	−0.01325
^{91}Zr	—	−0.014287	−0.013122	^{91}Zr	—	−0.01398	−0.012206
^{53}Cr	—	−0.0084451	−0.0085268	^{1}H	—	−0.034885	−0.0084595
^{1}H	—	−0.035156	−0.0082467	^{53}Cr	—	−0.0079444	−0.0080566

5. Conclusion

The lattice physics phenomena of the Canadian PT-SCWR 64-element design with fresh fuel were investigated. Isotopes, nuclides, and reactions with highest contributions to either nuclear data sensitivities or uncertainty were identified. Moreover, the different perturbed scenarios of CVR, FTC, CTC, and MTC were also investigated. The reactivity changes for different loss of coolant scenarios were investigated at the channel inlet and outlet.

The main conclusions from this work are:

1. The decreased lattice pitch of the SCWR relative to CANDU results in a harder neutron spectrum for the neutrons returning from the heavy-water moderator. This makes the resonance escape probability particularly sensitive to the light-water coolant properties in the fuel region of the assembly. The resonance escape probability also decreases with decreasing inner coolant density as expected.
2. Fast fission is also affected by the coolant properties in both the inner and outer coolant regions, mainly as a result of the high enrichment and harder spectrums with decreasing coolant densities.

3. As a result of the above, the partial voiding of a lattice where coolant in this fuel region is voided leads to a small positive reactivity, whereas voiding in the center tube results in a strong negative reactivity.
4. The fuel temperature reactivity largely behaves in a consistent manner as traditional CANDU designs.
5. Due to the very high temperature coolant, up-scattering into the low-lying fission and capture resonances leads is important and particularly affects the coolant temperature reactivity.

ACKNOWLEDGEMENTS

Funding to the Canada Gen-IV National Program was provided by Natural Resources Canada through the office of Energy Research and Development, Canadian Nuclear Laboratories (formerly Atomic Energy of Canada Limited), and the Natural Sciences and Engineering Research Council of Canada (Project NNAPJ 422784-11). The authors would also like to thank Professor Guy Marleau at École Polytechnique de Montréal for his valuable insight and discussions.

REFERENCES

[1] U.S. DOE Nuclear Energy Research Advisory Committee, 2002, "A Technology Roadmap for Generation IV Nuclear Energy Systems," GIF-002-00, http://gif.inel.gov/roadmap/pdfs/gen_iv_roadmap.pdf.

[2] L. Leung, M. Yetisir, W. Diamond, D. Martin, J. Pencer, B. Hyland et al, 2011, "A Next Generation Heavy Water Nuclear Reactor with Supercritical Water as Coolant," International Conference on the Future of Heavy Water Reactors (HWR-Future). Ottawa, ON.

[3] M. Yetisir, M. Gaudet, and D. Rhodes, 2013, "Development and Integration of Canadian SCWR Concept with Counter-Flow Fuel Assembly," The 6th International Symposium on Supercritical Water Reactor (ISSCWR-6). Shenzhen, Guangdong, China.

[4] J. Pencer and A. Colton, 2013, "Progression of the Lattice Physics Concept for the Canadian Supercritical Water Reactor," 34th Annual Conference of the Canadian Nuclear Society. Toronto, ON.

[5] J. Pencer, D. Watts, A. Colton, X. Wang, L. Blomeley, V. Anghel, and S. Yue, 2013, "Core Neutronics for the Canadian SCWR Conceptual Design," The 6th International Symposium on SCWR (ISSCWR-6). Shenzhen, Guangdong, China.

[6] D.W. Hummel, S.E. Langton, M.R. Ball, D.R. Novog, and A. Buijs, 2013, "Description and preliminary Results of a Two-dimensional Lattice Physics Code Benchmark for the Canadian Pressure Tube Supercritical Water-cooled Reactor (PT-SCWR)," The 6th International Symposium on Supercritical Water-Cooled Reactors (ISSCWR-6). Shenzhen, Guangdong, China.

[7] D.W. Hummel, S.E. Langton, M.R. Ball, D.R. Novog, and A. Buijs, 2013, "Description and Results of a Two-dimensional Lattice Physics Code Benchmark for the Canadian Pressure Tube Supercritical Water-cooled Reactor (PT-SCWR)," 34th Annual Conference of the Canadian Nuclear Society. Toronto, ON.

[8] J. Sharpe, F. Salaun, D. Hummel, A. Moghrabi, M. Nowak, J. Pencer et al, 2015, "A Benchmark Comparison of the Canadian Supercritical Water-cooled Reactor (SCWR) 64-element Fuel Lattice Cell Parameters Using Various Computer Codes," 35th Annual Conference of the Canadian Nuclear Society. Saint John, New Brunswick, Canada.

[9] G. Harrisson and G. Marleau, 2012, "Modeling of a 3-D SCWR Unit Cell," The 3rd China-Canada Joint Workshop on Supercritical-Water-Cooled Reactors (CCSC-2012). Xian, China.

[10] P. Adouki and G. Marleau, 2012, "Neutronics/Thermalhydraulics Coupling in a CANDU SCWR," The 3rd China-Canada Joint Workshop on Supercritical-Water-Cooled Reactors (CCSC-2012). Xian, China.

[11] D.W. Hummel and D.R. Novog, 2015, "Coupled 3D Neutron Kinetics and Thermalhydraulic Characteristics of the Canadian SCWR," The 7th International Symposium on Supercritical Water-Cooled Reactors (ISSCWR-7). Helsinki, Finland.

[12] M.A. DeHart and M.D. Jessee, 2011, "NEWT: A New Transport Algorithm for Two-dimensional Discrete-ordinates Analysis in Non-orthogonal Geometries," Tech. Rep. ORNL/TM-2005/39 Version 6.1 Sect. F21, Oak Ridge National Laboratory.

[13] Oak Ridge National Laboratories, 2013, SCALE: A Modular Code System for Performing Standardized Computer Analysis for Licensing Evaluation, Version 6.1.3.

[14] L.M. Petrie and B.T. Rearden, 2011, "MCDANCOFF Data Guide," Tech. Rep. ORNL/TM-2005/39 Version 6.1 Sect. M24. Oak Ridge National Laboratory.

[15] Oak Ridge National Laboratories, 2011, Scale: A Comprehensive Modeling and Simulation Suite for Nuclear Safety Analysis and Design, ORNL/TM-2005/39, Version 6.1. Radiation Safety Information Computational Center at Oak Ridge National Laboratory as CCC-785.

[16] S. Younan and D. Novog, 2016, "Important of Coolant Densities in TRITON Self-shielding Calculation for the Canadian SCWR," 40th Annual CNS/CNA Student Conference. Toronto, ON.

[17] E. Canuti, A. Petruzzi, F. D'Auria, and T. Kozlowski, 2012, "Sensitivity Studies for the Exercise I-1 of the OECD/UAM Benchmark," Science and Technology of Nuclear Installations.

[18] S.M. Bowman, 2011, "SCALE 6: Comprehensive Nuclear Safety Analysis Code System," Nuclear Technology, 174, pp. 126–148. doi: 10.13182/NT10-163.

[19] M.A. Jessee and M.D. Dehart, 2011, "TRITON: A Multipurpose Transport, Depletion, and Sensitivity and Uncertainty Analysis Module," Tech. Rep. ORNL/TM-2005/39 Version 6.1 Sect. T1, Oak Ridge National Laboratory.

[20] B.T. Reardon, 2011, "TSUNAMI-3D: Control Module for Three-dimensional Cross-section Sensitivity and Uncertainty Analysis for Criticality," Tech. Rep. ORNL/TM-2005/39 Version 6.1 Sect. C9, Oak Ridge National Laboratory.

[21] M.L. Williams, D. Wiarda, G. Arbanas, and B.L. Broadhead, 2011, "SAMS: Sensitivity Analysis Module for SCALE," Tech. Rep. ORNL/TM-2005/39 Version 6.1 Sect. F22, Oak Ridge National Laboratory.

[22] B.T. Rearden, M.L. Williams, M.A. Jessee, D.E. Mueller, and D.A. Wiarda, 2011, "Sensitivity and Uncertainty Analysis Capabilities and Data in SCALE," Nuclear Technology, 174, pp. 236–288. doi: 10.13182/NT174-236.

[23] C.R. Weisbin, J.H. Marable, J.L. Lucius, E.M. Oblow, F.R. Mynatt, R.W. Peelle, and F.G. Perey, 1976, Application of FORSS Sensitivity and Uncertainty Methodology to Fast Reactor Benchmark Analysis. Oak Ridge National Laboratory, Virginia, USA.

[24] M.L. Williams, D. Wiarda, G. Arbanas, and B.L. Broadhead, 2011, "SCALE Nuclear Data Covariance Library," Tech. Rep. ORNL/TM-2005/39 Version 6.1 Sect. M19, Oak Ridge National Laboratory.

[25] J. Pencer, M. McDonald, and V. Anghel, 2014, "Parameters for Transient Response Modelling for the Canadian SCWR," The 19th Pacific Basin Nuclear Conference (PBNC 2014). Vancouver, BC.

[26] D.W. Hummel, 2015, Coupled Nuetronic-Thermalhydraulic Transient Behaviour of Pressure Tube Type Supercritical Water-cooled Reactor. Hamilton, ON.

[27] L. Blomeley, J. Pencer, B. Hyland, and F.P. Adams, 2014, "Nuclear Data Sensitivity and Uncertainty for the Canadian Supercritical Water-Cooled Reactor," Annals of Nuclear Energy, 63, pp. 587–593. doi: 10.1016/j.anucene.2013.08.029.

[28] S.E. Langton, A. Buijs, and J. Pencer, 2015, "Nuclear Data Sensitivity and Uncertainty for the Canadian Supercritical Water-Cooled Reactor II: Full Core Analysis," Annals of Nuclear Energy, 75, pp. 635–644. doi: 10.1016/j.anucene.2014.09.017.

Chapter 5

Investigation of Fuel Burnup Impacts on Nuclear Reactor Safety Parameters in the Canadian Pressure Tube Supercritical Water-cool Reactor

This paper was accepted by the Journal of Nuclear Engineering and Radiation Science with digital object identifier given by doi:10.1115/1.4037895. It is cited as:

'Moghrabi A, Novog D., "Investigation of Fuel Burnup Impacts on Nuclear Reactor Safety Parameters in the Canadian Pressure Tube Supercritical Water-Cool Reactor," ASME. ASME Journal of Nuclear Radiation Science. 2017;4(1):011011-011011-11. doi:10.1115/1.4037895.'

This work expands the analysis performed in the previous publication which was limited to fresh fuel lattice cell. Rather, it compares and contrast between fresh and irradiated fuel to investigate the effects of fuel burnup on the lattice physics phenomena through a sensitivity and uncertainty analysis.

Investigation of Fuel Burnup Impacts on Nuclear Reactor Safety Parameters in the Canadian Pressure Tube Supercritical Water-Cool Reactor

Ahmad Moghrabi
Department of Engineering Physics,
McMaster University,
1280 Main Street West,
Hamilton, ON L8S 4L8, Canada
e-mail: moghraam@mcmaster.ca

David Raymond Novog
Department of Engineering Physics,
McMaster University,
1280 Main Street West,
Hamilton, ON L8S 4L8, Canada
e-mail: novog@mcmaster.ca

The Canadian pressure-tube super critical water-cooled reactor (PT-SCWR) is an advanced generation IV reactor concept which is considered as an evolution of the conventional Canada Deuterium Uranium (CANDU) reactor that includes both pressure tubes and a low temperature and pressure heavy water moderator. The Canadian PT-SCWR fuel assembly utilizes a plutonium and thorium fuel mixture with supercritical light water coolant flowing through the high-efficiency re-entrance channel (HERC). In this work, the impact of fuel depletion on the evolution of lattice physics phenomena was investigated starting from fresh fuel to burnup conditions (25 MW d kg^{-1} [HM]) through sensitivity and uncertainty analyses using the lattice physics modules in standardized computer analysis for licensing evaluation (SCALE). Given the evolution of key phenomena such as void reactivity in traditional CANDU reactors with burnup, this study focuses on the impact of fission products, ^{233}U breeding, and minor actinides on fuel performance. The work shows that the most significant change in fuel properties with burnup is the depletion of fission isotopes of Pu and the buildup of high-neutron cross section fission products, resulting in a decrease in cell k_∞ with burnup as expected. Other impacts such as the presence of protactinium and uranium-233 are also discussed. When the feedback coefficients are assessed in terms of reactivity, there is considerable variation as a function of fuel depletion; however, when assessed as Δk (without normalization to the reference reactivity which changes with burnup), the net changes are almost invariant with depletion. [DOI: 10.1115/1.4037895]

1 Introduction

The Canadian pressure tube super-critical water-cooled reactor (PT-SCWR) is a generation IV reactor concept utilizing a pressure tube design with supercritical light water as coolant. It is considered as an evolution of the Canada Deuterium Uranium (CANDU) reactor maintaining key features such as separation of the high-pressure coolant and the low-temperature and pressure heavy water moderator [1].

The PT-SCWR fuel channel design utilizes a re-entrant coolant flow path which is termed the high-efficiency re-entrant channel (HERC). As shown in Fig. 1 [2], the coolant flows from the inlet plenum at 350 °C and 25.8 MPa downward through the center flow tube in each fuel assembly. The coolant at the bottom of the channel is redirected upward around the fuel elements to the outlet plenum where it exits the fuel channel at 625 °C and 25.0 MPa. The Canadian PT-SCWR reference design includes a 64-element fuel assembly arranged in two concentric rings with 15% and 12% PuO_2 in ThO_2 in the inner and outer rings, respectively [3]. The PT-SCWR core is vertically oriented and batched fueled, where the fuel assembly has a 5 m active length and zirconium modified stainless steel cladding [3] with isotopic atomistic densities, material temperatures, and geometry specifications given by Hummel [2].

Owing to the significant differences in HERC fuel design relative to the standard CANDU reactor lattice, a benchmark analysis was performed comparing the two-dimensional (2D) lattice level neutronic behavior for the different lattice physics code applications [4]. Moreover, a recent sensitivity and uncertainty study for the PT-SCWR lattice cell with fresh fuel concluded that although the changes in net reactivity from lattice level perturbations were small (e.g., coolant density and fuel temperature feedbacks), these results were in fact driven by large and opposing changes in key lattice physics phenomena [5]. Given the considerable differences in fuel composition with burnup, the evolution of these offsetting reactivity differences must be considered. In this work, sensitivity and uncertainty analyses were performed using the standardized computer analysis for licensing evaluation (SCALE) code to assess the changes in these phenomena expected throughout a fueling cycle (25 MW d kg^{-1} [HM]).

2 Modeling and Calculation Methods

Simulations and lattice cell calculations were performed using the 238 energy group ENDF/VII.0 library distributed in SCALE version 6.3.1 [6,7]. Fuel burnup simulations were performed with the transport rigor implemented with time-dependent operation for neutronic depletion [8] module that employs new extended step characteristics-based weighting transport code (NEWT) [9] as multigroup transport solver. NEWT is a deterministic code that solves the neutron transport equation using the discrete ordinates method utilizing both the extended step characteristics approximation and the method of characteristics within the mesh. This makes it highly sensitive to the cell mesh, and therefore, a mesh-

Manuscript received May 23, 2017; final manuscript received August 24, 2017; published online December 4, 2017. Assoc. Editor: Thomas Schulenberg.

size sensitivity study was performed to determine the mesh quality necessary such that the code outputs' sensitivity to further mesh refinement was minimal [5]. NEWT was used to examine the reaction rates, the homogenized cross sections, flux spectrum, the components of the four-factor formula, and the neutron multiplication factor for the infinite lattice cell.

In addition to the geometrical input, NEWT requires information for self-shielding since the PT-SCWR lattice cell is characterized by concentric fuel rings which is different from the regular square lattice of light water reactors. Consequently, Dancoff factors (DFs), which are used by NEWT to perform accurate self-shielding calculations for fuels with nonsquare lattice pitch, were calculated a priori for all the study cases using Monte Carlo DANCOFF [10]. Ideally, DFs vary with the fuel pin positions; however, fuel pins located within the same ring have very similar DFs. A sensitivity study shows that the small changes in DFs have a minor effect on the transport calculations, and therefore, an average value was calculated for each fuel ring to be consistent with the previous study [5] and the SCALE manual recommendation [7]. NEWT performs the self-shielding calculation using the dan2pitch card that relies on the precalculated DFs to determine the equivalent lattice pitch. This approach has a limitation due to many constraints and factors, especially the coolant density [11]. As a result, an altered coolant density of 0.4 g/cm^3 was used in the self-shielding calculation when the coolant density in the fuel region drops below 0.4 g/cm^3 since this methodology proved to be the most consistent when compared to continuous energy results [11].

The nuclear data sensitivity and uncertainty analysis presented in this work was performed using tools for sensitivity and uncertainty analysis methodology implementation (TSUNAMI)-2D code [6–8,12,13]. TSUNAMI-2D executes the NEWT module in SCALE to calculate the forward and the adjoint flux solutions that are used by sensitivity analysis module for SCALE (SAMS) [6,14,15] to generate the sensitivity coefficients for k_∞ with respect to each cross section. SAMS determines the sensitivity coefficients for each energy group and reaction as nondimensional quantity defined as percentage effect on the system's neutron multiplication factor, k, to a percentage change in the nuclear reaction cross sections. For the cross section nuclear $\Sigma^i_{x,g}$ with the process x of nuclide i in energy group g, the sensitivity coefficient as a function of the neutron multiplication factor can be expressed as [15]

$$\text{sensitivity} = \frac{dk}{k}\frac{\Sigma^i_{x,g}}{d\Sigma^i_{x,g}} \tag{1}$$

In SCALE 6.3.1, SAMS modules calculate the total sensitivity (complete sensitivity) of the neutron multiplication factor as a combination of two factors: the implicit and the explicit terms. The total sensitivity is given by [15]

$$\left(S_{k,\Sigma^i_{x,g}}\right)_{\text{total}} = \left(S_{k,\Sigma^i_{x,g}}\right)_{\text{explicit}} + \left(S_{k,\Sigma^i_{x,g}}\right)_{\text{implicit}} = \frac{\Sigma^i_{x,g}}{k}\frac{\partial k}{\partial \Sigma^i_{x,g}} + \sum_j \sum_h \frac{\Sigma^j_{y,h}}{k}\frac{\partial k}{\partial \Sigma^j_{y,h}} \times \frac{\Sigma^i_{x,g}}{\Sigma^j_{y,h}}\frac{\partial \Sigma^j_{y,h}}{\partial \Sigma^i_{x,g}} \tag{2}$$

where $\Sigma^j_{y,h}$ represents the cross section nuclear data component for the process y of nuclide j in energy group h. The explicit sensitivity component relates to the sensitivity of the neutron multiplication factor to a direct perturbation in the cross section data, while the implicit sensitivity component determines the sensitivity resulting from self-shielding phenomena [15]. It is noteworthy that in both terms of sensitivity, $1/k$ is present, and hence, the sensitivities reported by NEWT are normalized to a reference multiplication constant, which itself is a function of burnup.

The scenario selection, geometry, and lattice meshing in this work are consistent with the methodology proposed by Moghrabi and Novog [5] used for fresh fuel, so a comparison between fresh and burnup fuels can be achieved. Based on this previous work, simulations were performed at two axial positions: 25 cm and 475 cm from the bottom of the channel to access the lattice cell characteristics at the bottom (channel inlet) and top (channel outlet) of the channel, respectively. The temperatures and properties of the different lattice cell components at 25 cm and 475 cm were taken from Sharpe et al. [4], and the DFs used are given in Moghrabi and Novog [5]. In this work, the effect of fuel irradiation (25 MW d kg^{-1} [HM]) on lattice cell physics phenomena was investigated through sensitivity and uncertainty analysis of the nuclear data library for the normal operating condition (NOC) and a set of perturbed cases as listed in Table 1.

3 Results

3.1 Normal Operating Conditions. To investigate the effects of fuel burnup, the components of the four-factor formula were examined and a comparison between fresh and burnup cases was performed at the bottom and top of the fuel channel as outlined below.

3.1.1 Effect of Depletion on the Four-Factor Formula. The value of each of the four factors was calculated for fresh and irradiated fuels at the bottom of the channel (at 25 cm from the

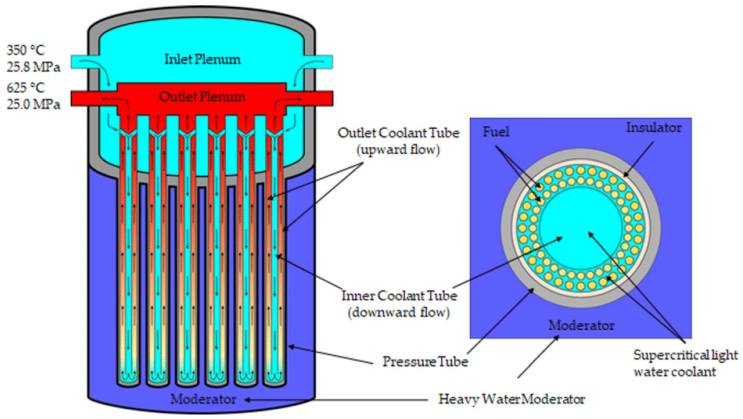

Fig. 1 Core and lattice cell cross section view of PT-SCWR HERC concept with the 64-element fuel assembly [2]

Table 1 Definition of sensitivity cases

Case name	Description
Reference (NOC)	Nominal temperatures and densities for each lattice cell component
Inner coolant voided	Coolant density in the central flow tube (inner tube) decreases to 0.001 g/cm^3 (unit for expressing the density was selected based on SCALE input parameters)
Outer coolant voided	Coolant density in the outer flow tube decreases to 0.001 g/cm^3
Total coolant voided	Coolant density in both tubes (inner and outer) decreases to 0.001 g/cm^3
Hot fuel	Fuel temperature increased by 100 K
Hot coolant	Inner and outer coolant temperature increased by 100 K
Hot moderator	Moderator temperature increased by 20 K

bottom of the channel) as shown in Table 2. Figure 2 shows a comparison of the multiplication constants and each of the four factors fresh and irradiated SCWR fuels as well as those for a typical CANDU reactor lattice. The main contributor to the decrease in neutron multiplication factor with burnup is the change in reproduction factor (η) as expected. The PT-SCWR is characterized by batch fueling giving rise to excess reactivity (at the beginning of cycle) compared to a conventional CANDU reactor which utilizes online refueling, and hence, has less excess reactivity at zero burnup. A direct comparison of all the factors of the four-factor formula shows that

— The reproduction factor in the PT-SCWR decreases sharply from 1.736 to 1.565 with depletion. The decrease in reproduction factor with burnup results from the depletion of fissile isotopes which directly reduces the reproduction factor. The enrichment of the SCWR fuel results in much higher reproduction factor than that of the natural uranium utilized in CANDU reactor.
— In the PT-SCWR, the thermal utilization factor decreases from 0.861 for fresh fuel to 0.853 at midburnup conditions. The decrease in the thermal utilization factor with fuel burnup is driven by the high absorption of fission products such as ^{135}Xe. Such changes are consistent with the sensitivity results from TSUNAMI that also demonstrate significant negative sensitivities to these isotopes in irradiated fuel. The PT-SCWR has a lower thermal utilization factor than the CANDU reactor due to the high thermal neutron absorption taking place in ^{1}H which was discussed thoroughly in Moghrabi and Novog [5].
— The resonance escape probability decreases slightly with fuel burnup from 0.675 to 0.670 in the PT-SCWR, mainly due to small increases in minor actinides and protactinium (which is bred from thorium). The TSUNAMI analysis discussed later shows that the sensitivities to these isotopes increase in magnitude with burnup, albeit these sensitivities are still small relative to other contributors. A comparison between the PT-SCWR and the CANDU reactor shows that the differences in the lattice pitch and fuel geometry play a significant role; the PT-SCWR is characterized by a tight lattice pitch compared to the CANDU reactor. Consequently, it possesses a harder neutron spectrum. This explains the significantly lower resonance escape probability in the PT-SCWR compared to a typical CANDU reactor.
— As shown in Table 2, the fast fission factor decreases from 1.276 for fresh fuel to 1.262 at midburnup conditions. It is also worthwhile to note that the fast fission is a misnomer in this regard. SCALE computes the fast fission factor in the four-factor formula as the ratio of all fission neutrons to thermal fission neutron with a thermal cut-off set at 0.625 eV. Therefore, the decrease in fissions within the epithermal regions appears as a decrease in fast fissions reported by the code. While SCALE's limitations in this regard show changes in fast-fission within the four-factor formula, a comparison between fission reaction rate spectra shows that high energy fissions, in fact, do not change appreciably with burnup. Given the harder spectrum in the SCWR compared to traditional CANDU reactor designs, the proportions of fissions above 0.625 eV are higher in the SCWR, and hence, SCALE reports this as a larger fast fission factor relative to the CANDU reactor value.

3.1.2 Sensitivity and Uncertainty Analysis. The most significant sensitivities calculated by TSUNAMI-2D for the reference case of the PT-SCWR at the bottom of the channel are presented in Table 3. These sensitivities are integrated over all energy levels and are broken down per reaction for each isotope. A comparison between fresh and irradiated fuels shows that the k_∞ isotopic sensitivities are almost identical. ^{2}H appears in the highest sensitivity list due to its essential role in the neutron moderation process. The most significant change with irradiation is that the system becomes highly sensitive to fission in ^{233}U and absorption in ^{135}Xe which is expected since (i) ^{232}Th is transmuted into ^{233}U with burn-up and (ii) Xenon effects increase with burnup until its concentration is saturated. Other isotopes such as higher order actinides and protactinium also are present in the irradiated case; however, their sensitivity magnitudes are less than those reported in Table 3. It is noteworthy that k_∞ is still highly sensitive to the

Table 2 Values of neutron multiplication factor (k_∞) and the four factors at the top and bottom of the channel

	Distance from bottom of channel			
	25 cm		475 cm	
Factor	Fresh fuel	Burnup fuel	Fresh fuel	Burnup fuel
Reproduction (η)	1.737	1.565	1.739	1.565
Utilization (f)	0.862	0.853	0.868	0.860
Resonance escape probability (p)	0.675	0.671	0.656	0.653
Fast fission (ε)	1.276	1.262	1.303	1.288
Nuetron multiplication (k_∞)	1.289	1.130	1.290	1.132

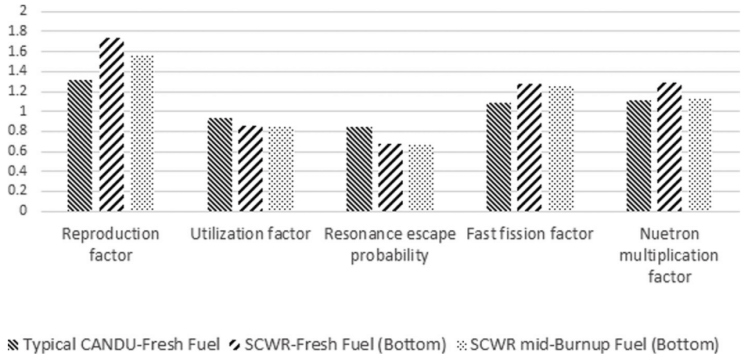

Fig. 2 A comparison between the conventional CANDU reactor and the Canadian PT-SCWR with fresh and burnup fuels

absorption in ^{1}H at midburnup even though it does not appear on the list of most sensitive isotopes. The ^{1}H overall sensitivity becomes small compared to the more sensitivity isotopes in the TSUNAMI analysis since the negative absorption sensitivity cancels the positive scattering contribution, yielding a relatively small total sensitivity compared to these other isotopes. In reality, the individual sensitivities of these reactions are high.

The sensitivities presented in Table 3 can be used to support the description of the physical phenomena in Secs. 2 and 3.1.1. The decrease in the reproduction factor is driven by the reduction in number density of the fissile isotopes relative to all other materials in the lattice. Overall, the sensitivities of the fissile isotopes become more positive, while the sensitivity to nonfissile fuel materials becomes more negative with burnup. This is expected since the number density of fissile components (except ^{233}U) decreases with time hence making the calculation of k more sensitive to the remaining material, while for nonfissile actinides their increasing absorption relative to fission isotopes drives the sensitivity to be more negative. The increase of the negative sensitivities of ^{232}Th and nonfissile Pu materials relative to the fissile materials supports the relative large reductions in the reproduction factor.

Absorption sensitivities of all fuel isotopes and the main structural materials increase except for ^{239}Pu which explains the slight decrease in resonance escape probability and thermal utilization factor through competing phenomena as described earlier. TSUNAMI results have shown less neutron thermal absorption in ^{1}H with burnup which has a positive impact on the thermal utilization factor that will be counterbalanced with the strong absorption (and high sensitivity) of Xe.

The uncertainty in k_{∞} due to uncertainties in the nuclear date library for irradiated fuel was found to be 7.13 mk which is marginally higher than the case for fresh fuel (6.96 mk) [5]. Nuclides with uncertainty contribution higher than 0.5 mk are listed in Table 4. The uncertainties in k_{∞} for ^{239}Pu(υ), which is the main contributor to the uncertainty, and [^{239}Pu(fission), ^{239}Pu(n, γ)] reactions decrease while there is a slight increase in all other uncertainties per isotope and reaction. The primary difference between fresh and burnup fuel cases is that ^{135}Xe (n, γ) uncertainty contributions increase with the increasing irradiation. The small increase in total uncertainty due to fuel burnup is consistent with the conventional behavior of CANDU reactor lattice cell uncertainty analysis. In conventional CANDU reactor, the uncertainty in k_{∞} decreases initially due to the ^{239}Pu peak and then increases thereafter [16]. The negative uncertainty contributions of ^{2}H shown in Table 4 are not truly negative; however, it is actually canceling the impacts of other (positive) uncertainty contributions by accounting for shared sources of uncertainty.

3.1.3 Effect of Elevation on Reactivity. Since the thermal-hydraulic conditions and moderating behavior change significantly from the bottom to the top of the core, the impact on reactivity as a function of elevation was investigated and discussed later. As shown in Table 2, the changes in multiplication and each of the four factors are consistent between the bottom and top of the channel albeit with slightly different magnitudes. The difference in reactivity between the inlet and outlet of the channel is 0.28 mk for fresh fuel and 2.05 mk for depleted fuel as shown in Table 5. Also shown in Table 5 is the contribution of each of the four-factors to the change in reactivity and shows that

Table 3 The top sensitive nuclides and breakdown by reaction at 25 cm for the reference case with fresh and burnup fuels

Fresh					Burnup				
Nuclide	Nubar	Fission	Capture	Total	Nuclide	Nubar	Fission	Capture	Total
^{239}Pu	0.71068	0.30942	−0.20704	0.10211	^{239}Pu	0.61414	0.30200	−0.16435	0.13760
^{240}Pu	0.00538	0.00316	−0.08229	−0.07813	^{241}Pu	0.30923	0.15991	−0.05007	0.10981
^{241}Pu	0.27523	0.12592	−0.04967	0.07616	^{232}Th	0.00824	0.00433	−0.10608	−0.10486
^{232}Th	0.00535	0.00248	−0.08271	−0.07432	^{240}Pu	0.00936	0.00596	−0.09413	−0.08779
^{2}H			−0.00061	0.06269	^{2}H			−0.00058	0.06234
^{56}Fe			−0.02314	−0.02511	^{56}Fe			−0.02149	−0.02316
^{58}Ni			−0.01261	−0.01376	^{233}U	0.05169	0.02545	−0.00368	0.02176
^{91}Zr			−0.01451	−0.01336	^{135}Xe			−0.0171	−0.01715
^{1}H			−0.03533	−0.00897	^{91}Zr			−0.01396	−0.01335
^{53}Cr			−0.00854	−0.00862	^{58}Ni			−0.01171	−0.01261

Table 4 Nuclear data contribution to k_∞ uncertainty in the reference, ICV, OCV, and total coolant void (TCV) cases at 25 cm from the bottom of the channel for fresh and burnup fuels

		Contribution to uncertainty (mk) at 25 cm							
		Fresh fuel				Burnup fuel			
Covariance matrix element		NOC	ICV	OCV	TCV	NOC	ICV	OCV	TCV
^{239}Pu ($\bar{\nu}$)	^{239}Pu ($\bar{\nu}$)	5.63	5.68	5.45	5.51	5.52	5.52	5.37	5.31
^{239}Pu (fission)	^{239}Pu (fission)	1.82	1.80	1.77	1.78	1.98	1.96	1.94	1.93
^{239}Pu (n, γ)	^{239}Pu (n, γ)	1.72	1.63	1.62	1.51	1.54	1.43	1.45	1.31
^{239}Pu (fission)	^{239}Pu (n, γ)	1.57	1.44	1.47	1.31	1.53	1.37	1.43	1.24
^{240}Pu (n, γ)	^{240}Pu (n, γ)	1.07	1.08	1.00	0.98	1.40	1.39	1.33	1.28
^{56}Fe (n, γ)	^{56}Fe (n, γ)	1.05	0.98	0.97	0.92	1.13	1.06	1.01	0.97
^{92}Zr (n, γ)	^{92}Zr (n, γ)	1.01	1.35	0.89	1.26	1.09	1.50	0.94	1.34
^{2}H (n, 2 n)	^{2}H (elastic)	−1.00	−1.39	−1.18	−1.80	−1.09	−1.56	−1.30	−1.95
^{2}H (n, 2 n)	^{2}H (n, 2 n)	1.04	1.22	1.14	1.34	1.08	1.28	1.17	1.39
^{2}H (elastic)	^{2}H (elastic)	0.95	1.55	1.20	2.38	1.08	1.85	1.43	2.69
^{241}Pu (fission)	^{241}Pu (fission)	0.69	0.66	0.68	0.68	0.97	0.95	0.96	0.98
^{232}Th (n, γ)	^{232}Th (n, γ)	0.63	0.74	0.57	0.54	0.84	1.08	0.86	1.10
^{91}Zr (n, γ)	^{91}Zr (n, γ)	0.75	1.01	0.69	0.99	0.81	1.12	0.73	1.06
^{241}Pu ($\bar{\nu}$)	^{241}Pu ($\bar{\nu}$)	0.58	0.66	0.63	0.68	0.80	0.84	0.80	0.85
^{90}Zr (n, γ)	^{90}Zr (n, γ)	0.65	0.87	0.58	0.82	0.71	0.97	0.61	0.87
^{242}Pu (n, γ)	^{242}Pu (n, γ)	0.53	0.62	0.49	0.54	0.67	0.77	0.64	0.68
^{58}Ni (n, γ)	^{58}Ni (n, γ)	0.62	0.58	0.57	0.54	0.66	0.62	0.59	0.57
^{135}Xe (n, γ)	^{135}Xe (n, γ)					0.63	0.60	0.63	0.63
^{53}Cr (n, γ)	^{53}Cr (n, γ)	0.56	0.51	0.51	0.48	0.59	0.56	0.53	0.50
Total of contributions above		6.92	7.09	6.67	7.02	7.06	7.27	6.84	7.15
Total from all contributions		6.96	7.14	6.71	7.06	7.13	7.35	6.91	7.24

— The resonance escape probability (p) is the dominant contributor to the reactivity change between the top and the bottom of the channel with a value of −22.28 mk and −23.17 mk in the case of fresh and burnup fuels, respectively. After investigating each reaction with and without the isotopes present with irradiation, we found no significant changes in physics phenomena with relatively insignificant changes in the escape probability. This is particularly evident when one considers that under irradiated conditions, the value of k is smaller, and hence, given k is used in both of the normalizations when calculating the reactivity and in the denominator of the sensitivity coefficients, all contributions are magnified slightly as burnup increases. Hence when we examine Δk, rather than ρ, while we see a large change in resonance escape on a reactivity basis (normalized to the depleted fuel's total reactivity) between the top and bottom of the core, there is almost no change in Δk (not normalized) over this height with burnup.
— The fast fission factor increases by 17.93 mk from the bottom to the top of the core which is slightly higher than the case of fresh fuel (15.96 mk). Since there is a large change in epithermal fission (due to the harder spectra at the top of the channel) between the bottom and top of the core and SCALE reports this as a change in fast fissions. However, these differences are not sensitive to fuel depletion, and again when one considers that the irradiated case has a smaller reference k (which acts to multiply the observed differences), the phenomena remain relatively unchanged. This is supported by examining Δk without normalization, which shows negligible change between the irradiated and a fresh fuel conditions.
— The thermal utilization factor increases with elevation by 7.18 mk for irradiated fuel as compared to 5.41 mk in the fresh fuel case. While the irradiated case shows lower values for both the lower and upper elevation, the absolute differences in k between the bottom and top of the core are very similar, again the reactivity changes reflecting that the absolute values of the reference k are lower in the depleted case.
— The reproduction factor is the largest contributor to k of the four factors and decreases strongly with burnup; however, the differences between the top and bottom of the core are negligible relative to the magnitude of their contribution (on the order of 1 mk or less).

Table 5 Contribution of the four-factors to the reactivity difference between the top and bottom of the channel

	Reactivity difference (mk) between top and bottom of the channel	
	Fresh fuel[a]	Burnup fuel
Reproduction factor (η)	1.20	0.11
Utilization factor (f)	5.41	7.18
Resonance escape probability (p)	−22.28	−23.17
Fast fission factor (ε)	15.96	17.93
Net reactivity change	0.28	2.05

[a]Fresh fuel results was taken from Moghrabi and Novog [5].

3.2 Coolant Density Reactivity. Several studies have identified interesting lattice physics phenomena for the Canadian PT-SCWR [2,5,16] for cases where nonequilibrium voiding conditions occur. Although the concept of coolant void is not relevant to supercritical coolants, it is nevertheless used here for consistency with the existing CANDU reactor literature and should be interpreted as the coolant density reactivity. These interesting lattice physics phenomena may occur during transient events where the inner flow channel coolant density remains relatively unperturbed while the outer coolant density decreases (outer coolant void (OCV)), or when the inner flow channel coolant density drops the outer channel coolant density remains relatively

Table 6 The reactivity change in each of the perturbed cases at the channel inlet and outlet with the corresponding breaking down contributions of the components of the four-factor formula

	Contribution (mk) at 25 cm					
	Fresh			Burnup		
	ICV	OCV	TCV	ICV	OCV	TCV
Reproduction factor (η)	−2.24	1.78	1.85	−7.53	−1.83	−10.64
Thermal utilization factor (f)	18.48	10.60	28.36	21.12	12.80	33.96
Resonance escape probability (p)	−108.52	−23.75	−150.64	−125.77	−25.96	−167.22
Fast fission factor (ε)	72.28	21.46	109.13	81.12	24.01	−121.57
Net reactivity change for the perturbed cases	−20.00	10.10	−11.31	−31.06	9.02	−22.33

unchanged (inner coolant void (ICV)). The term "total coolant void" (TCV) corresponds to the lattice case where the coolant density in the whole fuel assembly drops uniformly within both regions: inner and outer, and is often referred to as equilibrium voiding conditions. The reactivity behavior and the four factors have been investigated using sensitivity and uncertainty analyses for each of the voided cases (ICV, OCV, and TCV). Examination shows that fuel burnup effects at the top and bottom of the channel positions are characterized by the same behavior with a slight change in the degree of magnitude, and consequently, the discussion outlined below considers effects only at the bottom of the channel.

3.2.1 Inner Coolant Void Reactivity. The reactivity decreases in the ICV case at the bottom of the channel are −20.00 and −31.06 mk for fresh fuel and depleted fuel, respectively, as shown in Table 6. The sensitivities presented in Table 7 confirm such negative reactivity responses. These negative reactivity changes are due to large and offsetting physics phenomena. First of all, in the ICV case, neutron moderation through scattering with the ^{1}H in the central tube is eliminated, and consequently, neutrons would have to travel further to reach the heavy water moderator and thus the probability of resonance capture phenomena is increased [5], or alternatively the escape probability decreases (approximately −110 to −120 mk).

With the large reduction in moderation with inner coolant voiding, the neutron flux spectrum becomes harder, and given that SCALE reports any increase in epithermal fissions above 0.625 eV as a contributor to fast fissions, the reported fast fissions increase with voiding. Thus, the fast fission factor increases by 72.28 and 81.12 mk for fresh and depleted fuels although there is no discernable difference in the actual 1 MeV fission rate in either case. In examining the absolute values of the fast fission factor changes with ICV in Fig. 3, the effects are almost identical with the larger reactivity reported in the depleted case resulting from the normalization which has a lower denominator (i.e., k decreases with burnup).

The thermal utilization factor increases due to voiding as expected since the absorption in ^{1}H is reduced and this contributes approximately 18 mk toward the void reactivity. The contribution again increases with burnup due to the lower reference k in the depleted case, although the absolute changes in utilization are approximately identical in both the depleted and fresh fuel cases.

The uncertainty from the nuclear data library in ICV reactivity for the burnup case is slightly higher than the case of fresh fuel as shown in Table 4. The dominant contributor to uncertainty in k_∞ is ^{239}Pu($\bar{\nu}$) reaction consistent with the fresh fuel results. The slight increase in the total uncertainty in k_∞ can be explained based on the physics of the CANDU reactor found in the literature independent of the codes normalization process. The uncertainty in some of the ^{239}Pu reactions and particularly ^{239}Pu($\bar{\nu}$) decreases to counterbalance the increase in the uncertainties from the other reactions causing a slight increase in the total void uncertainty in the case of fuel burnup.

3.2.2 Outer Coolant Void Reactivity. The OCV case possesses a positive reactivity response which must be considered in the safety analysis during loss-of-coolant accident cases with non-equilibrium voiding in the channel. In outer coolant voiding conditions, the reactivity increases by 10.10 mk for fresh fuel and by 9.02 mk for burnup fuel as shown in Table 6. Mainly, the positive contributions of fast fission factor and thermal utilization factor are partially offset by the reduction in negative contribution of the resonance escape probability and the reproduction factor. It is interesting that in the OCV case, the reactivity associated with the

Table 7 The top nuclides for which the *k* calculation is sensitive, along with their components at 25 cm from the bottom of the channel for the ICV case with fresh and burnup fuels

Fresh fuel at 25 cm				Burnup fuel at 25 cm			
Nuclide	Fission	Capture	Total	Nuclide	Fission	Capture	Total
^{239}Pu	0.31104	−0.19936	0.11133	^{239}Pu	0.30135	−0.15338	0.14796
^{2}H		−0.00081	0.09962	^{232}Th	0.00506	−0.12858	−0.12708
^{232}Th	0.00291	−0.10069	−0.08901	^{241}Pu	0.16925	−0.04881	0.12041
^{241}Pu	0.13356	−0.04930	0.08413	^{2}H		−0.00077	0.10279
^{240}Pu	0.00383	−0.08590	−0.08077	^{240}Pu	0.00724	−0.09499	−0.08728
^{56}Fe		−0.02125	−0.02249	^{233}U	0.03039	−0.00415	0.02623
^{91}Zr		−0.01924	−0.01760	^{56}Fe		−0.02008	−0.02123
^{58}Ni		−0.01175	−0.01244	^{91}Zr		−0.01863	−0.01771
^{1}H		−0.00779	0.00958	^{135}Xe		−0.01593	−0.01597
^{242}Pu	0.00091	−0.00916	−0.00813	^{58}Ni		−0.01109	−0.01160

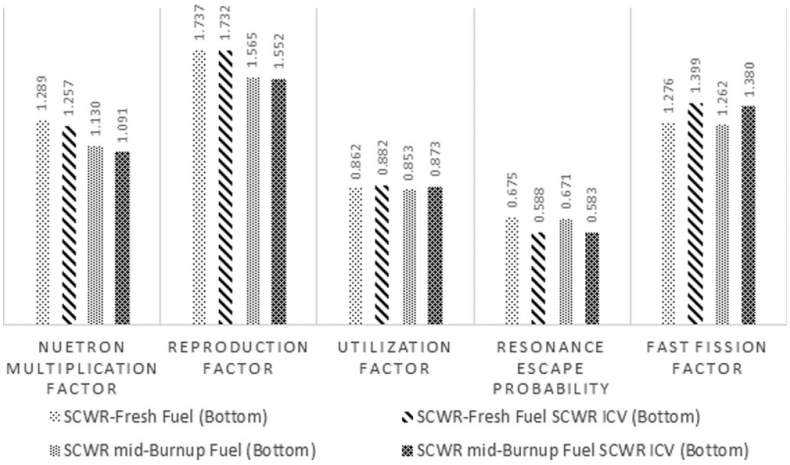

Fig. 3 The absolute values of k_∞ and all the four factors for the reference and the ICV cases for fresh and midburnup fuels at the bottom of the channel

lower density coolant in the outer region of the fuel decreases with burnup. The sensitivities presented in Table 8 confirm such positive reactivity variation at the channel inlet (at 25 cm from bottom of the channel).

Examination of the previous ICV case and top to bottom reactivity changes showed that phenomena were largely consistent in the depleted and fresh fuel cases, with the reactivity effects of these changes being larger in the depleted cases due to the lower reference k value used in the normalization. The same phenomenological behavior was observed for the OCV case. This was confirmed by comparing the change in each of the four factors for both types of fuel as shown in Fig. 4. While examining the changes in reactivity, one sees a significant change in some phenomena and the changes are driven by the denominator (i.e., k) in the normalization process. The relative contribution of the four factors to the OCV reactivity is larger for the irradiated fuel compared to the fresh fuel; however, the absolute change in their values is the almost unchanged with depletion, except for the reproduction factor. The reproduction factor in the OCV case increases by 1.78 mk for fresh fuel, while it decreases by 1.83 mk for depleted fuel, mainly due to less production in ^{239}Pu and ^{241}Pu. This was confirmed through the sensitivity analysis results that show a larger decrease in nubar in ^{239}Pu and ^{241}Pu for depleted fuel compared to fresh fuel. Similar to Secs. 3.1 and 3.2.1, SCALE normalizes the sensitivities to the k at each burnup step, and hence, reported sensitivities will tend to increase with burnup.

The uncertainty due to the nuclear data library for the OCV case with burnup fuel was found to be 6.91 mk which is slightly higher than the case of fresh fuel (6.71 mk) as shown in Table 4. As discussed previously, the decrease in the uncertainty of some of ^{239}Pu reactions and particularly the ^{239}Pu($\bar{\nu}$) reaction counterbalances the increase of the uncertainty in the other isotopes and reactions causing the small positive increase in the total uncertainty in k_∞.

3.2.3 Total Coolant Void Case. The reactivity decreases in the total coolant void case, as per the fundamental design requirements in case of loss-of-coolant accident. Consequently, neutron moderation is taking place only in the low-pressure heavy water moderator with negative reactivity changes of −11.31 mk and −22.33 mk for fresh and depleted fuels, respectively, as presented in Table 6. These reactivity effects are similar to those of the ICV case albeit lower in magnitude since the negative contribution from inner coolant void is partially offset from the effects of outer coolant that exists within the fuel region. As per Table 6, the negative contribution of resonance escape probability and reproduction factor counterbalances the positive contribution of the fast fission

Table 8 The top nuclides for which the k calculation is sensitive, along with their components at 25 cm from the bottom of the channel for the OCV case with fresh and burnup fuels

Fresh fuel at 25 cm from the bottom of the channel				Burnup fuel at 25 cm from the bottom of the channel			
Nuclide	Fission	Capture	Total	Nuclide	Fission	Capture	Total
^{239}Pu	0.30485	−0.19981	0.10471	^{239}Pu	0.29836	−0.15816	0.14015
^{240}Pu	0.00262	−0.00061	0.08022	^{232}Th	0.00463	−0.11260	−0.11160
^{241}Pu	0.12783	−0.08609	−0.07760	^{241}Pu	0.16152	−0.05027	0.11121
^{232}Th	0.00347	−0.05059	0.07711	^{240}Pu	0.00660	−0.09064	−0.08371
^{2}H		−0.07910	−0.07470	^{2}H		−0.00056	0.08223
^{56}Fe		−0.02169	−0.02404	^{233}U	0.02650	−0.00388	0.02260
^{58}Ni		−0.01199	−0.01337	^{56}Fe		−0.01966	−0.02156
^{91}Zr		−0.01435	−0.01260	^{135}Xe		−0.01742	−0.01747
^{1}H	0.00128	−0.00935	−0.00810	^{1}H		−0.02771	0.01344
^{53}Cr		−0.00798	−0.00809	^{91}Zr		−0.01352	−0.01233

factor and thermal utilization factor. Examining the absolute values of the four factors shows that they possess the same change in both types of fuel in TCV case. However, the depleted fuel has a lower reference value of k, and thus, the relative contribution to the total coolant void reactivity in both types of fuel is different. Based on the relative changes in reactivity, the resonance escape probability decreases by 152.64 mk and 167.22 mk for fresh and burnup fuels, respectively. On the other hand, the thermal utilization factor increases by 28.36 mk and 33.96 mk for fresh and burnup fuels, respectively. Due to the total loss of coolant, the neutron spectrum becomes harder compared to the reference case causing an increase in the epithermal fissions (above 0.625 eV) which was reported by SCALE as an increase of fast fissions. Thus, the fast fission increases by 109.13 mk for fresh fuel and by 121.57 mk for burnup fuel at the channel inlet. The most significant change in the case of fuel burnup is the larger negative contribution of the reproduction factor to the change in void reactivity due to the decrease of neutron reproduction in ^{239}Pu with burnup which is expected.

Similar to the previous discussion on the effects of fuel depletion on uncertainty, the total uncertainty in k_∞ due to the nuclear data for the TCV decreases slightly for depleted fuel as shown in Table 4. For the irradiated fuel, the total uncertainty found to be 7.24 mk compared to 7.06 mk for fresh fuel. The increase in the uncertainty of the different isotopes and reactions is counterbalanced by the decrease in the uncertainty of some of Pu reactions; in particular, ^{239}Pu($\bar{\nu}$) is the dominant contributor to the total uncertainty to cause a slight increase of uncertainty with burnup.

3.2.4 Comparison of SCWR and CANDU Reactor Voiding Phenomena. The Canadian PT-SCWR is an advanced nuclear energy system that has interesting and important lattice physics phenomena which are different from the conventional CANDU reactor. A comparison between the Canadian PT-SCWR and the typical CANDU reactor in case of coolant voiding is demonstrated in Fig. 5, where the net coolant void reactivity is shown along with the contributions of each factor of the four-factor formula as per the nuclear reactor design for fresh fuel. As shown in Fig. 5, CANDU reactors have a positive coolant void reactivity, while the PT-SCWR has a positive OCV and negative void reactivity response in both of the ICV and TCV conditions. The main difference between the two nuclear reactor designs is the lattice cell pitch size, multiple coolant flow paths, enrichment, and the subsequent effects on the neutron spectrum. The tight lattice pitch and enrichment in the PT-SCWR cause a harder neutron spectrum as compared to a typical CANDU reactor. In the PT-SCWR, the coolant has an important role in the neutron moderation process and losing the coolant has three major impacts on the lattice cell. First, a large decrease in the resonance escape probability occurs which contribute a large negative feedback. Second, an increase in the epithermal fissions which in SCALE is reported as an increase in fast fissions. Finally, the thermal utilization factor increases with less thermal neutron absorptions in ^{1}H causing a positive contribution to the reactivity. For ICV and TCV cases, the large changes in escape probability dominate, whereas in the OCV case the positive contributions overcome the escape phenomena and dominate. As shown in Fig. 5, the conventional CANDU reactor lattice cell experiences a small increase (compared to the PT-SCWR lattice cell) in the fast fission factor and the thermal utilization factor when the coolant density drops to a very low value. This increase causes a relatively small positive reactivity change (compared to the PT-SCWR) from phenomena similar to those discussed earlier. The CANDU reactor lattice cell is well moderated and the neutron spectrum dominated by thermal neutrons from the moderator. Under normal operating conditions, the thermal neutrons returning back from the moderator collide with the hot coolant and some fractions are up-scattered to energies within the resonance range. In the coolant voiding case, up-scattering with the coolant nuclides does not occur and a larger fraction of returning thermal neutrons will be absorbed directly within the fuel causing more fissions. In addition, there are small positive contributions resulting from the lack of coolant which allows fast neutrons to avoid scattering down to resonance energies during their travel from the fuel to the external moderator. In the PT-SCWR, the neutron spectrum returning from the moderator has a large fraction in the epithermal energy range, and under normal operating conditions, some of these neutrons become thermalized by the thin layer of coolant in the outer region of the bundle. For outer coolant voiding in the PT-SCWR, the phenomena are similar to that in a CANDU reactor with the exception that the contribution from resonance escape phenomena is smaller in magnitude.

3.3 Fuel Temperature Coefficient. The effects of fuel depletion on fuel temperature coefficient (FTC) were investigated at the top and the bottom of the channel. When the fuel temperature is increased by 100 K, the reactivity decreases by 1.20 mk and 1.03

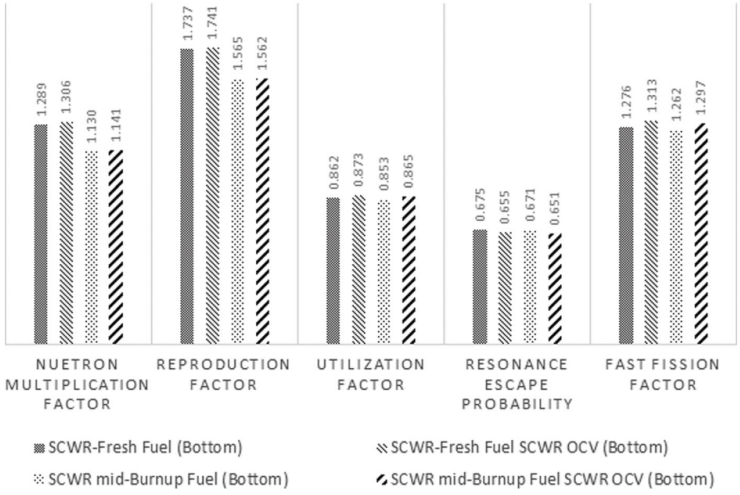

Fig. 4 A comparison between the values of k_∞ and all the four factors for the reference and the OCV cases at the bottom of the channel for fresh and depleted fuels

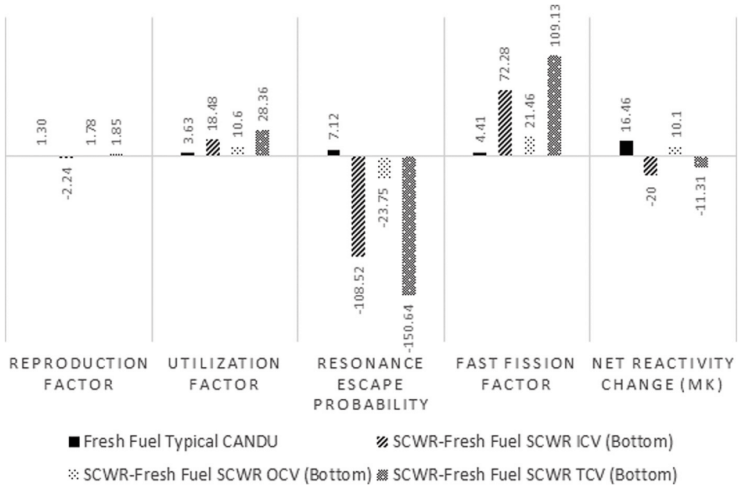

Fig. 5 A comparison of coolant void reactivity between the conventional CANDU reactor and PT-SCWR with a breakdown representing the contribution of each factor in the four-factor formula

Table 9 The reactivity change in each of the perturbed cases at the channel inlet and outlet with the corresponding breaking down contributions of the components of the four-factor formula

	Contribution (mk) at 25 cm					
	Fresh[a]			Burnup		
	FTC	CTC	MTC	FTC	CTC	MTC
Reproduction factor (η)	−0.03	−1.60	−0.19	0.09	1.38	0.18
Thermal utilization factor (f)	0.02	4.21	0.94	0.03	5.11	1.11
Resonance escape probability (p)	−1.30	−0.57	−0.05	−1.38	−0.68	−0.06
Fast fission factor (ε)	0.17	−0.35	−0.14	0.06	−1.10	−0.25
Net reactivity change for the perturbed cases	−1.14	1.69	0.56	−1.20	4.71	0.98

[a]Fresh fuel results were taken from Moghrabi and Novog [5].

mk corresponding to −0.012 mk/K and −0.0103 mk/K at the bottom and top of the channel, respectively. A comparison between fresh and burnt fuels at both positions along the channel shows that the difference in the total reactivity change due to fuel temperature perturbations is relatively small. The fuel temperature coefficient is negative for fresh and burnup fuels at both positions due to the Doppler broadening effect.

Examining the effects of the four factors shows that the Canadian PT-SCWR lattice cell experiences differing behavior to that of the typical CANDU reactor. In CANDU reactor, the low-lying ^{239}Pu peak plays an important role in the fuel temperature reactivity behavior with depletion. The CANDU reactor fresh fuel lattice cell has a small and negative fuel temperature coefficient which becomes much less negative as ^{239}Pu builds up with burnup. Given the increase in absorption in this low-lying fission peak with temperature, the accumulation of ^{239}Pu will tend to make the fuel slightly more reactive with the increasing temperature, although the net FTC remains negative. On the other hand, the PT-SCWR fuel initially contains high Pu loading, and hence, the fuel feedback for fresh fuel is lower in magnitude than CANDU

Table 10 The reactivity change in each of the perturbed cases at the channel inlet and outlet with the corresponding breaking down contributions of the components of the four-factor formula

	Contribution (mk) at 475 cm					
	Fresh[a]			Burnup		
	FTC	CTC	MTC	FTC	CTC	MTC
Reproduction factor (η)	−0.03	−1.08	−0.28	0.08	0.80	0.18
Thermal utilization factor (f)	0.03	3.78	0.84	0.04	4.51	0.98
Resonance escape probability (p)	−1.09	−0.35	−0.08	−1.17	−0.42	−0.10
Fast fission factor (ε)	0.10	−0.49	−0.10	0.02	−1.03	−0.23
Net reactivity change for the perturbed case	−0.99	1.86	0.38	−1.03	3.86	0.83

[a]Fresh fuel results were taken from Moghrabi and Novog [5].

Table 11 The top nuclear data sensitivity components at 25 cm for burnup fuel in case of fuel temperature reactivity coefficient

Nuclide	Nubar	Fission	Capture	Total
^{239}Pu	0.61425	0.30208	−0.16445	0.13759
^{241}Pu	0.30915	0.15989	−0.05007	0.10979
^{232}Th	0.00825	0.00434	−0.10633	−0.10510
^{240}Pu	0.00937	0.00597	−0.09411	−0.08776
^{2}H			−0.00058	0.06270
^{56}Fe			−0.02148	−0.02314
^{233}U	0.05165	0.02544	−0.00368	0.02174
^{135}Xe			−0.01708	−0.01713
^{91}Zr			−0.01397	−0.01335
^{58}Ni			−0.01171	−0.01260

reactor fuel. With fuel depletion, there is a reduction in ^{239}Pu concentration which would tend to make the fuel temperature coefficient more negative, which is consistent with the observed results.

The feedbacks are similar at the top and bottom of the core and throughout the depletion phase as shown in Tables 9 and 10. With the increasing fuel temperature, the dominant phenomenon is the resonance escape probability which decreases by 1.30 mk and 1.38 mk for fresh and depleted fuels, respectively. Such changes arise from Doppler broadening and are consistent with expectations. The effect is slightly higher for depleted fuel due to the relative dependence of the parameters on the reference k which is lower in case of depleted fuel as well as from changing isotopics (i.e., increases in nonfission absorptions). The increase in the absorption sensitivities in Table 11 in most of the fuel isotopes is consistent with the changes in resonance escape probability discussed earlier. The low-lying absorption resonances in ^{239}Pu fission resonance cause a small positive contribution in the thermal utilization factor for both fresh and depleted fuels. The behavior of the reproduction factor changes for depleted fuel compared to fresh fuel although the value of the reproduction factor is very small compared to the net reactivity change. Of note is that the changes in reproduction factor with temperature have different signs when comparing midburnup fuel to fresh fuel conditions. With burnup, the contribution of ^{233}U increases which has a lower capture to fission ratio as compared to the fresh fuel fission isotopes. Hence, when perturbing the fuel temperature, the low-lying ^{233}U fission resonances broaden and thus increase the proportion of fissions coming from ^{233}U which has a higher reproduction factor in general. Sensitivity results shown in Table 11 show the strong sensitivity to ^{233}U fission reaction in the depleted case and the sensitivity tends to increase in the perturbed fuel temperature cases, which is consistent with the rationale provided earlier.

Table 12 The top nuclear data sensitivity components at 25 cm for burnup fuel in case of coolant temperature reactivity coefficient

Nuclide	Nubar	Fission	Capture	Total
^{239}Pu	0.61820	0.30271	−0.16863	0.13403
^{241}Pu	0.30610	0.15790	−0.04996	0.10790
^{232}Th	0.00820	0.00430	−0.10501	−0.10375
^{240}Pu	0.00932	0.005924	−0.09331	−0.08701
^{2}H			−0.00058	0.06193
^{56}Fe			−0.02097	−0.02252
^{233}U	0.05091	0.02507	−0.00365	0.02140
^{135}Xe			−0.01629	−0.01633
^{91}Zr			−0.01393	−0.01331
^{1}H			−0.03113	0.01233

3.4 Coolant Temperature Coefficient. The coolant temperature coefficient (CTC) was investigated at the channel inlet and outlet in case of fuel burnup, and a 100 K increase in the coolant temperature causes the reactivity to increase by 4.71 mk and 3.86 mk for fresh and depleted fuels, respectively, corresponding to a coolant temperature coefficient of 0.0471 mk/K and 0.0386 mk/K.

As shown in Tables 9 and 10, the increase in the thermal utilization factor for fresh and depleted fuels at both positions is the most significant phenomenon related to coolant temperature perturbations. Again, the low-lying Pu fission resonances at approximately 0.3 eV are important contributors. The neutron up-scattering from hot coolant nuclides tends to shift thermal neutrons toward the low-lying Pu resonances. At the bottom of the channel, the thermal utilization factor increases by 4.21 mk and 5.11 mk for fresh and depleted fuels, respectively. The contribution to the relative reactivity change is slightly magnified due to its dependence on the value of k which is lower for irradiated fuel.

Interestingly, the behavior of the reproduction factor changes for burnup fuel compared to fresh due to coolant temperature perturbation. At the bottom of the channel, the reproduction factor decreases by 1.6 mk for fresh fuel, while it increases by 1.38 mk for depleted fuel. Such changes are consistent with the phenomena described in the fuel temperature coefficient results in that the importance of ^{233}U becomes more significant with burnup, and therefore, any changes that increase the proportion of fissions in uranium will tend to increase the overall reproduction factor (since the capture to fission ratio in ^{233}U is lower than that of Pu fuels). Given that higher coolant temperatures will tend to up-scatter neutrons to energies corresponding to the low-lying fission resonances of ^{233}U, the reproduction factor increases with the increasing temperature in depleted fuels where ^{233}U is present. The changes in fast-fission and resonance escape reported by SCALE were small with respect to coolant temperature changes.

The sensitivities of the highest contributing isotopes to the nuclear data sensitivity at the bottom of the channel are listed in Table 12 and confirm the discussion earlier. For fresh fuel, the sensitivity of Pu fissions increases with the increasing coolant temperature which is consistent with the increases in thermal utilization reported earlier. In depleted fuel, the increase in sensitivity in ^{233}U with fuel temperature indicated its increasing importance due to up-scattering within the coolant. As expected, when the coolant temperature is increased, the absorption sensitivity of ^{1}H increases so that it appears in the list of the isotopes with highest contribution to the nuclear data library sensitivities.

3.5 Moderator Temperature Coefficient. The moderator temperature coefficient (MTC) was calculated for depleted fuel by increasing the moderator temperature by 20 K, which causes the reactivity to increase by 0.98 mk and 0.83 mk corresponding to a MTC of 0.049 mk/K and 0.0415 mk/K at the channel inlet and outlet, respectively. Similar to fresh fuel, the outlet is slightly less sensitive to moderator temperature since the coolant temperature is higher in this region which affects the up-scattering and the increase in the thermal utilization factor. The physical phenomena affecting the MTC are identical to those affecting the coolant temperature coefficient.

4 Conclusion

The lattice physics phenomena of the Canadian PT-SCWR 64-element with fuel burnup were investigated. Sensitivity and uncertainty analysis was performed identifying the isotopes, reactions, and nuclides with highest contribution to uncertainty or sensitivity of k_∞ for the reference case and perturbed scenarios. The main conclusion of this work:

(1) The reactivity change and the four factor behavior in case of fuel burnup is quite similar to the fresh fuel case with some differences mainly due to the presence of Xenon and ^{233}U, and changes in the concentration of Pu isotopes.

(2) The tight lattice pitch of the PT-SCWR causes a harder neutron spectrum which increases the importance of the coolant in the neutron moderation process in both fresh and burnup fuel lattices as compared to traditional CANDU reactor designs.
(3) The decrease in neutron reproduction rate is considered as the main contributor to the decrease in reactivity with fuel burnup and results from the overall decrease in fissile content in the fuel with burnup. The system also becomes highly sensitive to ^{233}U and ^{135}Xe with fuel burnup as a consequence of the Th–Pu fuel mixture and fission product behavior.
(4) Overall, the feedback coefficients are consistent between fresh and depleted fuels with only minor changes occurring due to fission product, ^{233}U, and minor actinides build-up as well as Pu depletion. The most significant difference in fuel phenomena in depleted fuel is related to the reproduction factor which may differ significantly under moderator, coolant, or fuel temperature perturbations. These changes are driven by the increasing importance of ^{233}U with fuel burnup since ^{233}U possess a lower capture to fission ratio than that of the Pu fissile isotopes present in fresh fuel. Knowing that the concentration of produced ^{233}U is much smaller compared to the depletion of Pu, the Canadian SCWR is a thermal reactor with a total conversion ratio less than 1.
(5) The Canadian PT-SCWR design has interesting lattice physics phenomena that are different from the conventional CANDU reactor. The Canadian PT-SCWR is characterized by strong negative void reactivity which is important in case of safety analysis and some accident scenarios such as loss of turbine in boiling water reactor or rod ejection in pressurized water reactor; however, small positive void reactivities are possible under nonequilibrium voiding scenarios. These effects do not change significantly with fuel depletion.

Funding Data

- Natural Resources Canada.
- Natural Science and Engineering Research Council.
- Chalk River Nuclear Laboratories.
- The Canadian generation IV program.

Nomenclature

Greek Symbols

ρ = reactivity (mk)
Σ = neutron macroscopic cross section (cm^{-1})

Nondimensional Numbers

f = thermal utilization factor
k = neuron multiplication factor
k_∞ = infinite neuron multiplication factor
n = neutron
p = resonance escape probability
γ = gamma
ε = fast fission factor
η = reproduction factor

Acronyms

CANDU = Canada Deuterium Uranium
CTC = coolant temperature coefficient
DF = Dancoff factor
ENDF = evaluated nuclear data file
FTC = fuel temperature coefficient
HERC = high-efficiency re-entrant channel
HM = heavy metal
ICV = inner coolant void
MTC = moderator temperature coefficient
NEWT = new extended step characteristics-based weighting transport code
NOC = normal operating condition
OCV = outer coolant void
PT-SCWR = pressure tube super critical water-cooled reactor
SAMS = sensitivity analysis module for SCALE
SCALE = standardized computer analysis for licensing evaluation
TCV = total coolant void
TSUNAMI = tools for sensitivity and uncertainty analysis methodology implementation

References

[1] Leung, L. K. H., Yetisir, M., Diamond, W., Martin, D., Pencer, J., Hyland, B., Hamilton, H., Guzonas, D., and Duffey, R., 2011, "A Next Generation Heavy Water Nuclear Reactor With Supercritical Water as Coolant," International Conference on the Future of Heavy Water Reactors (HWR-Future), Ottawa, ON, Canada, Oct. 2–5, pp. 4–12.
[2] Hummel, D. W., 2015, "Coupled Neutronic-Thermalhydraulic Transient Behaviour of Pressure Tube Type Supercritical Water-Cooled Reactor," Ph.D. thesis, McMaster University, Hamilton, ON, Canada.
[3] Pencer, J., McDonald, M., and Anghel, V., 2014, "Parameters for Transient Response Modelling for the Canadian SCWR," 19th Pacific Basin Nuclear Conference (PBNC), Vancouver, BC, Canada, Aug. 24–28, pp. 3–13.
[4] Sharpe, J., Salaun, F., Hummel, D., Moghrabi, A., Nowak, M., Pencer, J., Novog, D., and Buijs, A., 2015, "A Benchmark Comparison of the Canadian Supercritical Water-Cooled Reactor (SCWR) 64-Element Fuel Lattice Cell Parameters Using Various Computer Codes," 35th Annual Conference of the Canadian Nuclear Society (CNS/CNA), Saint John, NB, Canada, May 31–June 2, pp. 7–17.
[5] Moghrabi, A., and Novog, D. R., 2016, "Investigation of Reactor Physics Phenomena in the Canadian Pressure Tube Supercritical Water Reactor," Can. Nucl. Lab. Nucl. Rev., **5**(2), pp. 253–268.
[6] ORNL, 2013, "SCALE: A Modular Code System for Performing Standardized Computer Analysis for Licensing Evaluation," Version 6.1.3, Oak Ridge National Laboratory, Oak Ridge, TN, Report No. NUREG/CR-0200.
[7] ORNL, 2011, "Scale: A Comprehensive Modeling and Simulation Suite for Nuclear Safety Analysis and Design," Version 6.1, Oak Ridge National Laboratory, Oak Ridge, TN, Report No. ORNL/TM-2005/39.
[8] Jessee, M. A., and Dehart, M. D., 2011, "TRITON: A Multipurpose Transport, Depletion, and Sensitivity and Uncertainty Analysis Module," Version 6.1 Sect. T1, Oak Ridge National Laboratory, Oak Ridge, TN, Technical Report No. ORNL/TM-2005/39.
[9] DeHart, M. A., and Jessee, M. D., 2011, "NEWT: A New Transport Algorithm for Two-Dimensional Discrete-Ordinates Analysis in Non-Orthogonal Geometries," Version 6.1 Sect. F21, Oak Ridge National Laboratory, Oak Ridge, TN, Technical Report No. ORNL/TM-2005/39.
[10] Petrie, L. M., and Rearden, B. T., 2011, "MCDANCOFF Data Guide," Version 6.1 Sect. M24, Oak Ridge National Laboratory, Oak Ridge, TN, Technical Report No. ORNL/TM-2005/39.
[11] Younan, S., and Novog, D., 2016, "Important of Coolant Densities in TRITON Self-Shielding Calculation for the Canadian SCWR," 40th Annual CNS/CNA Student Conference, Toronto, ON, Canada, June 19–22, pp. 2–5.
[12] Bowman, S. M., 2011, "SCALE 6: Comprehensive Nuclear Safety Analysis Code System," Nucl. Technol., **174**(2), pp. 126–148.
[13] Reardon, B. T., 2011, "TSUNAMI-3D: Control Module for Three-Dimensional Cross-Section Sensitivity and Uncertainty Analysis for Criticality," Version 6.1 Sect. C9, Oak Ridge National Laboratory, Oak Ridge, TN, Technical Report No. ORNL/TM-2005/39.
[14] Rearden, B. T., Williams, M. L., Jessee, M. A., Mueller, D. E., and Wiarda, D. A., 2011, "Sensitivity and Uncertainty Analysis Capabilities and Data in SCALE," Nucl. Technol., **174**(2), pp. 236–288.
[15] Williams, M. L., Wiarda, D., Arbanas, G., and Broadhead, B. L., 2011, "SAMS: Sensitivity Analysis Module for SCALE," Version 6.1 Sect. F22, Oak Ridge National Laboratory, Oak Ridge, TN, Technical Report No. ORNL/TM-2005/39.
[16] Ball, M. R., 2011, "Uncertainty in Lattice Reactor Physics Calculations," Ph.D. thesis, McMaster University, Hamilton, ON, Canada.

Chapter 6

Determination of the Optimal Few-Energy Group Structure for the Canadian Super Critical Water-cooled Reactor

This paper was published by the Annals of Nuclear Energy it is cited as:

A. Moghrabi, D.R. Novog, Determination of the optimal few-energy group structure for the Canadian Super Critical Water-cooled Reactor, Annals of Nuclear Energy, Volume 115, May 2018, Pages 27-38, ISSN 0306-4549, https://doi.org/10.1016/j.anucene.2018.01.011.

(https://www.sciencedirect.com/science/article/pii/S0306454918300100)

This work investigates the optimum few energy group homogenized structure that is suitable for a wide range of full-core diffusion based simulations for the Canadian PT-SCWR 64-element. A systematic study for the optimization of the few energy group structure is introduced where the energy group selection criterion is based on robust numerical computations.

Annals of Nuclear Energy 115 (2018) 27–38

Contents lists available at ScienceDirect

Annals of Nuclear Energy

journal homepage: www.elsevier.com/locate/anucene

Determination of the optimal few-energy group structure for the Canadian Super Critical Water-cooled Reactor

A. Moghrabi *, D.R. Novog

Department of Engineering Physics, McMaster University, 1280 Main Street West, Hamilton, Ontario L8S 4L8 Canada

ARTICLE INFO

Article history:
Received 16 October 2017
Received in revised form 11 January 2018
Accepted 12 January 2018

Keywords:
Reactor physics
Generation IV
Super Critical Water Reactor
Few-group structure

ABSTRACT

Most deterministic neutron transport codes implement the multi-group approximation theory to solve the linear Boltzmann equation by which the neutron flux and the interaction cross-sections are averaged over discretized energy groups. In order to further reduce the computational cost for large scale and/or time dependent problems, this multi-group information undergoes additional energy group condensation into the so-called few energy group structure which may be used in a broad range of diffusion based full-core analyses. The accuracy and efficiency of few-group based computations is dependent on the number and the boundaries of the discrete energy group structure. Since the flux spectrum used in the homogenization process may not be known a priori and indeed may evolve in space, with burnup, and during transients, the optimal energy group structure depends on reactor type, design, operating conditions, fuel type, and composition. The Canadian Pressure Tube Super-Critical Water-cooled Reactor (PT-SCWR) is a Generation IV advanced reactor system that uses light water above its thermodynamic critical point as coolant and a plutonium-driven thorium fuel mixture. Considering that the anticipated flux spectrum for such a design deviates significantly from the thermal-neutron dominated CANDU designs, there may be a need for improvements in the number and boundaries of the few-group nuclear data. This paper presents a systematic methodology for the delineation of few-group energy structure for the Canadian PT-SCWR. The methodology used the SCALE (Standardized Computer Analysis for Licensing Evaluation) code package to examine the effect of energy group homogenization and determine the structure which minimizes the sensitivity of the results to energy group partitioning. As such, it utilizes normal and off-normal operating conditions to determine the effect of energy homogenization and determines the minimal group of energy boundaries which can accurately capture the lattice physics phenomena within the lattice cell over a wide range of operating and accident conditions.

1. Introduction

The Generation IV International Forum (GIF) has identified six advanced reactor systems to be developed through an international collaboration of research and development (R&D) (U.S. DOE Nuclear Energy Research Advisory Committee, 2002). GIF has proposed four main goals for Generation IV advanced energy systems including enhancements in safety, economics, proliferation resistance, and sustainability (U.S. DOE Nuclear Energy Research Advisory Committee, 2002). The Canadian Pressure Tube Super-Critical Water-cooled Reactor (PT-SCWR) is a pressure tube design that uses supercritical light water as coolant and a separate low-pressure and temperature heavy water moderator (Leung et al., 2011).

Some of the key distinctions of the Canadian PT-SCWR from the fleet of the well-established CANDU reactors are the high-temperature supercritical light water coolant, the vertically orientated re-entrant channel, and the enriched plutonium driven thorium fuel mixture. The Canadian PT-SCWR is also characterized by a tight lattice pitch (25 cm lattice pitch) which results in an under-moderated lattice cell with a direct impact on the neutron energy spectrum (Moghrabi and Novog, 2016). Moreover, the fuel channel design features a High-Efficiency Re-entrant Channel (HERC) where the coolant flows downward through the central flow tube and then reverses direction to flow upward around the fuel elements to the channel outlet (Yetisir et al., 2013; Pencer et al., 2013; Pencer and Colton, 2013). Such design is characterized by strong variations in coolant density and temperature along the vertical fuel assembly. With such substantial changes the

* Corresponding author.
E-mail addresses: moghraam@mcmaster.ca (A. Moghrabi), novog@mcmaster.ca (D.R. Novog).

https://doi.org/10.1016/j.anucene.2018.01.011
0306-4549/

neutronic behavior is expected to be different from the conventional CANDU reactors. Consequently, many studies have been performed to investigate the important lattice physics phenomena (Moghrabi and Novog, 2016, 2017b,c) and for benchmarking lattice level neutronic behavior (Sharpe et al., 2015).

Deterministic physics codes solve for neutron transport within a reactor core using a number of approximations (Lewis and Miller, 1993). In general, the reactor physics calculations are carried out in three stages. First nuclear data from an established source (e.g., ENDF VII.1) are obtained and processed using a code such as NJOY in order to generate a large number of discrete energy-dependent cross sections (e.g., the 238-group library included in the SCALE code package). Such generic and large energy-group structure are often referred to as multi-group libraries. Secondly, transport simulations are performed utilizing this fine-group nuclear data for a specific lattice geometry. From these results, a further energy condensation is performed wherein the transport solution (flux and reaction rates) are used to derive equivalent macroscopic cross sections for a much smaller number of energy groups and for a homogenized region of space (i.e., the lattice cell). Third, these few-group homogenized cross sections are then passed to a core-level diffusion code such as PARCS or DONJON for full-core steady state and/or transient calculations. Such a procedure is applied in deterministic-full-core analysis packages such as SCALE (Laboratories, 2011) followed by PARCS (Downar et al., 2012) or DRAGON (Marleau et al., 1994) followed by DONJON (Varin et al., 2005). Although many deterministic lattice level codes are capable of generating the few-group homogenized cross-sections automatically, users are required to provide the energy boundaries for the few-group structure. Such few-group structure depends on the problem (reactor design, fuel type, coolant and moderator properties) and is often determined based on experience. In reactor physics analysis of thermal reactors, a general approach is to split the neutron energy spectrum into thermal and fast ranges with a cut-off energy of 0.625 eV. However, the energy barriers are not universally fixed and vary depending on the problem/model specifications. The proposed changes in Generation IV designs have driven renewed interest in the optimization of the few-energy group domain (Yi and Sjoden, 2013; Aristodemou et al., 2006; Akbari et al., 2012; Druska et al., 2009). This paper investigates the optimum few group-energy structure for the Canadian PT-SCWR 64-element design with fresh and depleted fuel.

Previous studies have suggested that the traditional two-energy group approach may not be sufficient to capture the steady and transient phenomena in the Canadian PT-SCWR given the fuel enrichment, flux spectrum, complex geometry and feedback behavior (Moghrabi and Novog, 2016, 2017b,c; Shen, 2012). It is also desirable that such a structure show minimal numeric sensitivity to boundary selection and/or group subdivision, a facet often referred to as discretization convergence in numerical methods literature (Fleming et al., 2005). For example, the shift in a boundary or the subdivision of energy groups should not cause an unreasonable change in the accuracy of a solution relative to the multi-group case, i.e., it is desirable to minimize the sensitivity of the solution to the movement of, or the addition/subtraction of a boundary. A proposed structure should also examine the effects of fuel depletion, delayed neutron effects, fuel temperature and coolant/moderator perturbations such that it captures such phenomena with acceptable accuracy as compared to the multi-group solution. In addition, the accuracy of the few-group boundaries needs to be evaluated against a consistent basis such as to avoid cancelation of errors. In particular, boundaries can be numerically selected as optimal in order to cancel a bias resulting from another boundary placed at a different energy. Such selection would then erroneously allow for boundaries with high bias, but opposite sign, as compared to the multi-group solution. Finally, selection of boundaries solely to eliminate a code-to-code bias between the diffusion code and a transport code should be avoided since such biases are code dependent, a function of fuel conditions, and may evolve in the course of a transient. As such it is desirable to assess potential boundaries within a single computational tool such as SCALE, rather than assessing behavior using full-core diffusion codes since the diffusion calculations are subjected to many more approximations (leakage, assembly discontinuities, etc...).

2. Materials and modelling methods

2.1. Description of the fuel channel and core geometry

The Canadian PT-SCWR core contains 336 pressurised fuel channels with 5 m long vertical fuel assemblies and zirconium modified stainless steel cladding (Pencer and Colton, 2013). The most recent design of the Canadian PT-SCWR 64-element fuel assembly geometry (Pencer et al., 2013; Pencer and Colton, 2013) with material atomic densities and geometry specifications were used in this study (Hummel, 2015). The coolant flow is characterized by a bi-directional flow path within the fuel channel (Pencer et al., 2013; Pencer and Colton, 2013). The coolant enters the inlet plenum at 350 °C and 25.8 MPa and flows downward through the central flow tube within each fuel channel, then reverses direction at the bottom of the fuel channel and flows upward through fuel containing outer assembly. The coolant exits the channel at 625 °C and 25.0 MPa (Fig. 1). The fuel is arranged in two concentric fuel rings of 32 elements each that are 12% and 15% by weight PuO_2 in ThO_2 in the outer and inner rings, respectively, creating a balanced radial power distribution (Pencer and Colton, 2013).

The PT-SCWR shares characteristics with the traditional Pressurized Heavy Water Reactor (PHWR) and Boiling light Water Reactors (BWR) and operates above the thermodynamic critical pressure. Consistent with PHWR designs the SCWR has a separate high pressure coolant and low pressure moderator. The low-temperature and low-pressure moderator is thermally isolated from the hot coolant through a ceramic insulator within the pressure tube. Similar to BWRs, the turbine is directly coupled to the reactor coolant outlet. The PT-SCWR utilizes a batch fuelled vertical core with enriched fuel similar to Light Water Reactor (LWR) technologies.

2.2. Description of computational codes

One of the primary goals in nuclear reactor analyses is to provide an accurate estimate of the neutron density in the nuclear reactor which itself is a function of time, space, energy, and direction. For practical reasons, traditional reactor analyses have used multi-scale methods wherein simulations at the lattice-level scale with high spatial and energy fidelity are used to derive inputs for full-core space-time kinetics calculations at lower spatial resolution. In this study, the lattice transport calculations were performed using the NEWT (Dehart and Jessee, 2011) code which is part of the SCALE (Standardized Computer Analysis for Licensing Evaluation) 6.1.3 package (Oak Ridge National Laboratories, 2013). Lattice cell simulations were performed using the 238 energy group ENDF/VII.0 library distributed in SCALE version 6.1.3. Fuel burnup simulations were performed with the TRITON (Jessee and Dehart, 2011) module that employs NEWT as a multi-group solver. NEWT is a deterministic transport solver that uses the discrete ordinate approach to solve the neutron transport equation. However, the discrete ordinate approach is difficult to apply directly to complicated non-orthogonal geometries due to the nature of the finite difference approximations. Consequently,

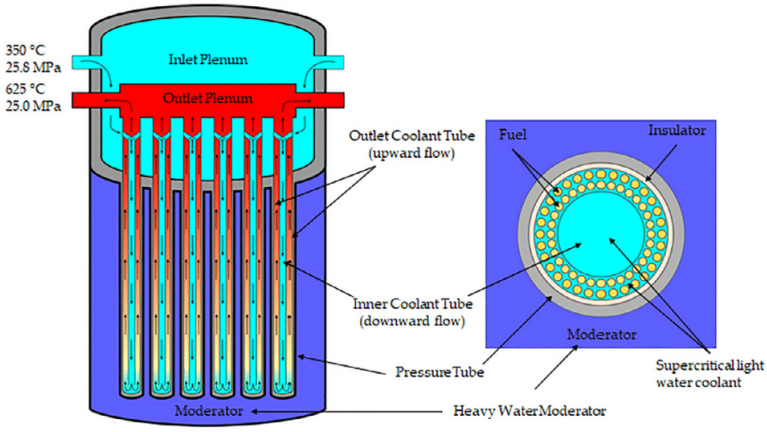

Fig. 1. Core and lattice cell cross-section view of PT-SCWR HERC concept with 64-element fuel assembly (Hummel, 2015).

NEWT uses the discrete ordinate approach followed by the Extended Step Characteristics (ESC) approximation that depends on the method of characteristics along discrete angular directions within the computational cell or mesh. While the ESC approximation is an efficient approach, its methodology is predicated on a fine spatial mesh. Therefore, optimal meshes were examined and used in this work through spatial-mesh sensitivity analysis. Moreover, a large number of simulations were performed as a benchmark to ensure the agreement of NEWT results with other lattice transport codes for the PT-SCWR analysis (Sharpe et al., 2015).

The Canadian PT-SCWR lattice cell contains concentric fuel rings which are different than the regular square lattice of LWRs. Consequently, NEWT requires the Dancoff Factors (DFs) to perform resonance self-shielding calculations. DFs were calculated using MCDANCOF (Petrie and Rearden, 2011) sequence included in SCALE package (Laboratories, 2011). NEWT performs the resonance self-shielding calculations using the dan2pitch card that requires the pre-calculated DFs to determine the equivalent lattice pitch. This approach has a limitation based on coolant and moderator densities which are of particular importance in the PT-SCWR (Younan and Novog, 2016). As a result, an altered coolant density of 0.4 g/cm^3 was used in the resonance self-shielding process when the coolant density within the fuel-containing region in the channel drops below 0.4 g/cm^3. This methodology proved to be the most consistent when compared to the continuous energy results over a wide spectrum of SCWR conditions (Younan and Novog, 2016).

2.3. Methodology

The objective in the homogenization process is to preserve the important physical phenomena and reaction rates. Nevertheless, there are many methods and criteria necessary to achieve these aims. The generation and the selection basis of the optimal boundaries for the few-group cross sections must consider the following:

i) The reference solution should have much higher fidelity in terms of energy discretization. For this reason, the reference solution was selected to be that for the infinite lattice with 238 groups and for a spatial mesh of sufficient refinement such that the grid independence is achieved. Such simulations have shown excellent agreement with the continuous energy stochastic solutions over a wide range of conditions in previous benchmarks (Sharpe et al., 2015). By using a deterministic solution as the reference, the simulations of fuel depletion and its effect on energy discretization can be done more economically than a Monte Carlo based continuous-energy solution.

ii) The optimal solution will depend on the merit function used to evaluate the level of agreement between the proposed few-group cases and that of the reference (or cost function to use terminology consistent with optimization literature). For each boundary included in the optimization, a unique cost-function should be derived such as to avoid cancelation of errors. For example, in selecting of two energy barriers it is possible that for some cost functions, barriers may be selected that generate cost function magnitudes and signs which cancel the errors relative to the reference case. Such barriers, while appearing to minimize the total error may not, in fact, be optimal (i.e., either boundary by itself causes a large, but offsetting, error). Using unique evaluation criteria for each barrier will ensure that cancelation of error effects are minimized.

iii) The overall bias between the few and multi-group solutions should be insensitive to further refinement in the few group energy structure, i.e., the subdivision of the few-groups into finer energy bands should not result in excessive change in the bias.

iv) When an optimal few-group structure is determined, its error should be small over a wide range of operating conditions since such data can be used for normal as well as accident analyses. Therefore, the fuel temperature, coolant and/or moderator density coefficients should be considered in the optimization process and the effects of the few group discretization on such important perturbations should be investigated.

Several potential methodologies are available to define these barriers. The first is to use engineering judgement and experience to define the optimal few-group energy structure, as has been done in the past (Lamarsh, 1983; Duderstadt and Hamilton, 1976). For example, for high temperature gas cooled reactors, key energy boundaries are in the 2–3 eV range while in thermal water cooled reactors a limit of 0.625 eV is common. Given that the SCWRs operating conditions and temperatures fall between these designs, a boundary or boundaries within this range may be optimal. The downside of purely knowledge-based boundary selection is that

the exact values remain uncertain and thus may be sub-optimal. Furthermore, it is not clear that such boundaries will be robust from a numerical methods standpoint (results show small sensitivities to group subdivision). Therefore, while important and useful for judging the validity of other methods, pure judgement approaches lack a rigorous formalism.

An alternative methodology would be to perform a brute force search where a transport solution is performed for a large number of possible energy group structures and each solution is judged against the reference solution using a cost function. If we assume that some combination of the 238 energy groups in the fine-structured SCALE library form the possible boundaries for the few-group case, then it would first appear that a brute force search may be appropriate since the number of combinations (238) seems small. Indeed, we can perform 237 simulations with NEWT, each one corresponding to a possible boundary for a two-group case of homogenized data and select the case which is most similar to the reference 238 group solution. Then one could proceed to select a second boundary in order to obtain a three-group structure by performing 236 simulations for each of the remaining possible barriers from the original SCALE library. Thus, one could keep adding groups until a satisfactory cost function was obtained. However, this approach assumes that once an energy barrier is set, such a barrier will remain optimal as further subdivisions are made which is clearly not the case. For example, on a search one may find that a barrier at 0.6 eV seems optimal for a two-group structure, then when searching for a second boundary the optimal cost function may be at 6 keV, and indeed such boundaries may provide a cost function near zero. Upon closer inspection of such barriers, we can observe that the case of 6 keV was selected to minimize the difference in the neutron multiplication factor (k_∞) between the cases with some residual in the cost function. The second boundary is then selected such as to zero out the residual in the cost function obtained from the first search, with little or no physical significance of that second boundary (i.e. the second barrier was selected solely to cancel the error in reaction rate obtained from the first barrier placement). While this three group (two boundaries) structure seems to minimize the cost function, the solution may be far from optimal in that i) subdivision of any of these boundaries would cause large changes in the cost function; ii) the second boundary may be completely unphysical (e.g., occurring in the middle of an important resonance) since it was selected solely to offset the error from the placement of the first boundary. In many multi-variate optimization problems, such propensity for bias cancelation can occur (Fleming et al., 2005; Sekhon, 2011) and is termed in this paper as an "error cancelation issue".

A variant of this second approach would be simultaneously solve for n boundaries over the entire solution of energy space. For example, when searching for two boundaries (three groups), transport solutions are performed for all possible combinations of two boundaries within the 238 possible choices. From this one can show that the number of transport solutions would be:

$$\textit{Total number of Possible collapsing scenarios} = \frac{237!}{(237-(n-1))!(n-1)!} \quad (1)$$

where n is the number of boundaries that can be placed. From this one can see that the number of transport solutions require to evaluate the optimum increases geometrically with the number of boundaries to be selected. Specifically, for two, three and four group structures 237, 27,966 and 2,190,670 transport solutions are required, respectively. Furthermore, since a majority of the batch-fueled core has undergone significant depletion, each one of these states would require analysis at some level of burnup, further increasing the solution times. Additionally, it is possible that a situation may arise wherein error cancelation between multiple boundaries leads to error cancelation issues as discussed above, albeit where one or more group boundaries are selected to cancel out the errors from other boundaries. While the issue of a large search space could be overcome using a non-parametric search algorithm, the error cancelation issue cannot be easily overcome using a single cost function.

A third approach could be implemented using an inverse selection method wherein successive NEWT simulations are performed starting with the finest possible structure and with a coarsening energy structure in each successive case (Moghrabi and Novog, 2017). In each successive case, the sensitivity to the removal of each remaining energy barrier is examined and the structure with the least sensitivity being selected to form the basis for the next set of cases. In this way, the number of groups is reduced from the original 238 down to a predefined number of few-groups or until the accuracy of the cost function deteriorates by more than 10%. Such a search is easy to implement and computationally tractable but suffers from a history effect in that boundaries may be removed at an early stage due to low sensitivity, but may become sensitive and important later on within the algorithm when fewer groups remain (Moghrabi and Novog, 2017). Since groups are not re-added in each stage the final group structure may be missing important boundaries that were eliminated in the early phase of the inverse selection process. Furthermore, barriers may again be removed for unphysical reasons solely to cancel out the error in the cost function resulting from some previous homogenization.

For this paper, a series of alternative methods, including brute force searches, alternative cost functions, inverse methods, and sensitivity analyses are used in order to establish an energy structure that has attributes outlined previously. As each method is implemented the optimal group structure is assessed against knowledge-based boundaries. The steps used in the methodology are outlined in Fig. 2. The reference case for the method involves a simulation of NEWT at 238 groups and is used to self-consistently homogenize the solution into any number of coarser structures. Once the homogenization into a specific group structure is complete, the results are used to generate a new NEWT library consistent with the fewer-group proposed energy group boundaries. The results of these new few-group NEWT simulations with the coarser group structure can then be directly compared against the original high-fidelity energy solution in 238 groups. Such a methodology has several advantages. First, the reference and grouping analyses are all performed within the same lattice code thereby avoiding any code-to-code biases that may obscure the optimization process. For example, if the reference case was run using a Monte Carlo code in continuous energy, biases resulting from the solution method would occur (for example due to the differences in solution, interpolation of temperature dependent data, etc.) (Sharpe et al., 2015). As such, the optimization process would add or remove boundaries in an attempt to eliminate the bias which was code-to-code driven, rather than boundary selection based on physical parameters. Code-to-code biases are a result of the approximations in each code and may be reactor, fuel or condition dependent. Thus, it is desirable to optimize energy structure in isolation and assess code biases independently or through validation. Secondly, the uncertainties and biases that arise from mathematical models used in the lattice code are eliminated and the effects of the energy group discretization are isolated and investigated independently from any other factors. To achieve that aim of assessing the effects due to the energy group discretization and collapsing process independently, all the NEWT lattice cell simulations (including the unclasped and the collapsed cases) were performed using the same optimal mesh which is depicted in Fig. 3. An additional homogenization step was added to the "reference case" where the 238 group solution is used to re-homogenize

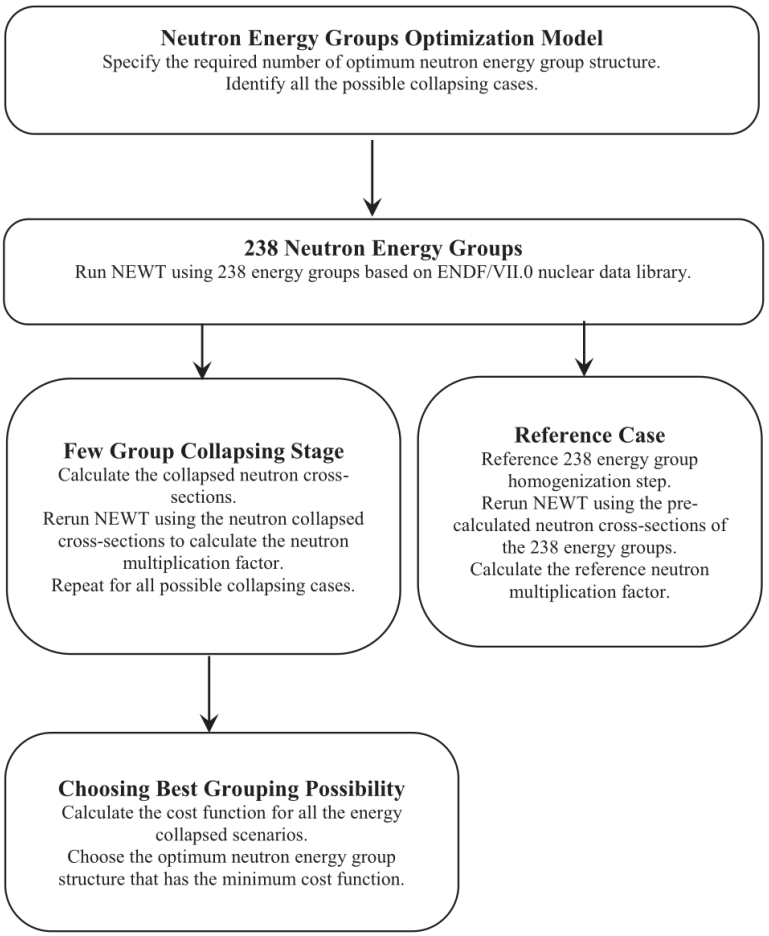

Fig. 2. Steps of the proposed model for neutron energy group collapsing procedure using the NEWT code.

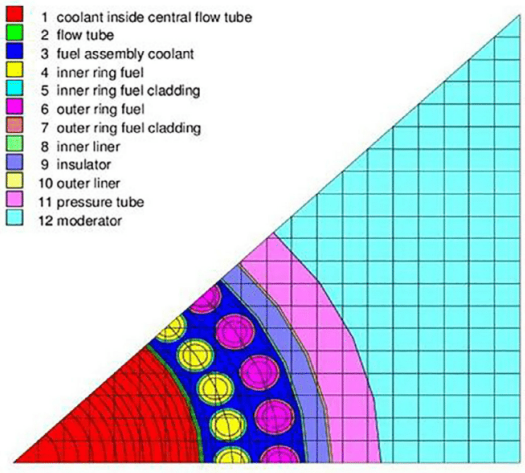

Fig. 3. The optimal mesh used in all executed NEWT simulations.

the 238 SCALE cross-sections using the problem specific flux distribution. This procedure aimed to provide a consistent basis for comparison with the few group collapsed simulations in order to minimize the biases due to numerical artifacts in the homogenization process (i.e., there is exact re-homogenization with the specific lattice geometry and flux distribution and spectrum done for both the reference and reduced energy group cases). Although the difference in k_{inf} due to this additional homogenization step is very small (~0.1 mk), such measures are included in this paper and are consistent with the methodology discussed in (Aristodemou et al., 2006).

3. Results and discussion

As mentioned above, the two-dimensional deterministic code NEWT was used to perform the lattice cell transport simulations. Given the large changes in moderation, fuel temperatures and other lattice physics inputs as a function of location within the core it is important to examine the possible effects of core location on group boundary selection. The group boundary selection is performed first considering core location effects and fresh fuel, then

including the depletion and finally including potential perturbations that occur in either normal or accident conditions.

3.1. Examination of core location effects and two-group selection

To investigate the effects of the core location on the selection of energy group boundaries, the proposed model illustrated in Fig. 2 was applied at three different locations along the vertical fuel channel. Simulations were performed at 25 cm, 250 cm, and 475 cm from the bottom of the channel corresponding to the channel inlet, middle, and channel outlet respectively. Given the sensitivity of the results to the cancelation of errors it is recommended to perform the optimization at each physical location along the fuel channel independently. Furthermore, such an approach allows one to isolate the differences in structure arising from the vastly different conditions along a channel that can be investigated.

Modelling the neutron energy spectrum by two groups would yield 237 possible cases as evaluated using Eq. (1) for each axial location. Such a search was performed for fresh and depleted fuel (25 MW d kg^{-1} [HM]) for the infinite lattice cell at the three locations of interest. The coolant densities and the materials temperature at the three locations are shown in Table 1 (Hummel, 2015). The cost function, which measures the relative error in neutron multiplication factor between the reference case using 238 energy groups and the collapsed case i, was calculated for each case as follows:

$$Cost\,Function(1) = \frac{|k_{inf.ref} - k_{inf.i}|}{k_{inf.ref}} \times 10^5 \quad (2)$$

where i varies from 1 to 237 for each of the 237 possible energy homogenization options. For a two energy group structure, the variation of k_{inf} (infinite multiplication factor) versus the value of the energy barrier selected is shown in Fig. 4. This Figure shows that k_{inf} is highly sensitive to the thermal energy barrier for the energy range between 0.05 eV and 3 eV. However, k_{inf} is characterized by a plateau with less sensitivity to the selection of the thermal energy cut-off barrier within the energy range between 3 eV and 20 eV. The sensitivity of k_{inf} to the thermal energy barrier selection for fresh and depleted fuel at the top, middle, and bottom of the fuel channel are similar. The optimal two-energy group structure at the three locations along the vertical channel are shown in Table 2. The thermal energy barriers were found to be 1.40 eV, 1.94 eV and 2.47 eV at the bottom, middle and top of the fresh fuel channel, respectively. While for mid-burnup fuel the recommended thermal cut-off is found to be 1.59 eV, 2.87 eV, and 3.06 eV at the same locations due to some spectral hardening in the cell. It is clearly shown in Table 2 and Fig. 4 that a higher thermal energy cut-off is recommended for the Canadian PT-SCWR as compared to more traditional CANDU designs and with small variation due to location. The minor variations in the selection of the thermal energy barrier for two groups along the fuel channel are mainly due to two dominating factors: i) the Doppler effect driven by the increase of the fuel temperature, and ii) the strong decrease in the coolant density with elevation along the vertical fuel assembly leading to a hardening neutron spectra. This was confirmed by the recent study which demonstrated that the large decreases in the coolant density along the vertical fuel channel is the dominant factor impacting the neutron spectrum and the different lattice physics phenomena in the PT-SCWR (Moghrabi and Novog, 2016). The same effects are influencing the lattice cell homogenized cross-sections in the case of fuel burnup (Moghrabi and Novog, 2017b,c).

In general, for few-group structures, the thermal energy cut-off boundary is usually placed such that the impact of thermal up-scatter in the coolant to a higher energy cross-section resonance is small. For thermal reactors, including the CANDU reactors, this boundary is typically placed at 0.625 eV. For High-Temperature Reactors (HTR) such a boundary is recommended to be between 2 eV and 4 eV due to the high coolant temperature (Duderstadt and Hamilton, 1976). Considering the SCWRs coolant temperature is between these designs the aforementioned boundaries of 1.4–3.1 eV are consistent with expectations and is consistent with recent studies related to the importance of neutron up-scattering in the PT-SCWR (Moghrabi and Novog, 2016, 2017b,c). Such boundaries are also consistent with cross-section behavior as shown in Fig. 5. In this Figure the two broadest and most significant fuel resonances occur below 2 eV with a third strong resonance occurring between 2 and 3 eV.

Given the relatively small changes in optimal-energy boundaries noted above, it is desirable to limit the search space to a single physical location along the channel to limit computational costs in subsequent optimization steps. To assess the effect of axial conditions on energy group discretization, the optimal two-group boundary at each axial elevation was analyzed using a mapping technique. First, the optimal boundary as derived for the lowest elevation was used to evaluate the neutronic phenomena at the downstream locations (i.e., the boundaries determined at the channel entrance were then used in the analysis of the downstream locations and the deviations in these downstream locations from the reference solutions were recorded). For example, using the boundary determine at the inlet location (i.e., 1.40 eV) to analyze the cost function at the middle of the channel produced a cost function of 102.9 for fresh fuel as compared to a value of 0.86 for the best energy barriers at that location. Next, the mid-plane optimized boundary were mapped to the other locations and again the changes in cost function were recorded. Finally, the optimized boundary at the channel outlet was used at the inlet and mid-plane locations to determine the cost function. By examining the cost function behavior for these mapping combinations it was determined that the group structure derived at the mid-plane of the core produced the best results when mapped to the other locations as shown in Table 3. All subsequent searches for multi-group boundaries are therefore performed using local thermalhydraulic and fuel conditions indicative of the mid-point of the fuel channel. Based on the analysis above, the optimal barrier for a two group energy structure was determined to be 1.94 to 2.87 eV depending on fuel depletion.

During the course of this work, many alternatives cost functions were explored including ones that depends on the difference in either fission, absorption or total reaction rates. However, the optimization using these alternative cost functions provided a similar and in some cases identical boundary results to the cost function relying on the difference in k_{inf} since these reactions strongly influence the value of k_{inf}. As an example, the difference in the total fission and absorption reaction rates between the reference case and the two group structure versus the selected energy barrier at the middle location of the mid-burnup fuel channel is shown in Fig. 6. The optimum thermal energy cut-off for the two energy group structure is located at ~2.87 eV which is similar to the previous discussion based on cost function that depends on k_{inf}. As a result, the multiplication constant was used as the primary cost function to determine the first energy barrier.

3.2. Additional group selection and limitations

The optimum three-group structure has been investigated for fresh and depleted fuel using the methods outlined previously. The results are summarized in Table 4 which shows the energy group barriers with the corresponding cost function and the reactivity difference between the reference and the optimum three-group cases.

Table 1
Coolant density and materials temperature at the bottom, middle, and top of the channel.

(cm)	Coolant Density (g/cm^3)		Component Temperature (K)						
	ρ_{out}	ρ_{in}	Outer Coolant	Cladding	Liner	Insulator	Pressure Tube	Inner Coolant	Fuel
25	0.51702	0.57896	647.40	683.04	640.78	537.68	410.38	636.45	1117.36
250	0.13998	0.58758	692.35	781.38	678.65	561.45	418.11	634.39	1550.53
475	0.07014	0.61903	890.62	1006.99	859.82	673.29	452.28	625.81	1539.91

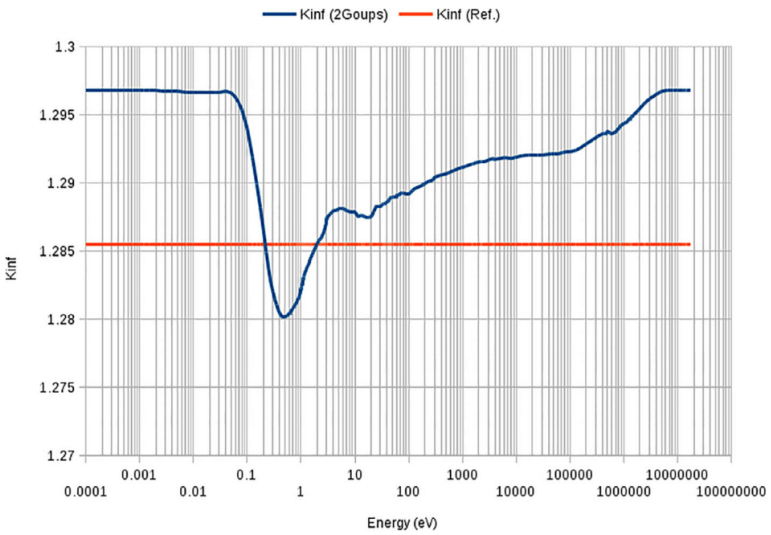

Fig. 4. Variation of k_{inf} versus energy barrier for the two-group structure at the middle of the fresh fuel channel.

Table 2
Optimal thermal energy group barrier with two group structure at the top, middle and bottom of the fuel channel.

Distance from the bottom of the channel	Best optimum thermal energy cut-off for two energy group structure (eV)		Cost Function	
	Fresh Fuel	Burnup Fuel	Fresh Fuel	Burnup Fuel
475 cm (Top)	2.47	3.06	0.222	1.489
250 cm (Middle)	1.94	2.87	0.859	0.454
25 cm (Bottom)	1.40	1.59	3.439	2.347

For the first optimization attempt, it is assumed that the optimal barrier from the two-group division is preserved and forms the first of the two-boundaries needed to create three groups. The main advantage of such an assumption is to decrease the search space for the second boundary. In this approach there exists 236 possible homogenization cases to be analyzed. For a fresh fuel lattice, a second energy barrier at 6 eV combined with the initial barrier set at 1.94 eV was determined to be optimal. The second optimization method involves simultaneous selection of both barriers without prior knowledge of the two-group results. Consequently, the number of possible homogenizations is higher than the fixed initial barrier method and is evaluated by Eq. (1) to be 27,966 possibilities. The optimum three-group structure obtained using the brute force search was determined to be 2.57 eV and 22.5 eV. The cost function of the three-group optimum structure for fresh fuel obtained using the brute force method is slightly smaller than the one obtained using the fixed 1st barrier approach, although it is relatively small in both cases.

As shown in Table 4, the optimal three-group structure for fresh fuel shows large errors when applied to irradiated fuel. The depleted fuel (25 MW d kg^{-1} [HM]) energy-group selection was then performed in a similar fashion as the fresh fuel case. The first iteration considers the best optimum two-group structure for fresh fuel and then adds a third group to accommodate the different isotopes that accumulate with burnup. In the case of the fresh fuel lattice, the optimum thermal energy barrier for the two group structure was found to be 1.94 eV using the fixed search strategy. Assuming that the first barrier remains optimum, a search of the remaining possibilities shows a minimal cost function is obtained at 950 eV as shown in Table 4. The second method mimics the fresh fuel case by simultaneously searching for the best two barriers based on the model outlined in Fig. 2. After simulating all the 27,966 possibilities, the model recommends two energy barriers at 2.97 eV and 2.87 eV with a very small cost function. From this result the following can be noted:

- As discussed in the previous section the optimum thermal energy cut-off for the two group structure was recommended at 2.87 eV and it is clearly shown in Table 4 that the brute force search approach for burnup fuel has recommended the same thermal energy cut-off barrier for three-group structure (i.e., the method selected a barrier of 2.97 eV which is in very close

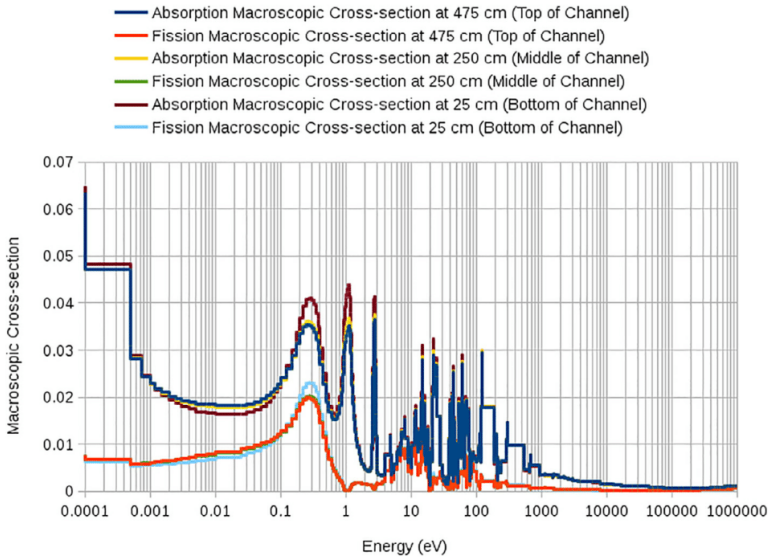

Fig. 5. The homogenized fission and absorption cross-sections versus energy for the fresh fuel lattice cell at 25 cm, 250 cm and 475 cm from the bottom of the channel.

Table 3
The values of the cost function at the top, middle, and bottom of the channel using the best optimum two energy group structure at each of the corresponding positions for fresh and burnup fuel lattice cell.

Best Optimum two energy group structure at	Value of cost function at the different locations of the fuel assembly							
	Fresh Fuel				Burnup Fuel			
	Top	Middle	Bottom	Max. cost function*	Top	Middle	Bottom	Max. cost function*
Top	–	48.2	172.8	172.8	–	48.9	197.8	197.8
Middle	50.8	–	108.1	108.1	41.6	–	149.8	149.8
Bottom	146.4	102.9	–	146.4	165.1	131.2	–	165.1

* The maximum values of the cost function is equivalent to the maximum value of $(\Delta k/k_{ref}) \times 10^5$.

proximity to the initial barrier of 2.87). It is worthwhile to mention that the 2.87 and 2.97 eV are almost identical and represent a single bin width in the fine structured 238 group case based on the ENDF/VII.0 nuclear data library build in within the SCALE 6.1.3 package (Laboratories, 2011). Such group structure with close energy barriers doesn't have a physical meaning and are not recommended from the reactor physics standpoint.

- This was also confirmed using Fig. 7, which represents the variation of k_{inf} versus the value of the second energy barrier for selected thermal cut-off energy barrier for three-group energy structure with burnup fuel (25 MW d kg^{-1} [HM]).
- In Fig. 7, each line has a fixed thermal energy cut-off (first energy barrier) and the value of k_{inf} varies versus the value of the second energy barrier. As shown in Fig. 7, the curves representing the value of k_{inf} converge at 2.87 eV.
- Based on Fig. 7 the cost function changes sign between 2.87 and 2.97 eV causing some cancelation issues to arise. Similar problems arise for other potential options at 0.07 eV, 2.97 eV, 6.5 eV and 305 eV where the cost function of those particular cases are depicted in Table 5. As discussed earlier in this work, the optimum group structure which is characterized by cancelation of errors is to be avoided since small deviations in lattice conditions or further subdivision of energy groups may provide erroneous results.

An important conclusion can be drawn regarding the thermal energy cut-off for the Canadian PT-SCWR in that the numerical search places both the first and second barriers very close to 2.87. As shown in Table 4 boundaries at or near 2.87 eV arise from searches for either a single or dual barrier search for depleted fuel, and is also in close proximity to the barrier of 2.57 eV selected for fresh fuel (i.e. within two energy groups of the original SCALE 238-group library). Therefore the 2.87 eV thermal barrier is utilized as the best possible thermal energy barrier. Based on the discussion on error cancelation for two boundaries, only a single boundary can be selected with this approach.

Finally, given that even at the Beginning Of cycle (BOC) at most 1/3 of the fuel is fresh and the remainder has some level of burnup, and that during a cycle all fuel has some level of depletion, the optimal boundary for depleted fuel at 2.87 eV is selected.

3.3. Group selection for reactivity coefficients

One of most important design basis accident scenarios in nuclear reactors is the Loss-Of-Coolant Accident (LOCA). Previous literature has identified interesting lattice physics phenomena for the PT-SCWR which indicates that coolant density reactivity effects must be considered in group structure delineation[1]. In such events

[1] It should be noted that the phenomenon of voiding does not occur in supercritical fluids and hence the term "void" reactivity is a misnomer. However, for consistency with existing literature we adopt the term void reactivity to denote the reactivity induced by a decrease in coolant density.

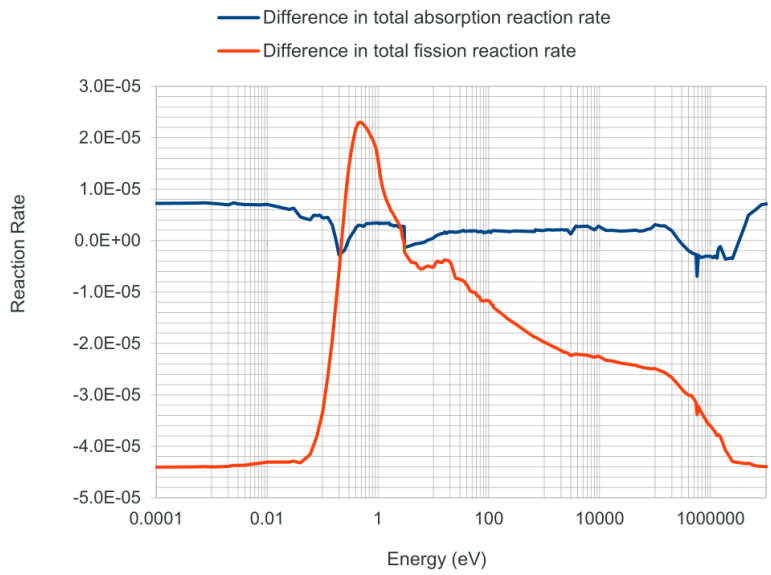

Fig. 6. Difference in total fission and absorption reaction rates between the reference case and two-energy-group structure as selected thermal energy barrier varies over energy range.

Table 4
The optimum three-energy group structure for fresh and burnup fuel (25 MW.d.kg^{-1} [HM]) and its corresponding value of the cost function and the reactivity difference between the optimum case and the reference case at the middle of the channel.

Type of fuel	Selection basis criteria	Energy group structure	Cost Function	Reactivity Difference (pcm)
Fresh	2G Fresh Fuel + 1G	20 MeV–6 eV–1.94 eV–0 eV	0.02334	0.01816
	Brute force search	20 MeV–22.5 eV–2.57 eV–0 eV	0.02256	0.01755
Burnup	3G Fresh fuel structure	20 MeV–22.5 eV–2.57 eV–0 eV	90.5498	80.3608
	2G Fresh Fuel (1.94 eV) +1G	20 MeV–950 eV–1.94 eV –0eV	0.48501	0.43005
	Brute force search	20 MeV–2.97 eV–2.87 eV–0 eV	0.05409	0.04796

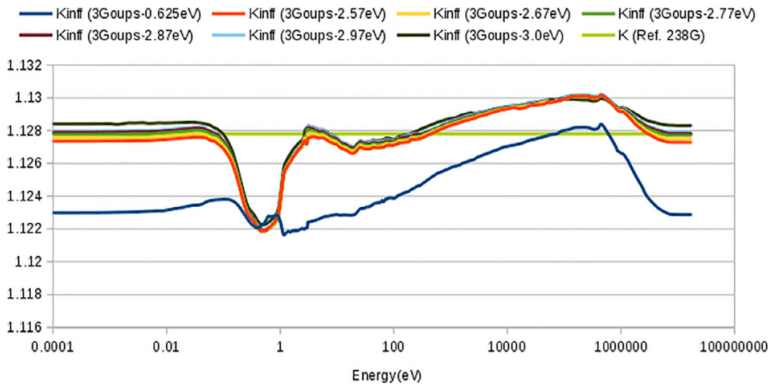

Fig. 7. Variation of lattice cell k_{inf} versus energy barrier for the three-group structure with burnup fuel at the middle of the channel for selected thermal energy cut-off.

it is conceivable that non-equilibrium voiding may exist for a short period of time wherein the coolant in the upward flowing fuel region of the channel may void prior to the coolant flowing downwards in the center for the channel. In such cases the resultant reactivity may be slightly positive for a brief period until such time as the density changes propagate to the central flow tube (since the total void reactivity is negative). Scenarios where the coolant density within the inner flow tube decreases while remaining relatively unchanged within the outer section are referred to as inner coolant void (ICV). When the coolant density decreases within the outer flow tube and stays comparatively unchanged in the inner tube, this is referred to the outer coolant void (OCV). The total coolant void (TCV) scenario refers to the equilibrium density changes in both flow tubes (inner and outer) within the fuel assembly.

Table 5
Best optimum three-group structure based on numerical analysis standpoint with thermal energy cut-off assigned at 2.87 eV at the middle of the channel for burnup fuel.

Energy Barriers (eV)	cost function	Reactivity Difference (pcm)
2.87–305	3.64955	3.23608
2.87–6.5	0.52668	0.46700
2.87–2.97	0.05408	0.04796
2.87–0.07	0.20571	0.18240

The coolant void reactivity for each region of the channel, the fuel temperature, and moderator temperature reactivity coefficients were investigated versus energy discretization for the depleted fuel lattice cell (25 MW d kg^{-1} [HM]). The fuel temperature coefficient (FTC) was calculated by perturbing the fuel temperature by 100 K, while the moderator temperature coefficient (MTC) was calculated by perturbing the moderator temperature by 20 K based on the recent sensitivity study (Moghrabi and Novog, 2016). The values of these parameters were calculated for the reference case using 238 energy groups, and for the different possible few-group options identified in the previous section. The best structure is the one that would minimize the differences in these parameters when calculated using a few-group structure.

Then to assess the merits of including additional groups to account for spectral changes due to perturbations in the fuel, coolant and moderator, additional groups were added to the existing 2.87 eV (two-group) structure. To add a second barrier (i.e., three groups), the energy boundaries were systematically tested and the differences in the predicted values of ICVR, OCVR, TCVR, FTC, MTC, and the reactivity between the reference solution and all the possible three energy groups scenarios were calculated as shown in Fig. 8. Given that the inner-coolant void reactivity for the PT-SCWR is negative, it was selected as an appropriate cost function for setting the next energy barrier. This additional cost function was calculated as follows:

$$Cost\ Function(2) = |ICVR_{ref} - ICVR_i| \quad (3)$$

where $ICVR_{ref}$ stands for the inner coolant void reactivity calculated using the reference case with high energy fidelity, and $ICVR_i$ stands for inner coolant void reactivity with three-energy-group structure. A brute-force search for a second boundary (third energy) group which minimized the error in ICVR was found to be at 820 keV. Further investigation also showed that such a boundary also minimized the error in TCVR (since IVCR is a component of the total void reactivity). Physically such a barrier also represents a segregation of neutron energies emitted from delayed neutron precursors. As shown in Table 6, the three-energy-group structure with energy barriers set as 2.87 eV and 820 keV is characterized by a small error in the calculations of TCVR, ICVR and OCVR. However, the error in overall bias in multiplication constant increases slightly as compared with the two-group results. While it may be possible to reduce this bias by searching for a third boundary, it is not recommended since setting this boundary solely to eliminate a bias in k_{inf} would amount to intentional error cancelation (from the authors point of view). For example, adding a third energy group barrier at 1.35 eV to form a four energy group structure would eliminate all the residual error in k_{inf} obtained with the previously chosen three group structure and would also preserve the small errors in TCVR, ICVR or OCVR. However, such a barrier appears to bi-sect some low lying resonances and hence may not have any physical meaning other than to cancel out errors from the earlier optimization stage.

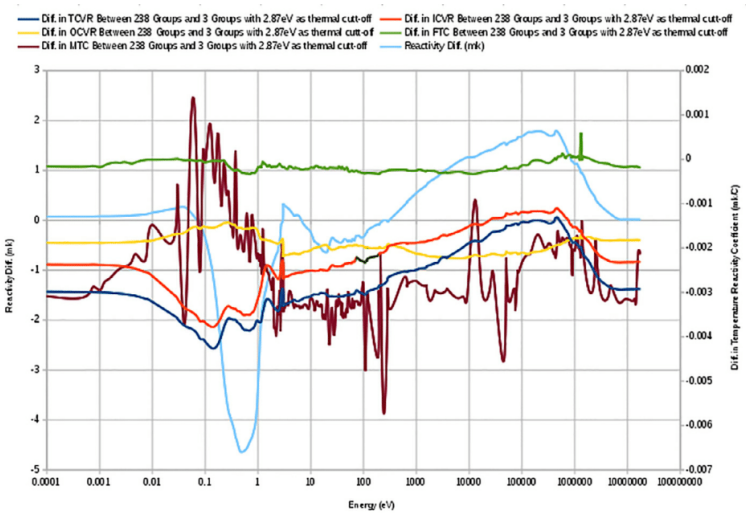

Fig. 8. The difference in reactivity, ICVR, OCVR, TCVR, FTC, and MTC between a three group structure with boundaries at (2.87 eV and energy E) and the reference solution.

Table 6
A detailed best optimum energy group structure based on selected perturbation of different design accident scenarios at the middle of the channel for burnup fuel.

Number of energy groups	Energy Barriers	Difference in Reactivity (mk)	Diff. in TCVR (mk)	Diff. in ICVR (mk)	Diff. in OCVR (mk)
2 Groups	2.87 eV	0.0136	−1.3739	−0.8378	−0.3910
3 Groups	2.87 eV –820 keV	1.2727	−0.3793	−0.0805	−0.3999

Table 7
Reactivity difference for selected optimum energy at mid (25 MW d kg^{-1} [HM])) and high (50 MW d kg^{-1} [HM])) burnup at selected location along the vertical fuel channel as compared to the reference simulations at that condition/location.

Number of Energy Groups	Energy Barriers	Distance from the bottom of the channel (Location)	Fuel Burnup (MW d kg^{-1} [HM])	Difference in Reactivity (mk)
2	2.87 eV	250 cm (Middle)	25	0.0136
2	2.87 eV	250 cm (Middle)	50	−0.9553
3	2.87 eV–820 keV	475 cm (Top)	25	1.098
3	2.87 eV–820 keV	250 cm (Middle)	25	1.273
3	2.87 eV–820 keV	250 cm (Middle)	50	0.723
3	2.87 eV–820 keV	25 cm (Bottom)	25	2.006

3.3.1. Verification of proposed group structure with core elevation and fuel burnup

The study that investigates the optimum energy group structure for the Canadian PT-SCWR was performed for fresh and depleted fuel with mid-cycle burnup assigned at 25 MW d kg^{-1} [HM]. In order to verify the proposed optimum group structure with burnup, the reactivity difference using the assigned two and three group structure were examined for fuel with higher burnup value (50 MW d kg^{-1} [HM]) at the middle of the channel. As depicted in Table 7, the reactivity difference from the reference solution at high fuel burnup value (50 MW d kg^{-1} [HM]) is small for the assigned optimum two and three energy group structures with an error less than 1 mk in both cases. This validates the pre-assigned optimum energy group structures with high fuel burnup.

The optimization of the energy group structure was performed at the core midplane since this position was shown to provide acceptable boundaries to elevations above and below the core mid-plane. In addition the proposed three-group structure obtained at the middle of the channel was verified against the reference solution at the top and bottom of the fuel assembly corresponding to 475 cm and 25 cm from the bottom of the channel, respectively. As shown in Table 7, the three-energy-group structure shows similar behavior and characteristics at all core elevations. Similar to the behavior of the optimum two-group structure discussed previously, the highest error in reactivity obtained using the optimum three-group structure occurs at the bottom of the core. However, the deviation from the mid-plane location is small (less than ~0.73 mk).

4. Summary and conclusion

This work investigated the optimal energy group structure for few-energy group homogenization for the advanced PT-SCWR lattice since previous studies showed that such few group structure depends on the nuclear reactor type, design, operating conditions and fuel nature. A sensitivity study of the optimum discretized few energy group structure was performed for the Canadian PT-SCWR 64 element with fresh and depleted fuel. One of the important findings of this work shows that a higher thermal cut-off barrier is recommended for the Canadian PT-SCWR than traditional CANDU or LWR designs. Based on minimizing the deviation in k_{inf}, a boundary at 2.87 eV is recommended for the two-energy group diffusion analysis.

Only a single barrier can be selected for a single cost function through numerical optimization. Using an additional cost function based on coolant density feedbacks an additional boundary at 820 keV is recommended. The optimum three energy group structure was determined based on the behavior of relevant feedback coefficients. This 820 keV barrier also delineates epithermal neutrons from those in the faster and delayed neutron range so as to minimize the deviation from the reference case feedback coefficients. Given the importance of these feedback phenomena it is recommended that all diffusion level transient calculations proceed with a minimum of three energy groups with barriers located at 2.87 eV and 820 keV.

Acknowledgments

The authors would like to thank Natural Research CANada (NRCAN), Natural Sciences and Engineering Research Council of Canada (NSERC) and the Canadian Generation IV program for their generous financial support of this work.

References

Akbari, M., Minuchehr, A., Zolfaghari, A., Khoshahval, F., 2012. An investigation for an optimized neutron energy-group structure in the thermal lattices using particle swarm optimization. Ann. Nucl. Energy 47, 53–61.

Aristodemou, E., Pain, C., Oliveria, C., Umpleby, A., Goddard, T., Harris, C., 2006. Energy group optimization for forward and inverse problems in nuclear engineering: application to downwell-logging problems. Geophys. Prospect. 54, 99–120.

Dehart, M.A, Jessee, M.D., 2011. "NEWT: A New Transport Algorithm for Two-dimensional Discrete-ordinates Analysis in Non-Orthogonal Geometries," Tech. Rep. ORNL/TM-2005/39 Version 6.1 Sect. F21, Oak Ridge National Laboratory.

Downar, T., Xu, Y., Seker, V., 2012. "PARCS v3.0 U.S.NRC Core Neutronics Simulator," USER MANUAL draft.

Druska, C., Kasselmann, S.t., Lauer, A., 2009. Investigation of space-dependent safety-related parameters of a PBMR-like HTR in transient operating conditions applying a multi-group diffusion code. Nucl. Eng. Des. 239, 508–520.

Duderstadt, J., Hamilton, J., 1976 Chapter 2. In: Nuclear Reactor Analysis. Wiley, New York, pp. 7–10.

Fleming, Peter J., Purshouse, Robin C., Lygoe, Robert J., 2005. Many-Objective Optimization: An Engineering Design Perspective. In: Coello Coello, C.A., Aguirre, A.H., Zitzler, E. (Eds.), Evolutionary Multi-Criterion Optimization: Third International Conference, EMO 2005, Guanajuato, Mexico, March 9-11, 2005. Proceedings. Springer Berlin Heidelberg, Berlin, Heidelberg, pp. 14–32.

Hummel, D.W., 2015. "Transient Neutronic-Thermalhydraulic Coupling in a PT-SCWR," Ph.D. Thesis, McMaster University, Hamilton, ON, Canada.

Jessee, M.A., Dehart, M.D., 2011. "TRITON: A Multipurpose Transport, Depletion, and Sensitivity and Uncertainty Analysis Module," Tech. Rep. ORNL/TM-2005/39 Version 6.1 Sect. T1, Oak Ridge National Laboratory.

Oak Ridge National Laboratories, 2011, Scale: A Comprehensive Modeling and Simulation Suite for Nuclear Safety Analysis and Design, ORNL/TM-2005/39, Version 6.1. Radiation Safety Information Computation Center at Oak Ridge National Laboratory as CCC-785.

Lamarsh, J.R., 1983. Introduction to Nuclear Engineering. Addison-Wesley, Reading, Mass.

Leung, L., Yetisir, M., Diamond, W., Martin, D., Pencer, J., Hyland, B., et al., 2011. A Next Generation Heavy Water Nuclear Reactor with Supercritical Water as Coolant. International Conference on the Future of Heavy Water Reactors (HWR-Future). Ottawa, Ontario, Canada.

Lewis, E.E., Miller, W.F., 1993. Computational Methods of Neutron Transport. American Nuclear Society, LaGrange Park, Illinois.

Marleau, G., Roy, R., Hebert, A., 1994. DRAGON: a collision probability transport code for cell and supercell calculations. Report IGE-157, Institute de génie nucléaire, École Polytechnique de Monteréal. Monteréal, Québec.

Moghrabi, A., Novog, D.R., 2016. Investigation of reactor physics phenomena in the canadian pressure tube supercritical water reactor. Canad. Nucl. Lab. Nucl. Rev. 5 (2), 253–268. https://doi.org/10.12943/CNR.2016.00031, avaialable online at: https://doi.org/10.12943/CNR.2016.00031.

Moghrabi, A., Novog, D., 2017a. Optimization Approach of Energy Group Structure for the Canadian Pressure Tube Supercritical Water Reactor. The 37th Annual Conference of the Canadian Nuclear Society. Niagara Falls, Ontario, Canada.

Moghrabi, A., Novog, D., 2017b. Investigation of fuel burnup impacts on nuclear reactor safety parameters in the Canadian Pressure Tube Supercritical Water-cool Reactor. ASME J. Nucl. Radiat. Sci. 4 (1). https://doi.org/10.1115/1.4037895.

Moghrabi, A., Novog, D.R., 2017c. Investigation of Fuel Burnup on Reactor Physics Phenomena in the Canadian Pressure Tube SuperCrticial Water-cool Reactor. Proceedings of the 8th International Symposium on SuperCritical Water Reactor (ISSCWR-8), Chengdu, China.

Oak Ridge National Laboratories, 2013, SCALE: A Modular Code System for Performing Standardized Computer Analysis for Licensing Evaluation, Version 6.1.3.

Pencer, J., Colton, A., 2013. Progression of the Lattice Physics Concept for the Canadian Superritical Water Reactor. 34th Annual Conference of the Canadian Nuclear Society. Toronto, Ontario, Canada.

Pencer, J., Watts, D., Colton, A., Wang, X., Blomeley, L., Anghel, V., Yue, S., 2013. Core neutronics for the Canadian SCWR conceptual design. The 6th International Symposium on SuperCritical Water Reactor (ISSCWR-6). Shenzhen, Guangdong, China.

Petrie, L.M., Rearden, B.T., 2011. "MCDANCOFF Data Guide," Tech. Rep. ORNL/TM-2005/39 Version 6.1 Sect. M24. Oak Ridge National Laboratory.

Sekhon, J.S., 2011. Multivariate and propensity score matching software with automated balance optimization: the matching package for R. J. Statist. Softw. 42 (7).

Sharpe, J., Salaun, F., Hummel, D., Moghrabi, A., Nowak, M., Pencer, J., et al., 2015. A Benchmark Comparison of the Canadian Supercritical Water-cooled Reactor (SCWR) 64-element Fuel Lattice Cell Parameters using Various Computer Codes. The 35th Annual Conference of the Canadian Nuclear Society. Saint John, New Brunswick, Canada.

Shen, W., 2012. Assessment of the traditional neutron-diffusion core-analysis method for the analysis of the Super Critical Water Reactor. Ann. Nucl. Energy 45, 1–7.

U.S. DOE Nuclear Energy Research Advisory Committee, 2002, "A Technology Roadmap for Generation IV Nuclear Energy Systems," GIF-002-00, http://gif.inel.gov/roadmap/pdfs/gen_iv_roadmap.pdf.

Varin, E., Hébert, A., Roy, R., Koclas, J., 2005. A User Guide for DONJON Version 3.01, Institut de génie nucléaire, Département de génie physique, École Polytechnique de Montréal, Montréal.

Yetisir, M., Gaudet, M., Rhodes, D., 2013. Development and Integration of Canadian SCWR Concept with Counter-Flow Fuel Assembly. The 6th International Symposium on SuperCritical Water Reactor (ISSCWR-6). Shenzhen, Guangdong, China.

Yi, C., Sjoden, G., 2013. Energy group structure determination using particle swarm optimization. Ann. Nucl. Energy 56, 53–56.

Younan, S., Novog, D., 2016. Important of Coolant Densities in TRITON Self-shielding Calculation for the Canadian SCWR. Important of Coolant Densities in TRITON Self-shielding Calculation for the Canadian SCWR," 40th Annual CNS/CNA Student Conference. Toronto, ON.

Chapter 7

Conclusions and Future Work

This work introduces a novel means and analysis that investigates the various lattice physics phenomena occur within the Canadian PT-SCWR to provide a comprehensive understanding of the neutronic behaviour within the lattice cell of such advanced GEN-IV nuclear energy system. Moreover, this work provided the most extensive examination of energy group boundaries for Pu-Th fuel mixture in high temperature reactors available up to date. The outcomes of the models were applied and the analysis performed lead to important conclusions related to the type of the fuel and design of such innovative GEN-IV nuclear reactor system which are summarized in this chapter. Recommendations for future work and a brief summary to the novel contribution to the knowledge created through the course of this work are also highlighted within this chapter.

The literature review discussed in this work shows that the Canadian PT-SCWR, which is an advanced GEN-IV nuclear energy system, has significant changes as compared to the conventional CANDU reactor. The multiple coolant flow-paths through the fuel channel, the Pu-Th fuel mixture, and the variation of the coolant properties through the fuel assembly lead to unique phenomena which have previously not been fully examined.

The first two papers investigate the lattice physics phenomena within the PT-SCWR through sensitivity and uncertainty analysis for fresh and depleted fuel. The third paper introduces a systematic study to examine the optimal discretized few energy group structure by which the minimum number of energy groups that corresponds to the highest computational accuracy were determined.

The three papers combined represent an in-depth analysis of the reactor physics phenomena for the Canadian PT-SCWR which lead to the following important conclusions:

- The Pu-Th fuel mixture is characterized by several large-magnitude and competing phenomena which cancels one another and gives rise to low sensitivities to important parameters such as coolant density. However, such large and competing phenomena also raise issues related to the robustness of the fuel design, since small changes in thermalhydraulic or fuel properties may give rise to undesirable behaviour.
- The tight lattice pitch of the PT SCWR compared to the conventional CANDU reactor results in a harder neutron spectrum. Such a spectrum appears well suited to the Pu-Th fuel, since it tends to increase the efficiency of fuel conversion.
- The coolant has an important contribution in the neutron moderation process. Consequently, the resonance escape probability and the fast fission factors become highly affected by the light water coolant properties in the fuel and flow tube regions. The PT-SCWR is characterized by a strong negative total coolant void reactivity dominated by the strong decrease in resonance escape probability. However as noted in the first paper, for non-equilibrium voiding cases the feedback may be positive.
- The PT-SCWR fuel channel is characterized by very high coolant temperature compared to the conventional thermal reactors. And thus the up-scattering phenomena into the low lying fission and capture resonances become very important and affect other phenomena such as the fuel, coolant and moderator temperature coefficients. Such importance is also reflected in the selection of the energy-group boundaries as discussed in the third paper.
- Fresh and depleted fuels are characterized by almost the same behaviour in terms of the reactivity changes and the behaviour of the four factors. The most important difference between fresh and depleted fuel is related to the fuel composition by which the overall fission content decreases with the Pu

depletion and the production of minor actinides, fission products, xenon and ^{233}U. The decrease in the reactivity observed for the depleted fuel is mainly due to the decrease in the reproduction factor as a consequence of fuel composition changes and the decrease in the fissile materials of the fuel.

- The optimum two and three energy group structures were identified based on numerical methods relying on the behaviour of the neutron multiplication factor and the different reactivity feedbacks. The third paper identified the importance of using multiple cost-function in the optimization process of energy group structure since multi-variate numerical search methodologies shows a limitation using one cost function.
- A two-group structure with an energy barrier set at 2.87 eV was observed to have an expected solution very close to the reference solution. Consequently, a higher thermal energy cut off compared with the conventional light water thermal reactors set at 2.87 eV is recommended for full core diffusion analysis for the PT-SCWR.
- Through numerical optimization, a unique barrier can be selected using singular cost function. The optimum three energy group structure was determined with additional barriers set at 820 keV based on the behaviour of reactivity feedback coefficients. The 820 keV barrier in the three group structure would separate the epithermal neutron range from the fast and delayed neutron range and minimize difference of other reactivity feedback coefficients from the reference solution. Additional energy group structure with a third energy barrier is set at 1.35 eV would minimize the bias in k_∞ and eliminate all the residual error in the neutron multiplication constant obtained due to the previously chosen three energy group structure. Also, the third energy barrier set at 1.35 eV would preserve the small errors in the calculation of the values of TCVR, ICVR and OCVR. Nevertheless, such additional barrier suffers from error cancelation.

7.1. Future Work

Completion of this work has identified many potential projects that can be pursued in the future, especially for the benefits of the development of the Canadian PT-SCWR project which has many participants through the different research institutions and universities. This includes, but is not limited to:

- The fuel nature and composition used in this study shows non-ideal behaviour in terms of large and opposing phenomena which cancel out. As a result, further investigation is recommended on the fuel design, type and percentage composition in order to have a fuel that is characterized by more stable behaviour.
- In this work, the optimum few energy group structure was determined based on the lattice cell transport approach. This approach has many benefits including the elimination of the code-to-code biases and the decrease in the computational cost. However, it is recommended that the outcomes of this study be validated with a full-core diffusion analysis and to compare the results with high energy fidelity reference solution obtained using the Monte Carlo continues energy like MCNP. Although a preliminary investigation of full-core analysis using PARCS was performed and confirmed the outcomes of this work but the in-depth comparisons were beyond the scope of this work.

7.2. Publications and presentations

In addition to the novel methods and analysis presented in this work, contribution to knowledge extents to the peer-reviewed studies, journal publications and presentations presented in international conferences which are listed as:

- **A. Moghrabi** and D.R. Novog, “Determination of the Optimal Few-Energy Group Structure for the Canadian Super Critical Water-cooled Reactor”, accepted by the Annals of Nuclear Energy on 12th Jan. 2018.
- **A. Moghrabi** and D.R. Novog, “Investigation of Fuel Burnup Impacts on Nuclear Reactor Safety Parameters in the Canadian Pressure Tube

Supercritical Water-cool Reactor," ASME. ASME Journal of Nuclear Radiation Science. 2017;4(1):011011-011011-11. doi:10.1115/1.4037895.

- **A. Moghrabi** and D.R. Novog, "Optimization Approach of Energy Group Structure for the Canadian Pressure Tube SuperCritical Water Reactor," Proceedings of the 37th Annual Conference of the Canadian Nuclear Society, Niagara Falls, ON Canada 2017.
- **A. Moghrabi** and D.R. Novog, "Investigation of Fuel Burnup on Reactor Physics Phenomena in the Canadian Pressure Tube SuperCritical Water-cool Reactor," Proceedings of the 8th International Symposium on SuperCritical Water Reactor (ISSCWR-8), Chengdu, China, 2017.
- **A. Moghrabi** and D.R. Novog,"Investigation of Lattice Physics Phenomena in the Canadian PT-SCWR in some Perturbed Scenarios," submitted to the 41th CNS/CNA Student Conference of the Canadian Nuclear Society, Niagara Falls, Ontario, Canada 2017.
- **A. Moghrabi** and D.R. Novog, "Investigation of Reactor Physics Phenomena in the Canadian Pressure Tube SuperCritical Water Reactor," Canadian Nuclear Laboratories Nuclear Review, Vol. 5, No. 2, 2016, pp. 253-268, doi:10.12943/CNR.2016.00031, available online at: http://dx.doi.org/10.12943/CNR.2016.00031
- **A. Moghrabi** and D.R. Novog," Nuclear Data Sensitivity and Uncertainty Analysis for the Canadian Supercritical Water- cooled Reactor (SCWR) 64 – element Fresh Fuel Lattice Cell," Proceedings of the 39th CNS/CNA Student Conference of the Canadian Nuclear Society, Saint John, New Brunswick, Canada, 2015.
- J. Sharpe, F. Salaun, D. Hummel, **A. Moghrabi**, M. Nowak, J. Pencer, D. Novog. A. Buijs, "A Benchmark Comparison of the Canadian SuperCritical Water-cooled Reactor (SCWR) 64-element Fuel Lattice Cell Parameters Using Various Computer Codes," Proceedings of the 35th Annual Conference of the Canadian Nuclear Society, Saint John, New Brunswick, Canada, 2015.

References

[1] "World Statistics Nuclear Energy Around the World," Nuclear Energy Institute, [Online]. Available: http://www.nei.org/Knowledge-Center/Nuclear-Statistics/World-Statistics. [Accessed 10 November 2016].

[2] U.S. DOE Nuclear Energy Research Advisory Committee and the Generation IV International Forum, "A Technology Roadmap for Generation IV Nuclear Energy Systems," 2002. [Online]. Available: https://www.gen-4.org/gif/jcms/c_40481/technology-roadmap. [Accessed 10 March 2014].

[3] OECD Nuclear Energy Agency for the Generation IV International Forum, "Technology Roadmap Update for Generation IV Nuclear Energy Systems," 2014. [Online]. Available: https://www.gen-4.org/gif/jcms/c_60729/technology-roadmap-update-2013. [Accessed 2 December 2016].

[4] NPR, "A Nuclear-Powered World," [Online]. Available: http://www.npr.org/2011/05/16/136288669/a-nuclear-powered-world. [Accessed 15 November 2016].

[5] Nuclear Energy Agency, "GIF Symposium Proceedings," in *Organization for Economic Co-operation and Development*, San Diego, USA, 2012.

[6] Y. Oka, "Review of High Temperature Water and Stream Cooled Rector Concepts.," in *First International Symposium on Supercritical Water-*

Cooled Reactors, Design and Technology, SCR-2000, Tokyo, Japan, 6-9 November, 2000.

[7] Y. Oka; S. Koshizuka; "Conceptual Design Study of Advanced Power Reactors," *Progress in Nuclear Energy,* vol. 32, no. 1, pp. 163-177, 1998.

[8] T. Schulenberg; L.K.H Leung; Y. Oka; "Review of R&D for Supercritical Water Cooled Reactors," *Progress in Nuclear Energy,* vol. 77, pp. 282 - 299, 2014.

[9] Y. Oka; S. Koshizuka; Y. Ishiwatari; A. Yamaji; "Super Light Water Reactors and Super Fast Reactors," Springer Science and Business Media, 2010.

[10] J. Licht; M. Anderson and M. Corradini; "Heat transfer to water at supercritical pressures in a circular and square annular flow geometry," *International Journal of Heat and Fluid Flow,* vol. 29, no. 1, pp. 156-166, 2008.

[11] The Generation IV International Forum, "Supercritical-Water-Cooled Reactor (SCWR)," [Online]. Available: https://www.gen-4.org/gif/jcms/c_42151/supercritical-water-cooled-reactor-scwr. [Accessed 8 December 2016].

[12] O. O. Gabriel; A. M.; Y.E. Chad-Umoren; "Science and Technology of Supercritical Water Cooled Reactors: Review and Status," *Journal of Energy Technologies and Policy,* vol. 3, no. 7, 2013.

[13] T. Schulenberg; L.K.H Leung; D. Brady; Y. Oka; K. Yamada; Y. Bae; G. Willermoz, "Supercritical Water-Cooled Reactor (SCWR) Development through GIF Collaboration," IAEA-CN-164-5S06.

[14] L. Leung; M. Yetisir; M. Diamond; D. Martin; J. Pencer; B. Hyland; H. Hamilton; D. Guzonas; R. Duffey, "A Next Generation Heavy Water Nuclear Reactor with Supercritical Water as Coolant," in *International*

Conference on the Future of Heavy Water Reactors (HWR-Future), Ottawa, Canada, 2011.

[15] D.F. Torgerson; B.A. Shalaby; S. Pang; "CANDU Technology for Generation III+ and IV Reactors," *Nuclear Engineering and Design,* vol. 236, pp. 1565-1572, 2006.

[16] C.K. Chow; H.F. Khartabil; "Conceptual Fuel Channel Designs for CANDU-SCWR," *Special issue on the 3rd international symposium on SCWR, Nuclear Engineering and Technology,* vol. 40(2), pp. 139-146, 2007.

[17] M. Yetisir; M. Gaudet; D. Rhodes; "Development and Integration of Canadian SCWR Concept with Counter-Flow Fuel Assembly," in *The 6th International Symposium on Supercritical Water Reactor (ISSCWR-6),* Shenzhen, Guangdong, China, 2013.

[18] J. Pencer; D. Watts; A. Colton; X. Wang; L. Blomeley; V. Anghel; S. Yue; "Core Neutronics for the Canadian SCWR Conceptual Design," in *The 6th International Symposium on Supercritical Water-Cooled Reactors (ISSCWR-6),* Shenzhen, Guangdong, China, 2013.

[19] D. Hummel; D. Novog;, "Coupled 3D Neutron Kinetics and Thermalhydraulic Characteristics of the Canadian Supercritical Water Reactor," *Nuclear Engineering and Design,* vol. 298 , pp. 78-89, 2016.

[20] G. Harrisson; G. Marleau; "Simulation Strategy for the Evaluation of Neutronic Properties of a Canadian SCWR Fuel Channel," *Science and Technology of Nuclear Installations,* Vols. 2013, Article ID 352757, 10 pages, 2013.

[21] P. Yang, L. Cao, H. Wu and W. Changhui , "Core Design Study on CANDU-SCWR with 3D Neutronics/Thermal Hydraulics Coupling," *Nuclear Engineering and Design,* vol. 241, no. 12, pp. 4714-4719, 2011.

[22] C. Yi; G. Sjoden; "Energy Group Structure Determination Using Particle Swarm Optimization," *Annals of Nuclear Energy*, vol. 56, pp. 53-56., 2013.

[23] E. Aristodemou, C. Pain, C. Oliveria and A. Umpleby, "Energy Group Optimization for Forward and Inverse Problems in Nuclear Engineering: Application to Downwell-Logging Problems," *Geophysical Prospecting*, vol. 54, pp. 99-120, 2006.

[24] M. Akbari; A. Minuchehr; A. Zolfaghari; F. Kho; "An Investigation for an Optimized Neutron Energy-Group Structure in the Thermal Lattices using Particle Swarm Optimization," *Annals of Nuclear Energy*, vol. 47, pp. 53-61, 2012.

[25] C. Druska; St. Kasselmann; A. Lauer; "Investigation of Space-Dependent Safety-Related Parameters of a PBMR-like HTR in Transient Operating Conditions Applying a Multi-Group Diffusion Code," *Nuclear Engineering and Design*, vol. 239, pp. 508-520, 2009.

[26] W. Shen, "Assessment of the Taditional Neutron-Diffusion Core-Analysis Method for the Analysis of the Super Critical Water Reactor," *Annals of Nuclear Energy*, vol. 45, pp. 1-7, 2012.

[27] I.L. Pioro; R.B. Duffey; “Heat Transfer and Hydraulic Resistance at Supercritical Pressures in Power Engineering Applications,” New York, NY: ASME Press, 2007, p. 334.

[28] Y. Oka; S. Koshizuka; "Supercritical-pressure, Once-through Cycle Light Water Cooled Reactor Concept," *Nuclear Science and Technology*, vol. 38, no. 12, pp. 1081-1089, 2001.

[29] Y. Oka; H. Mori; “Supercritical-Pressure Light Water Cooled Reactors,” Springer, 2014.

[30] T. Schulenberg; J. Starflinger; “High Performance Light Water Reactor, Design and Analysis,” Karlsruhe: KIT Scientific Publishing, 2012.

[31] X. Cheng; X.J. Liu; Y.H. Yang; "A Mixed Core for Supercritical Water-Cooled Reactors," in *3rd Int. Symposium on SCWR*, Shanghai, China, March, 2007.

[32] P.G. Boczar; W. Shen; J. Pencer; B. Hyland; P.S.W. Chan; R.G. Dworshak; "Reactor Physics Studies for a Pressure Tube Supercritical Water Reactor (PT-SCWR)," in *The 2nd Canada-China Joint Workshop on Supercritical Water-Cooled Reactors (CCSC-2010)*, Toronto, 2010.

[33] M.H. McDonald; B. Hyland; H. Hamilton; L.K.H. Leung; N. Onder; J. Pencer; R. Xu; "Pre-Conceptual Fuel Design Concepts for the Canadian Super Critical Water-Cooled Reactor," in *The 5th International Symposium on Supercritical Water-Cooled Reactors (ISSCWR-5)*, Vancouver, 2011.

[34] J. Pencer, M. McDonald and V. Anghel, "Parameters for Transient Response Modelling for the Canadian SCWR," in *The 19th Pacific Basin Nuclear Conference (PBNC 2014). Vancouver, BC.*, Vancouver, BC, 2014.

[35] G.I. Bell; S. Glasstone; "Nuclear Reactor Theory," NJ: Van Nostrand Princeton, 1970.

[36] I. Bondarenko; "Group Constants for Nuclear Reactor Calculations," New York: Consultants Bureau, 1964.

[37] Koclas, Jean, "Neutronic Analysis of Reactors," 1998.

[38] J. Duderstadt; L. Hamilton; "Nuclear reactor analysis," New York: Wiley, 1976.

[39] S. Glasstone; A. Sesonske; "Nuclear Reactor Engineering," 4th, Ed., New York: NY: Chapman & Hall, 1994.

[40] Y. Ronen, "High Converting Water Reactors", Boca Raton, Florida: CRC Press, 1990.

[41] L. Massimo, “Physics of High Temperature Reactors,” NY: Pergamon Press, 1976.

[42] M. H. Merrill, "Nuclear Design Methods and Experimental Data in Use at Gulf General Atomic," Gulf-GA-Al2652, Gulf Oil Company, San Diego, CA, July 1973.

[43] J. S. Han, "Sensitivity Study on the Energy Group Structure for High Temperature Reactor Analysis," 2008.

[44] J. Chang, "Nuclear Data Needs for Generation-IV reactors.," in *2003 Workshop on Nuclear Data Production and Evaluation*, Pohang, Korea, 2003.

[45] M. Driscoll; P. Hejzlar; "Reactor Physics Challenges in GEN-IV Reactor Design," *Nuclear Engineering and Technology,* vol. 37, pp. 1-10, 2005.

[46] R. Forrest, "Nuclear Science and Data Needs for Advanced Nuclear Systems," *Nuclear Procedia,* vol. 7, pp. 540-552, 2010.

[47] S. Pelloni; K. Mikityuk; "Nuclear Data Uncertainty Analysis for the Generation IV Gas-Cooled Fast Reactor," in *PHYSOR 2012: Advances in Reactor Physics - Linking Research, Industry and Education*, Knoxville, Tennessee, USA, 2012.

[48] K. Kozier; G. Dyck; "Sensitivity of CANDU-SCWR reactor physics calculations to nuclear data files," in *Nuclear Data Needs for Generation-IV Nuclear Energy Systems, Proceedings of the International Workshop*, Antwerp Belgium, 2005.

[49] S. Langton; A. Buijs; T. Zhu; D. Novog; "Monte Carlo Simulation of a Burnup-Average 78-Element Canadian SCWR and Similarity Study with ZED-2 Test Reactor," in *The 3rd China-Canada Joint Workshop on Supercritical Water Cooled Reactors (CCSC-2012)*, Xi’an, China, 2012.

[50] L. Blomeley; J. Pencer; B. Hyland; F.P. Adams; "Nuclear Data Sensitivity and Uncertinty for the Canadian Supercritical Water-Cooled Reactor," *Annals of Nuclear Energy,* vol. 63, pp. 587-593, 2014.

[51] D. Cacuci; SpringerLink (Online service); "Handbook of Nuclear Engineering," Boston, MA: Springer US, 2010.

[52] *Scale: A Comprehensive Modelling and Simulation Suite for Nuclear Safety Analysis and Design, ORNL/TM-2005/39, Version 6.1,* Available from Radiation Safety Information Computational Center Oak Ridge National Laboratory as CCC-785, June 2011.

[53] C. McEwan, "Covariance in Multigroup and Few Group Reactor Physics Uncertainty Calculations," Master Thesis, McMaster University, Hamilton, Canada, 2011.

[54] J. Taylor, "An Introduction to Error Analysis, Sausalito," USA: University Science Books, 1997.

[55] D. Cacuci, Sensitivity and Uncertainty Analysis Theory (Volume I), Boca Raton, Florida: CRC Press LLC, 2003.

[56] J. F. Ahearne, "Prospects for nuclear energy," *Energy Economics,* vol. 33, no. 4, pp. 572-580, 2011.

Appendix

1. PT-SCWR model input

The PT-SCWR lattice cell was modelled in SCALE. Thousands of input file have to be created for the optimum energy group structure analysis. Such process was automated using python language in conjunction with the SCALE code in order to generate the SCALE input files. It would be inconvenient to present all the input files in this report, rather a sample would be presented.

A sample of python file that creates all the allowed two-group structure lattice cell (237 files) is show below which also reflects PT-SCWR lattice cell modelling in SCALE:

```
import subprocess
import os
############################################################
# Middle of the Channel Input file top and bottom templates
############################################################
Middle_inputfile_top_template ='=t-xsec\n'\
'SCWR Lattice Cell (at 250 cm from bottom Channel / Middle of
channel) \n'\
'v7-238 \n'\
'read composition \n'\
'h2o 1 den=0.58758 1 634.39 end \n'\
      'wtpt-zr310ssIFT \n'\
      '      2   7.90      10 \n'\
      '   6000   0.034\n'\
      '  14000   0.51\n'\
      '  25055   0.74\n'\
      '  15031   0.016\n'\
      '  16000   0.002\n'\
      '  28000  20.82\n'\
      '  24000  25.04\n'\
      '  26000  51.738\n'\
      '  42000   0.51\n'\
      '  40000   0.59\n'\
      '1    663.99  end\n'\
      'h2o 3  den=0.13998 1 692.35 end\n'\
'    ag-107      4     Den=9.91    0     6.2281E-012 1550.53     end   \n'\
'    ag-109      4     Den=9.91    0     0.000016513 1550.53     end   \n'\
'    ag-111      4     Den=9.91    0     4.4363E-008 1550.53     end   \n'\
'    al-27 4     Den=9.91    0     1E-020      1550.53     end   \n'\
'    am-241      4     Den=9.91    0     0.000036693 1550.53     end   \n'\
'    am-242      4     Den=9.91    0     3.2175E-008 1550.53     end   \n'\
```

```
'    am-243      4     Den=9.91    0     0.000039255 1550.53     end   \n'\
'    ar-36 4     Den=9.91    0     1E-020      1550.53     end   \n'\
'    ar-38 4     Den=9.91    0     1E-020      1550.53     end   \n'\
'    ar-40 4     Den=9.91    0     1.0022E-020 1550.53     end   \n'\
'    as-75 4     Den=9.91    0     1.7175E-008 1550.53     end   \n'\
'    au-197      4     Den=9.91    0     1.0192E-020 1550.53     end   \n'\
'    b-10  4     Den=9.91    0     3.662E-018  1550.53     end   \n'\
'    b-11  4     Den=9.91    0     7.5781E-015 1550.53     end   \n'\
'    ba-130      4     Den=9.91    0     1E-020      1550.53     end   \n'\
'    ba-132      4     Den=9.91    0     6.6364E-012 1550.53     end   \n'\
'    ba-134      4     Den=9.91    0     0.000001661 1550.53     end   \n'\
'    ba-135      4     Den=9.91    0     6.9206E-009 1550.53     end   \n'\
'    ba-136      4     Den=9.91    0     1.5886E-006 1550.53     end   \n'\
'    ba-137      4     Den=9.91    0     2.5334E-006 1550.53     end   \n'\
'    ba-138      4     Den=9.91    0     0.000072562 1550.53     end   \n'\
'    ba-140      4     Den=9.91    0     0.000001154 1550.53     end   \n'\
'    be-9  4     Den=9.91    0     4.9886E-013 1550.53     end   \n'\
'    bi-209      4     Den=9.91    0     1.9697E-013 1550.53     end   \n'\
'    bk-249      4     Den=9.91    0     1.1303E-013 1550.53     end   \n'\
'    br-79 4     Den=9.91    0     2.5538E-010 1550.53     end   \n'\
'    br-81 4     Den=9.91    0     1.8199E-006 1550.53     end   \n'\
'    ca-40 4     Den=9.91    0     1E-020      1550.53     end   \n'\
'    ca-42 4     Den=9.91    0     1.0011E-020 1550.53     end   \n'\
'    ca-43 4     Den=9.91    0     1E-020      1550.53     end   \n'\
'    ca-44 4     Den=9.91    0     1.0069E-020 1550.53     end   \n'\
'    ca-46 4     Den=9.91    0     1E-020      1550.53     end   \n'\
'    ca-48 4     Den=9.91    0     1E-020      1550.53     end   \n'\
'    cd-106      4     Den=9.91    0     1.1919E-020 1550.53     end   \n'\
'    cd-108      4     Den=9.91    0     5.2466E-011 1550.53     end   \n'\
'    cd-110      4     Den=9.91    0     5.1317E-006 1550.53     end   \n'\
'    cd-111      4     Den=9.91    0     4.2797E-006 1550.53     end   \n'\
'    cd-112      4     Den=9.91    0     1.8648E-006 1550.53     end   \n'\
'    cd-113      4     Den=9.91    0     3.3468E-008 1550.53     end   \n'\
'    cd-114      4     Den=9.91    0     1.9009E-006 1550.53     end   \n'\
'    cd-116      4     Den=9.91    0     0.000000512 1550.53     end   \n'\
'    ce-136      4     Den=9.91    0     1E-020      1550.53     end   \n'\
'    ce-138      4     Den=9.91    0     2.2029E-013 1550.53     end   \n'\
'    ce-140      4     Den=9.91    0     0.000065946 1550.53     end   \n'\
'    ce-141      4     Den=9.91    0     2.7452E-006 1550.53     end   \n'\
'    ce-142      4     Den=9.91    0     0.000057939 1550.53     end   \n'\
'    ce-143      4     Den=9.91    0     1.0315E-007 1550.53     end   \n'\
'    ce-144      4     Den=9.91    0     0.000016777 1550.53     end   \n'\
'    cf-249      4     Den=9.91    0     2.5343E-014 1550.53     end   \n'\
'    cf-250      4     Den=9.91    0     2.8225E-014 1550.53     end   \n'\
'    cf-251      4     Den=9.91    0     8.4095E-015 1550.53     end   \n'\
'    cf-252      4     Den=9.91    0     1.6941E-015 1550.53     end   \n'\
'    cf-253      4     Den=9.91    0     1.2524E-018 1550.53     end   \n'\
'    cf-254      4     Den=9.91    0     2.2318E-020 1550.53     end   \n'\
'    cl-35 4     Den=9.91    0     1E-020      1550.53     end   \n'\
'    cl-37 4     Den=9.91    0     1.0044E-020 1550.53     end   \n'\
'    cm-241      4     Den=9.91    0     2.8001E-013 1550.53     end   \n'\
'    cm-242      4     Den=9.91    0     5.0745E-006 1550.53     end   \n'\
'    cm-243      4     Den=9.91    0     0.000000107 1550.53     end   \n'\
'    cm-244      4     Den=9.91    0     0.000010805 1550.53     end   \n'\
```

```
'    cm-245      4     Den=9.91    0     7.3209E-007 1550.53     end   \n'\
'    cm-246      4     Den=9.91    0     3.5894E-008 1550.53     end   \n'\
'    cm-247      4     Den=9.91    0     3.4237E-010 1550.53     end   \n'\
'    cm-248      4     Den=9.91    0     1.0818E-011 1550.53     end   \n'\
'    cm-250      4     Den=9.91    0     3.7882E-019 1550.53     end   \n'\
'    co-59 4     Den=9.91    0     1E-020      1550.53     end   \n'\
'    cr-50 4     Den=9.91    0     1E-020      1550.53     end   \n'\
'    cr-52 4     Den=9.91    0     1E-020      1550.53     end   \n'\
'    cr-53 4     Den=9.91    0     1E-020      1550.53     end   \n'\
'    cr-54 4     Den=9.91    0     1.0111E-020 1550.53     end   \n'\
'    cs-133      4     Den=9.91    0     0.000072161 1550.53     end   \n'\
'    cs-134      4     Den=9.91    0     0.000004817 1550.53     end   \n'\
'    cs-135      4     Den=9.91    0     0.000048944 1550.53     end   \n'\
'    cs-136      4     Den=9.91    0     4.0088E-008 1550.53     end   \n'\
'    cs-137      4     Den=9.91    0     0.000074212 1550.53     end   \n'\
'    cu-63 4     Den=9.91    0     1E-020      1550.53     end   \n'\
'    cu-65 4     Den=9.91    0     2.2916E-014 1550.53     end   \n'\
'    dy-156      4     Den=9.91    0     3.0097E-019 1550.53     end   \n'\
'    dy-158      4     Den=9.91    0     2.91E-015   1550.53     end   \n'\
'    dy-160      4     Den=9.91    0     2.0879E-008 1550.53     end   \n'\
'    dy-161      4     Den=9.91    0     5.3738E-008 1550.53     end   \n'\
'    dy-162      4     Den=9.91    0     2.6777E-008 1550.53     end   \n'\
'    dy-163      4     Den=9.91    0     1.6635E-008 1550.53     end   \n'\
'    dy-164      4     Den=9.91    0     4.8274E-009 1550.53     end   \n'\
'    er-162      4     Den=9.91    0     2.8299E-019 1550.53     end   \n'\
'    er-164      4     Den=9.91    0     5.2949E-014 1550.53     end   \n'\
'    er-166      4     Den=9.91    0     1.1619E-009 1550.53     end   \n'\
'    er-167      4     Den=9.91    0     1.1031E-010 1550.53     end   \n'\
'    er-168      4     Den=9.91    0     2.3476E-010 1550.53     end   \n'\
'    er-170      4     Den=9.91    0     1.3983E-011 1550.53     end   \n'\
'    es-253      4     Den=9.91    0     9.5144E-019 1550.53     end   \n'\
'    es-254      4     Den=9.91    0     1E-020      1550.53     end   \n'\
'    es-255      4     Den=9.91    0     1E-020      1550.53     end   \n'\
'    eu-151      4     Den=9.91    0     6.3861E-009 1550.53     end   \n'\
'    eu-152      4     Den=9.91    0     5.1797E-009 1550.53     end   \n'\
'    eu-153      4     Den=9.91    0     7.7686E-006 1550.53     end   \n'\
'    eu-154      4     Den=9.91    0     1.4927E-006 1550.53     end   \n'\
'    eu-155      4     Den=9.91    0     5.7145E-007 1550.53     end   \n'\
'    eu-156      4     Den=9.91    0     1.2946E-007 1550.53     end   \n'\
'    eu-157      4     Den=9.91    0     0.000000001 1550.53     end   \n'\
'    f-19  4     Den=9.91    0     1.2121E-020 1550.53     end   \n'\
'    fe-54 4     Den=9.91    0     1E-020      1550.53     end   \n'\
'    fe-56 4     Den=9.91    0     1.0253E-020 1550.53     end   \n'\
'    fe-57 4     Den=9.91    0     1E-020      1550.53     end   \n'\
'    fe-58 4     Den=9.91    0     2.9515E-020 1550.53     end   \n'\
'    ga-69 4     Den=9.91    0     9.4391E-011 1550.53     end   \n'\
'    ga-71 4     Den=9.91    0     6.712E-010  1550.53     end   \n'\
'    gd-152      4     Den=9.91    0     5.8908E-009 1550.53     end   \n'\
'    gd-154      4     Den=9.91    0     1.1493E-007 1550.53     end   \n'\
'    gd-155      4     Den=9.91    0     1.1546E-008 1550.53     end   \n'\
'    gd-156      4     Den=9.91    0     3.8867E-006 1550.53     end   \n'\
'    gd-157      4     Den=9.91    0     1.4465E-008 1550.53     end   \n'\
'    gd-158      4     Den=9.91    0     1.7884E-006 1550.53     end   \n'\
'    gd-160      4     Den=9.91    0     1.4718E-007 1550.53     end   \n'\
```

```
'    ge-70 4     Den=9.91    0     5.4033E-013 1550.53     end   \n'\
'    ge-72 4     Den=9.91    0     1.4903E-009 1550.53     end   \n'\
'    ge-73 4     Den=9.91    0     3.19E-009   1550.53     end   \n'\
'    ge-74 4     Den=9.91    0     7.6277E-009 1550.53     end   \n'\
'    ge-76 4     Den=9.91    0     3.646E-008  1550.53     end   \n'\
'    h-1   4     Den=9.91    0     1.5949E-008 1550.53     end   \n'\
'    h-2   4     Den=9.91    0     1.7094E-009 1550.53     end   \n'\
'    h-3   4     Den=9.91    0     1.603E-007  1550.53     end   \n'\
'    he-3  4     Den=9.91    0     1E-020      1550.53     end   \n'\
'    he-4  4     Den=9.91    0     0.000012718 1550.53     end   \n'\
'    hf-174      4     Den=9.91    0     1E-020      1550.53     end   \n'\
'    hf-176      4     Den=9.91    0     1.0131E-020 1550.53     end   \n'\
'    hf-177      4     Den=9.91    0     1E-020      1550.53     end   \n'\
'    hf-178      4     Den=9.91    0     1.5767E-020 1550.53     end   \n'\
'    hf-179      4     Den=9.91    0     1.7409E-020 1550.53     end   \n'\
'    hf-180      4     Den=9.91    0     1.3179E-020 1550.53     end   \n'\
'    hg-196      4     Den=9.91    0     1E-020      1550.53     end   \n'\
'    hg-198      4     Den=9.91    0     1.603E-020  1550.53     end   \n'\
'    hg-199      4     Den=9.91    0     1E-020      1550.53     end   \n'\
'    hg-200      4     Den=9.91    0     1.6999E-020 1550.53     end   \n'\
'    hg-201      4     Den=9.91    0     1E-020      1550.53     end   \n'\
'    hg-202      4     Den=9.91    0     1.0177E-020 1550.53     end   \n'\
'    hg-204      4     Den=9.91    0     1E-020      1550.53     end   \n'\
'    ho-165      4     Den=9.91    0     3.7506E-009 1550.53     end   \n'\
'    i-127 4     Den=9.91    0     4.5246E-006 1550.53     end   \n'\
'    i-129 4     Den=9.91    0     0.000013661 1550.53     end   \n'\
'    i-130 4     Den=9.91    0     3.4422E-010 1550.53     end   \n'\
'    i-131 4     Den=9.91    0     4.5672E-007 1550.53     end   \n'\
'    i-135 4     Den=9.91    0     2.8348E-008 1550.53     end   \n'\
'    in-113      4     Den=9.91    0     7.6894E-011 1550.53     end   \n'\
'    in-115      4     Den=9.91    0     2.843E-007  1550.53     end   \n'\
'    ir-191      4     Den=9.91    0     1E-020      1550.53     end   \n'\
'    ir-193      4     Den=9.91    0     1E-020      1550.53     end   \n'\
'    k-39  4     Den=9.91    0     1E-020      1550.53     end   \n'\
'    k-40  4     Den=9.91    0     1E-020      1550.53     end   \n'\
'    k-41  4     Den=9.91    0     1.0166E-020 1550.53     end   \n'\
'    kr-78 4     Den=9.91    0     7.0291E-020 1550.53     end   \n'\
'    kr-80 4     Den=9.91    0     3.0379E-011 1550.53     end   \n'\
'    kr-82 4     Den=9.91    0     3.6207E-008 1550.53     end   \n'\
'    kr-83 4     Den=9.91    0     3.4076E-006 1550.53     end   \n'\
'    kr-84 4     Den=9.91    0     6.5589E-006 1550.53     end   \n'\
'    kr-85 4     Den=9.91    0     0.000001565 1550.53     end   \n'\
'    kr-86 4     Den=9.91    0     0.000010119 1550.53     end   \n'\
'    la-138      4     Den=9.91    0     8.0904E-010 1550.53     end   \n'\
'    la-139      4     Den=9.91    0     0.000067626 1550.53     end   \n'\
'    la-140      4     Den=9.91    0     0.000000154 1550.53     end   \n'\
'    li-6  4     Den=9.91    0     1E-020      1550.53     end   \n'\
'    li-7  4     Den=9.91    0     1.9997E-020 1550.53     end   \n'\
'    lu-175      4     Den=9.91    0     1.0181E-020 1550.53     end   \n'\
'    lu-176      4     Den=9.91    0     1E-020      1550.53     end   \n'\
'    mg-24 4     Den=9.91    0     1.0003E-020 1550.53     end   \n'\
'    mg-25 4     Den=9.91    0     1E-020      1550.53     end   \n'\
'    mg-26 4     Den=9.91    0     1.0001E-020 1550.53     end   \n'\
'    mn-55 4     Den=9.91    0     1E-020      1550.53     end   \n'\
```

```
'    mo-100      4     Den=9.91    0     0.000074646 1550.53     end   \n'\
'    mo-92 4     Den=9.91    0     1.2466E-019 1550.53     end   \n'\
'    mo-94 4     Den=9.91    0     4.1973E-010 1550.53     end   \n'\
'    mo-95 4     Den=9.91    0     0.000045005 1550.53     end   \n'\
'    mo-96 4     Den=9.91    0     1.3083E-006 1550.53     end   \n'\
'    mo-97 4     Den=9.91    0     0.000060407 1550.53     end   \n'\
'    mo-98 4     Den=9.91    0     0.000064221 1550.53     end   \n'\
'    mo-99 4     Den=9.91    0     2.6262E-007 1550.53     end   \n'\
'    n-14  4     Den=9.91    0     7.0504E-013 1550.53     end   \n'\
'    n-15  4     Den=9.91    0     1.8753E-009 1550.53     end   \n'\
'    na-23 4     Den=9.91    0     1E-020      1550.53     end   \n'\
'    nb-93 4     Den=9.91    0     4.9973E-012 1550.53     end   \n'\
'    nb-94 4     Den=9.91    0     1.5694E-010 1550.53     end   \n'\
'    nb-95 4     Den=9.91    0     2.6209E-006 1550.53     end   \n'\
'    nd-142      4     Den=9.91    0     4.3833E-007 1550.53     end   \n'\
'    nd-143      4     Den=9.91    0     0.000046675 1550.53     end   \n'\
'    nd-144      4     Den=9.91    0     0.00003435  1550.53     end   \n'\
'    nd-145      4     Den=9.91    0     0.000033892 1550.53     end   \n'\
'    nd-146      4     Den=9.91    0     0.000032079 1550.53     end   \n'\
'    nd-147      4     Den=9.91    0     3.6471E-007 1550.53     end   \n'\
'    nd-148      4     Den=9.91    0     0.000019923 1550.53     end   \n'\
'    nd-150      4     Den=9.91    0     0.000011679 1550.53     end   \n'\
'    ni-58 4     Den=9.91    0     1E-020      1550.53     end   \n'\
'    ni-59 4     Den=9.91    0     1E-020      1550.53     end   \n'\
'    ni-60 4     Den=9.91    0     1.1001E-020 1550.53     end   \n'\
'    ni-61 4     Den=9.91    0     1.0001E-020 1550.53     end   \n'\
'    ni-62 4     Den=9.91    0     1E-020      1550.53     end   \n'\
'    ni-64 4     Den=9.91    0     1.002E-020  1550.53     end   \n'\
'    np-236      4     Den=9.91    0     1.2809E-013 1550.53     end   \n'\
'    np-237      4     Den=9.91    0     1.1154E-007 1550.53     end   \n'\
'    np-238      4     Den=9.91    0     1.4941E-010 1550.53     end   \n'\
'    np-239      4     Den=9.91    0     3.5041E-011 1550.53     end   \n'\
'    o-16  4     Den=9.91    0     0.045033    1550.53     end   \n'\
'    o-17  4     Den=9.91    0     5.1359E-009 1550.53     end   \n'\
'    p-31  4     Den=9.91    0     1.0003E-020 1550.53     end   \n'\
'    pa-231      4     Den=9.91    0     1.8758E-006 1550.53     end   \n'\
'    pa-232      4     Den=9.91    0     2.0763E-009 1550.53     end   \n'\
'    pa-233      4     Den=9.91    0     0.000012453 1550.53     end   \n'\
'    pb-204      4     Den=9.91    0     1.0149E-020 1550.53     end   \n'\
'    pb-206      4     Den=9.91    0     4.2022E-014 1550.53     end   \n'\
'    pb-207      4     Den=9.91    0     1.3284E-012 1550.53     end   \n'\
'    pb-208      4     Den=9.91    0     8.6853E-010 1550.53     end   \n'\
'    pd-102      4     Den=9.91    0     2.2512E-011 1550.53     end   \n'\
'    pd-104      4     Den=9.91    0     8.8453E-006 1550.53     end   \n'\
'    pd-105      4     Den=9.91    0     0.000059827 1550.53     end   \n'\
'    pd-106      4     Den=9.91    0     0.000033848 1550.53     end   \n'\
'    pd-107      4     Den=9.91    0     0.000040575 1550.53     end   \n'\
'    pd-108      4     Den=9.91    0     0.000028586 1550.53     end   \n'\
'    pd-110      4     Den=9.91    0     9.5149E-006 1550.53     end   \n'\
'    pm-147      4     Den=9.91    0     0.000011638 1550.53     end   \n'\
'    pm-148      4     Den=9.91    0     4.4113E-008 1550.53     end   \n'\
'    pm-149      4     Den=9.91    0     5.4387E-008 1550.53     end   \n'\
'    pm-151      4     Den=9.91    0     1.4314E-008 1550.53     end   \n'\
'    pr-141      4     Den=9.91    0     0.000057175 1550.53     end   \n'\
```

```
'    pr-142      4     Den=9.91    0     1.1712E-009 1550.53     end   \n'\
'    pr-143      4     Den=9.91    0     1.0147E-006 1550.53     end   \n'\
'    pu-236      4     Den=9.91    0     3.1473E-011 1550.53     end   \n'\
'    pu-237      4     Den=9.91    0     1.5299E-010 1550.53     end   \n'\
'    pu-238      4     Den=9.91    0     0.000075172 1550.53     end   \n'\
'    pu-239      4     Den=9.91    0     0.00061728  1550.53     end   \n'\
'    pu-240      4     Den=9.91    0     0.00079033  1550.53     end   \n'\
'    pu-241      4     Den=9.91    0     0.00033178  1550.53     end   \n'\
'    pu-242      4     Den=9.91    0     0.00029508  1550.53     end   \n'\
'    pu-243      4     Den=9.91    0     1.793E-008  1550.53     end   \n'\
'    pu-244      4     Den=9.91    0     6.2066E-009 1550.53     end   \n'\
'    rb-85 4     Den=9.91    0     5.8342E-006 1550.53     end   \n'\
'    rb-86 4     Den=9.91    0     0.000000001 1550.53     end   \n'\
'    rb-87 4     Den=9.91    0     0.000013202 1550.53     end   \n'\
'    re-185      4     Den=9.91    0     1E-020      1550.53     end   \n'\
'    re-187      4     Den=9.91    0     1.0495E-020 1550.53     end   \n'\
'    rh-103      4     Den=9.91    0     0.00006343  1550.53     end   \n'\
'    rh-105      4     Den=9.91    0     1.1525E-007 1550.53     end   \n'\
'    ru-100      4     Den=9.91    0     5.0477E-006 1550.53     end   \n'\
'    ru-101      4     Den=9.91    0     0.000066524 1550.53     end   \n'\
'    ru-102      4     Den=9.91    0     0.000071997 1550.53     end   \n'\
'    ru-103      4     Den=9.91    0     3.9478E-006 1550.53     end   \n'\
'    ru-104      4     Den=9.91    0     0.000070731 1550.53     end   \n'\
'    ru-105      4     Den=9.91    0     1.525E-008  1550.53     end   \n'\
'    ru-106      4     Den=9.91    0     0.000023215 1550.53     end   \n'\
'    ru-96 4     Den=9.91    0     1E-020      1550.53     end   \n'\
'    ru-98 4     Den=9.91    0     4.5375E-014 1550.53     end   \n'\
'    ru-99 4     Den=9.91    0     2.5362E-009 1550.53     end   \n'\
'    s-32  4     Den=9.91    0     1E-020      1550.53     end   \n'\
'    s-33  4     Den=9.91    0     1E-020      1550.53     end   \n'\
'    s-34  4     Den=9.91    0     1.0002E-020 1550.53     end   \n'\
'    s-36  4     Den=9.91    0     1E-020      1550.53     end   \n'\
'    sb-121      4     Den=9.91    0     3.6017E-007 1550.53     end   \n'\
'    sb-123      4     Den=9.91    0     4.5935E-007 1550.53     end   \n'\
'    sb-124      4     Den=9.91    0     1.6644E-009 1550.53     end   \n'\
'    sb-125      4     Den=9.91    0     0.000000764 1550.53     end   \n'\
'    sb-126      4     Den=9.91    0     3.4674E-010 1550.53     end   \n'\
'    sc-45 4     Den=9.91    0     1E-020      1550.53     end   \n'\
'    se-74 4     Den=9.91    0     2.4291E-014 1550.53     end   \n'\
'    se-76 4     Den=9.91    0     3.6036E-010 1550.53     end   \n'\
'    se-77 4     Den=9.91    0     7.9748E-008 1550.53     end   \n'\
'    se-78 4     Den=9.91    0     2.2178E-007 1550.53     end   \n'\
'    se-80 4     Den=9.91    0     0.00000098  1550.53     end   \n'\
'    se-82 4     Den=9.91    0     2.6315E-006 1550.53     end   \n'\
'    si-28 4     Den=9.91    0     1E-020      1550.53     end   \n'\
'    si-29 4     Den=9.91    0     1.0006E-020 1550.53     end   \n'\
'    si-30 4     Den=9.91    0     1.0028E-020 1550.53     end   \n'\
'    sm-144      4     Den=9.91    0     6.3359E-019 1550.53     end   \n'\
'    sm-147      4     Den=9.91    0     4.7122E-006 1550.53     end   \n'\
'    sm-148      4     Den=9.91    0     5.4994E-006 1550.53     end   \n'\
'    sm-149      4     Den=9.91    0     2.7546E-007 1550.53     end   \n'\
'    sm-150      4     Den=9.91    0     0.000014991 1550.53     end   \n'\
'    sm-151      4     Den=9.91    0     1.7637E-006 1550.53     end   \n'\
'    sm-152      4     Den=9.91    0     9.4639E-006 1550.53     end   \n'\
```

```
'    sm-153      4     Den=9.91    0     4.5501E-008 1550.53     end   \n'\
'    sm-154      4     Den=9.91    0     3.3027E-006 1550.53     end   \n'\
'    sn-112      4     Den=9.91    0     2.0555E-016 1550.53     end   \n'\
'    sn-114      4     Den=9.91    0     7.0404E-012 1550.53     end   \n'\
'    sn-115      4     Den=9.91    0     2.3373E-008 1550.53     end   \n'\
'    sn-116      4     Den=9.91    0     1.1188E-007 1550.53     end   \n'\
'    sn-117      4     Den=9.91    0     0.000000455 1550.53     end   \n'\
'    sn-118      4     Den=9.91    0     0.000000365 1550.53     end   \n'\
'    sn-119      4     Den=9.91    0     3.5594E-007 1550.53     end   \n'\
'    sn-120      4     Den=9.91    0     3.6027E-007 1550.53     end   \n'\
'    sn-122      4     Den=9.91    0     4.7436E-007 1550.53     end   \n'\
'    sn-123      4     Den=9.91    0     1.7497E-008 1550.53     end   \n'\
'    sn-124      4     Den=9.91    0     7.6774E-007 1550.53     end   \n'\
'    sn-125      4     Den=9.91    0     6.7809E-009 1550.53     end   \n'\
'    sn-126      4     Den=9.91    0     1.9403E-006 1550.53     end   \n'\
'    sr-84 4     Den=9.91    0     2.7128E-013 1550.53     end   \n'\
'    sr-86 4     Den=9.91    0     1.736E-008  1550.53     end   \n'\
'    sr-87 4     Den=9.91    0     2.797E-010  1550.53     end   \n'\
'    sr-88 4     Den=9.91    0     0.000017305 1550.53     end   \n'\
'    sr-89 4     Den=9.91    0     1.7174E-006 1550.53     end   \n'\
'    sr-90 4     Den=9.91    0     0.000024997 1550.53     end   \n'\
'    ta-181      4     Den=9.91    0     1E-020      1550.53     end   \n'\
'    ta-182      4     Den=9.91    0     1E-020      1550.53     end   \n'\
'    tb-159      4     Den=9.91    0     3.138E-007  1550.53     end   \n'\
'    tb-160      4     Den=9.91    0     5.6285E-009 1550.53     end   \n'\
'    tc-99 4     Den=9.91    0     0.000065824 1550.53     end   \n'\
'    te-120      4     Den=9.91    0     7.9964E-017 1550.53     end   \n'\
'    te-122      4     Den=9.91    0     1.7535E-008 1550.53     end   \n'\
'    te-123      4     Den=9.91    0     1.3076E-010 1550.53     end   \n'\
'    te-124      4     Den=9.91    0     0.00000001  1550.53     end   \n'\
'    te-125      4     Den=9.91    0     2.9954E-007 1550.53     end   \n'\
'    te-126      4     Den=9.91    0     3.5612E-008 1550.53     end   \n'\
'    te-128      4     Den=9.91    0     7.5282E-006 1550.53     end   \n'\
'    te-130      4     Den=9.91    0     0.000025272 1550.53     end   \n'\
'    te-132      4     Den=9.91    0     2.4948E-007 1550.53     end   \n'\
'    th-228      4     Den=9.91    0     3.0867E-009 1550.53     end   \n'\
'    th-229      4     Den=9.91    0     1.4746E-009 1550.53     end   \n'\
'    th-230      4     Den=9.91    0     1.7493E-008 1550.53     end   \n'\
'    th-232      4     Den=9.91    0     0.018908    1550.53     end   \n'\
'    ti-46 4     Den=9.91    0     1.0134E-020 1550.53     end   \n'\
'    ti-47 4     Den=9.91    0     1E-020      1550.53     end   \n'\
'    ti-48 4     Den=9.91    0     1E-020      1550.53     end   \n'\
'    ti-49 4     Den=9.91    0     1.0043E-020 1550.53     end   \n'\
'    ti-50 4     Den=9.91    0     1.0011E-020 1550.53     end   \n'\
'    u-232 4     Den=9.91    0     4.6017E-007 1550.53     end   \n'\
'    u-233 4     Den=9.91    0     0.00020538  1550.53     end   \n'\
'    u-234 4     Den=9.91    0     0.000012912 1550.53     end   \n'\
'    u-235 4     Den=9.91    0     1.3289E-006 1550.53     end   \n'\
'    u-236 4     Den=9.91    0     2.7385E-007 1550.53     end   \n'\
'    u-237 4     Den=9.91    0     3.5967E-010 1550.53     end   \n'\
'    u-238 4     Den=9.91    0     1.3777E-009 1550.53     end   \n'\
'    w-182 4     Den=9.91    0     1.1945E-020 1550.53     end   \n'\
'    w-183 4     Den=9.91    0     1.768E-020  1550.53     end   \n'\
'    w-184 4     Den=9.91    0     1.291E-020  1550.53     end   \n'\
```

```
'    w-186 4     Den=9.91    0     1E-020      1550.53     end   \n'\
'    xe-124      4     Den=9.91    0     1E-020      1550.53     end   \n'\
'    xe-126      4     Den=9.91    0     9.5678E-012 1550.53     end   \n'\
'    xe-128      4     Den=9.91    0     1.9637E-007 1550.53     end   \n'\
'    xe-129      4     Den=9.91    0     6.7194E-010 1550.53     end   \n'\
'    xe-130      4     Den=9.91    0     2.4625E-007 1550.53     end   \n'\
'    xe-131      4     Den=9.91    0     0.000035263 1550.53     end   \n'\
'    xe-132      4     Den=9.91    0     0.000065234 1550.53     end   \n'\
'    xe-133      4     Den=9.91    0     5.4012E-007 1550.53     end   \n'\
'    xe-134      4     Den=9.91    0     0.000088645 1550.53     end   \n'\
'    xe-135      4     Den=9.91    0     2.1102E-008 1550.53     end   \n'\
'    xe-136      4     Den=9.91    0     0.00011767  1550.53     end   \n'\
'    y-89  4     Den=9.91    0     0.000019954 1550.53     end   \n'\
'    y-90  4     Den=9.91    0     6.4164E-009 1550.53     end   \n'\
'    y-91  4     Den=9.91    0     2.5764E-006 1550.53     end   \n'\
'    zr-90 4     Den=9.91    0     8.449E-007  1550.53     end   \n'\
'    zr-91 4     Den=9.91    0     0.000026932 1550.53     end   \n'\
'    zr-92 4     Den=9.91    0     0.000035084 1550.53     end   \n'\
'    zr-93 4     Den=9.91    0     0.000043205 1550.53     end   \n'\
'    zr-94 4     Den=9.91    0     0.000048692 1550.53     end   \n'\
'    zr-95 4     Den=9.91    0     4.8156E-006 1550.53     end   \n'\
'    zr-96 4     Den=9.91    0     0.000055337 1550.53     end   \n'\
      'wtpt-zr310ssFCI\n'\
      '      5   7.90 10\n'\
      '   6000   0.034\n'\
      '  14000   0.51\n'\
      '  25055   0.74\n'\
      '  15031   0.016\n'\
      '  16000   0.002\n'\
      '  28000  20.82\n'\
      '  24000  25.04\n'\
      '  26000  51.738\n'\
      '  42000   0.51\n'\
      '  40000   0.59\n'\
      '1   781.38 end\n'\
'    ag-107      6     Den=9.87    0     5.9219E-012 1550.53     end   \n'\
'    ag-109      6     Den=9.87    0     0.000015169 1550.53     end   \n'\
'    ag-111      6     Den=9.87    0     3.9522E-008 1550.53     end   \n'\
'    al-27 6     Den=9.87    0     1E-020      1550.53     end   \n'\
'    am-241      6     Den=9.87    0     0.000026051 1550.53     end   \n'\
'    am-242      6     Den=9.87    0     2.7827E-008 1550.53     end   \n'\
'    am-243      6     Den=9.87    0     0.000037477 1550.53     end   \n'\
'    ar-36 6     Den=9.87    0     1E-020      1550.53     end   \n'\
'    ar-38 6     Den=9.87    0     1E-020      1550.53     end   \n'\
'    ar-40 6     Den=9.87    0     1.0031E-020 1550.53     end   \n'\
'    as-75 6     Den=9.87    0     1.7948E-008 1550.53     end   \n'\
'    b-10  6     Den=9.87    0     2.7166E-018 1550.53     end   \n'\
'    b-11  6     Den=9.87    0     6.5166E-015 1550.53     end   \n'\
'    ba-130      6     Den=9.87    0     1E-020      1550.53     end   \n'\
'    ba-132      6     Den=9.87    0     5.8619E-012 1550.53     end   \n'\
'    ba-133      6     Den=9.87    0     2.1414E-012 1550.53     end   \n'\
'    ba-134      6     Den=9.87    0     1.7507E-006 1550.53     end   \n'\
'    ba-135      6     Den=9.87    0     7.767E-009  1550.53     end   \n'\
'    ba-136      6     Den=9.87    0     1.4938E-006 1550.53     end   \n'\
```

```
'    ba-137     6     Den=9.87    0     2.4489E-006 1550.53     end   \n'\
'    ba-138     6     Den=9.87    0     0.000069165 1550.53     end   \n'\
'    ba-140     6     Den=9.87    0     1.0729E-006 1550.53     end   \n'\
'    be-9  6     Den=9.87    0     4.5215E-013 1550.53     end   \n'\
'    bi-209     6     Den=9.87    0     2.3307E-013 1550.53     end   \n'\
'    bk-249     6     Den=9.87    0     2.3217E-013 1550.53     end   \n'\
'    bk-250     6     Den=9.87    0     1.5003E-016 1550.53     end   \n'\
'    br-79 6     Den=9.87    0     2.5522E-010 1550.53     end   \n'\
'    br-81 6     Den=9.87    0     1.7754E-006 1550.53     end   \n'\
'    ca-40 6     Den=9.87    0     1E-020      1550.53     end   \n'\
'    ca-42 6     Den=9.87    0     1.0014E-020 1550.53     end   \n'\
'    ca-43 6     Den=9.87    0     1E-020      1550.53     end   \n'\
'    ca-44 6     Den=9.87    0     1.0092E-020 1550.53     end   \n'\
'    ca-46 6     Den=9.87    0     1E-020      1550.53     end   \n'\
'    ca-48 6     Den=9.87    0     1E-020      1550.53     end   \n'\
'    cd-106     6     Den=9.87    0     1.1602E-020 1550.53     end   \n'\
'    cd-108     6     Den=9.87    0     4.591E-011  1550.53     end   \n'\
'    cd-110     6     Den=9.87    0     5.2959E-006 1550.53     end   \n'\
'    cd-111     6     Den=9.87    0     4.0335E-006 1550.53     end   \n'\
'    cd-112     6     Den=9.87    0     1.7564E-006 1550.53     end   \n'\
'    cd-113     6     Den=9.87    0     2.4639E-008 1550.53     end   \n'\
'    cd-114     6     Den=9.87    0     1.7914E-006 1550.53     end   \n'\
'    cd-116     6     Den=9.87    0     4.7455E-007 1550.53     end   \n'\
'    ce-136     6     Den=9.87    0     1E-020      1550.53     end   \n'\
'    ce-138     6     Den=9.87    0     1.9648E-013 1550.53     end   \n'\
'    ce-140     6     Den=9.87    0     0.000063318 1550.53     end   \n'\
'    ce-141     6     Den=9.87    0     2.5534E-006 1550.53     end   \n'\
'    ce-142     6     Den=9.87    0     0.000055728 1550.53     end   \n'\
'    ce-143     6     Den=9.87    0     9.6755E-008 1550.53     end   \n'\
'    ce-144     6     Den=9.87    0     0.000015893 1550.53     end   \n'\
'    cf-249     6     Den=9.87    0     4.9467E-014 1550.53     end   \n'\
'    cf-250     6     Den=9.87    0     5.9696E-014 1550.53     end   \n'\
'    cf-251     6     Den=9.87    0     1.839E-014  1550.53     end   \n'\
'    cf-252     6     Den=9.87    0     5.123E-015  1550.53     end   \n'\
'    cf-253     6     Den=9.87    0     4.4617E-018 1550.53     end   \n'\
'    cf-254     6     Den=9.87    0     1.007E-019  1550.53     end   \n'\
'    cl-35 6     Den=9.87    0     1E-020      1550.53     end   \n'\
'    cl-37 6     Den=9.87    0     1.0053E-020 1550.53     end   \n'\
'    cm-241     6     Den=9.87    0     2.2096E-013 1550.53     end   \n'\
'    cm-242     6     Den=9.87    0     4.4683E-006 1550.53     end   \n'\
'    cm-243     6     Den=9.87    0     1.0173E-007 1550.53     end   \n'\
'    cm-244     6     Den=9.87    0     0.000011362 1550.53     end   \n'\
'    cm-245     6     Den=9.87    0     7.6992E-007 1550.53     end   \n'\
'    cm-246     6     Den=9.87    0     5.5154E-008 1550.53     end   \n'\
'    cm-247     6     Den=9.87    0     5.7203E-010 1550.53     end   \n'\
'    cm-248     6     Den=9.87    0     2.1007E-011 1550.53     end   \n'\
'    cm-250     6     Den=9.87    0     8.4015E-019 1550.53     end   \n'\
'    co-59 6     Den=9.87    0     1E-020      1550.53     end   \n'\
'    cr-50 6     Den=9.87    0     1E-020      1550.53     end   \n'\
'    cr-52 6     Den=9.87    0     1E-020      1550.53     end   \n'\
'    cr-53 6     Den=9.87    0     1E-020      1550.53     end   \n'\
'    cr-54 6     Den=9.87    0     1.0148E-020 1550.53     end   \n'\
'    cs-133     6     Den=9.87    0     0.00006783  1550.53     end   \n'\
'    cs-134     6     Den=9.87    0     5.0257E-006 1550.53     end   \n'\
```

```
'    cs-135      6     Den=9.87    0     0.000039142 1550.53     end   \n'\
'    cs-136      6     Den=9.87    0     3.6737E-008 1550.53     end   \n'\
'    cs-137      6     Den=9.87    0     0.00007077  1550.53     end   \n'\
'    cu-63 6     Den=9.87    0     1E-020      1550.53     end   \n'\
'    cu-65 6     Den=9.87    0     2.2108E-014 1550.53     end   \n'\
'    dy-156      6     Den=9.87    0     2.1693E-019 1550.53     end   \n'\
'    dy-158      6     Den=9.87    0     2.5291E-015 1550.53     end   \n'\
'    dy-160      6     Den=9.87    0     2.1387E-008 1550.53     end   \n'\
'    dy-161      6     Den=9.87    0     4.774E-008  1550.53     end   \n'\
'    dy-162      6     Den=9.87    0     2.6132E-008 1550.53     end   \n'\
'    dy-163      6     Den=9.87    0     1.6619E-008 1550.53     end   \n'\
'    dy-164      6     Den=9.87    0     4.1296E-009 1550.53     end   \n'\
'    er-162      6     Den=9.87    0     1.7676E-019 1550.53     end   \n'\
'    er-164      6     Den=9.87    0     4.7184E-014 1550.53     end   \n'\
'    er-166      6     Den=9.87    0     1.1645E-009 1550.53     end   \n'\
'    er-167      6     Den=9.87    0     9.2962E-011 1550.53     end   \n'\
'    er-168      6     Den=9.87    0     2.1929E-010 1550.53     end   \n'\
'    er-170      6     Den=9.87    0     1.2686E-011 1550.53     end   \n'\
'    es-253      6     Den=9.87    0     3.299E-018  1550.53     end   \n'\
'    es-254      6     Den=9.87    0     2.4587E-020 1550.53     end   \n'\
'    es-255      6     Den=9.87    0     1E-020      1550.53     end   \n'\
'    eu-151      6     Den=9.87    0     2.888E-009  1550.53     end   \n'\
'    eu-152      6     Den=9.87    0     2.2436E-009 1550.53     end   \n'\
'    eu-153      6     Den=9.87    0     0.000007711 1550.53     end   \n'\
'    eu-154      6     Den=9.87    0     1.5678E-006 1550.53     end   \n'\
'    eu-155      6     Den=9.87    0     5.4664E-007 1550.53     end   \n'\
'    eu-156      6     Den=9.87    0     1.3929E-007 1550.53     end   \n'\
'    eu-157      6     Den=9.87    0     8.6564E-010 1550.53     end   \n'\
'    f-19  6     Den=9.87    0     1.3485E-020 1550.53     end   \n'\
'    fe-54 6     Den=9.87    0     1E-020      1550.53     end   \n'\
'    fe-56 6     Den=9.87    0     1.0308E-020 1550.53     end   \n'\
'    fe-57 6     Den=9.87    0     1E-020      1550.53     end   \n'\
'    fe-58 6     Den=9.87    0     2.9394E-020 1550.53     end   \n'\
'    ga-69 6     Den=9.87    0     9.1251E-011 1550.53     end   \n'\
'    ga-71 6     Den=9.87    0     6.699E-010  1550.53     end   \n'\
'    gd-152      6     Den=9.87    0     0.000000004 1550.53     end   \n'\
'    gd-154      6     Den=9.87    0     1.2313E-007 1550.53     end   \n'\
'    gd-155      6     Den=9.87    0     0.000000007 1550.53     end   \n'\
'    gd-156      6     Den=9.87    0     0.000003975 1550.53     end   \n'\
'    gd-157      6     Den=9.87    0     8.2958E-009 1550.53     end   \n'\
'    gd-158      6     Den=9.87    0     1.7042E-006 1550.53     end   \n'\
'    gd-160      6     Den=9.87    0     0.000000138 1550.53     end   \n'\
'    ge-70 6     Den=9.87    0     5.6183E-013 1550.53     end   \n'\
'    ge-72 6     Den=9.87    0     1.48E-009   1550.53     end   \n'\
'    ge-73 6     Den=9.87    0     3.2365E-009 1550.53     end   \n'\
'    ge-74 6     Den=9.87    0     7.7483E-009 1550.53     end   \n'\
'    ge-76 6     Den=9.87    0     3.7361E-008 1550.53     end   \n'\
'    h-1   6     Den=9.87    0     1.4751E-008 1550.53     end   \n'\
'    h-2   6     Den=9.87    0     1.5789E-009 1550.53     end   \n'\
'    h-3   6     Den=9.87    0     1.5247E-007 1550.53     end   \n'\
'    he-3  6     Den=9.87    0     1E-020      1550.53     end   \n'\
'    he-4  6     Den=9.87    0     0.000011255 1550.53     end   \n'\
'    hf-174      6     Den=9.87    0     1E-020      1550.53     end   \n'\
'    hf-176      6     Den=9.87    0     1.0187E-020 1550.53     end   \n'\
```

```
'    hf-177      6     Den=9.87    0     1E-020      1550.53     end   \n'\
'    hf-178      6     Den=9.87    0     1.5493E-020 1550.53     end   \n'\
'    hf-179      6     Den=9.87    0     1.8251E-020 1550.53     end   \n'\
'    hf-180      6     Den=9.87    0     1.3577E-020 1550.53     end   \n'\
'    hg-196      6     Den=9.87    0     1E-020      1550.53     end   \n'\
'    hg-198      6     Den=9.87    0     1.6672E-020 1550.53     end   \n'\
'    hg-199      6     Den=9.87    0     1E-020      1550.53     end   \n'\
'    hg-200      6     Den=9.87    0     1.8498E-020 1550.53     end   \n'\
'    hg-201      6     Den=9.87    0     1E-020      1550.53     end   \n'\
'    hg-202      6     Den=9.87    0     1.0188E-020 1550.53     end   \n'\
'    hg-204      6     Den=9.87    0     1E-020      1550.53     end   \n'\
'    ho-165      6     Den=9.87    0     4.2259E-009 1550.53     end   \n'\
'    i-127 6     Den=9.87    0     4.2582E-006 1550.53     end   \n'\
'    i-129 6     Den=9.87    0     0.000012957 1550.53     end   \n'\
'    i-130 6     Den=9.87    0     4.0366E-010 1550.53     end   \n'\
'    i-131 6     Den=9.87    0     4.1632E-007 1550.53     end   \n'\
'    i-135 6     Den=9.87    0     2.5691E-008 1550.53     end   \n'\
'    in-113      6     Den=9.87    0     6.0341E-011 1550.53     end   \n'\
'    in-115      6     Den=9.87    0     2.4907E-007 1550.53     end   \n'\
'    ir-191      6     Den=9.87    0     1E-020      1550.53     end   \n'\
'    ir-193      6     Den=9.87    0     1E-020      1550.53     end   \n'\
'    k-39  6     Den=9.87    0     1E-020      1550.53     end   \n'\
'    k-40  6     Den=9.87    0     1E-020      1550.53     end   \n'\
'    k-41  6     Den=9.87    0     1.0226E-020 1550.53     end   \n'\
'    kr-78 6     Den=9.87    0     7.8431E-020 1550.53     end   \n'\
'    kr-80 6     Den=9.87    0     3.1714E-011 1550.53     end   \n'\
'    kr-82 6     Den=9.87    0     3.6859E-008 1550.53     end   \n'\
'    kr-83 6     Den=9.87    0     3.3482E-006 1550.53     end   \n'\
'    kr-84 6     Den=9.87    0     6.6682E-006 1550.53     end   \n'\
'    kr-85 6     Den=9.87    0     1.5964E-006 1550.53     end   \n'\
'    kr-86 6     Den=9.87    0     0.000010206 1550.53     end   \n'\
'    la-138      6     Den=9.87    0     7.2579E-010 1550.53     end   \n'\
'    la-139      6     Den=9.87    0     0.00006462  1550.53     end   \n'\
'    la-140      6     Den=9.87    0     1.4366E-007 1550.53     end   \n'\
'    li-6  6     Den=9.87    0     1E-020      1550.53     end   \n'\
'    li-7  6     Den=9.87    0     1.9997E-020 1550.53     end   \n'\
'    lu-175      6     Den=9.87    0     1.0558E-020 1550.53     end   \n'\
'    lu-176      6     Den=9.87    0     1E-020      1550.53     end   \n'\
'    mg-24 6     Den=9.87    0     1.0004E-020 1550.53     end   \n'\
'    mg-25 6     Den=9.87    0     1E-020      1550.53     end   \n'\
'    mg-26 6     Den=9.87    0     1.0002E-020 1550.53     end   \n'\
'    mn-55 6     Den=9.87    0     1E-020      1550.53     end   \n'\
'    mo-100      6     Den=9.87    0     0.0000705   1550.53     end   \n'\
'    mo-92 6     Den=9.87    0     1.0779E-019 1550.53     end   \n'\
'    mo-94 6     Den=9.87    0     3.7653E-010 1550.53     end   \n'\
'    mo-95 6     Den=9.87    0     0.000043263 1550.53     end   \n'\
'    mo-96 6     Den=9.87    0     1.3889E-006 1550.53     end   \n'\
'    mo-97 6     Den=9.87    0     0.000057555 1550.53     end   \n'\
'    mo-98 6     Den=9.87    0     0.000061037 1550.53     end   \n'\
'    mo-99 6     Den=9.87    0     0.000000238 1550.53     end   \n'\
'    n-14  6     Den=9.87    0     6.4493E-013 1550.53     end   \n'\
'    n-15  6     Den=9.87    0     1.731E-009  1550.53     end   \n'\
'    na-23 6     Den=9.87    0     1E-020      1550.53     end   \n'\
'    nb-93 6     Den=9.87    0     4.7117E-012 1550.53     end   \n'\
```

```
'    nb-94 6     Den=9.87    0     1.43E-010   1550.53     end   \n'\
'    nb-95 6     Den=9.87    0     2.4524E-006 1550.53     end   \n'\
'    nd-142      6     Den=9.87    0     5.1041E-007 1550.53     end   \n'\
'    nd-143      6     Den=9.87    0     0.000043289 1550.53     end   \n'\
'    nd-144      6     Den=9.87    0     0.000034828 1550.53     end   \n'\
'    nd-145      6     Den=9.87    0     0.000032146 1550.53     end   \n'\
'    nd-146      6     Den=9.87    0     0.000030972 1550.53     end   \n'\
'    nd-147      6     Den=9.87    0     3.3274E-007 1550.53     end   \n'\
'    nd-148      6     Den=9.87    0     0.000018946 1550.53     end   \n'\
'    nd-150      6     Den=9.87    0     0.000011021 1550.53     end   \n'\
'    ni-58 6     Den=9.87    0     1E-020      1550.53     end   \n'\
'    ni-59 6     Den=9.87    0     1E-020      1550.53     end   \n'\
'    ni-60 6     Den=9.87    0     1.1192E-020 1550.53     end   \n'\
'    ni-61 6     Den=9.87    0     1.0002E-020 1550.53     end   \n'\
'    ni-62 6     Den=9.87    0     1E-020      1550.53     end   \n'\
'    ni-64 6     Den=9.87    0     1.0024E-020 1550.53     end   \n'\
'    np-236      6     Den=9.87    0     7.6727E-014 1550.53     end   \n'\
'    np-237      6     Den=9.87    0     8.3424E-008 1550.53     end   \n'\
'    np-238      6     Den=9.87    0     1.2924E-010 1550.53     end   \n'\
'    np-239      6     Den=9.87    0     3.344E-011  1550.53     end   \n'\
'    o-16  6     Den=9.87    0     0.044888    1550.53     end   \n'\
'    o-17  6     Den=9.87    0     6.908E-009  1550.53     end   \n'\
'    p-31  6     Den=9.87    0     1.0003E-020 1550.53     end   \n'\
'    pa-231      6     Den=9.87    0     1.7292E-006 1550.53     end   \n'\
'    pa-232      6     Den=9.87    0     2.2294E-009 1550.53     end   \n'\
'    pa-233      6     Den=9.87    0     0.000014799 1550.53     end   \n'\
'    pb-204      6     Den=9.87    0     1.0114E-020 1550.53     end   \n'\
'    pb-206      6     Den=9.87    0     3.6848E-014 1550.53     end   \n'\
'    pb-207      6     Den=9.87    0     1.1895E-012 1550.53     end   \n'\
'    pb-208      6     Den=9.87    0     9.4192E-010 1550.53     end   \n'\
'    pd-102      6     Den=9.87    0     1.9681E-011 1550.53     end   \n'\
'    pd-104      6     Den=9.87    0     0.000010072 1550.53     end   \n'\
'    pd-105      6     Den=9.87    0     0.000055163 1550.53     end   \n'\
'    pd-106      6     Den=9.87    0     0.000032736 1550.53     end   \n'\
'    pd-107      6     Den=9.87    0     0.000037851 1550.53     end   \n'\
'    pd-108      6     Den=9.87    0     0.000026766 1550.53     end   \n'\
'    pd-110      6     Den=9.87    0     8.9565E-006 1550.53     end   \n'\
'    pm-147      6     Den=9.87    0     0.000010552 1550.53     end   \n'\
'    pm-148      6     Den=9.87    0     4.4464E-008 1550.53     end   \n'\
'    pm-149      6     Den=9.87    0     5.087E-008  1550.53     end   \n'\
'    pm-151      6     Den=9.87    0     1.2751E-008 1550.53     end   \n'\
'    pr-141      6     Den=9.87    0     0.000054777 1550.53     end   \n'\
'    pr-142      6     Den=9.87    0     1.3614E-009 1550.53     end   \n'\
'    pr-143      6     Den=9.87    0     9.509E-007  1550.53     end   \n'\
'    pu-236      6     Den=9.87    0     2.1342E-011 1550.53     end   \n'\
'    pu-237      6     Den=9.87    0     9.9256E-011 1550.53     end   \n'\
'    pu-238      6     Den=9.87    0     0.000055038 1550.53     end   \n'\
'    pu-239      6     Den=9.87    0     0.00038923  1550.53     end   \n'\
'    pu-240      6     Den=9.87    0     0.00059028  1550.53     end   \n'\
'    pu-241      6     Den=9.87    0     0.00025082  1550.53     end   \n'\
'    pu-242      6     Den=9.87    0     0.00024757  1550.53     end   \n'\
'    pu-243      6     Den=9.87    0     1.7908E-008 1550.53     end   \n'\
'    pu-244      6     Den=9.87    0     6.7476E-009 1550.53     end   \n'\
'    rb-85 6     Den=9.87    0     5.8964E-006 1550.53     end   \n'\
```

```
'    rb-86 6     Den=9.87    0     1.0859E-009 1550.53     end   \n'\
'    rb-87 6     Den=9.87    0     0.000013391 1550.53     end   \n'\
'    re-185      6     Den=9.87    0     1E-020      1550.53     end   \n'\
'    re-187      6     Den=9.87    0     1.0405E-020 1550.53     end   \n'\
'    rh-103      6     Den=9.87    0     0.00005767  1550.53     end   \n'\
'    rh-105      6     Den=9.87    0     9.8648E-008 1550.53     end   \n'\
'    ru-100      6     Den=9.87    0     5.3243E-006 1550.53     end   \n'\
'    ru-101      6     Den=9.87    0     0.000062464 1550.53     end   \n'\
'    ru-102      6     Den=9.87    0     0.000067797 1550.53     end   \n'\
'    ru-103      6     Den=9.87    0     3.4516E-006 1550.53     end   \n'\
'    ru-104      6     Den=9.87    0     0.000066099 1550.53     end   \n'\
'    ru-105      6     Den=9.87    0     1.3171E-008 1550.53     end   \n'\
'    ru-106      6     Den=9.87    0     0.000021229 1550.53     end   \n'\
'    ru-96 6     Den=9.87    0     1E-020      1550.53     end   \n'\
'    ru-98 6     Den=9.87    0     4.067E-014  1550.53     end   \n'\
'    ru-99 6     Den=9.87    0     2.4005E-009 1550.53     end   \n'\
'    s-32  6     Den=9.87    0     1E-020      1550.53     end   \n'\
'    s-33  6     Den=9.87    0     1E-020      1550.53     end   \n'\
'    s-34  6     Den=9.87    0     1.0004E-020 1550.53     end   \n'\
'    s-36  6     Den=9.87    0     1E-020      1550.53     end   \n'\
'    sb-121      6     Den=9.87    0     3.3513E-007 1550.53     end   \n'\
'    sb-123      6     Den=9.87    0     4.3692E-007 1550.53     end   \n'\
'    sb-124      6     Den=9.87    0     1.7258E-009 1550.53     end   \n'\
'    sb-125      6     Den=9.87    0     7.1786E-007 1550.53     end   \n'\
'    sb-126      6     Den=9.87    0     3.2007E-010 1550.53     end   \n'\
'    sc-45 6     Den=9.87    0     1E-020      1550.53     end   \n'\
'    se-74 6     Den=9.87    0     2.2501E-014 1550.53     end   \n'\
'    se-76 6     Den=9.87    0     3.8865E-010 1550.53     end   \n'\
'    se-77 6     Den=9.87    0     7.9818E-008 1550.53     end   \n'\
'    se-78 6     Den=9.87    0     2.2043E-007 1550.53     end   \n'\
'    se-80 6     Den=9.87    0     9.7047E-007 1550.53     end   \n'\
'    se-82 6     Den=9.87    0     2.6006E-006 1550.53     end   \n'\
'    si-28 6     Den=9.87    0     1.0001E-020 1550.53     end   \n'\
'    si-29 6     Den=9.87    0     1.0006E-020 1550.53     end   \n'\
'    si-30 6     Den=9.87    0     1.0029E-020 1550.53     end   \n'\
'    sm-144      6     Den=9.87    0     5.0852E-019 1550.53     end   \n'\
'    sm-147      6     Den=9.87    0     4.3725E-006 1550.53     end   \n'\
'    sm-148      6     Den=9.87    0     5.5691E-006 1550.53     end   \n'\
'    sm-149      6     Den=9.87    0     1.9433E-007 1550.53     end   \n'\
'    sm-150      6     Den=9.87    0     0.000014298 1550.53     end   \n'\
'    sm-151      6     Den=9.87    0     1.0886E-006 1550.53     end   \n'\
'    sm-152      6     Den=9.87    0     8.7975E-006 1550.53     end   \n'\
'    sm-153      6     Den=9.87    0     4.5625E-008 1550.53     end   \n'\
'    sm-154      6     Den=9.87    0     3.1045E-006 1550.53     end   \n'\
'    sn-112      6     Den=9.87    0     1.688E-016  1550.53     end   \n'\
'    sn-114      6     Den=9.87    0     6.0732E-012 1550.53     end   \n'\
'    sn-115      6     Den=9.87    0     2.1674E-008 1550.53     end   \n'\
'    sn-116      6     Den=9.87    0     0.000000114 1550.53     end   \n'\
'    sn-117      6     Den=9.87    0     4.2148E-007 1550.53     end   \n'\
'    sn-118      6     Den=9.87    0     3.4013E-007 1550.53     end   \n'\
'    sn-119      6     Den=9.87    0     3.3251E-007 1550.53     end   \n'\
'    sn-120      6     Den=9.87    0     0.000000338 1550.53     end   \n'\
'    sn-122      6     Den=9.87    0     4.4687E-007 1550.53     end   \n'\
'    sn-123      6     Den=9.87    0     0.000000016 1550.53     end   \n'\
```

```
'    sn-124     6     Den=9.87    0     7.2308E-007 1550.53     end   \n'\
'    sn-125     6     Den=9.87    0     6.1087E-009 1550.53     end   \n'\
'    sn-126     6     Den=9.87    0     1.8409E-006 1550.53     end   \n'\
'    sr-84 6    Den=9.87    0    2.5147E-013 1550.53     end   \n'\
'    sr-86 6    Den=9.87    0    1.8682E-008 1550.53     end   \n'\
'    sr-87 6    Den=9.87    0    2.7115E-010 1550.53     end   \n'\
'    sr-88 6    Den=9.87    0    0.000017605 1550.53     end   \n'\
'    sr-89 6    Den=9.87    0    1.7657E-006 1550.53     end   \n'\
'    sr-90 6    Den=9.87    0    0.000025034 1550.53     end   \n'\
'    ta-181     6     Den=9.87    0     1E-020      1550.53     end   \n'\
'    ta-182     6     Den=9.87    0     1E-020      1550.53     end   \n'\
'    tb-159     6     Den=9.87    0     2.9457E-007 1550.53     end   \n'\
'    tb-160     6     Den=9.87    0     5.7471E-009 1550.53     end   \n'\
'    tc-99 6    Den=9.87    0    0.000061904 1550.53     end   \n'\
'    te-120     6     Den=9.87    0     7.1844E-017 1550.53     end   \n'\
'    te-122     6     Den=9.87    0     1.7864E-008 1550.53     end   \n'\
'    te-123     6     Den=9.87    0     1.4103E-010 1550.53     end   \n'\
'    te-124     6     Den=9.87    0     1.0334E-008 1550.53     end   \n'\
'    te-125     6     Den=9.87    0     0.000000287 1550.53     end   \n'\
'    te-126     6     Den=9.87    0     3.372E-008  1550.53     end   \n'\
'    te-128     6     Den=9.87    0     0.000007212 1550.53     end   \n'\
'    te-130     6     Den=9.87    0     0.000024008 1550.53     end   \n'\
'    te-132     6     Den=9.87    0     2.276E-007  1550.53     end   \n'\
'    th-228     6     Den=9.87    0     3.3117E-009 1550.53     end   \n'\
'    th-229     6     Den=9.87    0     1.6527E-009 1550.53     end   \n'\
'    th-230     6     Den=9.87    0     1.6514E-008 1550.53     end   \n'\
'    th-232     6     Den=9.87    0     0.019455    1550.53     end   \n'\
'    ti-46 6    Den=9.87    0    1.0181E-020 1550.53     end   \n'\
'    ti-47 6    Den=9.87    0    1E-020      1550.53     end   \n'\
'    ti-48 6    Den=9.87    0    1E-020      1550.53     end   \n'\
'    ti-49 6    Den=9.87    0    1.0058E-020 1550.53     end   \n'\
'    ti-50 6    Den=9.87    0    1.0014E-020 1550.53     end   \n'\
'    u-232 6    Den=9.87    0    4.9394E-007 1550.53     end   \n'\
'    u-233 6    Den=9.87    0    0.00022747  1550.53     end   \n'\
'    u-234 6    Den=9.87    0    0.000015726 1550.53     end   \n'\
'    u-235 6    Den=9.87    0    1.6787E-006 1550.53     end   \n'\
'    u-236 6    Den=9.87    0    2.4676E-007 1550.53     end   \n'\
'    u-237 6    Den=9.87    0    3.4945E-010 1550.53     end   \n'\
'    u-238 6    Den=9.87    0    1.1495E-009 1550.53     end   \n'\
'    w-182 6    Den=9.87    0    1.1367E-020 1550.53     end   \n'\
'    w-183 6    Den=9.87    0    1.8148E-020 1550.53     end   \n'\
'    w-184 6    Den=9.87    0    1.3202E-020 1550.53     end   \n'\
'    w-186 6    Den=9.87    0    1E-020      1550.53     end   \n'\
'    xe-124     6     Den=9.87    0     1E-020      1550.53     end   \n'\
'    xe-126     6     Den=9.87    0     8.1819E-012 1550.53     end   \n'\
'    xe-128     6     Den=9.87    0     2.0061E-007 1550.53     end   \n'\
'    xe-129     6     Den=9.87    0     7.9265E-010 1550.53     end   \n'\
'    xe-130     6     Den=9.87    0     2.8614E-007 1550.53     end   \n'\
'    xe-131     6     Den=9.87    0     0.000032613 1550.53     end   \n'\
'    xe-132     6     Den=9.87    0     0.000062908 1550.53     end   \n'\
'    xe-133     6     Den=9.87    0     4.9119E-007 1550.53     end   \n'\
'    xe-134     6     Den=9.87    0     0.000084206 1550.53     end   \n'\
'    xe-135     6     Den=9.87    0     1.561E-008  1550.53     end   \n'\
'    xe-136     6     Den=9.87    0     0.00011946  1550.53     end   \n'\
```

```
'    y-89  6     Den=9.87    0     0.000020114 1550.53     end   \n'\
'    y-90  6     Den=9.87    0     6.4533E-009 1550.53     end   \n'\
'    y-91  6     Den=9.87    0     2.5518E-006 1550.53     end   \n'\
'    zr-90 6     Den=9.87    0     8.4562E-007 1550.53     end   \n'\
'    zr-91 6     Den=9.87    0     0.000026618 1550.53     end   \n'\
'    zr-92 6     Den=9.87    0     0.000034367 1550.53     end   \n'\
'    zr-93 6     Den=9.87    0     0.000041976 1550.53     end   \n'\
'    zr-94 6     Den=9.87    0     0.000047063 1550.53     end   \n'\
'    zr-95 6     Den=9.87    0     4.5014E-006 1550.53     end   \n'\
'    zr-96 6     Den=9.87    0     0.000052934 1550.53     end   \n'\
  'wtpt-zr310ssFCO\n'\
  '      7   7.90 10\n'\
  '   6000   0.034\n'\
  '  14000   0.51\n'\
  '  25055   0.74\n'\
  '  15031   0.016\n'\
  '  16000   0.002\n'\
  '  28000  20.82\n'\
  '  24000  25.04\n'\
  '  26000  51.738\n'\
  '  42000   0.51\n'\
  '  40000   0.59\n'\
  '1   781.38 end\n'\
  'wtpt-zr310ssIL\n'\
  '      8   7.90 10\n'\
  '   6000   0.034\n'\
  '  14000   0.51\n'\
  '  25055   0.74\n'\
  '  15031   0.016\n'\
  '  16000   0.002\n'\
  '  28000  20.82\n'\
  '  24000  25.04\n'\
  '  26000  51.738\n'\
  '  42000   0.51\n'\
  '  40000   0.59\n'\
  ' 1  678.65 end\n'\
  'wtpt-Inslator\n'\
  '      9   5.83 3\n'\
  '  40000  66.63\n'\
  '  39089   7.87\n'\
  '   8016  25.5\n'\
  ' 1  561.45 end\n'\
  'wtpt-zr310ssOL\n'\
  '     10   6.52 4\n'\
  '  50000   3.5\n'\
  '  42000   0.8\n'\
  '  41093   0.8\n'\
  '  40000  94.9\n'\
  ' 1  418.11 end\n'\
  'wtpt-zr310ssPT\n'\
  '     11   6.52 4\n'\
  '  50000   3.5\n'\
  '  42000   0.8\n'\
  '  41093   0.8\n'\
```

```
      '  40000  94.9\n'\
      ' 1  418.11 end\n'\
      'd2o 12 den=1.0851 0.99833 342.16 end\n'\
      'h2o 12 den=1.0851 0.00167 342.16 end\n'\
      'h2o 13 den=0.4 1 692.35 end\n'\
      'h2o 14 den=0.4 1 692.35 end\n'\
      'end composition\n'\
      'read celldata\n '\
      'latticecell squarepitch pitch=1.3621 13  fueld=0.83 4\n '\
      'cladd=0.95  5 end\n '\
      'centrmdata dan2pitch(4)=0.4362519063 end centrmdata\n '\
      'latticecell squarepitch pitch=1.53 14 fueld=0.88 6\n '\
      'cladd=1.0   7 end\n '\
      'centrmdata dan2pitch(6)=0.3818353438 end centrmdata\n '\
      'end celldata\n'\
      'end\n'\
      '=newt parm=centrm\n'\
      'SCWR Lattice Cell (at 250 cm from bottom Channel / Middle of
channel)\n'\
      'read parm\n '\
      'timed=yes echo=yes solntype=keff\n '\
      'cmfd=yes xycmfd=5 sn=6\n '\
      'collapse=yes kguess=1.28\n '\
      'converg=mix\n'\
      'end parm\n'\
      'read materials\n '\
      'mix=12  pn=3  com=\" Moderator\"                        end\n '\
      'mix=11  pn=1  com=\" Pressure Tube\"                    end\n '\
      'mix=10  pn=1  com=\" Outer Liner\"                      end\n '\
      'mix= 9  pn=1  com=\" Insulator\"                        end\n '\
      'mix= 8  pn=1  com=\" Inner Liner\"                      end\n '\
      'mix= 7  pn=1  com=\" Outer Ring Fuel Cladding\"         end\n '\
      'mix= 6  pn=1  com=\" Outer Ring Fuel\"                  end\n '\
      'mix= 5  pn=1  com=\" Inner Ring Fuel Cladding\"         end\n '\
      'mix= 4  pn=1  com=\" Inner Ring Fuel\"                  end\n '\
      'mix= 3  pn=3  com=\" Fuel Assembly Coolant\"            end\n '\
      'mix= 2  pn=1  com=\" Flow tube\"                        end\n '\
      'mix= 1  pn=3  com=\" Coolant inside Central Flow Tube\" end\n'\
      'end materials\n'\
      'read geom\n'\
      'unit 1\n'\
      'cylinder 100 0.300 sides=32\n'\
      'cylinder 101 0.415 sides=32\n'\
      'cylinder 102 0.475 sides=32\n'\
      'media 4 1 101\n'\
      'media 5 1 102 -101\n'\
      'boundary 102\n'\
      'unit 2\n'\
      'cylinder 200 0.300 sides=32\n'\
      'cylinder 201 0.440 sides=32\n'\
      'cylinder 202 0.5   sides=32\n'\
      'media 6 1 201\n'\
      'media 7 1 202 -201\n'\
      'boundary 202\n'\
```

```
'global unit 100\n'\
'wedge 101 12.5 12.5 12.5\n'\
'cylinder  3 1.138 sides=32\n'\
'cylinder  4 1.61  sides=32\n'\
'cylinder  5 1.972 sides=32\n'\
'cylinder  6 2.277 sides=32\n'\
'cylinder  7 2.546 sides=32\n'\
'cylinder  8 2.789 sides=32\n'\
'cylinder  9 3.012 sides=32\n'\
'cylinder 10 3.22  sides=32\n'\
'cylinder 11 3.415 sides=32\n'\
'cylinder 12 3.7   sides=32\n'\
'cylinder 13 3.9   sides=32\n'\
'cylinder 14 4.1   sides=32\n'\
'cylinder 15 4.3   sides=32\n'\
'cylinder 16 4.5   sides=32\n'\
'cylinder 20 4.6   sides=32\n'\
'cylinder 21 4.65  sides=32\n'\
'cylinder 22 4.70  sides=32\n'\
'cylinder 100 4.8  sides=32\n'\
'cylinder 30 4.925 sides=32\n'\
'cylinder 32 5.4   sides=32\n'\
'cylinder 32 5.875 sides=32\n'\
'cylinder 34 6.075 sides=32\n'\
'cylinder 35 6.575 sides=32\n'\
'cylinder 36 7.075 sides=32\n'\
'cylinder 37 7.2   sides=32\n'\
'cylinder 40 7.25  sides=32\n'\
'cylinder 50 7.80  sides=32\n'\
'cylinder 60 7.85  sides=32\n'\
'cylinder 70 9.05  sides=32\n'\
'hole 1 origin x=5.4\n'\
'hole 1 origin x=5.296241  y=1.053488\n'\
'hole 1 origin x=4.988949  y=2.066491\n'\
'hole 1 origin x=4.489936  y=3.000079\n'\
'hole 1 origin x=3.818377  y=3.818377\n'\
'hole 1 origin x=3.000079  y=4.489936\n'\
'hole 1 origin x=2.066491  y=4.988949\n'\
'hole 1 origin x=1.053488  y=5.296241\n'\
'hole 1 origin             y=5.4\n'\
'hole 2 origin x=6.575\n'\
'hole 2 origin x=6.448663  y=1.282719\n'\
'hole 2 origin x=6.074508  y=2.516144\n'\
'hole 2 origin x=5.466913  y=3.652874\n'\
'hole 2 origin x=4.649227  y=4.649227\n'\
'hole 2 origin x=3.652874  y=5.466913\n'\
'hole 2 origin x=2.516144  y=6.074508\n'\
'hole 2 origin x=1.282719  y=6.448663\n'\
'hole 2 origin             y=6.575\n'\
'media  1 1  20\n'\
'media  2 1  22 -20\n'\
'media  3 1  37 -22\n'\
'media  8 1  40 -37\n'\
'media  9 1  50 -40\n'\
```

```
      'media 10 1  60 -50\n'\
      'media 11 1  70 -60\n'\
      'media 12 1 101 -70\n'\
      'boundary 101 20 20\n'\
      'end geom\n'\
      'read bounds\n '\
      'all=refl\n'\
      'end bounds\n'\
      'read homog\n '\
      '100 Cell 1 2 3 4 5 6 7 8 9 10 11 12 end\n'\
      'end homog\n'\
      'read collapse\n'
#print(Middle_inputfile_top_template)
Middle_inputfile_bottom_template ='\n' \
                           'end collapse\n'\
                                 'end \n'\
                                 '=newt\n'\
                                 'SCWR Lattice Cell (at 250 cm from
bottom Channel) using collapsed x-s\n'\
                                 'read parm\n '\
                                 'xnlib=30 collapse=no restart=no
timed=yes echo=yes wtdlib=4 kguess=1.28\n'\
                                 'end parm\n'\
                                 'read materials\n '\
                                 'mix=12  pn=3  com=" Moderator"
end\n '\
                                 'mix=11  pn=1  com=" Pressure Tube"
end\n '\
                                 'mix=10  pn=1  com=" Outer Liner"
end\n '\
                                 'mix= 9  pn=1  com=" Insulator"
end\n '\
                                 'mix= 8  pn=1  com=" Inner Liner"
end\n '\
                                 'mix= 7  pn=1  com=" Outer Ring Fuel
Cladding"         end\n '\
                                 'mix= 6  pn=1  com=" Outer Ring Fuel"
end\n '\
                                 'mix= 5  pn=1  com=" Inner Ring Fuel
Cladding"         end\n '\
                                 'mix= 4  pn=1  com=" Inner Ring Fuel"
end\n '\
                                 'mix= 3  pn=3  com=" Fuel Assembly
Coolant"            end\n '\
                                 'mix= 2  pn=1  com=" Flow tube" end\n '\
                                 'mix= 1  pn=3  com=" Coolant inside
Central Flow Tube" end\n'\
                                 'end materials\n'\
                                 'read geom\n'\
                                 'unit 1\n'\
                                 'cylinder 100 0.300 sides=32\n'\
                                 'cylinder 101 0.415 sides=32\n'\
                                 'cylinder 102 0.475 sides=32\n'\
                                 'media 4 1 101\n'\
```

```
'media 5 1 102 -101\n'\
'boundary 102 \n'\
'unit 2\n'\
'cylinder 200 0.300 sides=32\n'\
'cylinder 201 0.440 sides=32\n'\
'cylinder 202 0.5   sides=32\n'\
'media 6 1 201\n'\
'media 7 1 202 -201\n'\
'boundary 202 \n'\
'global unit 100\n'\
'wedge 101 12.5 12.5 12.5 \n'\
'cylinder  3 1.138 sides=32\n'\
'cylinder  4 1.61  sides=32\n'\
'cylinder  5 1.972 sides=32\n'\
'cylinder  6 2.277 sides=32\n'\
'cylinder  7 2.546 sides=32\n'\
'cylinder  8 2.789 sides=32\n'\
'cylinder  9 3.012 sides=32\n'\
'cylinder 10 3.22  sides=32\n'\
'cylinder 11 3.415 sides=32\n'\
'cylinder 12 3.7   sides=32\n'\
'cylinder 13 3.9   sides=32\n'\
'cylinder 14 4.1   sides=32\n'\
'cylinder 15 4.3   sides=32\n'\
'cylinder 16 4.5   sides=32\n'\
'cylinder 20 4.60  sides=32\n'\
'cylinder 21 4.65  sides=32\n'\
'cylinder 22 4.70  sides=32\n'\
'cylinder 100 4.8  sides=32\n'\
'cylinder 30 4.925 sides=32\n'\
'cylinder 32 5.4   sides=32\n'\
'cylinder 32 5.875 sides=32\n'\
'cylinder 34 6.075 sides=32\n'\
'cylinder 35 6.575 sides=32\n'\
'cylinder 36 7.075 sides=32\n'\
'cylinder 37 7.2   sides=32\n'\
'cylinder 40 7.25  sides=32\n'\
'cylinder 50 7.80  sides=32\n'\
'cylinder 60 7.85  sides=32\n'\
'cylinder 70 9.05  sides=32\n'\
'hole 1 origin x=5.4\n'\
'hole 1 origin x=5.296241
y=1.053488\n'\
'hole 1 origin x=4.988949
y=2.066491\n'\
'hole 1 origin x=4.489936
y=3.000079\n'\
'hole 1 origin x=3.818377
y=3.818377\n'\
'hole 1 origin x=3.000079
y=4.489936\n'\
'hole 1 origin x=2.066491
y=4.988949\n'\
```

```
                                'hole 1 origin x=1.053488
y=5.296241\n'\
                                'hole 1 origin             y=5.4\n'\
                                'hole 2 origin x=6.575\n'\
                                'hole 2 origin x=6.448663
y=1.282719\n'\
                                'hole 2 origin x=6.074508
y=2.516144\n'\
                                'hole 2 origin x=5.466913
y=3.652874\n'\
                                'hole 2 origin x=4.649227
y=4.649227\n'\
                                'hole 2 origin x=3.652874
y=5.466913\n'\
                                'hole 2 origin x=2.516144
y=6.074508\n'\
                                'hole 2 origin x=1.282719
y=6.448663\n'\
                                'hole 2 origin             y=6.575\n'\
                                'media  1 1  20\n'\
                                'media  2 1  22 -20\n'\
                                'media  3 1  37 -22\n'\
                                'media  8 1  40 -37\n'\
                                'media  9 1  50 -40\n'\
                                'media 10 1  60 -50\n'\
                                'media 11 1  70 -60\n'\
                                'media 12 1 101 -70\n'\
                                'boundary 101 20 20\n'\
                                'end geom\n'\
                                'read bounds\n '\
                                'all=refl\n'\
                                'end bounds\n'\
                                'read homog\n '\
                                '200 Cell 1 2 3 4 5 6 7 8 9 10 11 12
end\n'\
                                'end homog\n'\
                                'end\n'
#print(Middle_inputfile_bottom_template)
##############################################################################
############################
# Creating all possible 2 Collapsed Energy Groups options and their input
files at Middle of Channel
##############################################################################
############################
group2_raw = [1,237]
groups_number = len(group2_raw)
#print(groups_number)
all2groups = []
r_num = 'r' * 2
#print(r_num)
r = list(r_num)  # creating list of rs equal to the number of energy
groups (Here 2 groups)
#print(r)
for i in range(0,237):
```

```
    groups2 = [0,0]
    groups2[0]=group2_raw[0]+i
    groups2[1]=group2_raw[1]-i
    groups2 = [str(groups2[i]) + r[i] for i in range(len(groups2))]  #
adding r to the energy groups
    num = list(range(1, groups_number+1))  # creating number list of
number of energy groups  [1,2]
    #print(num)
    groups2 = [(groups2[i]) + str(num[i]) for i in range(len(groups2))]
# adding the group order to the energy group list
    all2groups.append(groups2)
    #print(groups2)
#print(all2groups)
#print(len(all2groups))
for i in range(len(all2groups)):
    #print(i)
    creat_inputfile = open('' + str((i+1)) + '_' + str((237-i)) + "-
Middle.input", "w")
    # print top part of input file
    creat_inputfile.write(Middle_inputfile_top_template)
    count = 0;
    for s in all2groups[i]:
        count += 1
        creat_inputfile.write(s)
        if (count % 10 == 0):
            creat_inputfile.write('\n')
        else:
            creat_inputfile.write(' ')
            # print bottom part of input file
    creat_inputfile.write(Middle_inputfile_bottom_template)
    creat_inputfile.close()
```

2. Diffusion full-core analysis with PARCS

The proposed model in this work for the energy group discretization analysis identifies the optimum two and three energy group structures using the infinite lattice cell and utilizing the transport approach. The full-core diffusion simulations using PARCS [1] were performed to validate the outcomes of the transport model explained earlier. At the lattice transport level, it was proved that the 0.625eV is not a proper or suitable thermal cut-off barrier for the Canadian PT-SCWR that fuelled with a mixture of Pu and Th. Rather, a higher thermal energy cut-off was recommended and it was found to be 2.87 eV. The full-core simulations were executed using the Purdue Advanced Reactor Core Simulator (PARCS) [1] that uses the condensed and homogenized cross-sections calculated by SCALE. The US Nuclear Regulatory Commission used PARCS to performs the 3D reactor core neutronic simulations and analysis. GENPMAX [2] is used to convert the SCALE output files into the suitable and acceptable format required by PARCS. To account for the significant axial variations of coolant density and temperature along the vertical channel, it was divided into 20 nodal positions with materials temperatures and densities given in Hummel [3]. As a result, the lattice cell simulations were performed for each of the 20 locations using the specific materials specifications and temperatures. A multi-cell geometry was created with a set of fuel and reflectors cells to obtain the homogenized cross-sections within the reflector which were employed in PARCS simulations. The refueling scheme introduced by Salaun et al [4] was used along with the same axial and radial heavy water reflector thickness.

The effects of the proper selection of the thermal cut-off barrier for the two-group structure was investigated through the diffusion model using PARCS. The refuelling scheme introduced by Salaun et al [4] was used and an equilibrium core was achieved after multiple refuelling steps. The variation of the calculated radial peak power, axial peak power, and maximum channel nodal power after attaining an equilibrium core using two-group structure for selected thermal cut-off barrier are presented in Figure 1. The diffusion simulations confirm the infinite lattice transport model. The effectiveness of higher thermal energy cut-off is demonstrated

in the calculations of the maximum channel power, radial and axial peak powers for an equilibrium core. Moreover, it shows that the selection of the 0.625 eV is a poor cut-off barrier for the two-group structure. However, the diffusion approach shows a convergence (Plateau) with higher thermal energy barrier (more than 2 eV).

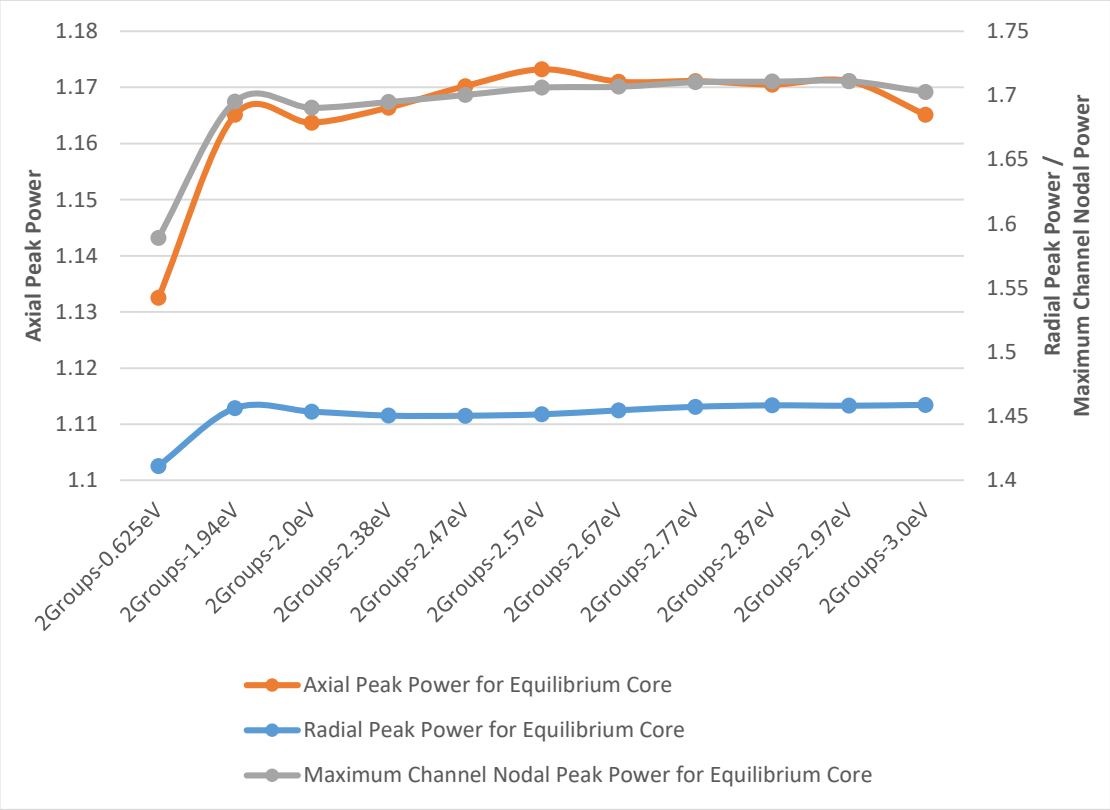

Figure 1: Radial peak power, axial peak power, and maximum channel power for equilibrium core using two-group structure with selected thermal energy cut-off in PARCS.

As shown in Figure 2, the fresh full-core excess reactivity was calculated employing the diffusion model for the optimum two and three energy group structures previously identified. The impacts of the proper selection of the thermal energy cut-off for the two-group structure was investigated and also presented in Figure 2 through a comparison between optimum two-group structure with thermal energy barrier set at 2.87 eV and the conventional energy barrier set at 0.625 eV

using the diffusion approach for fresh fuel-core. It was found at the lattice level that the two-group structure with an energy barrier set at 0.625 eV is characterized by less accurate results with an error that worth ~ 4 mk from the reference solution. While a two-group structure with an energy barrier set at 2.87 eV has the least error which is equivalent to ~ 0.4 pcm. The diffusion results confirm the transport analysis at the lattice level with less sensitivity where the difference calculated between the two energy barriers (0.625eV and 2.87 eV) at the diffusion level computed to be ~ 1.5 mk. The optimum three-energy group structure identified at the lattice level were investigated using the diffusion model with PARCS. The predicted solution shows a convergence between two and three energy group structure with full-core simulations as shown in Figure 2. However, the second barrier set at 820 keV was added due to ICVR transient case which its validation requires a transient full-core study analysis which is beyond the scope of this work. The comparison of the results of the fresh fuel full-core using the optimum two and three energy group structure with PARCS confirms the accuracy and the effectiveness of the selected optimum energy group structures. Moreover, the sensitivity of the results to the energy group structure presented in Figure 2 shows that a higher thermal cut-off energy is recommended for the Canadian PT-SCWR which characterized by a high coolant temperature and high propensity to up-scatter.

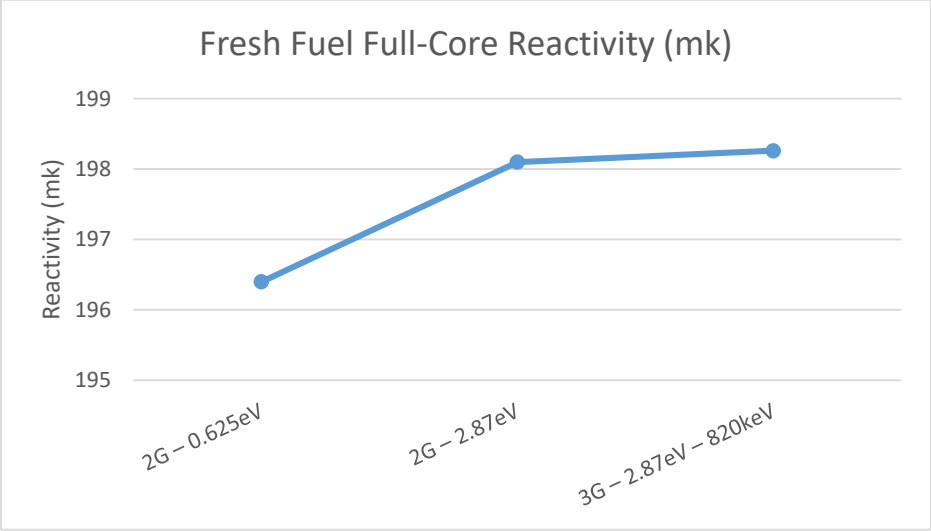

Figure 2: Full-core excess reactivity using PARCS for selected energy group structure

References for appendix:

[1] T. Downar, Y. Xu, and V. Seker, “PARCS v3.0 U.S.NRC Core Neutronics Simulator,” USER MANUAL draft.

[2] A. Ward, Y. Xu, and T. Downar, 2013, GenPMAXS—v6.1.2dev, Code for Generating the PARCS Cross Section Interface File PMAXS.

[3] D.W. Hummel, 2015, “Transient Neutronic-Thermalhydraulic Coupling in a PT-SCWR,” Ph.D. Thesis, McMaster University, Hamilton, ON, Canada.

[4] F. Salaun and D. Novog, 2016, “Spatial and Bulk Reactivity Systems Design and Optimization for the Canadian Supercritical Water Reactor,” Canadian Nuclear Laboratories Nuclear Review, Vol. 5, No. 2, 2016, pp. 285-298, doi:10.12943/CNR.2016.00037, available online at: http://dx.doi.org/10.12943/CNR.2016.000317.